Development And Characterisation Of MSC-Seeded Decellularised Airway Scaffolds For Regenerative Bioengineering

Hind Al Belushi

A thesis submitted to University College London for the degree of Doctor of Philosophy in the School of Life and Medical Sciences, Faculty of Medical Sciences

UCL Cancer Institute
University College London

September 2019

Declaration of Originality

I, Hind Khamis Al Belushi , confirm that the work presented in this thesis is my own. Where information has been derived from other sources, I confirm that this has been indicated in the thesis

Signature:

……..

Date

……..

Abstract

Tracheal tissue engineering (TE) is a potential solution for long tracheal lesions and recent clinical experience yielded promising results but challenges remain with respect to measurable criteria for acceptance of decellularised scaffolds, optimisation of cell seeding and understanding the biology of the seeded cells post attachment.

Confirming previous data from our group, I showed cellular clearance of DC scaffolds and significant reduction in total DNA levels but observed retention of residual nuclear materials within hyaline cartilage and submucosa. Evaluation of extracellular matrix components demonstrated retention of collagen and glycosaminoglycan and disrupted basement membrane components. The novel use of dynamic mechanical analysis (DMA) to measure the viscoelastic properties of tracheal cartilage in addition to tensile testing, provided the first demonstration of preservation of native viscoelastic mechanical properties after decellularisation.

To overcome the limitations of passive cell seeding, I conceived partial surface dehydration (PSD) conditioning of scaffolds which significantly improved cell seeding/attachment efficiency to (96.46% $\pm$1.710) and I confirmed survival of MSCs on the scaffold *in vitro*. Multiphoton imaging showed limited scaffold infiltration but revealed two, distinct cell morphologies dependent on the presence or absence of adventitia. These showed different RNA transcriptomic profiles and differential gene expression. Seeded MSCs upregulated transcripts of bioactive paracrine factors associated with tissue repair, including ECM remodelling, pro-angiogenesis, antifibrosis, chemoattraction and immunomodulatory properties. Cells seeded into the adventitial layer upregulated more bioactive factors and showed lower cellular stress, suggesting a favourable effect of maintaining adventitial layer.

The data presented herein form a coherent series of experiments providing novel data to the field of tracheal tissue engineering which address important GMP issues such as in-process acceptance criteria for scaffolds and data to support the rationale of autologous MSC seeding prior to implantation. These results allowed us to manufacture an improved clinical product for a compassionate case.

Impact statement

The data and observations generated from this thesis have gone some way towards enhancing our understanding of cell scaffold interactions and provided insights to help improve the manufacturing process. I have devised a reliable and cost-effective method for assessing circumferential mechanical stability of DC tracheal scaffolds based on DMA analysis of the viscoelastic properties of tracheal cartilage. Moreover, my data provided clues to improve recellularisation of scaffolds, as they suggested that the maintenance of an adventitial layer allows better cell attachment and enhanced physiological responses. Furthermore, to the best of our knowledge, I managed to present the first differential gene expression data of MSCs seeded onto DC tracheal scaffolds, these data were lacking since the beginning of the field in 2004. Our data will provide a foundation for subsequent studies to improve and optimise the current tracheal bioengineering approaches.

Also, my work in this thesis has had an impact outside the originally intended framework. Data generated from chapters 3, 4 and 6 have been submitted to the Medicines and Healthcare products Regulatory Agency (MHRA), UK to support two investigational medicinal product dossiers (IMPD), which have consequently resulted in:

1- The modification of the previous GMP-compliant process for the manufacture of long circumferential tissue engineered tracheal graft to an improved process which was used in a compassionate case with successful long-term outcome. The case was a 4-year paediatric patient who had a trachea-oesophageal fistula from swallowing a button battery (MHRA/MIA (IMP)11149). The tissue engineered implant engrafted without stent and has sustained her without any adverse incidents and without continued medial or surgical interventions for over three years.

2- A recent submission for the award of clinical trial authorisation in collaboration with Videregen Ltd and the Cell & Gene Therapy Catapult for the manufacture of tissue engineered tracheal patch grafts for Bronchopleural fistula (BPF), which is a life-threatening complication of pulmonary surgery that is associated with high mortality rates (up to 50%).

Overall the data generated from these cases will help provide a valuable insight and understanding of the safety and efficacy of this advanced tracheal tissue engineering therapeutic approach. Furthermore, the data generated from the trial in the manufacturing of the tracheal patch grafts might ultimately lead to the award of marketing authorisation for these tissue-engineered grafts, hence providing a solution for an unmet clinical need.

Dedication

This thesis is dedicated to my beloved parents; **Awatif AL-Hemaida** , my late father **Khamis Al-Belushi**. Thank you for your endless love, support, prayers, guidance, sacrifice, and everything you have done to give me a great life. Thank you for teaching me how to be strong, confident, compassionate, creative and how to strive for excellence. You are the secret of my success and the love of my life.

إلى والدي الحبيبين سر نجاحي ونور حياتي

لا حبيبا مثل أبي ولا قلبا مثل قلب أمي ولو بحثت دهرا

Acknowledgements

First and foremost, I would like to thank my beloved **GOD (Allah the Al mighty**) for giving me insight, strength, resilience and magic to sail through my PHD. I know I was naughty but thank you for your patience and support, I love it when you always reply to me and especially when you talk to me.

I am also extremely grateful to my supervisor **Professor Mark Lowdell** for believing in me and welcoming me in his facility. I am very indebted to him for his constant encouragement, valuable guidance, patience and the unforgettable fun and kind feelings throughout the course of my PHD. I am also very thankful to him for his inspiration and the experience I have gained in the world of translational medicine during my time in his facility, the Centre of Cell, Gene and Tissue Therapeutics CCGTT, Royal free hospital.

I am also very thankful to everyone in Prof. Mark Lowdell's research group and the Royal Free Hospital CCGTT team. Angela Tait thank you for your continues encouragement and the great time we spent discussing girls' stuff, culture and fashion. I am also very thankful to Faheem Gourbandi, for his brotherly support during the difficult times. Great thanks to Mr. John Yaxley for his help in all formal issues that I hated to do. I am very thankful to, Dr. Simin Li and Lorenzo Zani from Loughborough University, Wolfson School of Mechanical, Electrical and Manufacturing Engineering, for their help in DMA biomechanical analysis. Mark Turmaine for his help in SEM imaging, Alan Greig for his help in Multiphoton imaging and Stephen Henderson for his help in heat maps generation.

Special thanks for my friends, Maha, Safa, Amna, Wijdan and Mervat, thank you for your support, we shared great moments, we laughed, we cried, we complained a lot, and ended up shopping a lot more !

I am tremendously grateful for my beloved family, **MAMA, BABA**, my brothers and sisters :**Yousef, Kholoud, Maryam, Najat and Mohammad**, Thank you for your love, support, encouragement and inspiration. You are my treasure in this life and the most precious blessing from GOD.

This work was supported by our beloved father His **Majesty Sultan Qaboos bin Said**, Sultan of Oman special grant scheme through the Ministry of higher education and Ministry of Health. I am extremely grateful to him to grant me this opportunity to finish my higher education. May Allah bless his soul.

List of contents

List of figures

List of tables

List of Abbreviations

α-MEM	Alpha minimum essential medium
μCT	Micro computed tomography
μl	Microliter
μm	Micrometre
μg	Microgram
3D	Three dimensional
ACAN	Aggrecan
ADAM10	ADAM Metallopeptidase Domain 10
ADAM19	ADAM Metallopeptidase Domain 19
ADAM1A	ADAM Metallopeptidase Domain 1A
ADAM8	ADAM Metallopeptidase Domain 8
ADAM9	ADAM Metallopeptidase Domain 9
ADAMs	Adamalysins
ADAMTS	Proteinases with thrombospindin type-I-like repeats
ADAMTS15	ADAM Metallopeptidase With Thrombospondin Type 1 Motif 15
ADAMTS5	ADAM Metallopeptidase With Thrombospondin Type 1 Motif 5
ADM	Adrenomedullin
ALP	alkaline phosphatase
ANGPTL4	Angiopoietin Like 4
ANLN	Anillin Actin Binding Protein
ASCs	Adipose-derived stem cells
ASMCs	Airway smooth muscle cells
ATMPs	Advanced therapeutic medicinal products
AUC	Area under the curve
BABB	Benzyl alcohol: benzyl benzoate
BCL2A1	BCL2 Related Protein A1
bFGF	Basic fibroblast growth factor
BH	Benjamini-Hochberg
BM-MSCs	Bone marrow mesenchymal stromal cells
BMP1	Bone Morphogenetic Protein 1
BMP2	Bone Morphogenic protein-2

BMP4	Bone Morphogenic Protein 4
bp	Base pair
BSA	Bovine serum albumin
BSC	Biological safety cabinet
C11orf96	Chromosome 11 Open Reading Frame 96
C2CD4A	C2 Calcium Dependent Domain Containing 4A
C7orf69	Chromosome 7 Open Reading Frame 69
$CaCl_2$	Calcium chloride
CAM	Chicken chorioallantoic membrane
CCGTT	Centre for cell gene and tissue therapeutics
CCL2	C-C Motif Chemokine Ligand 2
CCL20	C-C Motif Chemokine Ligand 20
CCL7	C-C Motif Chemokine Ligand 7
CCNE2	Cyclin E2
CD	Cluster of differentiation
CFD	Computer Fluid Dynamics
CHI3L1	Chitinase 3 Like 1
CI	Confidence interval
CLEC18B	C-Type Lectin Domain Family 18 Member B
CNTN1	Contactin1
COL10A1	Collagen Type X Alpha 1 Chain
COL14A1	Collagen Type XIV Alpha 1 Chain
COL15A1	Collagen Type XV Alpha 1 Chain
COL18A1	Collagen Type XVIII Alpha 1 Chain
COL1A1	Collagen type I alpha 1 chain
COL24A1	Collagen Type XXIV Alpha 1 Chain
COL27A1	Collagen Type XXVII Alpha 1 Chain
COL6A1	Collagen Type VI Alpha 1 Chain
COL6A2	Collagen Type VI Alpha 2 Chain
COL7A1	Collagen Type VII Alpha 1 Chain
CSE	Cell seeding efficiency
CSE	Cell seeding efficiency
CSF2	Colony Stimulating Factor 2

CSF3	Colony Stimulating Factor 3
CT scanner	Computed tomography scanner
CXCL1	C-X-C Motif Chemokine Ligand 1
CXCL12	C-X-C Motif Chemokine Ligand 12
CXCL2	C-X-C Motif Chemokine Ligand 2
CXCL3	C-X-C Motif Chemokine Ligand 3
CXCL5	C-X-C Motif Chemokine Ligand 5
CXCL6	C-X-C Motif Chemokine Ligand 6
CXCL8	C-X-C Motif Chemokine Ligand 8
DAMPs	Damage associated molecular patterns
DAPI	4′, 6-diamidino-2-phenylindole
DC	Decellularised
DEGs	Differentially expressed genes
DEM	Detergent enzymatic method
DMA	Dynamic mechanical analysis
DMSO	Dimethyl sulfoxide
DNA	Deoxyribonucleic acid
DNases	Deoxyribonucleases
DOE	Design of experiments
DPBS	Dulbecco's Phosphate Buffered Saline
DPT	Dermatopontin
dsDNA	Double stranded Deoxyribonucleic acid
E.U.	European Union
E2F2	E2F Transcription Factor 2
ECM	Extracellular matrix
Ed	External diameter
EGF	Epidermal growth factor
eGFP	Enhanced green fluorescent protein
EHF	Epithelium-Specific Ets Transcription Factor 3
EIF2	*Eukaryotic Initiation Factor 2*
ELN	Elastin
ESCO2	Establishment Of Sister Chromatid Cohesion N-Acetyltransferase 2

EthD-1	Ethidium homodimer-1
EXO1	Exonuclease 1
FAM111B	Family With Sequence Similarity 111 Member B
FAM111B	Family With Sequence Similarity 111 Member B
FBS	Foetal bovine serum
FDA	Food and drug administration
FEA	Finite Element Analysis
FGF1	Fibroblast Growth Factor 1
FGF10	Fibroblast growth factor 10
FGF11	Fibroblast Growth Factor 11
FGF18	Fibroblast Growth Factor 18
FGF2	Fibroblast Growth Factor 2
FGF5	Fibroblast Growth Factor 5
FGF7	Fibroblast Growth Factor 7
FISH	Fluorescence in situ hybridization
FMO	Fluorescent minus one
G-CSF	Granulocyte colony stimulating growth factor
GAGs	Glycosaminoglycans
GDF15	Growth Differentiation Factor 15
GDNF	Glial cell-derived neurotrophic factor
GFBs	Gingival fibroblasts
GM-CSF	Granulocyte-Macrophage Colony Stimulating Factor
GMP	Good manufacturing practice
GO	Gene ontology
H&E	Haematoxylin and eosin
HBSS	Hanks' Balanced Salt Solution
HCL	Hydrochloric acid
HGF	Hepatocyte Growth Factor
HIF3A	Hypoxia Inducible Factor 3 Subunit Alpha
HLA	Human leukocytes antigen
HLA-A	Human leukocytes antigen, Class I, A
HLA-B	Human leukocytes antigen, Class I, B
HLA-C	Human leukocytes antigen, Class I, C

HMGB1	High Mobility Group Box 1
hrs	hours
HSA	Human serum albumin
HSD11B1	Hydroxysteroid 11-Beta Dehydrogenase 1
HSPA6	Heat Shock Protein Family A (Hsp70) Member 6
HSPA7	Heat Shock Protein Family A (Hsp70) Member 7
Hz	Hertz
I/E	Inspiration/ Expiration ratio
ICAM1	Intercellular Adhesion Molecule 1
ICAM3	Intercellular Adhesion Molecule 3
Id	Internal diameter
IGF	Insulin-like growth factor
IGF2	Insulin Like Growth Factor 2
IGFBP3	Insulin Like Growth Factor Binding Protein 3
IGFBP4	*Insulin Like Growth Factor Binding Protein 4*
IGFBP5	Insulin Like Growth Factor Binding Protein 5
IGFBP6	Insulin Like Growth Factor Binding Protein 6
IGFBP7	Insulin Like Growth Factor Binding Protein 7
IL11	Interleukin 11
IL15	Interleukin-15
IL15RA	Interleukin 15 Receptor Subunit Alpha
IL17F	Interleukin 17F
IL17RC	Interleukin 17 Receptor C
IL19	Interleukin 19
IL1A	Interleukin 1 Alpha
IL1B	Interleukin 1 Beta
IL1RN	Interleukin 1 Receptor Antagonist
IL23A	Interleukin 23 Subunit Alpha
IL24	interleukin 24
IL32	Interleukin 32
IL33	*Interleukin 33*
IL34	Interleukin 34
IL4I1	Interleukin 4 Induced 1

IL4R	*Interleukin 4 Receptor*
IL6	Interleukin 6
IL8	Interleukin 8
INF	Interferon
INFA2	Interferon Alpha 2
INFG	Interferon Gamma
IPA	Ingenuity pathway analysis
IPKB	Ingenuity pathway knowledge base
iPSC	Induced pluripotent cells
IPSCs	*Induced pluripotent stem cells*
ISCT	International Society for Cellular Therapy
K4Fe (CN)6	Potassium Ferrocyanine
KCNJ6	Potassium Voltage-Gated Channel Subfamily J Member 6
KIAA1161	Uncharacterized Family 31 Glucosidase KIAA1161
KIF20A	Kinesin Family Member 20A
kPa	Kilopascal
LIF	Leukaemia inhibitory factor
LINC00707	Long Intergenic Non-Protein Coding RNA 707
LRRTM3	Leucine Rich Repeat Transmembrane Neuronal 3
MCM10	Minichromosome Maintenance 10 Replication Initiation Factor
mg	Milligram
$MgCL_2$	Magnesium Chloride
MHC	Major histocompatibility complex
MHRA	Medicines and Healthcare products Regulatory Agency
MIR614	MicroRNA 614
miRNAs	MicroRNA
ml	Millilitre
mm	Millimetre
mm^2	Square millimetre
MMP1	Matrix metalloproteinase-1
MMP10	Matrix metalloproteinase-10
MMP12	Matrix metalloproteinase-12
MMP13	Matrix metalloproteinase-13

MMP14	Matrix metalloproteinase-14
MMP16	Matrix metalloproteinase-16
MMP2	Matrix metalloproteinase-2
MMP3	Matrix metalloproteinase-3
MMP8	Matrix metalloproteinase-8
MMPs	Metalloproteinases
MOI	Multiplicity of infection
MPa	Megapascals
MRI	*Magnetic resonance imaging*
MSCs	Mesenchymal stromal cells
MT1F	Metallothionein 1F
MT1G	Metallothionein 1G
MT1H	Metallothionein 1H
MT1JP	Metallothionein 1J
MT1M	Metallothionein 1M
MTT	4,5Pdimethylthiazol -2)-2,5Pdiphenyltetrazolium bromide
MYPN	Myopalladin
NA	Native
NaCl	*Sodium chloride*
NFKB	Nuclear Factor Kappa B Subunit 1
ng	Nanogram
NHSBT	Health Service Blood and Transplant
NK	Natural killer
nm	Nanometre
NUPR1	Nuclear Protein 1, Transcriptional Regulator
OCN	Osteocalcin
OCT	Optimum Cutting Temperature
p38 MAPK	*P38* mitogen-activated protein kinases
PAS	Periodic acid Schiff
PBS	Phosphate buffered saline
PET	Polyethylene terephthalate
PFA	Paraformaldehyde Fixative
PGA	Polyglycolic acid

PGE2	Prostaglandin E Synthase 2
pH	Potential hydrogen
PKP2	Plakophilin 2
PLCE1-AS1	PLCE1 Antisense RNA 1
PLGA	Polylactic-co-glycolic acid
POSS-PCU	Polyhydral oligomeric silsesquioxane covalently bonded to a polycarbonate (urea) urethane soft segment PCU chain
PPARG	Peroxisome Proliferator Activated Receptor Gamma
PSD	Partially surface dehydrated
PTGES	Prostaglandin E Synthase
PTPN20	Protein Tyrosine Phosphatase Non-Receptor Type 20
PU	Polyurethane
RELA	RELA Proto-Oncogene
RGCC	Regulator Of Cell Cycle
RIN	RNA Integrity Number
RN7SK	RNA Component Of 7SK Nuclear Ribonucleoprotein
RNA	Ribonucleic acid
RNAseq	RNA sequencing
RPM	Revolutions per minute
rRNA	Ribosomal Ribonucleic acid
RT-PCR	Real time polymerase chain reaction
RUNX2	Runt-related transcription factor 2
SD	Standard deviation
SDC	Sodium deoxycholate
SDF1	Stromal cell-derived factor 1
SDS	*Sodium dodecyl* sulphate
SEM	Scanning electron microscopy
sGAG	Sulphated glycosaminoglycan
SIS	Small intestinal submucosa
SLC27A2	Solute Carrier Family 27 Member 2
SOX9	SRY (Sex Determining Region Y)-Box 9
SPC24	SPC24 Component Of NDC80 Kinetochore Complex
SPC25	SPC25 Component Of NDC80 Kinetochore Complex

STC1	Stanniocalcin 1
TE	Tissue Engineering
TERM	Tissue Engineering and Regenerative Medicine
TGFβ	Transforming growth factor beta
TGFB1	Transforming Growth Factor Beta 1
TGFB2	Transforming Growth Factor Beta 2
TGFBI	Transforming growth factor beta induced
Th1	T helper 1
Th2	T helper 2
TIMP1	Metallopeptidase Inhibitor 1
TIMP2	Metallopeptidase Inhibitor 2
TIMP3	Metallopeptidase Inhibitor 3
TIMPs	Tissue inhibitors of metalloproteinases
TLR3	Toll Like Receptor 3
TNF	Tumour necrosis factor
TNFRSF11B	Tumour Necrosis Factor Receptor Superfamily, Member 11b
TNFRSF18	Tumour Necrosis Factor Receptor Superfamily Member 21
TNFRSF1B	Tumour Necrosis Factor Receptor Superfamily Member 1B
TNFRSF21	Tumour Necrosis Factor Receptor Superfamily Member 21
Treg	T regulatory cells
TREM1	Triggering Receptor Expressed On Myeloid Cells 1
TREM1	Triggering Receptor Expressed On Myeloid Cells 1
TU	Transducing Units
U.K.	United Kingdom
UC-MSCs	Umbilical cord mesenchymal stromal cells
UCL	University college London
UW	University of Wisconsin solution
VAD	Vacuum assisted detergent enzymatic decellularisation
VCAM1	Vascular Cell Adhesion Molecule 1
VEGF	Vascular endothelial growth factor
VEGFA	Vascular Endothelial Growth Factor A
VEGFB	Vascular Endothelial Growth Factor B
VEGFC	Vascular Endothelial Growth Factor C

YHWAZ	Tyrosine 3-Monooxygenase/Tryptophan 5-Monooxygenase Activation Protein Zeta
ZCCHC5	Zinc Finger CCHC Domain-Containing Protein 5
ZNF439	Zinc Finger Protein 439

1 General Introduction

1.1 Trachea anatomy and physiology

The trachea is an essential part of the respiratory system (Figure 1.1). It is a fibro-elastic cartilaginous tube that forms a conduit between the larynx and the bronchi. It facilitates air flow to the lungs as well as purifying it from foreign particles and microorganisms. The trachea develops during the fourth week of gestation from the ventral foregut epithelium forming a tracheobronchial diverticulum. Then it dilates and grows ventrocaudally branching into lung buds. Thus, the inner lining of the trachea is of endodermal origin and it continues to bifurcate by interaction with the surrounding splanchnic mesoderm that will give rise to the cartilaginous and muscle components of the trachea and the lungs. Several major signalling pathways such as fibroblast growth factor 10 (FGF10), insulin-like growth factor (IGF) and epidermal growth factor signalling pathways mediate these interactions (Brand-Saberi and Schäfer, 2014).

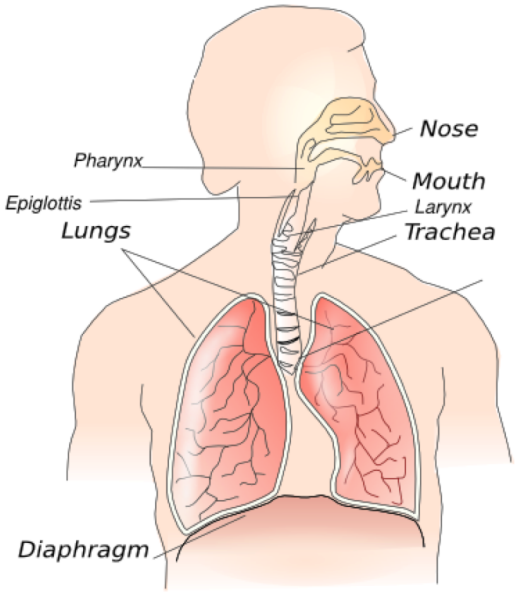

Figure 1.1: The respiratory system.
Image reproduced from (LLC, 2019)

1.1.1 General Anatomy

The trachea extends from the lower portion of the larynx starting at the cricoid cartilage at the level of the sixth cervical vertebra descending from the neck to the level of the fourth thoracic vertebra (Figure 1.2), where it bifurcates at the (carina) to the two bronchi of the lungs (Brand-Saberi and Schäfer, 2014). The level will vary during respiration, cervical flexion and extension, spinal curvature and also among individuals depending on their body build. On average the length of the trachea ranges between 10-13 cm with a coronal diameter of 2.3cm in adult males, 2cm in adult females and a sagittal diameter of 1.8cm in the adult male and 1.4 cm in adult female and approximately 1-3 mm wall thickness (Grillo, 2004).

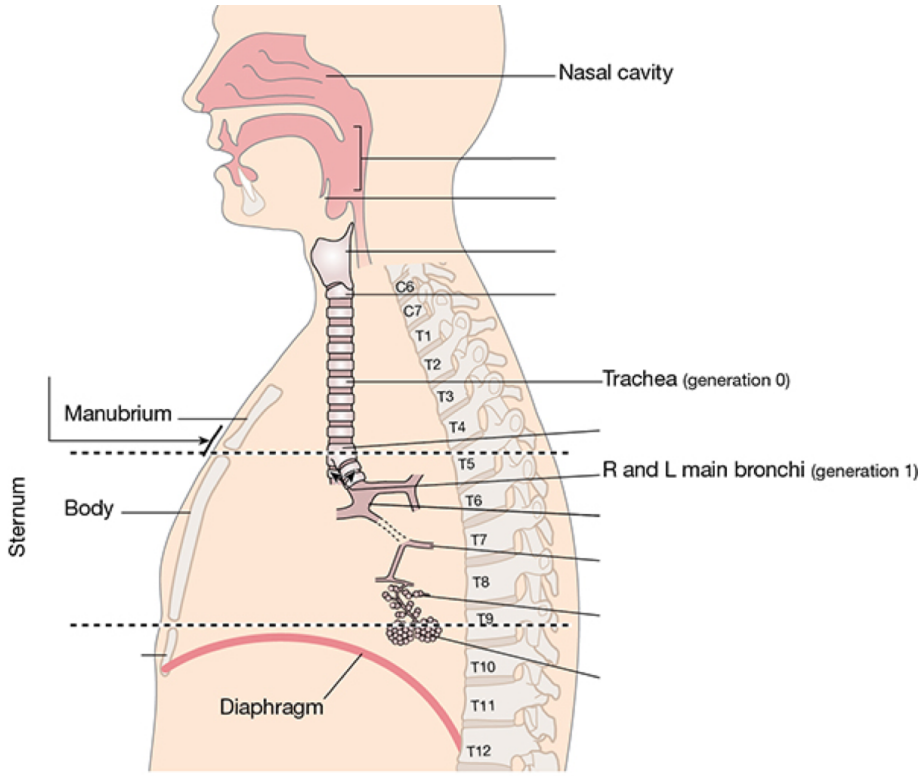

Figure 1.2: Location of trachea relative to vertebrae.

The trachea descends from the level of the sixth vertebra (C6) to the level of the fourth vertebra (C4). Image reproduced from (Ward et al., 2010).

The scaffolding of the human trachea is reinforced with 15-20 incomplete C shaped cartilaginous rings of hyaline cartilage forming the anterior and lateral circumference (Figure 1.3) (Marchant, 2005). Cartilage comprises up to two-thirds of the trachea circumference. The rings are joined posteriorly by a fibrous tissue and smooth muscle (the trachealis muscle). An intercartilaginous narrow fibrous membrane (annular ligament) connects the inferior edge of each cartilage ring to the superior edge of the cartilage below. There are approximately two cartilaginous rings per centimetre of trachea. The cartilage rings are embedded in an elastic fibrous membrane, which consist of two layers, a thicker layer that covers the outer surface of the rings and a thinner layer covering the inner surface. The two layers blend together to form a single membrane which connects the rings to one another (Furlow and Mathisen, 2018).

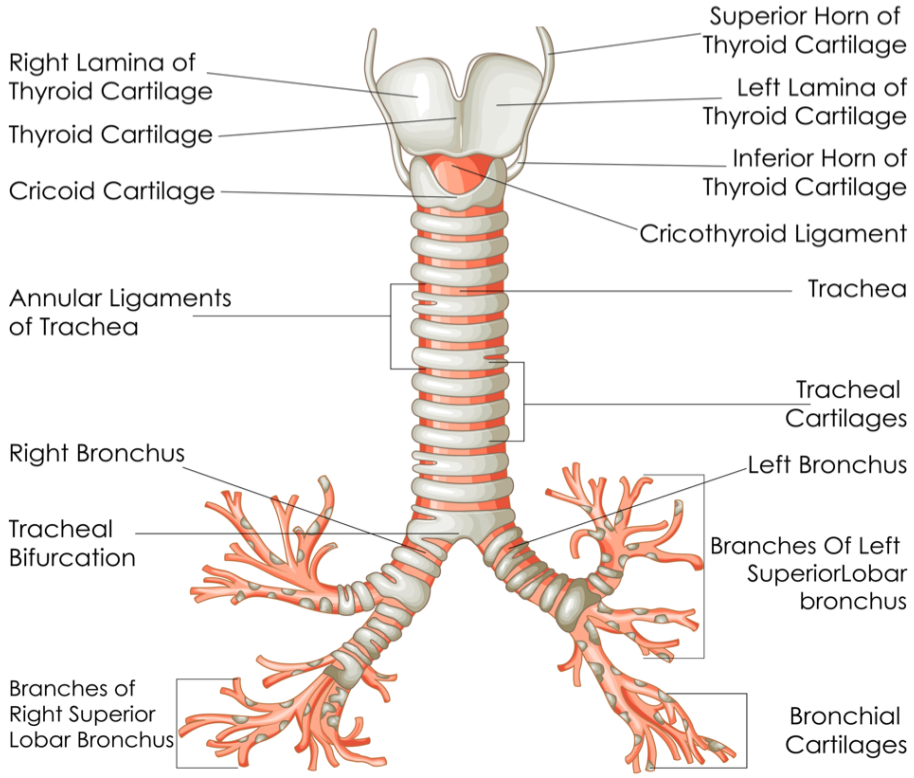

Figure 1.3: The overall structure of the trachea.

Trachea structure as a fibroelastic tube reinforced with cartilaginous rings. Image reproduced from(Shutterstock, 2019).

The cross-section shape of the tracheal lumen is circular at birth, then the lumen takes an ovoid shape as the child grows into an adult. Though, this circular shape may persist as a normal adult variant (Furlow and Mathisen, 2018). The tracheal lumen flattens at the posterior side. The trachea is covered anteriorly by the cervical fascia and the infrahyoid muscle. The oesophagus lies posteriorly to the trachea with the recurrent laryngeal nerve between them (Marchant, 2005). The thyroid lobes, carotid sheath and inferior thyroid artery lie in the lateral sides and it is crossed by the jugular venous arch and isthmus of the thyroid. In the thorax the trachea is crossed by the brachiocephalic artery and by the left brachiocephalic vein (Marchant, 2005). The tracheal wall is composed of four distinct tissue layers (Figure 1.4): (1) Respiratory mucosa (mucus membrane) covering the lumen and containing the ciliated columnar pseudostratified epithelium, (2) Submucosal layer, (3) Hyaline cartilaginous layer (4) adventitial layer which is the outermost connective tissue layer. Details of the composition and microstructure of these different layers are described in the following section.

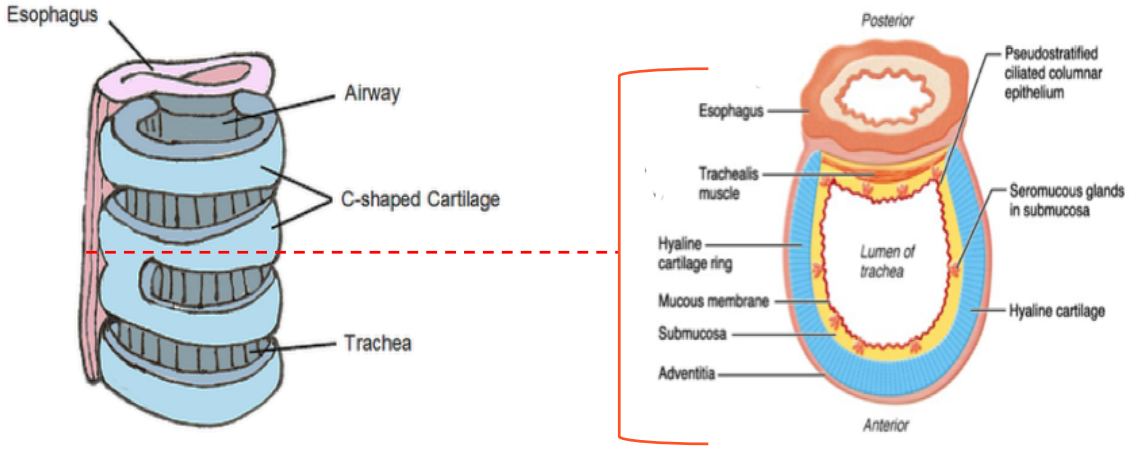

Figure 1.4: Cross sectional view of trachea and oesophagus.

Schematic showing an overview of the main tissue layers comprising the tracheal wall. Image modified from (Player, 2019, Blendspace, 2019)

1.1.1.1 Microstructure of the trachea

The tracheal lumen is lined with a specialised respiratory mucosa that forms an effective barrier which reduces the inhalation of any harmful particulates' agents in to the lung. It consists of a ciliated columnar pseudostratified epithelium, mucus secretory (goblet) cells, neuroendocrine cells, brush cells and basal cells, all resting on a well-defined basement membrane (Brand-Saberi and Schäfer, 2014). There are typically 250 cilia per ciliated cell in the epithelium, they beat in a coordinated manner away from the lungs (1,300 times /minutes) to remove noxious particulates that are trapped by the mucus away from the lungs (Martin, 1988). The function of the neuroendocrine cells is still debatable but they are suggested to act as chemosensory cells. The brush cells display apical microvilli and function as sensory cells controlling breathing and diameter of trachea (Brand-Saberi and Schäfer, 2014). A subpopulation of the basal cells is characterised as stem/progenitor cells that can develop to ciliated cells or goblet cells in response to injury to replace the sloughed or injured surface. Under the epithelium there is a loose connective tissue layer (lamina propria) which contain blood vessels, elastic connective tissue fibers and where various cells can migrate into and out of the blood stream like dendritic cells and mast cells (Martin, 1988). Below this is the submucosal layer comprised of a loose meshwork of connective tissues that contain nerves, large blood vessels, and numerous mucus glands (Seromucinous glands) that have their ducts extending and opening to the surface (Minnich and Mathisen, 2007). These glands produce considerable volumes of mucus to lubricate the inner surface of the trachea and they are found abundantly exterior to the trachealis muscle. Earlier reports have described presence of stem /progenitor cells in the seromuncinous glands (Martin, 1988).

Then below this lies the perichondrium, which is a dense fibrous porous tissue which wraps around the cartilage layer and facilitate nourishment of the cartilage. Several studies showed that perichondrium has limited regenerative potential because it contains stem/ progenitor cells that have chondrogenic potentials (Yoon et al., 2013, Wiggenhauser et al., 2017). Below this layer is the cartilaginous layer, which is a hyaline type cartilage with many chondrocytes encapsulated in their lacunas. Then covering the cartilage from outside is the adventitial layer. The tracheal adventitia is divided in to two layers an outer loose and an inner dense fibrous layer (Ohkimoto et al., 1997). The schematic bellow shows the main micro- components of the tracheal wall (Figure 1.5)

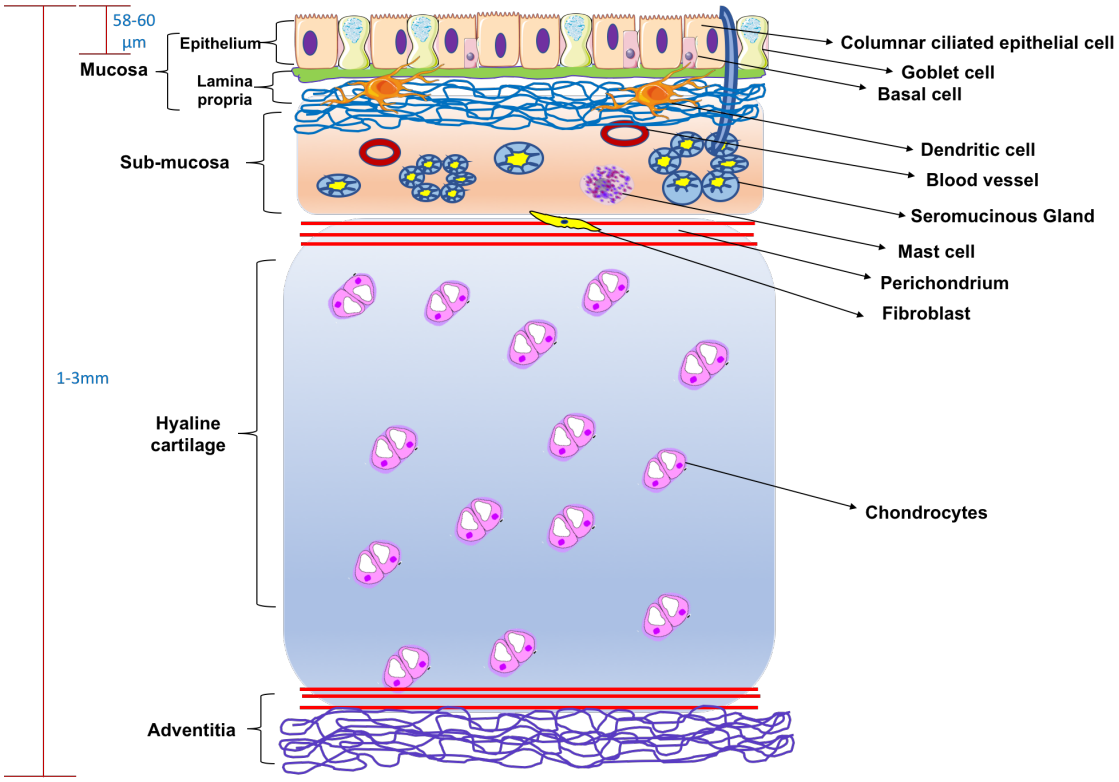

Figure 1.5: schematic showing the microstructure of the trachea.
Diagram shows various tissue layers in the trachea and the main cellular components of the: mucosa, submucosa, hyaline cartilage, and adventitia.

1.1.1.2 Trachea blood supply

The blood supply of the trachea is a unique intricate network that is difficult to reconstruct (Figure 1.6). The upper section of the trachea (cervical) is supplied by the tracheoesophageal branches (first, second and third tracheoesophageal branches) of the inferior thyroid arteries and the lower part of the trachea (thoracic) is supplied by the bronchial arteries (superior, middle and inferior bronchial arteries) that arise directly from the aorta (Furlow and Mathisen, 2018). The arteries are feeding the trachea by approaching it laterally and vascularising the trachea in a segmental pattern along its longitudinal access. The arteries branch superiorly and inferiorly forming anastomoses with the segmental arteries above and below. The tracheal arteries run within the intercartilaginous ligament (annular ligament) and branch again travelling circumferentially within the tracheal wall forming anastomoses with the corresponding arteries from the contralateral side (Furlow and Mathisen, 2018). This network feeds the submucosal capillaries found beneath the endotracheal mucosa and the tracheal cartilage receives its nourishment from the capillary bed by diffusion (Salassa et al., 1977) .The blood supply of the posterior membrane of the trachea comes from the oesophageal arteries and their branches. The vagus, and the recurrent laryngeal nerve innervates the trachea for pain and secretomotor functions and from the sympathetic nerves to blood vessels and smooth muscle (Fishman et al., 2014b).

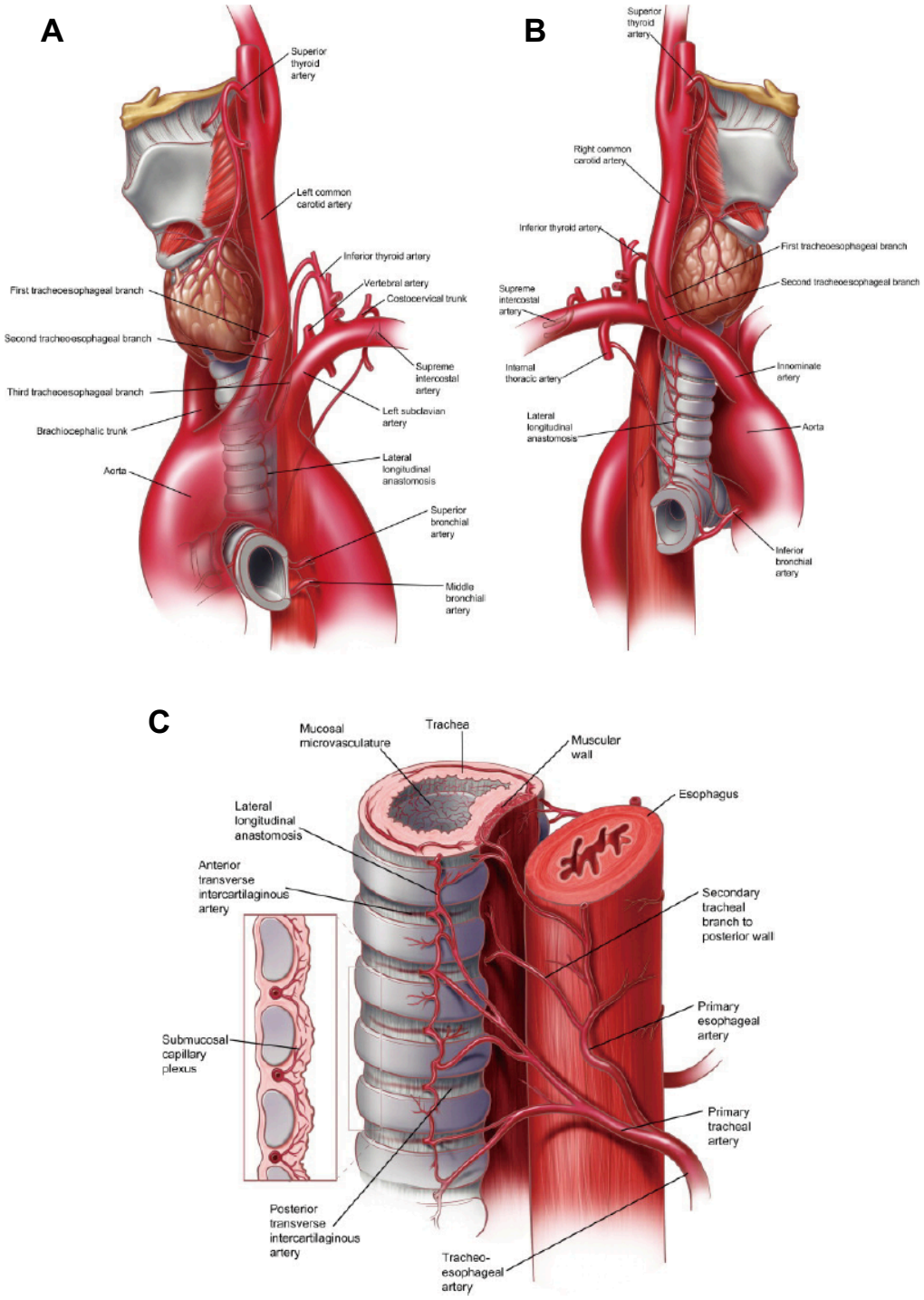

Figure 1.6: Blood supply of the trachea.

Left anterior oblique view (A), right anterior oblique view (B), (C) segmental blood supply of the trachea and relationship to oesophagus. Images reproduced from (Furlow and Mathisen, 2018)

1.1.2 Trachea physiological functions

The trachea physiological functions by far exceeds simple conduction of air between larynx and the lungs. It serves two main functions, a mechanical role (structural) maintaining a patent airway despite of inter-thoracic pressure generated by respiration to facilitate airflow and an immunologic role keeping the lung sterile and trapping pathogens going through the airway by mucociliary escalator system. A detailed description of these functions is described below:

1.1.2.1 Maintenance of a patent airway to facilitate air flow

The trachea is the proximal part of the respiratory system conducting zone acting as a patent conduit to allow air transport as well as air conditioning to the lungs. Air transport is dependant in the inner diameter of the trachea. During inspiration and expiration, the pressure gradient generated between the atmospheric pressure and pressure in the alveoli is necessary to produce air flow to the lung (Fiel, 1992). This pressure gradient is directly affected by the resistance caused by friction of air on the airway wall (Fiel, 1992). The resistance to flow is inversely proportional to inner radius of the trachea raised to the fourth power as represented by the Hagen-Poiseuille law when the flow is laminar (Brand-Saberi and Schäfer, 2014). The resistance will increase at higher flow rates when the airflow is turbulent. Therefore, conditions that reduces the inner diameter of the trachea such as: mucosal swelling, tumours and constriction of airway muscles will substantially increase the resistance to airflow (Brand-Saberi and Schäfer, 2014). It has been estimated that a 50% reduction in the diameter of the trachea will cause a 16-fold increase in resistance if the flow is laminar and 32-fold with turbulent airflow (Epstein, 2005). In addition to that the resistance will also affect the tracheal compliance, which is a measure of tracheal expansibility during breathing (Fiel, 1992). Furthermore, during breathing the inspired air will be conditioned by warming to 37^{o}C and also humidification to avoid dehydration and cooling of the sensitive lung tissue (Fiel, 1992, Kandjov, 2001).

Hence mechanically the trachea is finely tuned for its intended function with its anisotropic structural combination of fibrous annular ligaments, cartilaginous rings and trachealis muscle that makes it longitudinally flexible enabling mobility of the head and circumferentially stiff to resist collapse. On which the tracheal rings are responsible for maintaining the open airway, while trachealis muscle and annular ligaments allows for changes in the diameter and length (Bouhuys, 1977). Therefore, these principle components will define the overall mechanical behaviour and any change in their mechanical properties will negatively affect the flow in the airway and will compromise the biological function (Malvè et al., 2011, Trabelsi et al., 2010). The trachea undergoes significant deformation during breathing, sneezing and coughing, where muscle contraction or expansion and interthoracic pressure leads to cartilage rings bending and thus modulating the diameter of the airway to regulate air flow (Malvè et al., 2011).

The mechanical properties of the cartilaginous rings are attributed to its hyaline matrix composition of collagen fibers predominately collagen II, as well as other types of collagen like: III, V, VI and collagen X. The collagen fibers entraps large aggregate of hydrophilic proteoglycans. The predominant proteoglycan in hyaline cartilage is aggrecan, which consist of a protein core and keratin sulphate glycosaminoglycan GAGs chains which interact with hyaluronic acid. The highly negatively charged proteoglycan contents attracts large volume of water (60-85%) and dissolved electrolytes generating an osmotic swelling pressure that is balanced by tension in the collagen fibers (Schulz and Bader, 2007, Boazak and Auguste, 2018) . The functional coupling of this hydrated matrix gives the tissue its resilient properties (Roberts et al., 1997). On which tensile properties are governed by the collagen fibers, while proteoglycans engenders the cartilage compressive properties (Knudson and Knudson, 2001). During breathing the tracheal rings are loaded in a way that generates tensile loads in the outer regions of the rings and compressive loads on the core of the rings. Therefore, the tracheal cartilage is described mechanically by being a biphasic, non-linear viscoelastic material that shows higher strength in compression compared to tension (Teng et al., 2009b, Boazak and Auguste, 2018).

The trachealis muscle is a highly cellular tissue and is considered as the active component of the trachea (Teng et al., 2012). The contraction of the muscle regulate trachea diameter and enhances maximum airflow during breathing (Macklem and Mead, 1968). The deformation ability of the trachealis muscle compared to tracheal rings contribute significantly to tracheal compliance (Boazak and Auguste, 2018). Mechanically It is considered a non-linear reinforced hyperplastic material with two orthogonal collagen fibers, this orientation allow the muscle to support longitudinal tissue deformation during swallowing, while the transverse fibers support deformation in the circumferential direction (Trabelsi et al., 2010). The annular ligament facilitate the longitudinal flexibility of the trachea; however, no studies are available that directly assessed their matrix components and also their mechanical characterisation is challenging due to their short inter-length (Boazak and Auguste, 2018).

1.1.2.2 Protective barrier functions of trachea against inspired debris and aspirated microorganism.

The second most important function of the trachea is forming a protective barrier against inspired noxious materials and germs. The Goblet cells and submucosal mucus glands continuously secrete mucus that lines the respiratory epithelium forming a mechanical barrier of approximately of 10-20μm thickness (Martin, 1988). These secretions are controlled by the autonomic nervous system and are modulated by many inflammatory mediators (Brand-Saberi and Schäfer, 2014). The mucous secretions consist generally of two layers: a less viscous sol layer lining the epithelium to allow the ciliary beating, and a top gel layer that entraps particulates substances and germs (Martin, 1988). The process of mucociliary clearance is a highly regulated mechanical process coordinated by cilia beating and airflow during expiration (Brand-Saberi and Schäfer, 2014). On which epithelial cells cilia beat at a rate of 1300 times/ minute in the sol layer with their tips hitting the bottom of the gel layer, thus propelling mucus with its trapped debris and microorganism away from the lungs towards the epiglottis to be expectorated or swallowed (Martin, 1988).

Also, during coughing, the tracheal lumen narrows increasing the velocity of the airflow, and this helps dislodge mucus and trapped foreign particles. It is estimated that a whole new layer of mucus covers the trachea every 30 to 60 minutes (Martin, 1988). This mucus lining of the trachea also prevents excessive loss of water during air humidification. Dry air can increase mucus viscosity and hence impeding clearance of mucus by ciliated epithelium (Martin, 1988). In addition to that the system will be more prone to infection because the trapped microorganisms can penetrate the underlying cells (Martin, 1988).

1.2 Indications for tracheal replacement

Many pathological conditions can cause significant tracheal lesions that require resection and reconstruction. The disease aetiologies vary from congenital malformation such as congenital tracheal stenosis and tracheomalacia to acquired lesions secondarily to post traumatic injuries, tumours, infections, chronic airway inflammation and post intubation stenosis (Fishman et al., 2014b, Hong et al., 2012, Kojima and Vacanti, 2014). Generally, most tracheal lesions can be resected and reconstructed with primary end-to-end anastomosis and rarely require whole organ replacement like pathologies of other organs such as blood vessels, lung, and liver (Udelsman et al., 2018). In some other cases core out granulation tissue, bronchoscopic dilation, and laser therapy are employed (Ghorbani et al., 2017). However, there remains a rare subset of patients with extensive disease conditions presenting with long segment tracheal lesions (more than 50% of adult tracheal length and more than 30% of the paediatric tracheal length) with complexities that preclude conventional reconstruction methods (Chiang et al., 2016, Maughan et al., 2017). In these cases, conventional management ways using end-to-end anastomosis will lead to high level of mechanical tension in the anastomotic joints causing severe and fatal post operation complications (Mulliken and Grillo, 1968). These cases are devastating life-threatening conditions necessitating replacements of the long defected tracheal segment. The replacement of trachea remains one of the most difficult and vital procedures in ortholaryngology/ head and neck surgery.

1.3 Requirements of an ideal tracheal substitute

Many authors have outlined the desirable characteristics required for an ideal tracheal replacement (Belsey, 1950, Ott et al., 2011, Grillo, 2002, Neville et al., 1990). The prerequisites included maintenance of adequate structural and mechanical compatibility by displaying lateral rigidity and longitudinal flexibility. Moreover, it must provide air tight lumen and must be non-toxic, biocompatible, non-immunogenic, non-carcinogenic with the ability to integrate with the surrounding tissue without causing chronic inflammation and granulation tissue. Also, it must not dislocate or erode with time and must avoid accumulation of secretions and to be impervious to bacterial colonization. In addition to that tracheal replacement should permit resurfacing and growth of the epithelium. Although some authors have highlighted that, having an intact epithelial lining might not be strictly necessary if the patients maintained an effective cough mechanism (Etienne et al., 2018).

1.4 Therapeutic approaches for tracheal replacement

The pursuit for an ideal tracheal replacement has been directed toward the development of tracheal replacements that can comply with the above criteria and are able to maintain consistent and predictable long-term functions necessary for survival. Several approaches are being developed to aid the creation of tracheal substitutes. Each of these approaches has its own advantages and limitations. A brief description of the main approaches is described below:

1.4.1 Synthetic stents and prosthesis

Many types of materials have been used to manufacture stents such as silicon, Teflon, vitallium, glass, polyethylene, Avalon, and poly (vinyl alcohol). However, the most common are silicon and metal-based stents. With regards to prosthesis, there are two main types of prosthesis that have been described, solid prosthesis and porous prosthesis (Etienne et al., 2018). The main advantage of this approach is the readily availability of these devices.

Nevertheless, there are many disadvantages mainly associated with lack of biocompatibility, increase risk of granulation, obstruction, erosion, infection, lack of epithelial coverage and poor mechanical properties. All leading to high rate morbidity and mortality (Etienne et al., 2018, Ghorbani et al., 2017). For example, when considering solid prosthesis, a clinical trial by Neville *et al*. using Neville prosthesis which are (silicon rubber prosthesis with non- terminal Dacron ring) have reported high rate mortality of prosthesis-related complications and development of suture-line granulomas. Therefore, solid prosthesis is not considered a long term viable tracheal substitute. Hence the porous prosthesis were developed to counter problems of solid prosthesis and had an advantage of allowing ingrowth and incorporation of connective tissue and epithelial cells due to the porous nature of the devices. Although some studies showed improved epithelisation and incorporation, other studies still reported overgrowth of scar tissue, obstruction, stenosis, subsequent infection and poor mechanical properties (Ghorbani et al., 2017). Recent advances on stents and prosthesis involved fabrication of hybrid prosthesis by addition of biological biocompatible materials like collagen and Dacron (Sato et al., 2010).

1.4.2 Non-viable tissues

This approach involves pre-treatment of cadaveric trachea, aorta, and other tissues with freezing, lyophilization or chemical fixation to reduce antigenicity and improve biocompatibility. Few studies have used this approach (Ghorbani et al., 2017) and have reported drawbacks related to granulation, scar formation as well as poor biomechanical properties requiring permanent stenting (Grillo and McKhann, 1964, Grillo, 2002, Agathos et al., 2010, Elliott et al., 1996). However, with the introduction of bioengineering this approach has been modified to be used as bio-scaffolds for bioengineering applications (Ghorbani et al., 2017).

1.4.3 Autogenous tissues

This approach involves using autologous tissues such as : pulmonary, omentum, fascia, skin, forearm flaps, pleura, and synovial membranes which can be tubularised in to a tracheal segment. Still, they require support with prosthesis (Udelsman et al., 2018). Another modification of this approach involves fabricating a composite autogenous graft, where the patient's own rib or costal cartilage struts are fashioned and used to reinforce the tissue (Figure 1.7) (Etienne et al., 2018, Ghorbani et al., 2017). The main advantage of this approach is biocompatibility and the vascular autonomy of the tissue that could help improve healing (Etienne et al., 2018). However major drawbacks of this approach include the surgical procedure risk during harvesting of the autogenous tissue and the lack of epithelium that leads to loss of mucociliary escalator functions (Etienne et al., 2018). Furthermore, the need for stents for mechanical support (Udelsman et al., 2018).

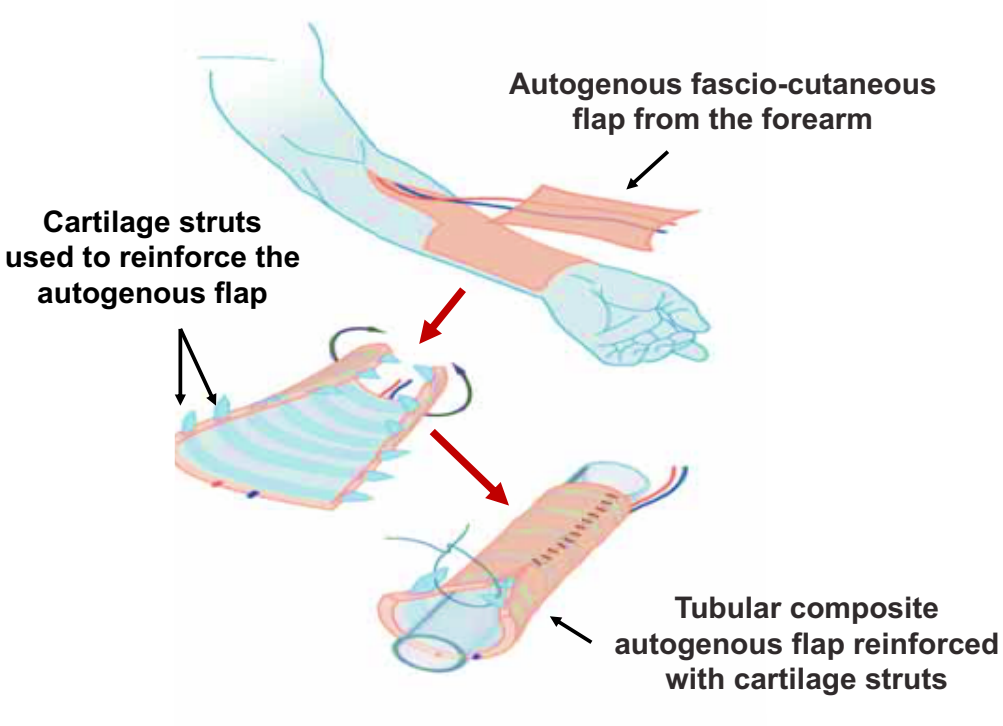

Figure 1.7: schematic of the fabrication of a composite autogenous tracheal replacement.

Image modified from(Etienne et al., 2018)

1.4.4 Aortic allografts

This approach involves tracheal replacement using fresh or cryopreserved aortic grafts. The advantages of this approach are in the potential off-shelf availability and the lack of the need for immunosuppression. But the downsides are lack of lateral rigidity and the requirement for stents to prevent malacia as well as the lack of the respiratory epithelium (Udelsman et al., 2018). The largest clinical study was reported by Wurtz *et al*. for six patients using fresh and cryopreserved aortic grafts. The results showed high morbidity and stents could not be withdrawn due to lack of stiffness, absence of epithelium and no cartilage regeneration as well as inflammatory infiltration (Wurtz et al., 2010). These results were not in line with the reported pre-clinical animal studies that showed neo-cartilage formation and restoration of the epithelium (Seguin et al., 2009). In addition to that, other downsides reported include: contraction, calcification of the aortic graft and lack of vascularisation (Ghorbani et al., 2017, Etienne et al., 2018).

1.4.5 Tracheal allografts

This approach involves the transplantation of allogenic trachea and requires the use of immunosuppression to avoid rejection. However, multiple studies over the last century have already concluded that the use of de-vascularised tracheal allografts is not reliable even with immunosuppression administration with only limited success seen when replacing short segment tracheal defects (Neville et al., 1976). In attempts to resolve the antigenicity of the graft, studies involved other approaches like merthiolate-treatment and cryopreservation of the allografts. The cryopreserved grafts re-epithelialised for short segments but failed over longer lengths in addition to the concerns with regards to cellular remnants that could lead to rejection (Sotres-Vega et al., 2009, Haykal et al., 2014a). The chemically treated grafts gave mixed results having high morbidity rates and requirement for stenting, repeated interventions with long term cannulation (Propst et al., 2011, Etienne et al., 2018).

The literature implies that re-vascularisation is one of the central challenges for tracheal replacement regardless of the approach used. That said the trachea as previously described has a complex blood supply with vessels of tiny diameter and segmental distribution, hence lacking an identifiable vascular pedicle that would make direct anastomosis to the recipient's vessels in the neck very challenging (Etienne et al., 2018). Therefore, to avoid the need for direct re-vascularisation, an interesting strategy was developed which is based on pre-vascularisation by wrapping the allograft in a heterotopic tissue (vascularised and perfused with identifiable vascular pedicle from the recipient (Etienne et al., 2018). This can be done as a one-step procedure like performing omentopexy of the graft (Levashov Yu et al., 1993), or as a two-step procedure by implanting the allograft initially in a heterotopic position like the sternocleidomastoid muscle, and once the trachea is perfused with the recipient vascular pedicle it will be transferred to the orthotopic position (Rose et al., 1979).

The best clinical application of this technique was reported by Delaere *et al*. who performed a two stage pre-vascularised allotransplantation in a 55-year-old patient post traumatic tracheal stenosis (Delaere et al., 2010). The allograft had been pre-vascularised by implantation heterotopically in the forearm of the recipient with immunosuppression administration (Figure 1.8). However, during the first few weeks the posterior membranous sheath had undergone avascular necrosis, therefore it was removed and replaced by recipient buccal mucosa. After 4 months the allograft had full mucosal lining comprised of chimeric patchwork of both recipient and donor cells as confirmed by FISH analysis as both donor and recipient were of different gender and the trachea was viable and vascularised. The trachea was later transferred to the orthotopic position and immunosuppression was withdrawn. But donor derived epithelium disappeared after withdrawal of immunosuppression, and no impact was noticed on the cartilage (Delaere et al., 2010). This indicate immune sensitisation and rejection of the donor derived cells. However, it is speculated that due to the physical isolation of chondrocytes in the dense avascular matrix, they were hidden from the immune system (Den Hondt and Vranckx, 2017, Sykes, 2010).

This technique was performed on 4 other patients and has shown promising variable results having an advantage of pre-vascularisation (Delaere et al., 2012). However, the main disadvantages of this approach is the lack of circumferential re-vascularisation, necrosis of the posterior wall, requirement of extended periods of immunosuppression to avoid graft rejection and this cause higher susceptibility to infection as well as the requirement of several months of heterotopic development (Udelsman et al., 2018). Nevertheless, this technique is a very promising approach for long segment tracheal replacement despite of the inherent challenges. In fact, this strategy can be considered as combined allotransplantation and tissue engineering approach as recipient cells were used to reconstruct the graft.

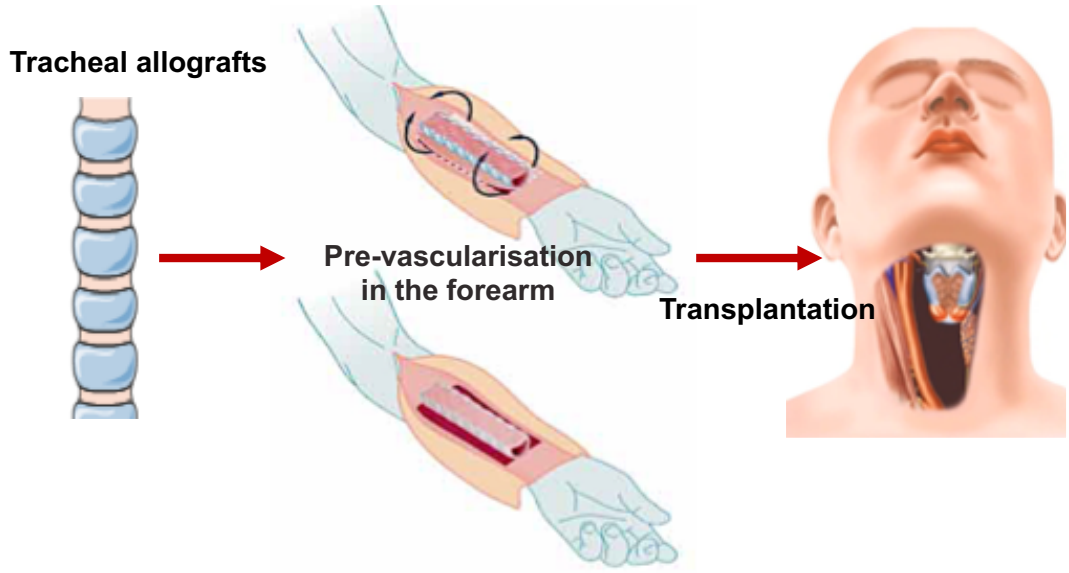

Figure 1.8: schematic of tracheal allograft pre-vascularisation in the forearm prior to implantation in the final orthotopic site.
Image modified from (Delaere et al., 2010, Etienne et al., 2018)

Overall, given the challenges, limitations, and dissatisfaction with these approaches in providing a curative replacement for end stage tracheal defects, the interest has shifted to the relatively new discipline of **Tissue Engineering and Regenerative Medicine** (TERM). Which is an interdisciplinary approach that combines the principles and methods of bioengineering, material and life sciences, transplantation and cellular therapeutics with the aim to develop biological substitutes that restore, repair, regenerate, maintain and improve biological function of a tissue or a whole organ (Langer and Vacanti, 1993). Therefore, the following sections will review the current status of tracheal tissue engineering.

1.5 Tracheal tissue engineering

1.5.1 Principles

Tissue engineering (TE) represents the most attractive promising approach to create safe and efficacious tracheal replacements that may circumvent the limitations faced by the other interventions. The basic principle of TE approach is to manufacture a customised functional biocompatible implant that mimics the native biological tissue. i.e. the creation of a functional neo-organ. Given that, the unique tissue functional characteristic and architecture is governed by the synergetic combination of cells, biochemical and physical cues in the body (Guilak et al., 2014). The basic pillars for TE strategies is based on using a biological triad of **a)** scaffolds able to mimic and maintain structural support while acting as an inductive template for tissue growth and development, **b)** cellular constituents to repopulate and support tissue growth and function, and **c)** Providing the necessary boosting biochemical and/or mechanical signals and conditions to guide cell repopulation, differentiation and neo-tissue development (Butler et al., 2008).

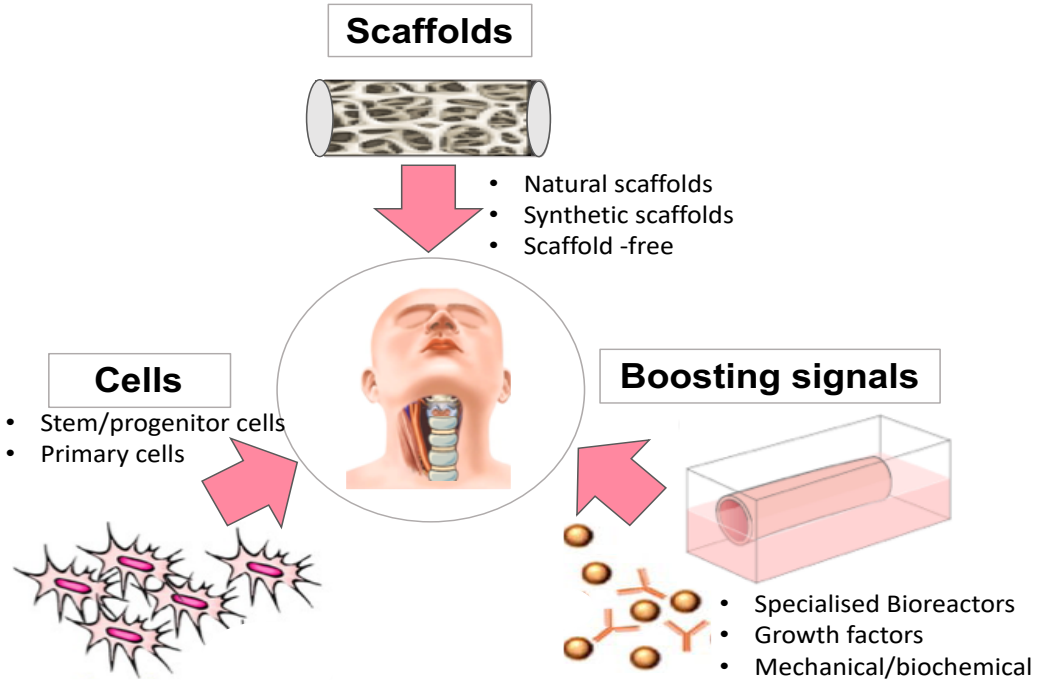

Figure 1.9: Schematic showing the classical tissue engineering design components.

1.5.2 Approaches for the creation of bioengineered tracheal grafts

Tracheal tissue engineering (TE) approaches are generally classified in to four main strategies (Fishman et al., 2014b, Chiang et al., 2016). These approaches are based on the use of either synthetic or biologic scaffolds seeded with one or more cell types. They are:

1.5.2.1 *In vitro* culture TE approach

In this strategy the cells are pre-seeded in to airway scaffold *in vitro* in specialised bioreactors with +/- bioactive or physical boosting signals (Fishman et al., 2014a). This approach allows cells attachment, expansion, and ECM deposition. In addition to that it permits co-culturing different types of cells and allows the directed differentiation with stimulating signals (Chiang et al., 2016). Yet it is a time-consuming approach that requires specialised cultivation resources and has a higher risk of contamination (Chiang et al., 2016).

1.5.2.2 *In vivo* TE (Cell-free scaffolds approach)

In this approach cell-free scaffolds are implanted in its orthotopic position with the rational of using the body as bioreactor. The aim is to activate endogenous regenerative and wound healing mechanisms (Jungebluth et al., 2012). On which stem, progenitor and other cells are recruited to facilitate tissue remodelling (Fishman et al., 2014a). This approach has an advantage of ready availability but will require a mechanically functional implant at the time of implantation (Chiang et al., 2016).

1.5.2.3 *In vivo* TE with (Perioperative cell seeding approach)

This approach is based on using the body as a bioreactor as well by implanting the scaffold in the orthotopic position, but with an additional in situ seeding of autologous cells and stem cells at the time of operation (Hori et al., 2002, Nakamura et al., 2011, Chiang et al., 2016). It also requires a mechanically functional construct at the time of operation (Chiang et al., 2016).

1.5.2.4 Ectopic TE approach

This approach is based on implanting seeded or non-seeded tracheal scaffold in an ectopic position initially to allow *in vivo* development and pre-vascularisation. It also permits the use of pedicled flap at the time of orthotopic transplant. However, it is a time-consuming approach that require 2-14 weeks for tissue development (Chiang et al., 2016, Tsao et al., 2014)

1.5.3 The onset of tracheal tissue engineering field

In 1994 the Vacanti's group have reported the first pioneering experimental tissue engineered tracheal study (Sakata et al., 1994). In their study, they have manufactured cartilage tubes of chondrocytes harvested from calves and seeded it onto synthetic nonwoven mesh of polyglycolic acid (PGA) fibers that were wrapped around silastic tubes. Then tracheal epithelial cells isolated from new-born lambs were injected into the cylindrical tubes and the constructs were implanted into subcutaneous pockets of 10 node mice. The study reported the development of an epithelial lining in four of the implanted tubes, but the rest became infected due to lack of epithelial layer (Sakata et al., 1994). The group also tested the feasibility of this method for the replacement of large circumferential tracheal defect created in nude (athymic) rats, where they have reported hyaline cartilage formation (Vacanti et al., 1994). Then Kojima and co-workers from Vacanti's group have reported the manufacturing of autologous tissue engineered cartilage constructs shaped in to helix to mimic the structural components of tracheal rings (Kojima et al., 2002). In their study they harvested and cultured fibroblasts and chondrocytes from the nasal septum and seeded them onto separates sheets of polyglycolic acid (PGA) mesh. The sheets were later formed in to tubes and implanted under sternocleidomastoid muscle prior to tracheal replacement in sheep. The study reported animal survival up to 7 days after surgery (Kojima et al., 2002). Since then many groups have designed tissue engineered constructs using a wide variety of techniques.

1.5.4 The first proof of concept clinical cases

The reconstruction of extensive tracheal lesions for patients with end stage tracheal diseases remains a major surgical and technical challenge. So, it becomes sometimes a serious and an acute threat to patient life (Weiss et al., 2014). Therefore, tracheal bioengineering has been one of the first fields in TE to witness clinical application on compassionate grounds. Several patients have been treated on compassionate basis and their reported outcomes were a landmark that created much enthusiasm and excitements as well as evoked debate for the potentials of tissue engineering in treating extensive tracheal lesions.

In 2004, Macchiarini and colleagues reported the use of a bioengineered tracheal patch to treat a tracheal defect in a 58-year-old patient who had undergone a right completion carinal pneumonectomy and radical lymphadenectomy for a relapsing lung cancer (Macchiarini et al., 2004). The bioartificial patch was manufactured by seeding autologous fibroblast and muscle cells in a collagen matrix from a decellularised porcine proximal jejunum segment. Endoscopic examination at twelve weeks post operation revealed epithelial coverage and patch integration with adjacent tissues with lack of granulation tissue or chronic inflammation (Macchiarini et al., 2004).

In 2005, Omori *et al* group in Japan have constructed a bioengineered composite graft using a tubular scaffold of porous Marlex mesh covered by a collagen sponge derived from porcine dermal atelocollagen (Omori et al., 2005). The bioartificial construct was used to repair a tracheal defect of a 78-year thyroid cancer patient. At two-month post operation epithelial growth was observed on the graft and the group reported good epithelialisation of the luminal surface without any complications after two years of operation (Omori et al., 2005).

In 2008, the ground breaking first full segmental TE tracheal replacement was reported by Macchiarini *et al*. for a 30-year-old patient presenting with end stage left-main bronchus malacia secondarily to tuberculosis (Macchiarini et al.). In this case a decellularised bronchial allotransplant of a deceased donor was repopulated *in vitro* using autologous bronchial epithelial cells and chondrocytes derived from bone marrow mesenchymal stromal cells (BM-MSCs) in an air-liquid rotating bioreactor. The recipient showed no signs of rejections two months post operation, no anti-donor HLA antibodies were detected and no immunosuppression was administrated. The development of proximal graft stenosis was reported six months post-surgery. Bronchoscopic biopsies showed evidence of recellularisation at one year and epithelialisation at two years post operation. A 5-year follow-up report demonstrated a patent graft with no stenosis at the distal bronchial anastomosis, however the patient required 16 bronchoscopies in 5 years, 14 of these required stenting (Gonfiotti et al., 2014). This case has evoked great attention from both professional groups and mass media as the first tissue engineered organ with great promises in the field of tissue engineering. Conversely it has also raged much debate, criticism and controversy particularly questioning the mechanism of how healing and regeneration would have been achieved with the lack of blood supply in the graft which challenge the current knowledge (Delaere, 2010). In addition to the lack of clear evidence of stem cells repopulation of the scaffolds and role they play in promoting tissue regeneration (Delaere, 2010). Yet the authors claimed the presence of microvasculature as measured by contact bleeding and laser-Doppler readings at 4-months post operation. They argued that endogenous angiogenesis is another means of neovascularisation and more work is needed to investigate if it is sufficient and how it can be stimulated (Macchiarini and Birchall, 2010). The authors also commented on the rationale of using undifferentiated mesenchymal stromal cells is to stimulate in situ tissue regeneration by supply of appropriate signals. They indicated that it is unclear yet how the seeded cells could have contributed to healing and warranted that data is urgently needed with regards to bioengineered constructs healing (Macchiarini and Birchall, 2010).

In 2010, Delaere *et al*. conducted a promising allotransplantation post pre-vascularisation in a patient forearm that have been described in an earlier section in details 1.4.5). It is of interest to include the case as it represent a fusion between allo-transplantation and tissue engineering principles, on which recipient buccal mucosa was used to repopulate the graft (Delaere et al., 2010).

In 2012, Elliott and colleagues published a two-year follow-up report of the first paediatric TE tracheal case for a 10-year-old boy who suffered from congenital tracheal stenosis (Elliott et al., 2012). The graft was manufactured in 2010 using a decellularised tracheal scaffold which was seeded intraoperatively with BM-MSCs and epithelial patches. In addition to that recombinant erythropoietin, transforming growth factor beta (TGFβ) and granulocytes colony stimulating growth factor (G-CSF) were administrated to encourage angiogenesis, chondrogenesis and the recruitment of progenitor cells. Authors reported angiogenesis one-week post operation evidenced by contact bleeding and laser-Doppler fluximetry as well as a strong neutrophil response in the first 8 weeks. The study also reported that the graft itself was malacic and the patient required dilation for secretions clearance, granulation removal and stenosis as well as required stenting. At 15 months, complete epithelialisation was achieved. At 6 months post operation the graft was patent and the patient returned to school and had re-gained normal lung functions. A four-year follow-up reports showed that the patient's need for intervention declined up to late 2013 and that the only major intervention was performed due to infection and stenosis within the tracheal stents. Nevertheless, the child recovered and returned to school again. (Hamilton et al., 2015). It is worth noting that debates continued with demands for more evidence with regards to mechanism of cell-scaffold interaction and tissue healing (Delaere, 2013), but the authors clearly stated that compassionate cases use evolving technologies to provides hope for patients and also help gives some clues to inform the necessary science. While little is known about how the graft integrates and maintains its function, it calls for more research work and formal trials to learn and understand cell scaffolds interactions (Birchall et al., 2013).

The first GMP (good manufacturing practice)-compliant TE tracheal graft was also operated in 2012 (Elliott et al., 2017). Following the promising outcomes of the seeded decellularised TE tracheal grafts for the adult and the paediatric patients, another compassionate case was operated for a teenage girl suffering from a critical tracheal stenosis that failed conventional reconstructive techniques. The graft was based on an allogenic decellularised tracheal scaffold that was *in vitro* seeded with expanded BM-MSCs and nasal derived epithelial cells in a specialised bioreactor. However, in this case the TE graft was manufactured to full European GMP standards, where all constituents' cells, scaffolds and the end composite graft were prepared in a fully licensed facility following validated standard protocols that had undergone extensive risk assessments and quality control before being finally approved by the United Kingdom (U.K.) Medicines and Healthcare products Regulatory Agency (MHRA). It is worth noting that scaffolds containing human cells are regulated as tissue-engineered advanced therapeutic medicinal products (ATMPs) in the European Union (E.U.) and was released for implantation as an unlicensed medicine according to predefined criteria. In this case the graft was not stented in order to preserve the seeded epithelial cells and to avoid morbidities that were associated with absorbable stent as in the previous case. The initial results were encouraging and the patient's exercise tolerance was improved. However, 3-weeks post operation the patient encountered an acute event hypothesised to be an intrathoracic bleed or an acute malacia that lead to airway obstruction and death of the patient. The authors were not able to rule out the mechanism for the acute obstruction if it was primarily a failure of the graft or due to extraluminal obstruction because patient relatives declined post-mortem retrieval of the graft. It was hypothesised that the weakening of mechanical integrity at the initial stages of implantation could be a result of tissue remodelling which might necessitate the use for stenting during the first few months of implantation. The authors also warranted that more research work is needed to address mechanical integrity of the graft pre and post implantation into relevant *in vivo* models especially that these changes were not observed in their preclinical porcine studies (Elliott et al., 2017, Go et al., 2010).

Taken as a whole and while the working mechanism and the process of *in vivo* remodelling of the tissue-engineered grafts are still not fully defined. However, the encouraging results observed have prompted active research and derived the development of bioengineering approaches by different groups in Europe and North America that have taken different routes in the investigation and optimisation of this new technology (Weiss et al., 2014). Therefore, the following sections endeavours to provide a summary of the current status of tracheal bioengineering field highlighting main concepts and themes of clinical and preclinical work as well as highlighting limitations and knowledge gaps.

1.5.5 Scaffolds options for tracheal bioengineering

Scaffolds play an essential role in the manufacturing of three-dimensional TE organs. They make the basic templates to provide important functions these are: structural and mechanical support, allowing cell attachment, proliferation and neo-tissue formation as well as facilitating vascularisation. Therefore, their composition and mechanical properties are of great importance in tracheal TE. The optimal scaffold type remains a source of debate in the field (Crapo et al., 2011). Scaffolds being developed in tracheal bioengineering can be broadly classified to three types each having its pros and cons, these are: (1) synthetic scaffolds, (2) scaffold-free biological constructs, and (3) biological scaffolds (Baiguera et al., 2010a).

1.5.5.1 Synthetic scaffolds

Synthetic scaffolds have been developed since the advent of tracheal bioengineering in many experimental models (Vacanti et al., 1994, Kojima et al., 2002). They are typically composed of a variety of modified polymers that can be combined with other biological materials. These are further divided in to non-biodegradable and degradable scaffolds (Bogan et al., 2016). Numerous options are available for example: polyglycolic acid (PGA) (Gunatillake et al., 2003), polylactic-co-glycolic acid (PLGA) (Luo et al., 2009), Polyethylene terephthalate (PET), and polyurethane (PU) (Ajalloueian et al., 2014) and Pluronic F-127 (Kamil et al., 2004).

Synthetic scaffolds have many advantages, for example: the ability to customise their size and shape to patients' specific requirements. Hence, offering a promising approach for providing customised off-the shelf scaffolds (Fishman et al., 2011). Furthermore, they offer the ability to tune and control scaffolds mechanical properties, porosity and biodegradation rate to some extent (Fishman et al., 2014a). However, several challenges are still under investigation and need to be resolved and tested before these scaffolds can be clinically translated. For example, matching the macro and micro-scaffold architecture to native tracheal tissue, immune response to synthetic scaffolds, mechanical mismatch, effect and toxicity of scaffold degradation products, vascularisation, poor incorporation with the native tissue and graft migration (Bogan et al., 2016, Fishman et al., 2014a). Moreover, studies have shown that synthetic scaffolds are inferior to biologic scaffold with regards to supporting cells attachments and growth (Lutolf and Hubbell, 2005).

It is worth mentioning that despite the high hopes, tracheal TE field was setback and in particular, the use of synthetic scaffolds for tracheal bioengineering has lost preference and evoked much more concerns as a result of scientific and ethical research misconduct. On which, the same leading scientist who pioneered the landmark first human decellularised TE tracheal constructs (Macchiarini et al., 2008) was found guilty of scientific misconduct after reporting the clinical use of artificial synthetic scaffolds made from a nanocomposite polymer POSS-PCU (Polyhedral oligomeric silsesquioxane covalently bonded to a polycarbonate (urea) urethane soft segment PCU chain) in to nine patients between 2011 and 2014.(Claesson-Welsh and Hansson, 2016, Ott and Mathisen, 2011, Frostell et al., 2017, Cyranoski, 2014, The Lancet, 2016, The, 2018, Vogel, 2013, Delaere and Van Raemdonck, 2014). Reports from internal and external investigators have confirmed lack of sufficient preclinical *in vitro* and *in vivo* animal studies that support the clinical translation of POSS-PCU for tracheal TE, moreover published reports of clinical success of these synthetic scaffolds was overstated and patients had actually developed devastating fatal complications (UCL, 2017, KI, 2016).

Nevertheless, synthetic scaffolds remain a promising research approach for tracheal bioengineering. Indeed, Chiang *et al* have conducted a comprehensive review of *in vivo* animal TE tracheal graft studies, where they have evaluated critical outcomes of the grafts. In their review they have found that while cartilage regeneration did not appear to be associated with a specific scaffold type, the bulk of progress in cartilage regeneration was mainly achieved with synthetic scaffolds (Chiang et al., 2016). In addition to that mechanical failure and stenosis was mostly associated with the use of synthetic scaffolds, yet epithelialisation was reported regardless of the scaffold type (Chiang et al., 2016). Overall this approach can take an advantages of innovative technologies such as 3D-printing, electrospinning to design smart biodegradable polymers decorated with structural or bioactive molecular cues to support remodelling and growth (Maughan et al., 2017). And this is highly desirable for paediatric patients, where scaffolds need to incorporate and grow with them (Bogan et al., 2016).

1.5.5.2 Scaffold free/biological constructs

Unlike the traditional TE strategy that relies on using a three-dimensional (3D) scaffolds, this approach is based on developing tissue like structures by taking the advantage of cells natural ability to synthesise tissues without utilising exogenous 3D materials as templates for cells seeding (Athanasiou et al., 2013). It is based on harnessing self-organisation and self-assembly techniques such as: cell sheet engineering, bioprinting, and aggregate technologies (Athanasiou et al., 2013). This approach offers an advantage of avoiding the drawbacks that are normally associated with scaffold-based approaches like immunogenicity and inflammatory response that results from introduction or degradation of foreign scaffold to the body or the potential alteration of the cells phenotype as a result of cells interactions with the underlying scaffolds (Darling and Athanasiou, 2003, Chiang et al., 2016, Ott et al., 2011). Moreover, it provides a biomimetic microenvironment allowing higher degree of cell-cell communications and hence maintaining cellular phenotype (Athanasiou et al., 2013).

However, this approach may compromise mechanical integrity and most scaffold-free approaches will need to rely on temporary stents to maintain the shape of the trachea. For example, in a study by Tani *et al*. chondrocytes sheet was wrapped around a silicon tube in a rotating bioreactor, but when removing the silicon tube the sheet maintained the tracheal tubular shape but had only one third of the elastic intensity of the native tracheal cartilage as measured by rheometer. Generally, studies in this approach focused on chondrocytes and cartilage formation (Ott et al., 2011, Dikina et al., 2015). For example, in one study by Weidenbecher *et al*, fabricated chondrocytes sheets obtained from auricular cartilage were layered with a muscle flap around a silicon tube and then allowed to mature in an ectopic position prior to implantation to treat a tracheal defect in rabbits (Weidenbecher et al., 2009). The study demonstrated cartilage formation and vascularisation but all rabbits expired between 1 and 39 days due to obstruction of the lumen with fibrous tissue and stenosis (Weidenbecher et al., 2009). Also, in another study epithelial cell-based sheets were constructed using temperature responsive dishes that were later implanted in to rabbits after a period of ectopic maturation. The study reports formation of a pseudostratified columnar epithelium on the construct lumen (Kanzaki et al., 2006). Overall, there have been few studies that have utilised this approach in tracheal bioengineering (Ott et al., 2011).

1.5.5.3 Biological scaffolds

This category represents scaffolds that are constructed or derived from natural biological sources.

1.5.5.3.1 Natural ECM derivatives

Natural ECM derivatives represent constructs that are made from derivative components of extracellular matrix (ECM) such as collagens, alginate, fibrin, and hyaluronic acid. Although these components have all proven to be cell compatible but they still possess limitations related to lack of consistencies and their structural malleability. However, several tracheal bioengineering studies have taken the advantage of these materials and attempted combining them with other materials or prosthesis to achieve better results (Ott et al., 2011). For example, the use of collagen-coated polypropylene mesh reinforced with polypropylene mesh cylinders have been extensively studied as composite prosthesis (Ott et al., 2011).

One interesting clinical study by Omori *et al* have utilised collagen-conjugated prosthesis composed of polypropylene Marlex mesh coated with collagenous sponge to replace laryngeal and tracheal tissue in four patients (Omori et al., 2008). Follow-up reports showed no signs of graft rejection and have demonstrated re-epithelisation of the grafts after three years. Other approaches involved manufacturing a cell-loaded gel to either coat the outer tracheal side or to regenerate the epithelial luminal side of the trachea (Sato et al., 2010, Tada et al., 2008, Nomoto et al., 2008). In a recent study by a collaborative group, Hamilton *et al* and colleagues have combined human epithelial/stem and progenitor cells with collagen hydrogel to make a mechanically stable epithelial sheet that was later implanted in to a pre-vascularised decellularised tracheal scaffolds in a rat model. The study demonstrated an engraftment of keratin positive cells after one week of implantation (Hamilton et al., 2019).

1.5.5.3.2 Decellularised (DC) scaffolds

1.5.5.3.2.1 Decellularisation technique

The other type of biological scaffolds that is most commonly used for tracheal TE are decellularised scaffolds. Decellularisation is a technique that uses a combination of chemical, enzymatic or physical treatments methods (agitation, sonication or pressure) to disrupt and remove cellular contents while reserving the three-dimensional (3D) architecture and the natural structural and functional ECM proteins and glycosaminoglycans composition of the treated tissues and organs (Gilbert et al., 2006, Crapo et al., 2011, Parmaksiz et al., 2016). The rationale of the decellularisation process is to produce non-immunogenic scaffolds by removing cellular components and antigens and thus eliminating the risk of inflammatory and immunological rejection of grafts.

The technique was first popularised by Badylak and colleagues in 1995 when they have decellularised porcine small intestinal submucosa (SIS) using detergents (Badylak et al., 1995, Badylak et al., 1998). Human allografts and porcine xenografts have been investigated as possible sources of scaffolds (Badylak and Gilbert, 2008). A decellularisation protocol generally involves lysis of cellular membranes using either physical methods or ionic solutions, then an enzymatic treatment to separate cellular components from the ECM, then solubilisation of cellular cytoplasmic and nuclear components using detergents and finally removal of the cellular debris from the tissue (Gilbert et al., 2006). These steps will be used in different combination and using different reagents depending on the tissue type.

Various decellularised scaffolds were developed and have been used successfully in many pre-clinical animal studies and human clinical studies without the formation of anti-HLA antibodies (Spector, 2016, Parmaksiz et al., 2016, Gilbert et al., 2006). For example, skin (Chen et al., 2004), bladder wall (Chen et al., 1999) , tendon (Cartmell and Dunn, 2000), ligament (Woods and Gratzer, 2005), adipose tissue (Flynn, 2010), vasculature (Grandi et al., 2011)

pericardium (Morticelli et al., 2013) and even whole organ like lungs (Weymann et al., 2015), kidney (Liu et al., 2015), and heart (Ott et al., 2008). In fact, there are over thirty decellularised scaffolds that are commercially available and are obtained from either human or xenogeneic sources for tissue engineering and regenerative applications (Parmaksiz et al., 2016, Badylak et al., 2009).

1.5.5.3.2.2 Advantages

The decellularised (DC) scaffolds have many advantages compared to synthetic scaffolds. For example, they circumvent the need for top-down design of the 3D macro and micro architecture as they maintain the complex natural ECM structure unique for the anatomic location. Moreover, DC scaffolds retain mechanical cues and many conserved bioactive molecular cues that support cellular attachment, ingrowth, survival, differentiation, angiogenesis, and proliferation. For example, they act as a reservoir of many structural and functional proteins like collagen types, glycosaminoglycans and growth factors such as basic fibroblast growth factor (bFGF), transforming growth factor beta (TGF-β) and vascular endothelial growth factor (VEGF) (Badylak, 2014, McDevitt et al., 2003, Parmaksiz et al., 2017). An additional advantage of DC scaffolds that they are degradable substrates that release an additional reserve of non-toxic potent bioactive (matricriptic) peptides that influence cellular behaviour resulting in a diverse array of bioprocesses like chemotaxis, angiogenesis and adhesion and recruitment of stem and progenitor cells among others (Brown and Badylak, 2014).

Moreover, DC scaffolds have been found to promote and induce site appropriate constructive tissue remodelling and hence help avoiding scar formation (Brown and Badylak, 2014). In fact, achieving functional site appropriate remodelling in response to tissue TE-construct implantation is the aim of tissue engineering paradigm. Nevertheless, the bio-inductive profile of DC scaffolds and the mechanisms by which DC scaffolds induce constructive tissue remodelling are not fully elucidated (Brown and Badylak, 2014). But a wealth of studies has demonstrated that ECM based scaffolds are able to promote and modulate host immune response towards a pro-healing response by modulating the phenotype

of the cells involved through the interaction with scaffolds surface ligands and bioactive ECM degradation products . For example, studies showed that DC scaffolds promote the switch of macrophages from the proinflammatory M1 macrophages phenotype that predominate immediately following implantation and which is normally associated chronic inflammation, encapsulation and scarring to the anti-inflammatory pro-healing M2 macrophage phenotype (Brown et al., 2009, Allman et al., 2001, Badylak et al., 2008, Brown et al., 2011). Furthermore, ECM scaffolds have been found to promote a T helper 2 (Th2) immune response which is conventionally associated with graft acceptance (Allman et al., 2001). Moreover, decellularised scaffolds promote tissue specific cell phenotypes and site-specific cell differentiation (Fishman et al., 2014a).

1.5.5.3.2.3 Disadvantages

The decellularisation process is a delicate process that needs to maintain a fine balance between eliminating antigenic components without jeopardising ECM integrity while retaining chemical and biomechanical cues necessary to support tissue regeneration. Therefore, decellularisation processing methods will have a substantial effect on the final product and every manipulation step will affect or alter ECM structure and composition to some extent. It should be stressed that it is impossible to completely eliminate cellular materials (Crapo et al., 2011). In fact, studies have already demonstrated that even commercially available decellularised products still contain residual cellular remnants (Gilbert et al., 2009, Iannotti et al., 2006).

Moreover, many studies have also demonstrated that inefficient decellularisation and the presence of residual cellular debris, residual DNA, damage associated molecular patterns (DAMPs) can adversely affect the regenerative process *in vivo* by attenuating the beneficial inductive remodelling properties of biological scaffolds promoting an adverse proinflammatory responses (Qin et al., 2010, Brown et al., 2009, Nagata et al., 2010, Brown and Badylak, 2014). Furthermore, excessive decellularisation protocols may disrupt ECM components like collagen and proteoglycans content and structure, hence compromising the overall mechanical properties of the obtained ECM scaffold (Sun et al., 2018, Kawecki et al., 2018). It is worth noting that decellularised scaffolds are FDA classified as

medical devices, but no standard quality criteria are established yet. Nevertheless, a minimum quantitative criteria for decellularisation has been proposed by Crapo *et al* based on a review of studies where constructive remodelling have been observed *in vivo* and adverse host response have been avoided (Crapo et al., 2011). These criteria were recently updated by Kawecki *et al* and the full list is displayed in (Table 1.1) below (Kawecki et al., 2018).

Table 1.1: Minimum criteria for efficient decellularisation

Minimum criteria to satisfy the intent of decellularisation (Kawecki et al., 2018, Crapo et al., 2011)
• **<50 ng dsDNA per mg ECM dry weight**
• **<200 bp(base pair) DNA fragment length**
• **lack of visible nuclear material in tissue sections stained with 4',6-diamidino-2-phenylindole (DAPI) or H&E**
• **the lack of intracellular membrane compartments (e.g. Mitochondria).**
• **the lack of cell membrane elements**
• **the presence of unremoved and undamaged ECM elements (collagen, GAGs, fibronectin, etc.)**
• **the lack of cytotoxicity of the obtained ECM scaffold**

Hence, the choice of the decellularisation method and the efficiency of the process are critical determinant of clinical success of the decellularised tissue and it should be optimised depending on the nature and the composition of the tissue being processed. Other caveats that need to be accounted for are adverse effects due to long term-storage and risk of disease transmission to recipient (O'Leary et al., 2015). Another major downside of using decellularised scaffolds is the dependence on cadaver organ supply. But this problem can be ameliorated if xenogeneic sources have been validated safe for human use. Interestingly a study by Badylak and colleagues has demonstrated that the α-gal epitope that was previously considered a barrier to xenotransplantation has not posed significant rejection problem post decellularisation (Badylak and Gilbert, 2008). This might be a promising future solution of cadaveric organ shortage allowing the use porcine tissues that might offer an unlimited source of tissues (Fishman et al., 2014b).

Turning back to tracheal bioengineering, several decellularised scaffolds have been attempted to reconstruct tracheal defects, these included: aortic grafts (Seguin et al., 2009), jejunum (Walles et al., 2004a, Macchiarini et al., 2004), bladder (Gilbert et al., 2008) and trachea (Go et al., 2010, Jungebluth et al., 2009, Macchiarini et al., 2008). Since this thesis is focused on development and investigation of decellularised tracheal scaffolds for airway TE, the following section is dedicated to present the development of decellularised tracheal scaffolds in the field.

1.5.5.3.2.4 Development of the decellularised tracheal scaffolds

There is currently a general consensus that decellularised scaffolds are the best reported scaffolds in the clinical setting compared to their synthetic counterparts in terms of safety and efficacy (Maughan et al., 2017, Crapo et al., 2011). Various decellularisation protocols have been published using different reagents. The most commonly utilised protocol for tracheal decellularisation is based on a detergent–enzymatic method (DEM) that was initially developed by Conconi and colleagues (Conconi et al., 2005). This method however, was originally derived from Meezan *et al*. who developed it to isolate intact basement membranes from bovine blood vessels, rabbits' renal tubules and rat renal glomeruli (Meezan et al., 1975).

The Conconi *et al*. protocol mainly involved an initial washing step with distilled water followed by a detergent step using an ionic detergent, sodium deoxycholate (SDC) that is effective in solubilising cytoplasmic and nuclear membranes and may also disturbs protein-protein interactions (Gilbert et al., 2006) and an enzymatic step using Deoxyribonucleases (DNases) that helps cleaving nucleic acid sequences and so aid the removal of cell residues after cell lysis in tissues (Crapo et al., 2011). These steps were repeated for multiple cycles (18-22 cycle) to ensure efficient decellularisation of the porcine trachea which required in total 72 to 88 working days (Conconi et al., 2005). After 18 days of process, the study demonstrated complete clearance of cells along with major histocompatibility complex (MHC) class I and II from mucosal and submucosal layer but chondrocytes were still visible in the cartilage. However, at 22 cycles, complete

clearance of cellular components was evident but the mechanical properties of the scaffolds were compromised. It was also demonstrated that the scaffolds were able to support *in vitro* adhesion of chondrocytes and tracheal epithelial cells post seeding (Conconi et al., 2005).

The same protocol was later adapted and used by Macchiarini and colleagues to manufacture the first adult TE tracheal graft (Macchiarini et al., 2008). However, upon translating the protocol for clinical use on human tracheal samples, it was noted that 18 cycles were not sufficient to completely eliminate donor cells. Thus, the number of treatment cycles was increased to 25 cycles and the overall graft production time was increased to 90 days (Macchiarini et al., 2008). But the effect of these additional cycles on the scaffold structural integrity was not addressed in the paper.

In their follow-up experimental work on porcine trachea, the decellularisation protocol was modified to include only 17 treatment cycles in order to reduce the length of the process to 35 days. In their study they have demonstrated the loss of MHC-I and MHC-II staining, as well as cellular clearance from all reigns except the cartilaginous layer. In addition to that they have tested uniaxial tensile strengths of the scaffolds and verified the maintenance of the mechanical integrity. The study also confirmed that the generated scaffolds were not-immunogenic by performing heterotopic implantation in to an allogenic and xenogeneic settings for 30 days (Jungebluth et al., 2009). In another study Go *et al*. from the same group, have demonstrated successful seeding of the tracheal matrices with chondrocytes derived from bone marrow stromal cells (BM-MSCs) and epithelial cells as confirmed by scanning electron microscopy (SEM) (Go et al., 2010). Furthermore, orthotopic allo-transplantation of the seeded matrices showed that the uniaxial tensile mechanical properties were not altered after 60 days of implantation when two types of cells (epithelial cells and chondrocytes) were seeded into scaffolds in contrast to non-seeded or single cell-seeded matrices (Go et al., 2010). In addition to that their study indicated that epithelial cell seeding is necessary to prevent bacterial and fungal infection (Go et al., 2010). The authors suggested that seeding two types of cells help maintain

mechanical integrity *in vivo*. However, the studies were ambiguous that it did not specify how the mechanical analysis was performed.

The same group have also modified their clinical decellularisation protocol of human trachea to make it more clinically relevant for patients requiring urgent intervention. On which they have re-adjusted the duration of the single treatment steps without altering the total number of treatment steps (25 cycles) to reduce the processing time to 3 weeks (Baiguera et al., 2010b). Histological analysis, SEM imaging, uniaxial mechanical testing and quantitative RT-PCR analysis were used to confirm that the revised protocol was able to maintain efficient nuclear clearance while preserving the structural and mechanical properties of the generated matrices. The study also showed that the decellularised tracheal scaffolds retain proangiogenic properties. This was demonstrated by immunocytochemical staining for basic fibroblast growth factor (bFGF), *in vitro* endothelial migration assay and Chicken chorioallantoic membrane (CAM) angiogenic assay (Baiguera et al., 2010b).

Conversely, Partington *et al*. have used the same (DEM) detergent enzymatic protocol on porcine samples and reported a significant reduction in the uniaxial tensile mechanical properties of the decellularised tracheal rings but the compressive properties were not altered (Partington et al., 2013). In addition to that the study reported a substantial reduction in glycosaminoglycan GAGs levels post decellularisation (Partington et al., 2013). The author suspected that the loss of circumferential tensile tracheal strength could lead to TE construct collapse *in vivo* and warranted the need to further optimise the decellularisation protocol *(Partington et al., 2013).*

Similarly, Haykal *et al*. have evaluated and compared the structural and mechanical properties of three different decellularisation protocols including the DEM method and still reported a substantial loss of GAGs and loss of biomechanical properties in all methods (Haykal et al., 2012). This study was distinct compared to other studies because it applied a different method of mechanical analysis which is based on compliance measurement at physiological

air way pressures using CT scanner (Haykal et al., 2012). While this approach of biomechanical testing offers simulation of the *in vivo* mechanical stress that the trachea encounter but it requires the use of whole tracheal segment for analysis and this might not be a practical approach especially for quality control during manufacturing.

Then with the vison of reducing the lengthy processing time of the DEM method to make it more feasible for clinical and commercial translation, Lange and colleagues introduced the new vacuum assisted detergent enzymatic decellularisation (VAD) protocol that only require 9-11 days to complete (Lange et al., 2015). Their new protocol mainly involves an initial freeze thawing step followed by a detergent and an enzymatic step as the conventional protocol, however vacuum (negative pressure) was applied throughout the cycles which were all performed in an automatic shaker. The underlying hypothesis is that the applied negative pressure would draw reagents deeper and faster in the tissue and hence expediting the overall process (Lange et al., 2015). The authors interestingly reported complete clearance of cellular components even

within the cartilaginous layer their results were meeting the suggested minimum criteria for efficient decellularisation (Crapo et al., 2011) with an overall maintenance of collagen and GAGs levels. Furthermore, uniaxial tensile mechanical characterisation of the decellularised cartilage rings revealed preservation of the mechanical strengths.

Then a follow-up study that compared vacuum assisted decellularisation method to the conventional detergent enzymatic method revealed similar findings and that both protocols were comparable (Butler et al., 2017b). This study also demonstrated that vacuum assisted decellularised scaffolds were able to support the attachment of epithelial cells as well possessed proangiogenic response by direct Chicken chorioallantoic membrane (CAM assay and by subcutaneous implantation in mice. The study also highlighted that a loss of basement membrane was observed with both methods and warranted more research work to investigate its retention or reconstruction (Butler et al., 2017b). Of notice was the lack of agreement in mechanical characterisation between this study and

Partington *et al* study (Partington et al., 2013) despite using the same uniaxial tensile test setup and sample size. Moreover, in this study a conceptual methodological weakness was noted in one setup of the tensile mechanical analysis performed, on which dumbbell samples dissected from the longitudinal plane were tested. Given that the heterogenous structure of the trachea, this sample will contain both cartilage and annular ligament segment at variable proportions and this will eventually cause the sample to fail mainly within the weakest ligament side and this is not the ideal setup for a tensile test. Furthermore, lateral, and anteroposterior compression analysis (full ring compression assay) were also performed, this assay will not give a reliable representation of the tissue mechanical properties because it describes an extrinsic property of the tissue that varies with size and shape depending on the donor and is difficult to normalise. It is worth noting that vacuum assisted detergent enzymatic decellularisation (VAD) protocol is used by our team and is used to produce the decellularised tracheal samples in this thesis.

Taken together, while an improvement was achieved in terms expediting the processing time and cellular clearance and the removal of MHC-I and II, there appear to be conflicting results with regards to mechanical properties reported with some showing compromised properties (Haykal et al., 2012, Partington et al., 2013, Jungebluth et al., 2009). Of notice was that the majority of studies utilised uniaxial tensile testing as a way of assessing the mechanical properties of the generated constructs relative to native tissue. Although this is one of the basic mechanical assays that reflects the linear failure mechanics of materials, it require careful setup to conduct and might not be sufficient or reliable to reflect the complex biomechanical properties of the trachea being non-homogenous anisotropic viscoelastic properties (Boazak and Auguste, 2018). Indeed, mechanical characterisation in general is a challenging task in the field with most biological tissues possessing complex properties such as linearity, non-linearity, viscoelasticity and tribological properties (Butler et al., 2000). While it is impossible to match and characterise all properties of the tissue in question, a prioritisation approach must be adapted to select the most critical properties depending on the tissue mechanical characteristics and requirement (Butler et al., 2000, Guilak et al., 2014).

1.5.5.4 Current status of scaffolds in tracheal bioengineering

Overall considering scaffolds types in tracheal bioengineering, the optimal scaffold type that will support tissue regeneration is yet to be defined. However, based on the present pre-clinical and clinical studies in the field, the use of biological scaffolds and specially decellularised scaffolds is the most common as current data suggest that they possess better safety and efficacy compared to synthetic scaffolds (Fishman et al., 2014a, Maughan et al., 2017, Chiang et al., 2016). Despite the reported promising outcomes with regards to cell attachment and re-epithelisation of the scaffolds, similar findings with regards to chondrogenic regeneration or vascularisation and cell/ scaffolds interactions remain not fully explored (Chiang et al., 2016). Moreover, Mechanical stability remains a major issue in tracheal TE with most preclinical and clinical studies reporting mechanical collapse or stenosis with the need intermittent stenting (Elliott et al., 2012, Gonfiotti et al., Boazak and Auguste, 2018). Whilst, the mechanisms and the pathology leading to this biomechanical weakness is not yet fully understood, there is an identified need to focus on structural characterisation of and means to evaluate pre and post manufacturing as well as pre and post implantation.

1.5.6 Cells used in tracheal tissue engineering

The main goal of tracheal TE is build a construct that can recapitulate the tracheal tissue biomechanical structure, restore a functional mucosa, and can be vascularised to ensure tissue and cells survival. The trachea has a complex structure consisting of different specialised cell types that define the overall tissue function these include: ciliated pseudostratified epithelial cells, chondrocytes, smooth muscle cells, fibroblasts, and endothelial cells. Therefore, the cells seeding choices for tracheal tissue engineering were mainly a reflection of the native tracheal composition. Yet it is not clear yet which cell type should be seeded to tracheal scaffolds prior to transplantation to promote functional regeneration of the TE construct. Currently the three most widely employed cell types for seeding in tracheal bioengineering in pre-clinical and clinical studies are: chondrocytes, epithelial cells, and mesenchymal stromal cells (MSCs).

1.5.6.1 Chondrocytes

Chondrocytes are used with the aim to regenerate a functional hyaline cartilage to maintain structural support of the trachea. They have been used at Vacanti's initial attempt to bioengineer trachea.(Vacanti et al., 1994). Chondrocytes were mostly used in pre-clinical tracheal bioengineering studies and mainly in combination with synthetic scaffolds (Maughan et al., 2017, Chiang et al., 2016). The only reported clinical use of chondrocytes was in the first reported adult human TE tracheal case (Macchiarini et al., 2008).

The main sources for harvesting chondrocytes are: auricular, nasal septum, tracheal and costal cartilage. The cells can be isolated and expanded *in vitro*. While auricular cartilage harvesting is considered one of the safest, easiest and is minimally invasive, studies have shown that it forms an elastic type cartilage that has suboptimal properties compared to the native hyaline cartilage required for tracheal constructs (Weidenbecher et al., 2009, Weidenbecher et al., 2008). In contrast Kojima *et al*. compared PGA engineered trachea fabricated from nasal septal and chondrocytes and found that nasal septal chondrocytes developed cartilage histologically and mechanically similar to tracheal cartilage (Kojima et al., 2003a). Moreover, it has an advantage that it allows the isolation of other types of cells from the same biopsy like epithelial cells and connective tissue cells (Kojima et al., 2003b). Costal and tracheal chondrocytes have the potential to produce hyaline cartilage, but the invasiveness of their harvesting procedures make them clinically less desirable sources (Walles et al., 2004b, Ott et al., 2011).

That said harvesting cells for cartilage generation remains a challenge in TE and the optimal cell source is still not defined. Additionally, one limitation with the generation of cartilage is the dedifferentiation potential during *in vitro* culture regardless of the source that needs to be resolved. The ideal source needs to afford simplicity, safety, and minimal invasiveness during harvesting as well as production of non-immunogenic large number of cells of stable phenotype (Kojima and Vacanti, 2014).

Therefore, research has focused on deriving chondrocytes from other stem cell sources. It is worth noting that while embryonic stem cells can be used as a source for chondrocytes generation, but ethical and safety concerns limit their translational use (Fishman et al., 2014a). Moreover, induced pluripotent cells (iPSC) have been used to generate hyaline cartilage in small animal models (Brian et al., 2012), but their clinical safety have not been established yet (Fishman et al., 2014a). Currently the most promising alternative source for chondrocytes generation is the differentiation of multipotent mesenchymal stromal cells (MSCs). They possess many advantages like ease of isolation, safety, *in vitro* expandable in considerable numbers and can be isolated from different sources like bone marrow, adipose tissues, and many others. MSCs have been used for tracheal cartilage regeneration in several tracheal TE studies (Fuchs et al., 2003, Go et al., 2010). Of interest were studies performed by Kojima and Vacanti that coculture MSCs with chondrocytes to improve cartilage formation and avoid the use of differentiation growth factors like TGF-β1 and dexamethasone (Kojima and Vacanti, 2014).

Preclinical studies seeding chondrocytes for tracheal bioengineering revealed variable outcome results, for example : neocartilage formation was reported in several studies using synthetic (Komura et al., 2015, Hong et al., 2014, Grimmer et al., 2004, Nomoto et al., 2008) and decellularised scaffolds (Go et al., 2010). It was noted that few of these studies did not include un-seeded control and hence making the analysis of the outcomes difficult. In addition to that some studies reported deposition of appropriate matrix components like collagen , GAGs, and elastin (Luo et al., 2013, Grimmer et al., 2004, Tsao et al., 2014). Other studies showed persistent of chondrocytes post transplantation for more than 14 weeks (Komura et al., 2015, Kojima et al., 2002, Hong et al., 2012, Nomoto et al., 2012). However mechanical failure (Luo et al., 2013, Grimmer et al., 2004, Gilpin et al., 2010, Kojima et al., 2002) and stenosis (Kunisaki et al., 2006, Weidenbecher et al., 2009) (Lin et al., 2009) were also observed in some studies. In fact, a review study by Chiang and colleagues analysed outcomes of segmental orthotopic tracheal preclinical animal studies, and reported that tracheal cartilage regeneration was more dependent on the cell type used with an advantage towards the use of differentiated chondrocytes. In addition to that

it was not linked to a particular scaffold material type. Yet most of the progress in cartilage regeneration in the field was achieved with combination of synthetic scaffolds (Chiang et al., 2016).
Taken as a whole more research is still required to define the best cell source/ scaffold and strategy of utilising chondrocytes in generating cartilage for tracheal TE.

1.5.6.2 Epithelial cells

As previously described epithelial cells play an essential role in the airway forming a protective barrier against infections. Indeed, compromised mucociliary clearance is a serious challenge after tracheal transplantation due to accumulation of secretions at the distal anastomosis site promoting infection and obstruction (Santacruz and Mehta, 2009). Therefore, restoration of a functional epithelium is one of the main targets of tracheal TE. Several sources were used to isolate epithelial cells and have reported success in both preclinical and clinical tracheal TE studies, these include: tracheal and bronchial brush biopsies (Macchiarini et al., 2008, Kobayashi et al., 2010), nasal septum (Mohd Heikal et al., 2010), buccal mucosal (Delaere et al., 2010), and skin (Kim et al., 2004).

While the aim is to achieve long term regeneration by direct epithelial cells engraftment, analysis of clinical cases that have incorporated epithelial cells or explant biopsies to the graft have shown that the process of re-epithelialisation was slow and had taken up to two years for segmental tracheal replacement (Hamilton et al., 2015, Gonfiotti et al., 2014). These results indicate that it is unlikely that the seeded cells have survived and contributed to epithelial regeneration and that restoration happened by slow epithelial cell migration from adjacent tissue. Moreover, evidence from preclinical studies has demonstrated epithelial cell migration from the anastomotic sites (Nakamura et al., 2009, Won Suh et al., 2001, Rawlins and Hogan, 2008).The lack of engraftment can be due to the lack of sufficient blood supply to ensure epithelial cells survival. In fact, this is supported by studies that have demonstrated improved epithelialisation when employing periods of heterotopic pre-vascularisation (Komura et al., 2015, Tsao et al., 2014, Kanzaki et al., 2006). Moreover, when looking at literature from skin tissue engineering, studies have demonstrated that epithelial cells survival is

higher on well vascularised wound surfaces. All of this highlight the importance of improving vascularisation of TE tracheal constructs to achieve better outcomes. That said until this is achieved, the incorporation of engineered epithelial layer, remains indispensable as it can still provide barrier functions and probably signalling to enhance regeneration without the need for long term engraftment by acting as a biological dressing to avoid mucus plugging and graft infection and the associated complications that compromise success of the transplantation.

It is well known that the interaction between epithelial cells and mesenchymal elements such as fibroblasts play a role in tissue morphogenesis. Indeed, fibroblasts have been used during *in vitro* epithelial cells culture and found to improve epithelial cells survival (Wiszniewski et al., 2006, Skibinski et al., 2007). Pre-clinical animal studies have demonstrated that fibroblasts expedited re-epithelialisation. (Kobayashi et al., 2010, Nomoto et al., 2008, Mohd Heikal et al., 2010), for example Kobayashi *et al*. constructed bioengineered grafts (collagen sponge with a spiral polypropylene mesh) containing gingival fibroblasts (GFBs) and adipose-derived stem cells (ASCs) and implanted them into rat tracheal defects. The authors report expedited regeneration of highly ciliated epithelium within 2 weeks (Kobayashi et al., 2010).

Interestingly other studies also revealed that co-seeding of epithelial cells with MSCs have been associated with improved re-epithelialisation as well (Go et al., 2010, Han et al., 2011, Nakamura et al., 2009), for example Nakamura *et al*. have reported faster epithelialisation and fewer complications related to stenosis when seeding BM-MSCs into bioengineered mesh type prosthesis coated with atelocollagen that were used to replace tracheal defect in dogs in comparison to peripheral blood (Nakamura et al., 2009). It is possible that the paracrine effects of MSCs have contributed to this effect.

In other regards it is important to stress there are still many challenges associated with epithelial cells generation for tracheal TE applications that are still not fully resolved. For example, the optimal source for isolating epithelial cells is still ill defined, obtaining epithelial cells in sufficient numbers and efficient time for

urgent cases is another major challenge in the field (Zhang et al., 2015, Butler et al., 2016).

This is because epithelial cells tend to expand slowly in culture. Moreover, primary epithelial cells lack phenotypic stability and tend to dedifferentiate rapidly with increasing passage number and loss of specialised cells (Zhang et al., 2015). Therefore, several approaches were suggested and are under development to enhance their growth such as : co-culture with fibroblast cells (Kobayashi et al., 2006, Butler et al., 2016) , or the use of an air-liquid interface when culturing them (Fulcher and Randell, 2013), or cell sheet engineering for example using thermos-responsive poly (N-isopropylacrylamide) (PIPAAm)-coated dishes to produce epithelial sheets (Kanzaki et al., 2006) and extracellular matrix mimicking systems like the use of decellularised allo-dermis (Ansari et al., 2017).

1.5.6.3 Mesenchymal stromal cells (MSCs)

MSCs have gained extensive interest over the past decades as a promising therapeutic tool in clinical settings. They are multipotent cells capable of self-renewal and can differentiate to various specialised cells like osteoblast, chondrocytes, tenocytes, adipocytes, cardiomyocytes and neurocytes (Bai et al., 2016). They have been isolated from various sources such as bone marrow, umbilical cord tissue, peripheral blood, dermis, dental pulp, adipose tissue, liver and many others (Rhee et al., 2015). They were described first in 1970 by A.J Freidenstein as plastic adherent non-hematopoietic cells that can form fibroblastic colonies *in vitro (Friedenstein et al., 1966)*. The International Society for Cellular Therapy (ISCT) have proposed minimal criteria for defining them, these include: (1) plastic adherence in culture, (2) tri-lineage differentiation potential to osteocytes, chondrocytes and adipocytes, (3) cell-surface expression of CD90, CD105 and CD73, and lack of cell surface CD45, CD34, CD14, CD79 and HLA-DR (Dominici et al., 2006b). In addition to their differentiation potentials, they display dramatic homing capabilities towards pathological sites, inflammation and injury sites (Bai et al., 2016). Furthermore, MSCs releases numerous paracrine bioactive molecules such as growth factors, cytokines, chemokines, miRNAs and microvesicles (exosomes), (Boazak et al., 2017).

These factors exert a wide range of biological effects on local cellular dynamics. The paracrine effects of these factors have been classified in to main categories: immunomodulatory, anti-apoptotic, anti-scarring, angiogenesis, chemoattraction, support of cellular growth, differentiation, pro-regeneration and nurturing (da Silva Meirelles et al., 2009). These paracrine factors play principle role in mediating the cells therapeutic effects and promoting regenerative responses, anti-inflammatory, healing and tissue repair (Kusuma et al., 2017). Furthermore, their ease of isolation with a high *in vitro* proliferative capacity, make them an accessible source for clinical applications. In fact, many preclinical trials and studies have demonstrated their therapeutic efficacy and encouraging signs of clinical activity in various conditions, such as inflammatory, degenerative diseases, autoimmune, rheumatic diseases (Maumus et al., 2013), musculoskeletal regeneration, spinal cord injuries and wound healing (Bai et al., 2016, Wang et al., 2016, Maxson et al., 2012, Maumus et al., 2013). The promising results from pre-clinical studies have prompted a sharp upsurge in the number of clinical trials that use MSCs to treat a variety of diseases (James et al., 2014) and with an enviable safety record in clinical practice (Giordano et al., 2007).

All these criteria have made MSCs an excellent candidate for cellular therapy, regenerative medicine, and tissue engineering. In tissue engineering they are already a popular choice that have been widely incorporated in various therapeutic models that ranged from cardiac repair, cartilage and bone TE, tendon and skeletal TE, intervertebral disk repair and many others (Kusuma et al., 2017).

In tracheal bioengineering, MSCs have been used in several pre-clinical and clinical studies with the rationale of taking an advantage of either their differentiation potential or their paracrine effects to promote natural tissue remodelling and regeneration (Murphy et al., 2013). Indeed, autologous BM-MSCs have been used in three first human TE tracheal cases (Elliott et al., 2012, Macchiarini et al., 2008, Elliott et al., 2017).

Some groups have focused on harnessing the multi-differentiation potentials MSCs as source for chondrocytes derivations (Go et al., 2010, Fuchs et al., 2003, Kojima and Vacanti, 2014, Macchiarini et al., 2008). Other groups have utilised the cells the cells by directly seeding them in to scaffolds or by co-seeding them with other types of cells like chondrocytes and epithelial cells.

Few pre-clinical studies in tracheal bioengineering have demonstrated that seeding MCSs in tracheal scaffolds have a beneficial effect. For example, a study by Suzuki *et al*. reported an accelerated neovascularisation and epithelialisation in an adipose derived MSC seeded in to collagen sponge artificial graft within two weeks of implantation into rats' tracheal defects in contrast to 2 months in non-seeded grafts (Suzuki et al., 2008). Another study by Haykal *et al*. constructed a tracheal graft by co-seeded MSCs with epithelial cells into decellularised porcine trachea and then implanted in a heterotopic position in pigs (Haykal et al., 2013). Results of the study showed increased infiltration of regulatory T lymphocytes and delayed macrophages infiltration and scaffold degradation compared to un-seeded scaffolds. This study suggests that MSCs might be evoking an immunomodulatory effect. In another study it was found that co-seeding of MSCs with chondrocytes in Poly (L-lactic-co-glycolic acid) (PLGA) scaffolds in an ectopic culture in the abdominal wall of rabbits was associated with increased matrix deposition, improved epithelialisation and vascularisation (Tsao et al., 2014). As previously described MSCs seeding have been associated with enhanced epithelialisation (Go et al., 2010, Han et al., 2011, Nakamura et al., 2009, Gray et al., 2012).

Overall, the exact role, contribution, and relevance of seeding MSCs in tracheal bioengineering remains controversial. Even more, the concept of MSCs involvement has been challenged by other studies that have demonstrated low engraftment showing that cells do not persist long after implantation or systemic administration (Galderisi and Giordano, 2014, Minguell et al., 2013, Karp and Leng Teo, 2009, Wagner et al., 2009, Freyman et al., 2006), Moreover, the concept of utilising MSCs in tracheal TE have been also critiqued as it is unclear yet the role of the cells and how they exert their effect and if it by directly engrafting or by releasing other factors (Delaere, 2010).

1.5.6.4 Cell seeding techniques in tracheal tissue engineering

Over the past decades various seeding techniques have been developed in an effort to facilitate recellularisation of three-dimensional scaffolds and to improve cell seeding efficiency, uniform delivery, and permeation. The seeding techniques ranged from simple static passive seeding of cells by applying them directly to scaffold surface (Xiao et al., 1999, Song et al., 2018) to more complex techniques that involve the use of bioreactor based dynamic systems with different delivery principles and designs such as : perfusion (Petersen et al., 2010), rotational (Godbey et al., 2004), vacuum (Nieponice et al., 2008), electrostatic (Bowlin et al., 2001) or magnetic seeding approaches (Shimizu et al., 2007). Other approaches of seeding involved the use of biological glues like fibrin (Pawlowski et al., 2004, Salacinski et al., 2001) or injection seeding (Urbani et al., 2018). The delivery system may be further complicated by incorporating hybrid delivery and cultivation modes like injection seeding coupled to perfusion (Zhou et al., 2016), or other biophysical stimuli to mimic *in vivo* environment in order to induce maturation and function to seeded cells for example: electrical stimuli (Ott et al., 2008) mechanical stretch (Petersen et al., 2010), or shear stress (Lovett et al., 2009).

When reviewing cell seeding techniques in tracheal tissue engineering, a search of clinical and preclinical literature shows that seeding has been attempted in several ways. These techniques included: in situ (*in vivo*) recellularisation, where harvested islands of epithelial cells and total mononuclear cells suspension from bone marrow were directly applied into tracheal allograft during the operation (Jungebluth et al., 2012, Elliott et al., 2012). Other reports utilised perfusion-based seeding in custom designed double chamber bioreactor that allow separate seeding of two cell types and different media flow for both luminal and abluminal compartment (Haykal et al., 2014b, Go et al., 2010). Another study employed vacuum based seeding technique of bone marrow derived mononuclear cells to a polymeric nanofiber scaffold (Clark et al., 2016).

Nevertheless, the most common technique of seeding cells in tracheal tissue engineering remains as static passive cell seeding. On which cells are drop-seeded onto the scaffold surface, then allowing cells to sit relatively undisturbed to maximise cells attachment and permeation (Godbey et al., 2004). This step is followed by cultivation in media, in specially designed bioreactors for a variable length of time under either static conditions or under dynamic movement of the graft, media or both (Batioglu-Karaaltin et al., 2015, Kunisaki et al., 2006, Lee et al., 2002, Fuchs et al., 2003, Lin et al., 2009, Gray et al., 2012, Elliott et al., 2017, Macchiarini et al., 2008).

1.5.6.5 Current status of cell choices and seeding techniques in tracheal bioengineering

Overall data from literature suggest that seeded scaffolds outperform and support tissue integration more than unseeded scaffolds (Chiang et al., 2016, Suzuki et al., 2008, Kanzaki et al., 2006, Go et al., 2010, Tsao et al., 2014, Mohd Heikal et al., 2010, Gray et al., 2012). Moreover, based on preclinical studies seeding multiple types of cells appear to be beneficial especially with regards to MSCs (Go et al., 2010, Kojima et al., 2002, Tsao et al., 2014, Kobayashi et al., 2010). But, it is not clear yet which type of cells /or cells combination is optimal for tracheal tissue engineering and how they contribute to regeneration (Maughan et al., 2017). There is also a lack of studies that have addressed critical cell seeding variables like the optimal cell seeding density, optimal seeding technique and how to seed, evaluation of seeding efficiency, evaluation of cells survival, fate, and interactions to ensure achieving a reproducible seeding success. Furthermore, most studies relied upon qualitative methods like histology and endoscopy to evaluate constructs integration making interpretation of outcomes a challenging task (Maughan et al., 2017). Although some studies have employed cells pre-labelling techniques like transfecting with florescent proteins to facilitate cells tracking (Gray et al., 2012, Haykal et al., 2014b, Seguin et al., 2013, Suzuki et al., 2008), but false positive results is still possible from dead, phagocytosed cells. Therefore, one of the current challenges is tracking of cells fate and more research work is required to explore new techniques to facilitate cells tracking.

1.5.7 Boosting signals in tracheal bioengineering

Boosting signals represents all the conditions that will prepare the construct for implantation by providing the necessary biochemical and/or mechanical signals to support and guide cell/scaffolds repopulation, differentiation, and neo-tissue development (Fishman et al., 2011). These will include *in vitro* culture or *in vivo* implantation or a combination of these steps. For example, the use of certain growth factors, or specialised bioreactors for cultivation or simulation of *in vivo* condition as well as the use of certain re-vascularisation techniques.

1.5.7.1 Growth factors

Growth factors have been used in several pre-clinical and clinical studies in order to boost certain processes and assist in the regeneration and remodelling, for example peripheral mobilisation of cells and recruitment and differentiation and proliferation of cells/ progenitor cells and promotion of re-vascularisation. One of the first paediatric clinical compassionate cases by Elliott *et. al*. have topically administrated, G-CSF to facilitate progenitor cell recruitment and human recombinant erythropoietin to encourage angiogenesis, and TGF- β to support chondrogenesis in decellularised tracheal scaffold (Elliott et al., 2012). But it is still not clear yet how these factors might have participated in the construct integration process. Moreover, bolus application of growth factors is limited by the inherent instability of these proteins *in vivo* and their effect cannot be controlled at distant sites (Fishman et al., 2011). One pre-clinical study reported improved proangiogenic vessel formation in an *ex vivo* CAM assay post perfusion of VEGF through degraPol scaffolds (Tan et al., 2007).

In order to allow localised slow release of these factors, investigator have incorporated growth factors in biodegradable polymers, for example one study involved encapsulation of bFGF in gelatine sponges and placing it in chondrocytes seeded-PGA scaffolds which have resulted in enhanced chondrogenesis after implantation in tracheal defect in rabbits (Kojima et al., 2004). Several studies also adapted similar approaches incorporating growth factors like bone morphogenic protein-2 (BMP2) (Igai et al., 2008), TGF- β to improve chondrogenesis (Komura et al., 2008). Overall a deeper understanding of how these factors can be utilised, and how it should be incorporated is still

required. And in the context of decellularised scaffolds, an evaluation of the growth factors retention has to be established too.

1.5.7.2 Bioreactors

1.5.7.2.1 *In vitro* bioreactor

Bioreactors are devices in which biological and/or biochemical processes develop under closely monitored and tightly controlled environmental and operating conditions (e.g. pH, temperature, pressure, nutrient supply and waste removal) and are used for *in vitro* culture devices to study and improve TE constructs (Fishman et al., 2011) . The general purposes of bioreactor are to provide optimal physiological conditions to promote cell adhesion, achieve uniform cells seeding and distribution in 3D constructs, improve mass transport of nutrients and oxygen, and delivering chemical or mechanical stimulations (convective mixing, perfusion, pressure, electrical, mechanical etc.) that imitate conditions of growing organs to enhance cells growth and differentiation (Martin et al., Badylak et al., 2011). Various designs are available and differ in, size, shape, and design complexity subject to the requirements of the engineered tissue/organ (Zhao et al., 2016, Plunkett and O'Brien, 2011).

In tracheal tissue engineering the majority of bioreactor models used have focused on improving seeding of the constructs to overcome problems related to static culture conditions by improving distribution and mass transport. For example, a study showed that the use of dynamic perfusion bioreactors might improve chondrocytes distribution in chondrocytes seeded Poly-(ethylene glycol)-terephthalate–poly (butylene terephthalate) scaffolds compared to static methods (Tan et al., 2009).

Another study designed an air-liquid (half filled with media) rotating bioreactor in its longitudinal axis was designed for primary chondrocyte proliferation on a 1cm long synthetic tracheal scaffold (poly 3-caprolactone-type II collagen scaffolds). The results of the study demonstrated an enhanced cell proliferation and increased level of GAG and collagen was also reported (Lin et al., 2009). The scaffold was implanted into a rabbit model of small tracheal defect and showed

good re-epithelialisation and granulation of tissue outgrowth (Lin et al., 2009). A double-chamber bioreactor was also used to deliver different culture media on either side of the trachea with rotation along the longitudinal axis to expose graft to culture media and incubator atmosphere. A commercial version was made by Harvard Bioscience Inc. and it was utilised for the first tracheal engineering adult human case (Asnaghi et al., 2009). Few other studies used a model based on pulsatile radial distention coupled with dynamic flow. For example, a study by Ghezzi and colleagues demonstrated that pulsatile flow stimulation of dense collagen constructs seeded with airway smooth muscle cells (ASMCs) increased collagen content, improved circumferential strength, and showed an up regulation of α-smooth muscle actin (Ghezzi et al., 2013). Haykal *et.al* used a double chamber rotating perfusion bioreactor to improve epithelial and MSC cell seeding into long segment porcine tracheal grafts. The study reported an improved distribution and increased cells attachment compared to static culture as determined by histology staining. But no labelled cells were detected on the abluminal side 3 days post implantation and no epithelial cells were observed in the first two weeks (Haykal et al., 2014b). No blinding of the histology results was mentioned in this study. It is therefore, unclear if the cells did not survive post implantation or the seeding was not optimal as predicted.

1.5.7.2.2 *In vivo* bioreactor

This approach uses the recipient body as a natural bioreactor. It is based on harnessing the body ability to activate endogenous regenerative and wound healing mechanisms (Bader and Macchiarini, 2010). It has many advantages compared to conventional *in vitro* approach overcoming limitation associated with extensive in vitro manufacturing time, increased risk of contamination during cell/construct manipulations, the high cost for specialised bioreactors and culture systems and the need for specialised trained staff (Jungebluth et al., 2012). The construct will be implanted with cells or other boosting factors during operation to facilitate the remodelling process. Several studies in tracheal TE have utilised this approach (Elliott et al., 2012, Nakamura et al., 2009, Ruszymah et al., 2005, Kajbafzadeh et al., 2015).

1.5.7.3 Re-vascularisation

As previously described re-establishment of blood supply is a major challenge in tracheal bioengineering due to the lack of discrete vasculature that will be amenable for anastomosis. Therefore, a graft of substantial length will be at a risk of undergoing necrosis because they are slow to establish vascular connections to support cell growth and tissue integration. Several approaches have been proposed to try solve this problem. For example, delivery of angiogenic growth factors as previously described in section (1.5.7.1), or pre-vascularisation by pre-implantation in a heterotopic position prior to tracheal transfer as free or pedicled flap (Delaere et al., 2012, Komura et al., 2015) or performing an interposition graft or omental/pericardial wrapping if the tissue is available (Macchiarini et al., 2004, Elliott et al., 2012). One concern, is that seeded cells might not survive the pre-vascularisation periods and hence multiple post-operative seeding or delayed seeding might be required to overcome this problem (Maughan et al., 2017).

Taken as whole, the optimal combination of conditions and boosting signals or techniques to facilitate tissue engineered tracheal integration and regeneration are yet to be defined and opens up new research paths to optimise this developing technology.

1.6 Summative statement and motivation of the thesis

Replacement of long segment tracheal lesions is one the most difficult and vital procedures with no optimal replacement available currently. The recent history of tracheal tissue engineering represents a series of proof of concept studies, but, the approaches used remain diverse and there is no consensus yet on the best approach to be employed. It also highlights many scientific gap of knowledge, clinical and translational challenges that need to be thoroughly investigated and optimised. The international society for cellular and gene therapy (ISCT) has released a position statement with regards to the current practice in tracheal bioengineering (Weiss et al., 2014). The summit behind this paper have identified key questions, gaps of knowledge and recommendations from the basic science, pre-clinical and clinical, regulatory and industry aspects that need to be addressed to ensure progress in the field (Weiss et al., 2014).

The expert's conclusion stressed the importance of collaborative coordinated efforts between, basic translational, clinical, and commercial groups. It also emphasised the importance of incorporating a strong element of basic research and discovery science to fill the knowledge gap, and to consider all practical aspects of the clinical application. All of which will help propel progress in the field yielding optimisation of the current technology to provide an effective novel therapy for patients.

1.7 Scope and aims of the thesis

Scope

This thesis is focused in development and characterisation of MSC-seeded decellularised tracheal scaffolds for airway tissue engineering. We have identified, addressed, and investigated three main knowledge gaps related to the manufacturing of these constructs, these are: (1) evaluation of structural and mechanical stability, (2) Improving cell seeding efficiency (3) Investigation of the interaction, relevance and expected effect of seeding MSCs into decellularised tracheal scaffolds.

Main aims of this thesis

1. Evaluation of cellular clearance, biochemical and biomechanical structural properties of tracheal scaffolds following vacuum assisted decellularisation technique (VAD). The central focus is to explore and introduce the use of dynamic mechanical analysis (DMA) for the assessment of the viscoelastic mechanical properties of tracheal cartilage to be a new representative measure of scaffold mechanical properties.
2. Improvement of passive cell seeding efficiency of MSCs on decellularised tracheal scaffolds. and the analysis of cells/scaffolds interactions with regards to attachment, viability, proliferation, infiltration, and spatial distribution.
3. Analysis of differential gene expression of MSCs post seeding onto decellularised human tracheal scaffolds aiming to seek scientific justification for MSC seeding pre-implantation. The focus is in exploring the expression of paracrine bioactive factors produced by MSCs that are of relevance to tissue remodelling and integration.

2 Materials and Methods

2.1 Tissue Procurement

2.1.1 Porcine trachea

Adult porcine tracheae were commercially obtained from Animal Organs for Research (From Cheale Meats Ltd. Abattoir, Brentwood, UK). Porcine tracheas were trimmed onsite to obtain the trachea from the larynx to the carina. They were packaged in to plastic bags, which were surrounded by wet ice, in a polystyrene box and then transported by a courier to the laboratory. Upon arrival, porcine tracheae were trimmed to remove excess tissue, cricoid cartilage from the proximal region and bronchus from the distal region of trachea. The loose visceral fascia was gently removed from the organ and then tissues were washed twice using sterile phosphate buffered saline (PBS). The tracheae were either used fresh or stored frozen in PBS at -80°C for future use as required.

2.1.2 Human trachea

Human tracheae were procured by National Health Service Blood and Transplant (NHSBT) retrieval team. Cadaveric donors were identified through the (NHSBT), by agreement and with appropriate consent, following the current clinical practice for nonliving tissue retrieval in the U.K. Ethical approval was obtained through the National Research Ethics Committee (REC reference NO: 11.LO.1522). Tracheae were retrieved less than 48 h post mortem and were removed in their entirety from cricoid to carina. Donor tracheae were immediately rinsed in 1 L (0.9% NaCl w/v) normal saline and surrounding tissue was dissected away. The tracheae were stored and shipped in UW (University of Wisconsin solution) (Bridge to life UK) and stored at -80 °C freezer for future use.

2.2 Vacuum Assisted Chemical Enzymatic Decellularisation (VAD)

Porcine trachea decellularisation was performed as per established protocol using Vacuum Assisted Chemical Enzymatic decellularisation (VAD) method (Lange et al., 2015). All processes were performed within a class II biological safety cabinet where maintenance of sterility was required. Human tracheae were decellularised using the same protocol by the NHSBT team.

2.2.1 Tissue preparation for decellularisation

Frozen tracheal tissue was thawed overnight at 4°C. Then the tissue was aseptically placed in a sterile container to perform decontamination step by submerging the tissue in 20% (v/v) chlorhexidine (Alpha aesar) solution and leaving it static, protected from light for 5 minutes, followed by three washes with sterile normal saline (NaCl 0.9% w/v), (Baxter Healthcare, UK) of 5 minutes each (Figure 2.1).

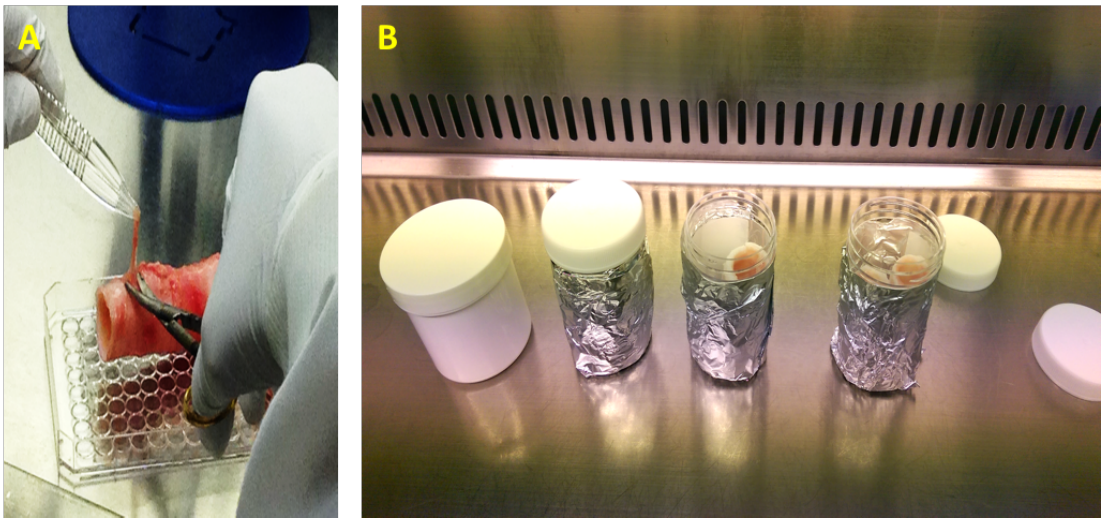

Figure 2.1: Tissue preparation and decontamination.

Tracheal tissue is dissected to remove excess tissue(A), Then trachea is decontaminated with 20% chlorhexidine for 5 minutes (B), then washed 3 times with sterile Normal saline.

2.2.2 Solutions preparation, sterile filtration, and transfer to bags

All reagent solutions were prepared one day prior to commencing the decellularisation process; except the DNase/RNase solutions (Enzymatic steps), which were added to designated transfer bags immediately prior to use. Unless otherwise stated, all solutions had a final volume of 250 ml. Sterile solutions were all transferred to sterile transfer bags (Terumo, UK) using a peristaltic pump (Watson Marlow, UK), via individual sterile haematology pump segments (Quest Biomedical, UK) and coupler-luer lines (Quest Biomedical, UK) as shown in (Figure 2.2). All solutions prepared contained 1% (v/v) antibiotic/antimicotic (Gibco, USA).

2.2.2.1 Detergent solution

Triton X-100 (0.25% v/v) (Sigma) / Sodium deoxycholate SDC (0.25% w/v) (Sigma Aldrich) solution was prepared in 250ml of Hanks' Balanced Salt Solution (HBSS) without $CaCl_2$ and $MgCl_2$ (Gibco), Then filtered using filtering unit system (Corning) and vacuum pump. And then transferred in to a sterile 300ml transfer bag as described above.

2.2.2.2 Washing solutions

Seven transfer bags (Terumo, UK) were filled with 250ml HBSS without $CaCl_2$ and $MgCl_2$ (Gibco, UK) each.

2.2.2.3 DNase/RNase solutions (Enzymatic step)

Two sterile transfer bags (Terumo, UK) were filled with a stock solution of HBSS with calcium and magnesium (Gibco, UK). On the day of use, RNase type I (Roche, Switzerland) 0.1 g/L and 2000 Kunitz units /L DNase I (Sigma-Aldrich, UK), were added to the stock solution transfer bags using injection site couplers (Origen). All reagent solutions were stored at 4 °C, and removed from the fridge to adapt to room temperature 1 hour prior to requirement.

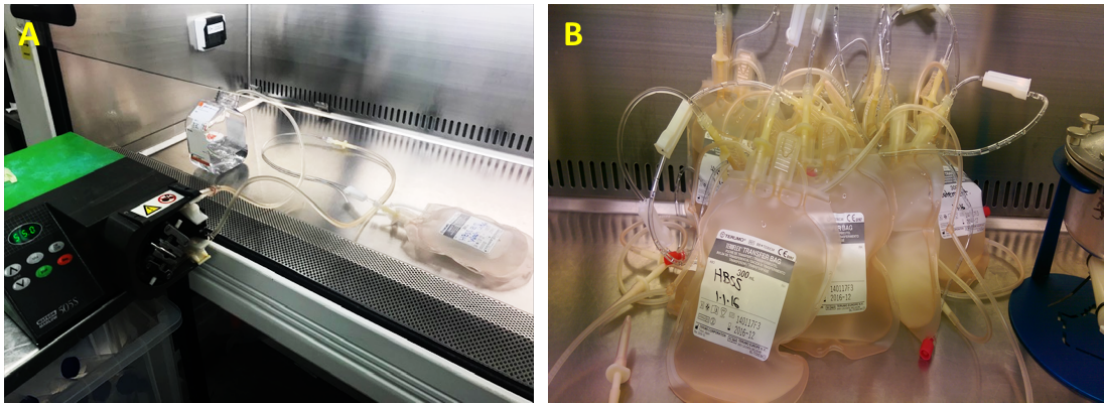

Figure 2.2: Decellularisation solution filling in sterile transfer bags.

Sterile solutions were all transferred to sterile transfer bags using a peristaltic pump.

2.2.3 Preparation and assembly of Bioreactor (Ricordi chamber) for decellularisation

The decellularisation process was performed in a specially designed chamber capable of withstanding negative pressure/vacuum (BioRep, USA). A day prior to starting the process the Ricordi chamber parts (chamber, chamber lid, O- ring and thumb nail screws), three (1/4") inch inner diameter (ID) polypropylene male luer thread barbs (Value Plastics, USA), three vacuum tubing lengths of Tygon® E-603 non-DEHP (Cole-Parmer, UK), 60 mm x 1/4" inch (ID), all were sterilised by autoclaving.

2.2.3.1 Assembly steps

Aseptically female –male combi stopper caps (VWR International, UK) were attached to the three-luer thread barbs without touching the barb ends (Figure 2.3, A), and each barb was inserted to one end of the three-vacuum tubing. Then two vacuum tubing lines were attached to the lower ports of the chamber and one attached to the chamber lid (Figure 2.3, A, B). Then three way-stopcocks (BD Infusion Therapy, Sweden) were firmly attached to each barb end of the tubing. On the lid, additional 2 miniSart filters 0.2µm (Sartorius stedim) and a three-way stopcock was also attached in tandem (Figure 2.3, C). All ports were finally capped with female-male luer sterile combi-stoppers (VWR International, UK). All three-way stopcocks were adjusted at lock position. The O-ring was then fitted on the groove of the chamber without passing over the chamber body opening (Figure 2.3, D). Finally, the tissue was placed in the chamber and the lid was closed and thumb screws tightened (Figure 2.3, D, E). Cable ties were also attached over each barb connections at opposing ends of each tubing segments and tightened using cable ties (Figure 2.3, E). The fully assembled decellularisation chamber is shown in (Figure 2.3, F)

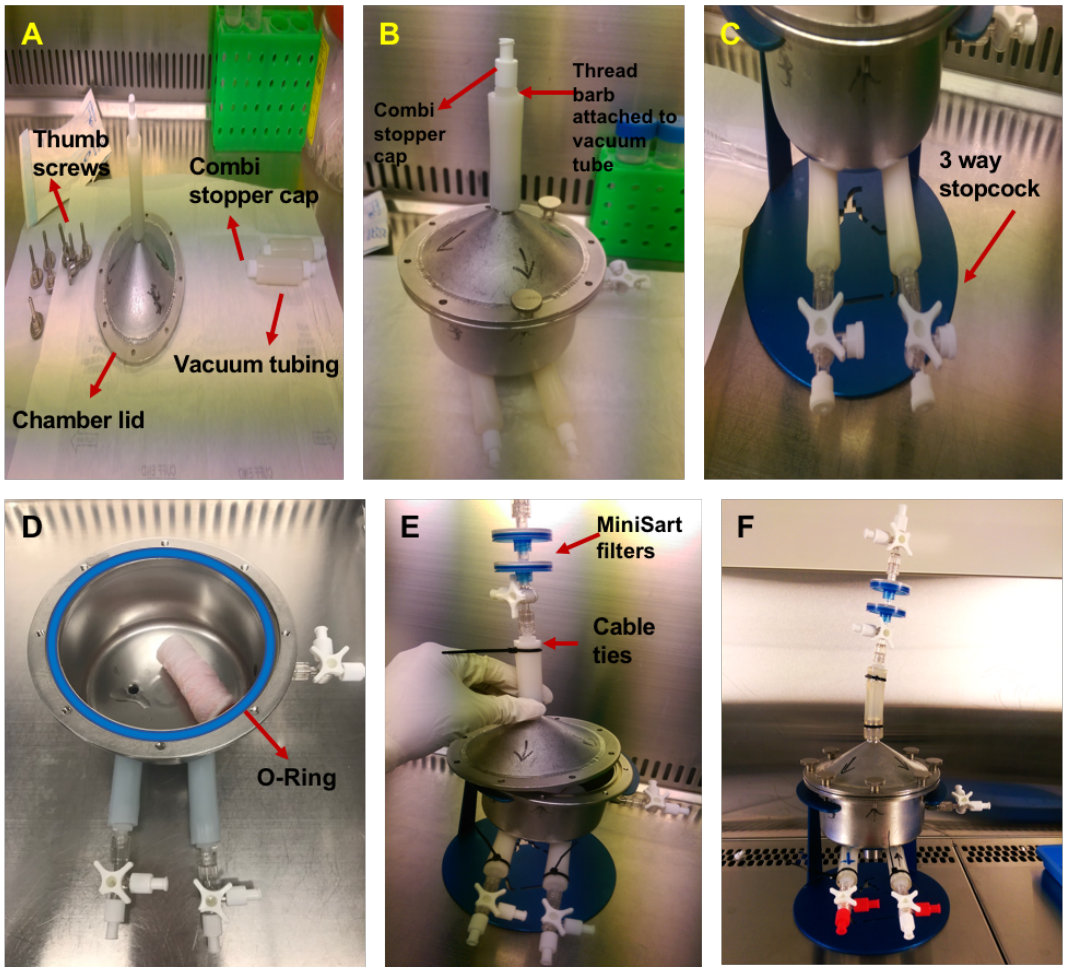

Figure 2.3: General assembly steps of decellularisation chamber.

Luer thread barbs were inserted in the 3 vacuum tubing segments and capped by combi stoppers before attaching them in chamber lid port and chamber two lower ports (A, B). Then 3-way stopcock are threaded in all ports and tissue is aseptically placed in the chamber (C, D), Also, miniSart filters were attached to the lid port with an additional a 3 way-stopcock and cable ties used to tighten connected tubing (E). Fully assembled decellularisation (Recordi chamber) (F).

2.3 Decellularisation Process

The decellularisation process proceeded as described in Table 2.1. Distinct ports on the base of the chamber were used for filling and draining throughout the process reagents were transferred to the Ricordi Chamber by gently squeezing each bag (Figure 2.4, A). Draining was done, under gravity (Figure 2.4, B). De-pressurization was done through the lid port using a Telstar 2F-10 rotary vane vacuum pump and vacuum was set at 1500 ATM/1000u (Figure 2.4, B). All steps were agitated in a Stuart orbital incubator SI500 (Bibby Scientific, UK) at 125 rpm.

Table 2.1: VAD Decellularisation steps

Procedure day	Step	Duration	Agitation (rpm)	Temperature (°C)
1	Detergent	24h±4h	125 rpm	37
2	Wash step	2x 20m		2-6
2-4	Wash step	48-72		2-6
4-5	DNase/ RNase	24h±4h		37
5	Wash step	2x 20m		2-6
5-7	Wash step	48-72		2-6
7-8	DNase/ RNase	24h±4h		37
8-10	Wash step	48-72h		2-6

*h (hour), m (Minute), rpm (revolution per minute),

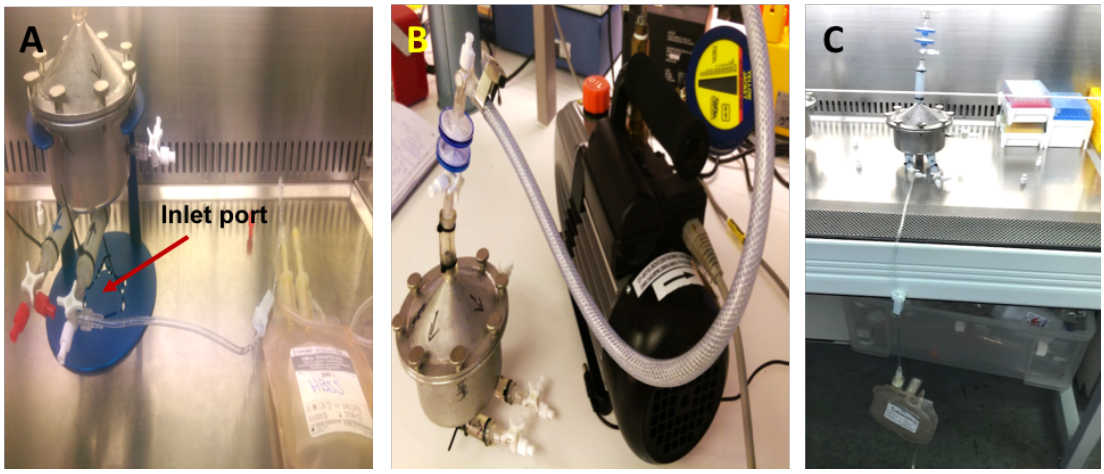

Figure 2.4: Illustration of decellularisation solutions filling, draining and vacuum application.

Reagent filling the chamber through inlet port (A), De-pressurization step using vacuum pump (B), Draining step of reagent (C).

2.4 Histochemical stains of paraffine sections

2.4.1 Paraffin sections preparation, embedding and sectioning

Paraffin sections were used for histochemical staining of native and decellularised scaffolds. Paraffin sections were prepared and stained by technical staff from the division of neuropathology in UCL Institute of Neurology. The staining protocols are briefly described below:

2.4.2 Deparaffinisation and rehydration

Paraffin sections of native and decellularised scaffolds prior to staining were first de-waxed and rehydrated. Slides were first dipped in two changes of Xylene for 3 minutes, then were dipped in (1:1) Xylene: 100% ethanol solution for 3 minutes. Then slides were dehydrated in graded ethanol (100%, 95%, 70%, 50% v/v ethanol), 3 minutes each. The slides were finally rinsed with distilled water.

2.4.3 Haematoxylin and eosin (H&E)

This is a general-purpose stain that was used to differentiate the full cellular details and micro-architecture of tracheal sections pre and post decellularisation. Paraffin sections were first de-waxed and rehydrated in distilled water then immersed haematoxylin (Sigma) for 10 minutes. Slides were quickly dipped in 1% (v/v) acid alcohol and then were rinsed in distilled water for 2 minutes. Then slides were fixed gently in running tap water until the stain stop streaking. Sections were stained with eosin (Fisher scientific) for 1 minute and then washed with distilled water until eosin stops streaking. Finally, sections were dehydrated in graded alcohol, cleared in xylene, and mounted with DPX (Sigma).

2.4.4 Picrosirius red staining

Picrosirius red staining kit (Abcam, ab150681) was used to visualise and assess retention of collagen fibers in tracheal tissue. Picrosirius red is an acidic hydrophilic stain that is widely used to stain collagen I, collagen III, and muscle in tissue sections. The specificity of this dye can be enhanced when used with polarised light microscopy due to its birefringent properties that allows selective discrimination of collagen types. Briefly, paraffin tissue sections were first de-waxed and rehydrated in distilled water. Slides were then immersed in picrosirius red solution and incubated for one hour. Then they were rinsed with two changes of acetic acid solution followed by another rinse in absolute ethanol. The slides were finally dehydrated with two changes of absolute ethanol and then cleared with xylene and mounted with DPX(Sigma).

2.4.5 Safranin O staining

Safranin O is a widely used stain for cartilage GAG and proteoglycans. It binds to the carboxyl and sulphate groups (negative charged) of glycosaminoglycans (GAGs). The intensity of safranin O is proportional to the GAG and proteoglycan contents. Safranin O (Sigma) was used to stain tissue sections of native and decellularised scaffolds as follow, slides were first de-waxed and rehydrated in distilled water. Then slides were stained with Wiegert's iron haematoxylin working solution for 10 minutes and then washed with running tap water. Slides were later stained with 0.05% fast green solution for 5 minutes and then quickly rinsed with 1% acetic acid solution for 10-15 seconds. Then slides were stained with 0.1% safranin O solution for 5 minutes. The slides were finally dehydrated with 95% ethanol, absolute ethanol, and xylene, using 2 changes each, 2 minutes each. Slides are finally cleared in xylene and mounted with DPX (Sigma)

2.4.6 Toluidine blue staining

Toluidine blue (Sigma) was used to stain cartilage GAGs. It is basic thiazine metachromatic dye that has high affinity for acidic tissue components. Briefly, tissue sections were first de-paraffinised and rehydrated. Then slides were stained with toluidine blue working solution (PH 2.0-2.5) for 2-3 minutes. Then slides are washed in three changes of distilled water. Slides were dehydrated quickly through 95% ethanol and 2 changes of absolute ethanol (10 dips each as stain fades quickly in ethanol). Finally, slides were cleared in xylene and mounted with DPX (Sigma).

2.4.7 Periodic acid Schiff (PAS) staining

PAS staining Kit (Roche Ltd) was used to detect the presence of glycoproteins and it also stain basement membrane, it acts by oxidizing compounds that have free hydroxyl group. Slides are first dewaxed and rehydrated in distilled water. Then slides are immersed in 0.5% periodic acid solution for 5 minutes and then rinsed with distilled water. Then the slides were placed in Schiff reagent for 15 minutes. The slides were later washed with tap water for 5 minutes and then counterstained with Mayer's haematoxylin solution for 1 minutes and washed with tap water for 5 minutes. Finally, slides were dehydrated in graded ethanol and cleared with xylene before mounting with DPX.

2.5 Frozen tissue sections preparation, embedding and sectioning in Optimum Cutting Temperature (OCT) compound

Frozen tissue sections were prepared for analysis tracheal tissues components with histochemical stains and immunofluorescence labelling. Tracheal tissues were cut in to 3-4mm pieces and then fixed in 4% (w/v) PFA (Paraformaldehyde Fixative) for 3 hours, then immersed in 30% (w/v) sucrose (Sigma Aldrich, Poole, UK) overnight at 4°C to cryoprotect tissue structure. Tissue sections were then blotted in Dulbecco's Phosphate Buffered Saline (DPBS) (Sigma) to remove external sucrose solution. Cryomolds were filled with Optimum Cutting Temperature (OCT) compound (Cell Path Ltd). Tissue sections were then fully submerged in OCT compound with the desired sectioning plane facing the bottom of the mould, ensuring there were no bubbles around the tissue. Cryomolds were frozen placing them in beaker of a pre-cooled 2-Methylebutane (Sigma) in liquid nitrogen to ensure uniform freezing to a solid white block. Frozen moulds were finally stored at -80°C freezer until sectioned. Thermo scientific Cryotome FE cryostat (Thermo Scientific, Loughborough, UK) was used to section. Frozen blocks were first mounted on to cryocassette using OCT compound and then clamped on the cryostat just behind the blade. The block was then trimmed to remove overlaying OCT compound until the tissue was fully exposed and then 7µm thick tissue sections were picked up on to a positively charged adhesion microscope slides (Thermo Scientific, UK). Slides were then air dried and finally stored at -20°C until further analysis.

2.6 Immunofluorescence staining of ECM components

All steps of incubations were performed in a humidified chamber to avoid drying of tissue sections. Optimization process of the protocol involved working out optimum dilution of primary antibody and it was investigated at 1:50, 1:100, 1:200 and 1: 500 dilutions. In addition, optimum fixation of tissue sections in 4% (w/v) PFA for 5 minutes was utilised in comparison to cold acetone.

Frozen tissue sections were brought to room temperature and then fixed with 4% (w/v) PFA for 10 minutes. Then slides were washed and incubated for 15 minutes with DPBS with 0.1% (v/v) triton X-100 (Sigma Aldrich). The sections were blocked with DPBS (Sigma) containing 1% (w/v) goat serum albumin, 0.1% (v/v) Tween (Fisher Scientific) for 1hour to reduce non-specific staining. The sections were then incubated with primary antibodies diluted with blocking solution overnight at 4°C. The sections were then rinsed with DPBS (Sigma) with 0.1% triton X-100 (Sigma Aldrich) three times 10 minutes each. Fluorophore conjugated secondary antibodies were diluted with blocking solution and applied to the sections, then were incubated for 1 hours in the dark to avoid photo bleaching. Following incubation with secondary antibodies, the sections were washed three times with DPBS for 10 minutes each. Finally, sections were briefly rinsed with DPBS with 0.1% triton X-100 (Sigma Aldrich) three times 10 minutes each and mounted cover-slipped using anti-fade mounting media (Molecular probes, Life technologies). As a negative control, parallel sections where stained by omitting primary antibody addition step and carrying out the staining steps as detailed above. Imaging was performed using Nikon eclipse microscope and Image J software was used to annotate the images. The panel of primary and secondary antibodies used for the immunofluorescence staining of ECM components of native and decellularised tracheal scaffolds are detailed in Table 2.2.

Table 2.2: Panel of primary and secondary antibodies used for ECM immunofluorescence staining.

Primary Antibody	Dilution	Secondary Antibody	Dilution
Rabbit polyclonal Anti collagen-II (ab3092, Abcam, Cambridge, UK)	1:100	Alexafluor 594 goat anti rabbit (Life technologies)	1:100
Rabbit polyclonal Anti- laminin (ab11575, Abcam, Cambridge, UK)			
Rabbit polyclonal anti Fibronectin (ab23516, Abcam, Cambridge, UK)			
Rabbit polyclonal Anti-Elastin (ab21610, Abcam, Cambridge, UK)			
Rabbit polyclonal Anti-Collagen IV (ab21610, Abcam, Cambridge, UK)			
Rabbit polyclonal Anti-Collagen I (MA1-26771, Invitrogen)	1:200		1:1000
DAPI (4′,6-diamidino-2-phenylindole) (Sigma)	1:1000		

2.7 Biochemical Assays

2.7.1 Quantitative analysis of total DNA content

DNA was extracted from tissues using the DNeasy Blood and Tissue kit (Qiagen, Crawley, UK). Approximately 20mg of dry tissue was lysed overnight shaking at 56°C using 180µl ATL lysis buffer and 20µl in proteinase K solution. Then 400µl of (1:1) ethanol/ Buffer AL is added to lysate. The mixture is then pipetted in to a DNeasy mini spin column, where the DNA will be selectively bound to the DNeasy membrane of mini spin column (Qiagen, Crawley, UK), the steps involved centrifugation and washing with buffer and then finally elution in 100µl AE buffer. The Total DNA contents were measured using NanoDrop (ND1000; NanoDrop Products, Wilmington, USA). The concentration of DNA was normalised to the tissue weight for each test and the mean ± SD was determined. Paired t-test was used to determine any statistical difference between native and decellularised tissue (GraphPad Prism).

2.7.2 Quantitative analysis of total collagen content

Collagen was extracted from native and decellularised tissues using Qiuckzyme Total Collagen assay (2B Scientific, Upper Heyford, UK). The assay is based on measurement of collagen specific hydroxy-proline by a chromogenic reaction. Hydroxyproline is a non-proteinogenic amino acid, which in mammals occurs in elastin and collagen. Briefly, 50mg of dry tissue was lysed overnight in 6 M Hydrochloric acid (HCL) (Sigma, Pool, UK) at 95°C. Then the lysate was further diluted (1:75) in 4M HCL (Sigma, Pool, UK). Then after centrifugation the supernatant was oxidised first then mixed with the detection reagent for 1 hour at 60°C to form a chromogen. The absorbance was read at 570nm using Victor X3 PerkinElmer plate reader and compared to 0-300µg/ml standard curves. The concentration of total collagen was normalised to the tissue weight and the Mean ± SD was determined. Paired t-test was used to find any statistical differences between Native and decellularised tissues (GraphPad Prism).

2.7.3 Quantitative analysis of sulphated Glycosaminoglycan (sGAG)

The Blyscan GAG assay Kit (Biocolor Ltd, Carrickfergus, UK) was used to quantify sGAG content of Native and decellularised tissue samples. This is a dye-binding assay to quantify total sGAG. The dye label in this assay is 1,9-dimethylmethelene blue and employed to label sulphated polysaccharides component of proteoglycans or the protein free sulphated glycosaminoglycan chain. Briefly, 25mg of minced dry tissue was lysed using papain-based digestion buffer (Sigma, Poole UK) at 65°C overnight. Then after centrifugation the lysate was diluted 1:50 using distilled water. Then 20µl of the diluted lysate was added to 1ml dye reagent and mixed on a mechanical shaker for 30 minutes. Then sGAG-dye complex was pelleted by centrifugation and unbound dye was drained off. Then 500µl of blyscan dissociation reagent is added to release the bound dye to solution. The Absorbance was finally read at 656nm using Victor X3 PerkinElmer plate reader and compared to a 0-5µg/ml standard curve. For each sGAG assay the concentration of sGAG was normalised to tissue weight and mean ±SD was determined. Paired t-test was used to statistically analyse any significant difference between native and decellularised tissue (GraphPad Prism).

2.8 Mechanical analysis

2.8.1 Uniaxial tensile test

The uniaxial tensile test was used to evaluate the tensile properties of tracheal scaffolds pre and post decellularisation which include: tensile modulus (Young's modulus), ultimate tensile strength (stress at failure) and ultimate tensile strain (extension at failure) using Zwick Roell tensile machine with the help of technical staff from department of mechanical engineering UCL. 10X2mm dumbbell shaped samples were punched out of the trachea at the circumferential direction insuring a homogenous cartilage section (Figure 2.5, A). Then the length, thickness and width were measured using a digital calliper (Figure 2.5, B). Samples were maintained in DPBS prior to test to maintain hydration. Samples were gripped at both ends using serrated type grips with sand paper to prevent slipping during test (Figure 2.5, C). Then uniaxial tension was increased at a constant slow rate (20mm/min) until sample rupture in the middle and all parameters were determined by initially converting the resultant force: displacement curves to stress- strain curves using the following equations:

Stress $\sigma = \frac{F}{A_\circ}$, expressed in Megapascals (MPa)

Strain $\varepsilon = \frac{\Delta L}{L_\circ}$, expressed as a percentage (%)

Where

$\mathbf{F}$ is the measured force concerned, expressed in Newton (N).

$\mathbf{A_o}$ is the initial cross-sectional area of the specimen, expressed in square millimetres(mm^2).

L_o is the gauge length of the test specimen expressed in millimetres (mm^2).

$\mathbf{\Delta L}$ is the increase of the specimen length, expressed in millimetres (mm^2).

Young's (tensile) modulus $\mathrm{E} = \frac{\sigma 2 - \sigma 1}{\varepsilon 2 - \varepsilon 1}$, expressed as Megapascals (MPa).

This is calculated from the slope of the linear reign of the stress strain curve at 10% strain.

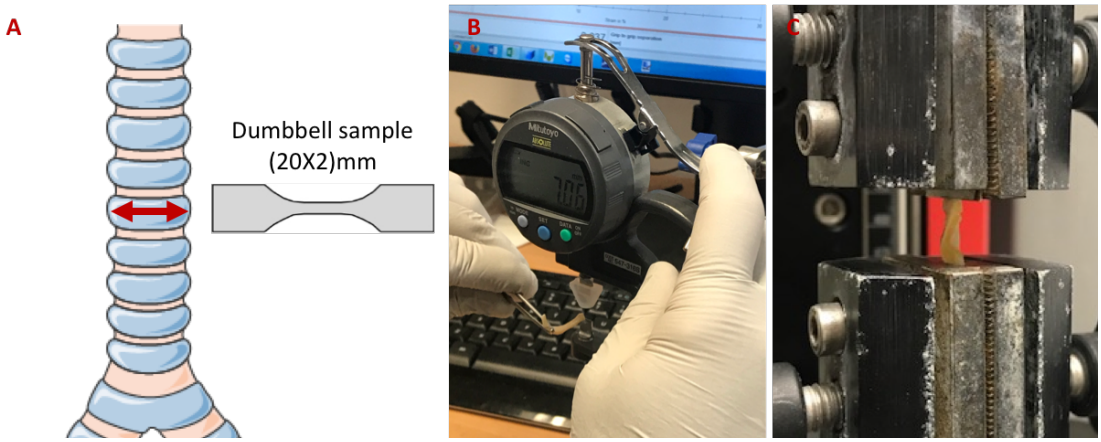

Figure 2.5: Uniaxial tensile test setup.

Dumbbell shaped samples punched out from tracheal cartilaginous rings using a standard cutter (A), Measurement of sample width using digital calliper (B), Then samples are clamped using serrated grips and stretched until failure (C).

2.8.2 Dynamic Mechanical Analysis (DMA) frequency sweep test

Dynamic mechanical analysis (DMA) was used to assess the mechanical and viscoelastic of native and decellularised tracheal cartilage. The analysis was performed by the technical staff at Loughborough University, Wolfson school of mechanical, electrical, and manufacturing engineering utilising the DMA/SDTA861^{e} STAR system (Mettler Toledo).

DMA works by applying a sinusoidal deformation to a sample of known geometry. The sample can be subjected to a controlled stress or a controlled strain. A sinusoidal signal is applied and the complex modulus, loss modulus, storage modulus and phase angle are recorded. For our purpose we have designed a physiologically tailored frequency sweep test to breathing rates to exploit the viscoelastic nature of tracheal cartilage. Since breathing is a cyclical activity consisting of expiration and inspirations repeated over time, the protocol involved running the test at 37C^{o} under displacement control on stretch mode in the circumferential direction with an oscillation amplitude centred at 10% of sample length that was deemed physiological. A sine wave of 5 seconds duration that mimics normal Inspiration: Expiration (I: E) ratio was established. A range of frequencies from (0.1-1Hz) were selected that span over a range of normal and abnormal breathing rates (10-60 breath/minute). Dumbbell shaped samples (20mm lengths X 2mm width) were cut using a special cutter. The sample was mounted between two clamps and subjected to sinusoidal movement (Figure 2.6). To prevent samples from drying, samples were covered with wet tissue paper. With the strain fixed, the frequency of the signal was adjusted to record the material viscoelastic response curves of the samples. The resultant data were analysed using DMA/SDTA861^{e} STAR system (Mettler Toledo) software. In DMA, viscoelastic materials display a phase lag between stress applied and material response (Figure 2.7), δ is the measured phase angle, and for viscoelastic materials it ranges between $0 > \delta > 90^{o}$, while for an elastic material the applied stress and strain are in phase and the δ=0 and for a viscous material the lag of phase angle δ= 90^{o}.

The outcome measures of DMA material properties are

1. Storage modulus (Solid-like/ Elastic-like) M'= M*Cos δ
2. Loss modulus (Viscous-like) M''= M*sin δ
3. Complex modulus M*=M'+M''
4. Tan Delta measure of dumping (energy dissipated by system) (Tan δ) = M'/M'

DMA analyser simultaneously calculates these values at frequency range tested. Then raw data for each measure were plotted versus frequency to compare response curves of both native and decellularised samples. Viscoelastic measures curves of both native and decellularised scaffolds were then analysed semi-quantitively by calculating Area Under the Curve (AUC) using trapezoid rule then a paired t-test was used to determine if there is a significant different of the calculated AUC between the two groups. Paired t-test was used to find any statistical differences between Native and decellularised tissues (GraphPad Prism). A parallel validation experiment was also conducted to demonstrate the reliability of DMA analysis in detecting changes in viscoelastic properties of tracheal cartilage. Since the cartilage is the principle component of the trachea displaying the viscoelastic nature, the experiment involved comparing the difference in the viscoelastic response between native porcine tracheal cartilage and collagenase digested (overnight) cartilage samples. The collagenase treated samples were used as positive control displaying reduced stiffness. This was also confirmed when physically mounting the samples in the DMA analyser. The results of the validation (Figure 2.8) confirmed the ability of DMA analysis to detect a distinct viscoelastic response between native and collagenase treated samples. Collagenase digested samples showed reduced storage, loss and complex modulus and an increase in the tan delta indicating reduced stiffness.

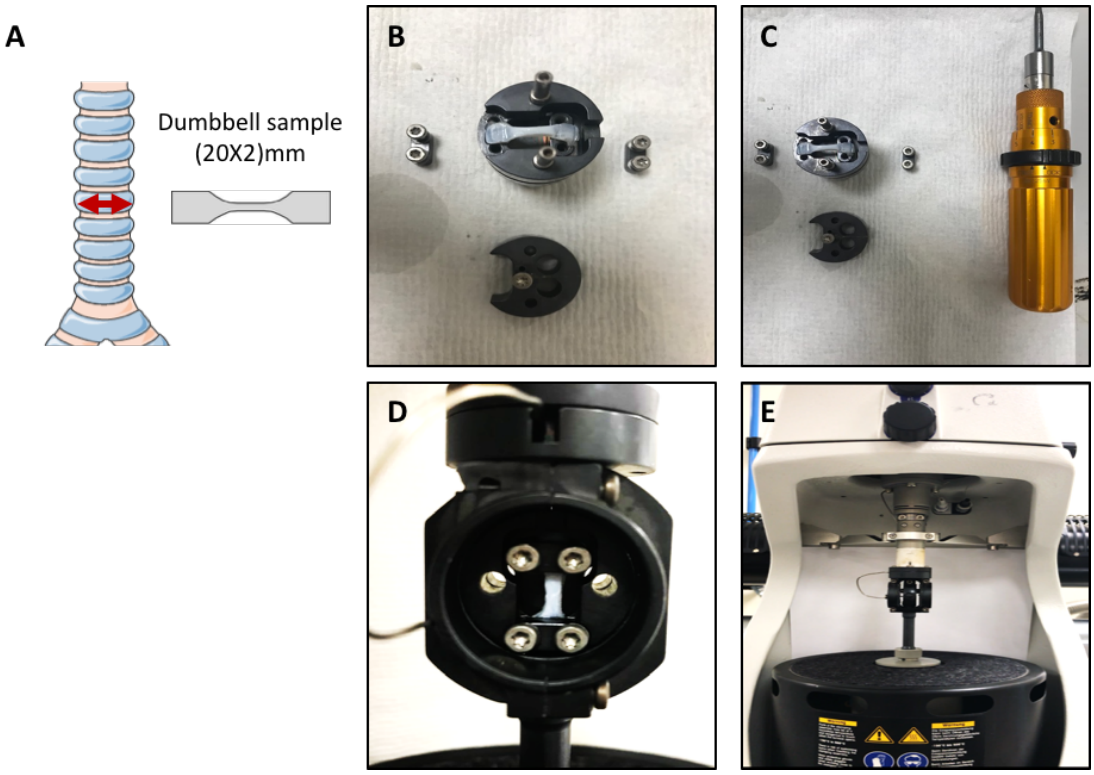

Figure 2.6: Sample setup for Dynamic mechanical analysis (DMA).
Dumbbell shaped samples punched out from tracheal cartilaginous rings using a standard cutter (A). Sample clamped between grips and compiled in the DMA analyser (B-E).

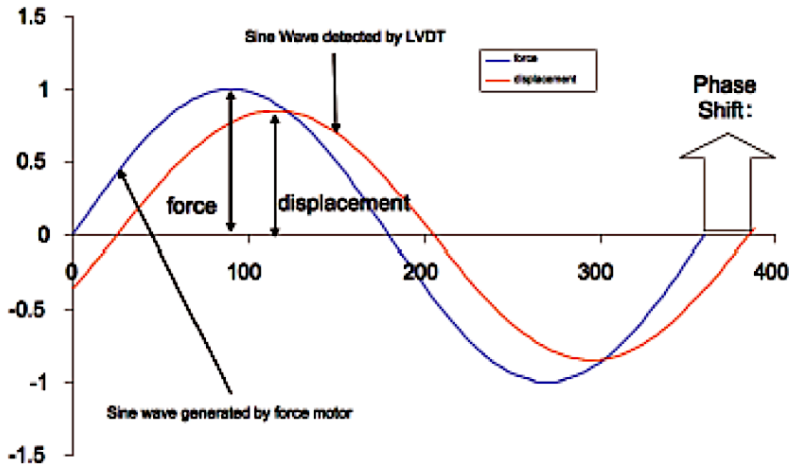

Figure 2.7: Phase shift of a viscoelastic material undergoing cyclical stretch.

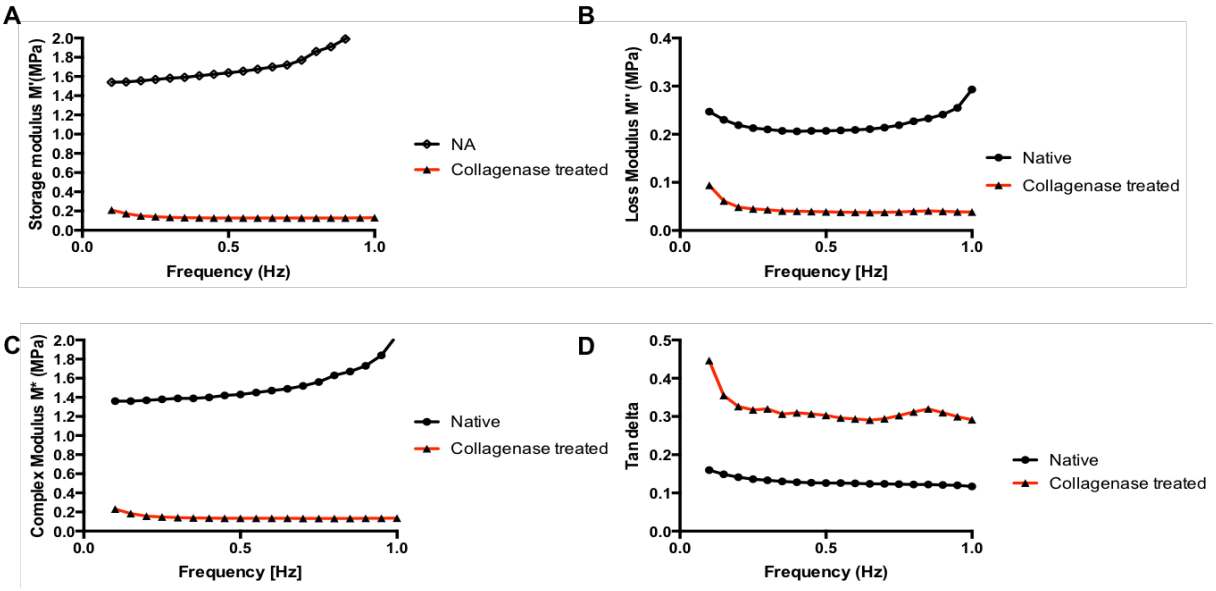

Figure 2.8: validation of DMA analysis utilising collagenase treated tracheal cartilage samples.

DMA analysis comparison between native porcine tracheal cartilage and collagenase treated samples demonstrating distinct viscoelastic response between both groups. The result show reduced storage modulus (A), loss modulus (B), complex modulus (C) and an increase in tan delta (D) in collagenase treated samples.

2.9 Umbilical cord mesenchymal stromal cells (UC-MSCs) culture and routine passage and preservation.

Umbilical cord MSCs (UC-MSCs) were provided by centre for cell gene and tissue therapeutics (CCGTT) facility, Royal free hospital. Alpha minimum essential medium (α-MEM) (GIBCO) supplemented with 10% (v/v) foetal bovine serum (FBS) (GIBCO) and 1% antibiotic antimycotic (Gibco) was used for routine cell culture and passage. It is worth noting that UC-MSCs have been used throughout this project as an alternative source of BM-MSCs, this is because they were a cost effective readily available source for this study.

2.9.1 Cryogenic revival

Cryovials were removed from liquid nitrogen storage and resuspended immediately in warm culture medium upon dissolution from ice to reduce damage to the cell, 20 ml of medium was added and cell suspension was centrifuged at 300xg for 5 minutes and then supernatant was discarded removing freezing solution and finally resuspended in 1ml of complete culture medium. Cells viability and quantitation was done using trypan blue exclusion cell count method. Briefly 10μl of trypan blue was mixed with 10μl of cell suspension, then 10μl of mixture was placed in the haemocytometer and examined immediately under microscope. Viable cells were counted and was calculated using the following equation:

Viable cells/ml = cell count /mm^2 x 10^4 (volume of the chamber) x 2(dilution factor).

Percentage viable cells (%) = (1- (Number of blue cells÷ Number of total cells)) x100.

Then cells were plated at a seeding density of 1000 cell/cm^2 in T175cm^2 cell culture flasks (easy flask Nunc) and medium was changed twice a week.

2.9.2 Routine passage

When 70% confluency of cell culture was reached, cells were washed with DPBS (Sigma), then cells were detached using 7ml TryplE Express dissociation reagent (Gibco) by incubating for approximately 5 minutes at 37^{o}C , 5% CO_2 incubator. Then TryplE was neutralised using equal volume of complete culture medium and topped up with an extra 15ml of complete culture medium for centrifugation for 5minutes at 300xg. Supernatant was discarded and cell pellet was resuspended in 1ml of culture medium. As required cells were either passaged and plated as described above, or used immediately for seeding experiments or cryopreserved for later use.

2.9.3 Cells cryopreservation

Freezing medium was prepared by preparing 20% (v/v) dimethyl sulfoxide (DMSO), (Origen) in 4.5% human serum albumin (HSA). Then equal volume of cold freezing medium was added to cell suspension and cells were aliquoted in 1.8 ml cryovials as (1x106 cells/ml)/each. Cryovials were first cooled slowly by placing them in cryofreezing containers (Mr. Frosty Nalgene) in - 80 mechanical freezer prior to final storage at liquid nitrogen storage.

2.10 MSCs characterisation and immunophenotyping

Cells culture flasks were examined frequently under microscope to confirm that they exhibit the typical plastic adherent spindle shape morphology of MSCs. Prior to cells seeding, cells were immunophenotyped using flowcytometry to confirm that they conform to the international society of cellular therapy (ISCT) minimum criteria for MSCs. Where ≥95% of MSCs must express specific surface antigen, CD105, CD73 and CD90, while lacking (≤2 %) expression of CD45, CD34, CD11b, CD79 alpha or CD19 and HLA class II.

Prior to setting up the staining panel, compensation was performed to correct for spectral overlap between the different fluorochromes used in the staining panel. Compensation was conducted using a negative control (unstained cells) and a set of single stained controls beads (one comp eBeads) stained individually with each antibody used in the experiment). Automatic compensation was then performed using flowcytometry (Novocyte, ACEA biosciences Inc.). Approximately 1-2x10^6 cells were used for staining by first washing and resuspension in DPBS (Sigma) and then 50-100ul of suspension were distributed in prelabelled tubes (minimum of 100x10^3 /tube). Then the staining protocol was set up according to the panel detailed in (Table 2.3), by adding 1µl of each fluorochrome conjugated monoclonal antibody and incubation of samples for 20 minutes in the dark at room temperature. Then samples were centrifugated at 300xg for 5 minutes and supernatant was discarded. Finally, samples were resuspended in DPBS ready for flowcytometry acquisition. Fluorescent minus one controls (FMO) were used to help assess the spread of fluorophores and to set the gates properly.

Multilineage differentiation potentials of UC-MSCs to chondrogenic, adiopogenic and osteogenic lineages have been performed and confirmed by Dr. Ben Weil, from CCGTT.

Table 2.3: MSCs immunophenotyping panel.

	FITC	PE	PE-Vio770	APC
Unstained control	-	-	-	-
Staining mix	CD14/CD19/CD34/CD45/HLA-DR	CD90	CD73	CD105
FMO controls*	-	CD90	CD73	CD105
	CD14/CD19/CD34/CD45/HLA-DR	-	CD73	CD105
	CD14/CD19/CD34/CD45/HLA-DR	CD90	-	CD105
	CD14/CD19/CD34/CD45/HLA-DR	CD90	CD73	-

*FMO controls: Fluorescent minus one controls

2.11 Passive cell seeding protocol

DC scaffolds for this project were either seeded as full tracheal rings 1cm^2 or as 6mm punch biopsies depending on the experiment required. The seeding was done on a 6 well culture plate. Prior to MSCs seeding, DC scaffolds were preconditioned in complete culture medium for 1-3 hours. Then scaffolds were partially surface dehydrated (PSD) in a 37^{o}C, 5% CO_2 incubator for 1-2 hours in order to remove excess moisture and improve cells retention. Then MSCs were resuspended in culture medium and seeded by drop seeding on the abluminal surface of DC scaffolds at a seeding density of 500x10^3 /cm^2 as 25µl aliquots. Then seeded scaffolds were incubated undisturbed for 15 minutes in a 37^{o}C, 5% CO_2 incubator to allow cells attachment. Then cell-seeded scaffolds were topped up with an additional 20 µl of culture media and incubated for an extra 15 minutes before finally being topped up fully with culture media to cover scaffold. Seeded scaffolds were kept undisturbed in the incubator. Media was changed every 3 days by removing 50% of media and replacing it with fresh media. When seeding tracheal rings, total surface area of the scaffold was first estimated to determine the total number of cells required for seeding. Total surface area of the trachea was calculated using the following formula by assuming a uniform cylinder shape of the trachea:

Total surface area = πhd, h = total length, and d = external diameter of trachea. The seeding was attempted by seeding a quarter at a time as displayed in (Figure 2.9).

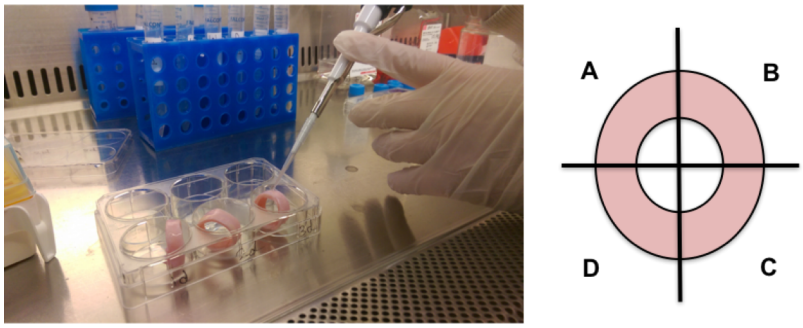

Figure 2.9: Passive cell seeding of UC-MSCs on DC tracheal scaffolds rings. Passive seeding of tracheal scaffolds was attempted by dividing scaffolds to four quarters (A, B, C, D) and seeding a quarter at a time.

2.12 Quantification of cell seeding efficiency (CSE)

Cell seeding efficiency (CSE) quantification was conducted to evaluate the efficacy of the seeding process, it reflects the percentage of cells that were successfully derived and attached to the scaffolds relative to the initial number of cells seeded. Total dsDNA assay using Quant-iT picogreen dsDNA assay Kit (Invitrogen) was used for cell quantification. Picogreen is an asymmetrical cyanine dye that exhibit > 1000-fold fluorescence enhancement upon binding selectively to dsDNA. In this study an indirect quantification approach was adopted, where CSE was derived by calculating the ratio of unattached cells (total dsDNA) in the residual seeding medium to the number of cells (total dsDNA) seeded initially. The analysis was performed according to the manufacturer's instructions. Briefly, (1ng/ml-1ug/ml) DNA standard curve was first prepared using the provided DNA standard. Then serial dilution of known number of cells as well as test samples (unattached) cells from seeding experiment were resuspended in 1ml DNase free water (Millipore) and then lysed by 3 freeze thaw cycles at -80^{o}C freezer. The test samples were diluted 1:10 in TE buffer (200mMTris-HCl,20mM EDTA) provided prior to analysis. Picogreen reagent was diluted 1:200 in TE buffer and was protected from light to prevent photodegradation. Then, working picogreen reagent was added to test and standard samples at a ratio of (9:1) and incubated for 5 minutes before final fluorescent measurement at 480nm and 520nm using the spectrophotometer (Victor X3 PerkinElmer plate reader). Finally, unattached cell numbers were interpolated from standard curve and the cells seeding efficiency (CSE) was calculated using the following formula:

CSE (%) = 1- (Number of unattached cells in medium ÷Number of cells seeded) x100

2.13 PKH26 staining of MSCs

PKH26 is a yellow orange fluorescent dye with long aliphatic tails that can incorporate in to lipid regions of the cell membrane. It is used as a cell linker dye for *in vitro* and *in vivo* cell tracking studies. In this study it was used to pre-label cells for immunofluorescent detection of cells post seeding in to DC scaffolds. PKH26 red fluorescent cell linker kit (Sigma Aldrich) was used. Briefly, cells were first washed with DPBS and then centrifuged at 300xg and supernatant was discarded. The target cell pellet was later resuspended in 500μl of diluent C. In a separate polypropylene tube PKH26 dye solution was prepared by adding 4μl dye to 496μl diluent C. Then the dye solution mix was immediately added to cells suspension and mixed by pipetting and incubated for 5 minutes at room temperature to allow dye incorporation. After that, staining was stopped by adding 10ml of complete culture medium. Finally, the cells were centrifuged at 300xg for 5 minutes and supernatant was discarded and cell pellet was resuspended in culture medium ready for seeding experiments.

2.14 Assessments of viability and metabolic activity

2.14.1 Live /dead staining

Live/ dead staining was used to determine the percentage cell viability on cell seeded scaffolds at different time point of culture. The assay is based on using 2 colour fluorescent cell dyes to discriminate between live and dead cells. In this assay ethidium homodimer-1 and Hoechst 3342 dye (Thermo fisher scientific) were used. Ethidium homodimer-1 (EthD-1) can only enter cells with damaged membranes and binds nucleic acids producing bright red fluorescent signal. Whilst Hoechst 3342 is a cell permeant nuclear stain that binds dsDNA and stains both live and dead cells is used as a counter stain. Whole mount staining of 6mm punch biopsies of DC scaffolds seeded with UC-MSCs were used in this assay. The protocol involves adding EthD-1 (20 ul/10ml culture medium) and Hoechst 3342 at (1:2000) dilution to cell seeded scaffolds and then incubating them in CO_2 incubator for 20 minutes. Then scaffolds are washed with DPBS prior to imaging using confocal microscope (Leica SP8 laser scanning confocal microscope (LSCM) equipped with titanium sapphire multiphoton laser (Coherent Chameleon Vision II Ti: Sapphire laser). Objective: 25x N.A, Excitation AF594.).

2.14.2 MTT assay

MTT (4,5Pdimethylthiazol -2)-2,5Pdiphenyltetrazolium bromide) reagent is used to measure cell growth and viability. The yellow MTT solution is bio reduced by metabolically active cells in part by the action of mitochondrial dehydrogenases to form dark blue formazan insoluble salts and the resulting formazan can be solubilised and quantified by spectrophotometry. MTT assay Kit (Sigma Aldrich) was used on cell seeded scaffolds as per manufacturer protocol. Briefly MTT solution was added in an amount equal to 10% (v/v) of culture volume. Then seeded scaffolds were incubated for 4 hours in CO_2 incubator. Then the solution is removed and formazan precipitate is inspected and lysed using the MTT solvent provided (0.1N HCl anhydrous isopropanol). Absorbance of the resulting solution can be measured at 570nm using spectrophotometer (Victor X3 PerkinElmer plate reader) referenced at 630nm.

2.14.3 Alamar blue assay

Alamar blue reagent is a non-toxic resazurin based solution that is wildly used as an indicator of cells metabolic activity and can be used in to estimate cells proliferation. Resazurin (Blue non-fluorescent) the active ingredient in alamar blue reagent is bioreduced by metabolically active cells to form resorufin a pinkish red highly fluorescent compound that can be quantitated using either absorbance or fluorescent based spectrophotometry. Alamar blue reagent kit (Thermo Fisher Scientific) was used in this study. On which alamar blue was added in 1/10 volume of the culture medium of the cell- seeded DC scaffolds. then seeded scaffolds were incubated for 4 hours in 37^{o}C, 5% CO_2 incubator protected from direct light. Then fluorescence of the resultant solution was measured at 560nm and 590 nm using spectrophotometer (Victor X3 PerkinElmer plate reader).

2.15 KI 67 immunofluorescence staining

KI 67 expression have been used as a marker to predict cells proliferation on DC scaffolds. It is a nuclear protein that is present in all active phases of cell cycle (G1, S, G2, mitosis) but it is absent during resting phase (G0). The assay was performed on whole mount (6mm punch biopsies) seeded scaffolds.

Briefly: cell seeded scaffolds were first fixed with 4% (w/v) PFA for 10 minutes, then washed X3 times with DPBS. Then seeded scaffolds were incubated for 15 minutes with DPBS with 0.1% (v/v) triton X-100 (Sigma Aldrich). After that they were placed in blocking buffer (DPBS containing 1% (v/v) goat serum albumin, 0.1% (v/v) Tween (Fisher Scientific) for 2 hours to reduce non-specific staining. The scaffolds were later incubated with primary antibody AntiKI67(Rabbit monoclonal to KI67, ab16667) diluted (1:300) with blocking solution overnight at 4°C. Then scaffolds were then rinsed with DPBS (Sigma) containing 0.1% triton X-100 (Sigma Aldrich) three times 10 minutes each. Fluorophore conjugated secondary antibody Alexa flour 594 (Invitrogen, mouse anti rabbit mAb) was diluted (1: 1000) with blocking solution and applied to scaffolds and incubated for 1 hour in the dark to avoid photo bleaching. Following incubation with the secondary antibody, whole mount sections were washed three times with DPBS with 0.1%(v/v) triton X-100 (Sigma Aldrich) three times 10 minutes each. As a negative control, parallel seeded scaffolds where stained by omitting primary antibody and carrying staining steps as detailed above. Then DPBS was added to stained seeded scaffolds ready for imaging using confocal microscope (Leica SP8 laser scanning confocal microscope (LSCM) equipped with titanium sapphire multiphoton laser (Coherent Chameleon Vision II Ti: Sapphire laser). Objective: 25x N.A, Excitation AF594.

2.16 Scanning Electron Microscopy (SEM)

Imaging was performed by trained staff in electron microscopy facility, UCL division of biosciences. Samples were initially fixed in Karnovsky's fixative prior to sending them to SEM imaging. The protocol for sample preparation for SEM involves washing samples for three times/10 minutes each in 0.1M phosphate buffered saline (PBS). Then samples were post fixed in 1% osmium tetroxide solution / 1.5% Potassium Ferrocyanine K4Fe (CN)6) in 0.1m cacodylate buffer at 3^{o}C for 1 ½ hrs. After that samples were rinsed in distilled water and dehydrated in a graded ethanol. Then samples were dried using critical point dryer. Dried samples were later mounted on aluminium stubs using sticky carbon tabs. Then the mounted samples were coated using a sputter coater (10nm layer of gold Au). Finally, samples were imaged with FEI quantum series SEM.

2.17 Zs.green Lentiviral transduction of UC-MSCs

To aid visualisation and localization of cells on the DC scaffolds, UC-MSCs were transduced with a lentiviral reporter vector expressing Zs.green fluorescent protein (Vectalys). Zs.green is a bright green fluorescent protein derived from *zoanthus sp.reef* coral that is 4X brighter than the classical eGFP. The transduction protocol was conducted as per manufacturer's instructions with an optimal multiplicity of infection (MOI) = 6. UC-MSCs at P3 were cultured as per routine culture protocol in T175 culture flask until cells reached 50% confluency at the day of transduction. A parallel flask of cultured cells was used to estimate cell number. Then the volume of viral vector required to achieve the target MOI was calculated using the following equation:

Viral vectors volume required (μl) = (Number of cells seeded ÷ viral vector titer (TU/ml) x MOI x1000., (Viral vector titer is provided as per lot number).

The transduction mix was prepared by adding the required volume of thawed viral particles to complete media containing polybrene at (800μg/ml, making a final concentration of 4ug/ml) in 35ml final volume of culture medium. Then medium in the designated cell culture flask was discarded and transduction mix was added slowly and flask was rocked gently side to side to mix viral vector in to target cells. Then cells were incubated with the transduction mix overnight (maximum 16 hrs) in a 37^{o}C, 5% CO_2 incubator. After this step, the transduction mix was discarded and cells were washed with DPBS and replaced by fresh culture medium. The flask was incubated for 2 days before characterisation of transgene expression by flowcytometry (ACEA biosciences Inc.) and fluorescent microscopy (Leica DMI4000B microscope).

2.18 Optical clearing protocol

Optical clearing is a technique that aim to improve visualisation and deep imaging of thick tissue sections by increasing transparency of the 3-dimensional opaque tissues and allowing exogenous staining of tissues. It is based on reducing light scattering by reducing refractive indices mismatch of tissue components. This is done by treating tissue with specialised reagents that either remove some components or change the hydration status of protein and hence modifying the optical properties. In this study BABB (v/v) (1:2 benzyl alcohol: benzyl benzoate) optical clearing mixture to clear Zs.green transduced UC-MSCs seeded on decellularised scaffolds. The protocol briefly involves fixing seeded scaffolds in 4%(w/v) PFA for 10 minutes followed by 3X washes with DPBS 10 minutes each. Then seeded scaffolds were dehydrated in graded ethanol 5 minutes each. After that seeded scaffolds were placed in (1:1) solution of BABB: absolute ethanol for an additional 5 minutes. Finally, scaffolds were placed in BABB mixture and inspected until tissue rendered transparent, this step takes 5-10 minutes, samples were mounted in BABB. Because BABB is a hazardous solvent that can dissolve polycarbonate and damage microscope eyepieces, a specialised chamber slides were prepared using Sylgard-148 (Sigma) to fit the size of scaffolds (6mm punch biopsies) and protect the eyepiece of microscope from contacting BABB during image acquisition. The slides were prepared by placing a cap of a small 2ml screw top vial in the centre of the slide and then Sylgard was applied around the cap using an applicator cartridge and allowed to cure under the fume hood. When Sylgard has cured, the vial cap was removed leaving a central well where microscopy cleared sample can be placed mounted in BABB and covered with a glass cover slip. Finally, samples were imaged within 2 hours using multiphoton microscopy (Leica SP8 laser scanning confocal microscope (LSCM) equipped with titanium sapphire multiphoton laser (Coherent Chameleon Vision II Ti: Sapphire laser) using Objective: 25x N.A. 0.95 IRAPO (Infrared apochromat).

2.19 Image processing

Image processing and rendering throughout this project was performed using both Fiji and Imaris Version 8.4.1 (Bitplane, AG).

2.20 RNA extraction from UC-MSCs seeded DC scaffolds

RNA extraction of cell seeded DC scaffolds was performed to perform RNA sequencing and RT-PCR for differential gene expression analysis of cells seeded on DC scaffolds. Four different RNA extraction methods were compared to establish a method that give the highest RNA yield and quality suitable for analysis. The methods were:

2.20.1 Extraction method A

In this method RNeasy lipid tissue kit (Qiagen) was used. It is based on the initial cryopulverisation of cell seeded scaffolds (6mm). the protocol was conducted as per manufacturer's instructions. Briefly cells seeded scaffolds (6mm punch biopsies), where first cryopluverised on a liquid nitrogen precooled tissue pulveriser to reduce sample to fine powder. Then grounded sample was immediately transferred to nuclease free Eppendorf tube and 1ml of Qiazol (Qiagen) reagent was added. The sample was later incubated for 5 minutes at room temperature to permit complete dissociation of nucleoprotein. This step was followed by the addition of 200μl chloroform and sample was shacked vigorously for 15 seconds. Then sample was centrifuges at 12000xg at 4^{o}C for 15 minutes. Then the upper aqueous phase containing RNA was transferred to a new Eppendorf tube and 1 volume of 70% ethanol was added. Finally, RNA was purified using RNeasy spin column by performing several washes of the column membrane using buffer RW1 and buffer RPE (x2) and centrifugation at 8000xg for 15 second each. Finally, the RNA is eluted in 20 μl RNase free water.

2.20.2 Extraction method (B)

This method is based on initial detachment of cells from seeded scaffolds using TryplE (Gibco) prior to RNA extraction and purification using column based PicoPure kit (Acturus). The process started by initially washing 1cm^2 seeded DC scaffolds with DPBS. Then adding 25 μl of TryplE cell dissociation reagent on top of scaffolds followed by 5 minutes incubation in 37^{o}C, 5% CO_2 incubator. Then TryplE was neutralised with 1ml complete culture medium and cells were pelleted with centrifugation at 300xg for 5 minutes. Then cell pellet was resuspended in 100μl extraction buffer (XB) provided and cells were resuspended by pipetting. Then cells were incubated at 42^{o}C for 30 minutes and then centrifuged at 3000xg for 2 minutes. Supernatant was carefully transferred to a new RNase free microtube and 100μl of 70% ethanol was added to cell extract and mixed well by pipetting. Then as per manufacturer's protocol, spin column was first preconditioned with conditioning (CB) buffer for 5 minutes at room temperature and then centrifuged at 16000xg for 1 minute in the provided collection tube to remove conditioning buffer. Then cell extract ethanol mixture is pipetted in the conditioned column and is centrifuged at 100xg for 2 minutes to bind RNA followed by 30 seconds centrifugation at 16000xg to remove the flowthrough. Then spin column was washed initially with 100μl wash buffer (W1) and centrifuged at 8000xg for 1 minutes, followed by two extra washes using wash buffer 2 (W2) and final centrifugation at 16000xg for 2 minutes to remove wash buffer. The final step involves transferring spin column to a new 0.5ml RNase free microtube and pipetting 15μl elution buffer (EB) directly to membrane with the tip touching the membrane gently to ensure buffer delivery. The elution buffer is incubated in the column at room temperature for 1 minute before final centrifugation at 16000xg for 1minute to elute RNA.

2.20.3 Extraction method (C)

This extraction method is based on direct lysis of cells on scaffolds using Trizol reagent. TRIzol reagent and phasemaker tube complete system (Invitrogen) was used. Phasemaker tubes were centrifuged for 30 seconds at 16000xg prior to use. Then 1ml of ice cold TRIzol reagent was added to ($1cm^2$) seeded scaffolds to directly and was pipetted up and down to lyse attached cells. The lysate was later centrifuged for 5 minutes at 12000xg at 4°C and the supernatant was transferred to a new RNase free microtube. Then lysate was transferred to a phasemaker tube and incubated for 5 minutes for complete dissociation of nucleoproteins complex. After that 200μl of chloroform was added and the tube was shacked vigorously and then incubated for 2-3 minutes before centrifugation at 12000-16000xg at 4°C for 5 minutes. Then the upper aqueous layer containing RNA was carefully transferred to a new microtube. Precipitation of RNA involved an addition of 10μg of RNase free glycogen (Invitrogen) to coprecipitate with RNA, then adding 0.5ml isopropanol to the aqueous phase and incubating it for 10 minutes before centrifugation at 12000xg at 4°C for 10 minutes. The supernatant was discarded and the gel-like pellet was resuspended and washed with 1ml 75% ethanol. Then the sample was centrifuged for 5 minutes at 7500xg at 4°C and supernatant was discarded. Finally, the pellet was allowed to air dry for 10 minutes before final resuspension in 20μl of RNase free water and incubation in a heat block set at (55-60)°C for an extra 15 minutes to solubilise RNA.

2.20.4 Extraction Method (D)

This method is based on using RNA protect (Qiagen) and cell scarping to detach cells from scaffolds prior to RNA extraction using column-based method PicoPure kit (Acturus). The protocol incubating cell seeded scaffolds (1cm2) with 1 ml of RNA protect for 5 minutes at room temperature and then scrapping and transferring detached cells suspension to a new microtube. Then the sample was centrifuged at 300xg for 5 minutes to pellet cells. The supernatant will be discarded and sample will be processed following same steps as per PicoPure kit instructions that was detailed in extraction method (B) above.

2.20.5 Genomic DNA elimination from RNA preparations

TURBO DNA-free kit (Invitrogen) was used to remove contaminating genomic DNA from the extracted RNA prior to analysis. The kit utilises DNase enzyme that have high catalytic activities and marked affinity for DNA that digest contaminating DNA to levels below the limit of detection of downstream analysis like RT-PCR and RNA sequencing. The protocol was conducted as per manufacturer's instructions. On which, 0.1 volume of TURBO DNase buffer was added and mixed with the extracted RNA sample. Then 1μl of TURBO DNase enzyme was added to the sample and was incubated at 37°C for 30 minutes. Then 0.2 volumes of DNase inactivation reagent was added, mixed properly, and incubated for 5 minutes. Finally, the sample was centrifuged at 1000xg for 1.5 minutes and supernatant containing RNA was transferred to a new RNase free microtube for storage at -80°C or for further analysis.

2.21 Assessment of RNA quality

RNA extracted from seeded scaffolds quality was checked based on yield, purity, and integrity. The RNA yield and purity were measured using a NanoDrop spectrophotometer (ND1000; NanoDrop Products, Wilmington, USA) with a 1.50μl sample volume. RNA, ssDNA and dsDNA absorb at 260nm.The purity is estimated based on the UV absorbance ratio 260/280 and 260/230. Ideally a pure RNA preparation should have an absorbance reading of (1.8-2.1) for 260/280 ratio and (2-2.2) for 260/230 ratio. Deviations from these values is indicative of the presence of impurities that might interfere with downstream analysis. The integrity of RNA which is a measure of RNA degradation was also checked by trained staff in UCL (Institute of child health genomics center) using the Agilent 2200 bioanalyzer (Agilent technologies). The bioanalyzer is based on a fluorescent-tag microfluidic capillary electrophoresis. The RNA will be separated in the channels of the microfabricated chip based on molecular weight and will be ultimately detected with a fluorescent detector. The integrity is expressed as an RNA Integrity Number (RIN). RIN is assigned based on the ratio of ribosomal RNA, 28S and 18S rRNA. A RIN number higher than 7 is indicative of high integrity RNA.

2.22 RNA sequencing (RNAseq)

RNA sequencing was conducted for comparative differential gene expression analysis of MSCs seeded on DC tracheal scaffolds at day 3 of culture. RNA was extracted from scaffolds as per method (D) as it gave the highest yield and quality RNA. RNA sequencing was conducted by trained staff at UCL institute of child health (ICH) genomics centre.

2.22.1 Wet lab

For library preparation 1ng of good quality total RNA (RIN ~8) were amplified using a template switching method to generate full length cDNA This was followed by conversion to sequence-ready libraries using the NEB DNA Ultra™ II FS workflow coupled with IDT xGen adaptors. Multiplexed libraries were sequenced on an Illumina NextSeq 500 run (75bp single read, plus 8bp UMI) after being pooled in equimolar quantities, calculated from Qubit and Tapestation fragment analysis.

2.22.2 Data analysis

Reads were demultiplexed and fastq files were generated using Illumina's bcl2fastq software (v2.19). Resulting fastq were pre-processed to remove adaptor contamination and poor-quality base-calls (fastp v0.19.3.3) before guided alignment to the human genome (build, UCSC hg38) using RNA-STAR (v2.5.2b). UMI contained in the sequencing reads were used to deduplicate the data (JE-Suite v1.2.1, a fork of Picard Tools) before reads-per transcript were estimated using FeatureCounts (v1.6.3). Count data was then analysed for differential expression using the Bioconductor SARTools (v 0.1.0), a DESeq2 wrapper. All sequence and annotation was downloaded from the Illumina iGenomes repository: http://emea.support.illumina.com/sequencing/sequencing_software/igenome.html. Genes were considered as differentially expressed if the adjusted P value (BH corrected with benjamini Hochberg algorithm) was <0.05 and had a fold change of ≥ log2 fold change.

2.23 Bioinformatics

To further analyse DEGs data sets, data were filtered using more stringent cut-off values to select only for the most significant differentially expressed genes (DEGs) where only DEGs with ≥ (±1.5) log2 fold change and an adjusted P value of ≤ 0.001 were considered. Data analysis pipeline of differentially expressed genes (DEGs) were conducted using different bioinformatics tools , these included:

2.23.1 Functional gene ontology (GO) enrichment analysis.

Gene ontology enrichment analysis is a de facto standard bioinformatics tool that is used with high throughput techniques like RNA seq to facilitate the interpretation of the large sets of gene expression data produced. The analysis is based on classifying gene sets and inferring their biological functions based on the predefined gene ontology classification terms (Cellular process, molecular functions, and cellular component). The gene ontology consortium (http://www.geneontology.org), is a worldwide consortium that define ontologies to annotate the biological knowledge we have or predicted for a given gene function. Then it will identify the most significant overrepresented (enriched) GO terms to infer a functional profile of the most significant terms that describe the data set. GO enrichment analysis was performed using GOrilla web-based application (Eden et al., 2009), Version used (April 2019). One GO category was only considered in this study, which is GO- Biological processes.

2.23.2 Pathway enrichment analysis

Ingenuity pathway analysis IPA software (Qiagen), was used as a tool for this type of analysis. Data set as lists of DEGs gene identifiers (upregulated and downregulated) with their corresponding gene expression values were uploaded to the software. The software will analyse the RNA expression data by mapping each gene identifier to its corresponding gene object in the ingenuity pathway knowledge base (IPKB) and relating it to the body of information in the context of known biological responses, regulatory networks, and higher order response pathways. Then it will identify biological processes, canonical pathways,

upstream regulators and signalling networks that were most significantly enriched in the data set. In all analysis Fisher exact test was used to calculate a P value, that reflect the probability that each biological function assigned to data set was due to chance alone. It will also make prediction about the direction of the observed change (activation or inhibition) by comparing the observed direction of change in the data set to what is expected from literature. The overall activation/ inhibition status is calculated using Z score algorithm, which denotes the negative log of the P value derived from Fisher exact test. In this study IPA was used to perform an initial core analysis function of the data set followed by a comparative analysis function of the identified subgroups.

2.23.3 Identification of selected gene families that are associated with MSCs paracrine therapeutic effects.

The data set was specifically investigated for the differential expression of selected gene sets representing known bioactive paracrine factors produced by MSCs. These factors were compiled from literature and have been found to mediate cells therapeutic potentials and tissue repair. The selected gene families included factors associated with ECM remodelling, anti-fibrotic, anti-scarring, anti-apoptotic, chemoattraction, supportive and immunomodulatory effects. The gene families investigated were grouped as:

1. ECM remodeling
2. Chemokines and interleukins
3. Growth factors (A)
4. Growth factors (B)/ adhesion and other paracrine factors.

2.24 Quantitative real time polymerase chain reaction (RT-PCR).

RT-PCR was used to confirm RNA sequencing data. It was performed by qstandard, UCL facility trained staff. Four differentially expressed genes were selectively verified using RT-PCR. The genes of interests included VEGFA (Vascular endothelial growth factor A), BMP4 (Bone morphogenic Protein 4), PTGES(PGE2) and CSF2. YHWAZ (Tyrosine 3-Monooxygenase/Tryptophan 5-Monooxygenase Activation Protein Zeta) was used as housekeeping gene to normalise gene expression values. Samples of cells growing on DC scaffolds gene expression were compared to cells pre-seeding (Control group).

2.24.1 Reverse transcription

Up to 500 ng of RNA were reverse transcribed using the Qiagen Quantitect reverse transcription Kit (Qiagen) in a 20 μL reaction according to the manufacturer's instructions. The steps involved adding genomic DNA (gDNA) wipeout buffer (1X) to the template RNA and an incubation step at 42^{o}C for 2 minutes. Then the template RNA samples were placed immediately on ice. The reverse- transcription master mix was prepared by mixing quantiscript reverse transcriptase (1μL), Quantiscript RT buffer (4μL at 1X) and RT primer mix (1μL). The reverse transcription master mix was then added to the template RNA samples and incubated for 15 minutes at 42^{o}C. Then the inactivation step of the reaction involved incubation of samples at 95 for 3^{o}C minutes. The completed reaction was diluted 10-fold with 0.5 μg/mL tRNA in Rnase free water.

2.24.2 RT-PCR

Four microliters of cDNA were amplified in a 20μL reaction using customer-supplied probe mix and TaqMan assays according to the manufacturer's instructions (Life technologies). All samples were run in duplicates.

Amplification parameters:

1. Hold at 50°C for 2 minutes.
2. Enzyme activation 95°C for 2 minutes.
3. Denaturation at 95°C for 15 seconds.
4. Anneal/extension 60°C for 1 minute.
5. Number of cycles: 45 cycles

2.24.3 Data analysis

Relative quantification was performed the Pfaffl method (Pfaffl, 2001) an amendment of the delta delta C_T method ($\Delta\Delta C_T$) which accounts for differences in primer efficiencies to increase reproducibility. Normalised expression ratio was calculated using the following formula:

Normalised Relative Quantity = $E^{\Delta CT(\text{Gene of interest})} / E^{\Delta CT(\text{Reference gene})}$

C_T = Cycle threshold value

E = Primer efficiency

$\Delta C_T = C_{T\,(\text{Control average})} - C_{T\,(\text{Average CT})}$.

2.25 General statistical analysis

Throughout this thesis, data were statistically analysed using Graph Pad prism software. The statistical tests used are denoted in each Results section and associated figure legends in each Results chapter. The statistical significance was accepted considering a 5% confidence level. All data sets were tested for normality using a Shapiro-Wilk test in order to determine the appropriate statistical analysis used. The number of biological repeats for each experiment is indicated in the figure legends of the data presented. At least three technical repeats were maintained in all experimental setup where possible.

3 Biochemical and biomechanical evaluation of decellularised tracheal scaffolds

3.1 Introduction

Decellularisation of tracheal extracellular matrix (ECM) is a front-running strategy to produce scaffolds for tracheal tissue engineering. To date the clinical use of decellularised tracheal scaffolds have been documented in several proof of concept cases and on compassionate basis with promising and varying success levels (Macchiarini et al., 2008, Jungebluth et al., 2011, Elliott et al., 2012, Gonfiotti et al., 2014, Hamilton et al., 2015, Elliott et al., 2017).

The most common decellularisation methods for tracheal tissues were based on the use of Detergent Enzymatic Method (DEM) (Macchiarini et al., 2008, Conconi et al., 2005, Meezan et al., 1975). However (DEM) decellularisation protocols are lengthy protocols that require serval weeks (> 3 weeks) before a scaffold is ready for final processing and hence making it less desirable for clinical translation (Baiguera et al., 2010a). Therefore, Vacuum Assisted Decellularisation (VAD) was developed by P.Lange and colleagues as a modification of (DEM) by incorporation of intermittent vacuum (negative pressure) steps to improve reagent impregnation and have resulted in an accelerated decellularisation protocol of (9-11) days (Lange et al., 2015). The VAD protocol is currently in use by our team for clinical translation of tracheal bioengineering (Elliott et al., 2017).

Overall, the ultimate goal of any decellularisation protocol is the removal of cellular and immunogenic materials, while minimising damage to the extracellular matrix (ECM) components as well as preservation of structural, biomechanical and bioactive cues that are necessary to guide tissue remodelling and integration (Gilbert et al., 2006).

Trachea serves an important structural function maintaining the patency of the airway despite changes of intrathoracic pressure during breathing (Roberts et al.,

1997). Therefore, one of the crucial requirements of tracheal decellularisation protocols is maintenance of the structural integrity and mechanical properties of its components, as this will facilitate post-operative extubation and might help avoiding the need for long term intraluminal stenting. Despite the initial encouraging success of few tracheal tissue engineering cases in patients, published follow-up reports of decellularised constructs reported suboptimal mechanical properties requiring dilatation and stenting intermittently (Elliott et al., 2012, Hamilton et al., 2015, Gonfiotti et al., 2014, Badylak et al., 2012). Though, the mechanisms of the pathology leading to this biomechanical weakness is not yet fully understood, but it draws attention to importance of mechanical characterisation of decellularised tracheal scaffolds to assist understanding of the mechanisms involved and aid clinical translation.

Pioneers studies regarding structural and mechanical stability of VAD or even DEM decellularised tracheal scaffolds have mainly focused on using uniaxial tensile test (stretch to failure) in order to assess mechanical stability post decellularisation (Lange et al., 2015, Butler et al., 2017a, Jones et al., 2014, Philipp et al., 2014, Partington et al., 2013). Although this type of assessment is useful in determining the overall tensile strength of the tissue, it is limited in that it only reflect the linear elastic properties of the tissues and is unable to fully describe the complex nonlinear mechanical properties of tracheal tissues and in particular cartilaginous rings (Rains et al., 1992, Teng et al., 2008, Suki, 2014). Moreover, there are considerable variations in the reported data that make comparison between studies a challenging task as a result of different experimental setups and lack of standardised technique to perform and report data (Boazak and Auguste, 2018).

Two other interesting studies on tracheal decellularised scaffolds mechanical stability have employed a new approach by measuring compliance of the whole tracheal graft from pressure volume curve relationships using CT scanner (Haykal et al., 2012, Den Hondt et al., 2017), Although this method has many advantages such as: it allows physiological simulation of the passage of air during breathing and allow testing the graft as a whole, as well as being a non-destructive method that opens possibilities of automation in data collection.

However, a major drawback of the approach is that it is not practical for routine use and quality check-up.

Moreover, mechanical parameters for pressure volume relationships have not yet been well established for isolated trachea and the predictability of tracheal collapse need to be first clarified (Aoki and Moriya, 2018). Furthermore, other studies have reported conflicting findings that either showed maintenance of mechanical properties post decellularisation (Lange et al., 2015, Butler et al., 2017a) or loss of mechanical properties (Partington et al., 2013, Haykal et al., 2012).

In light of the above findings, there is an identified demand to improve biomechanical assessment tools of decellularised tracheal scaffolds and a need to seek better measures that can predict structural and mechanical stability of tissues post decellularisation. Therefore, the goal of this chapter was to tackle this particular issue by performing initially a comprehensive biochemical and mechanical assessment and re-evaluation of our inhouse VAD tracheal decellularisation protocol using conventional methods. And secondly exploring new mechanical measures that could reflect the mechanical functional demand of tracheal cartilage which can be performed using simple practical mechanical tools.

The process of selecting a new mechanical measure started by exploring and prioritising the most critical property that could better inform about the tracheal cartilage *in vivo* mechanical strategy. Tracheal cartilage from a mechanical stand point displays a nonlinear, anisotropic viscoelastic mechanical properties (Butler et al., 2000, Safshekan et al., 2017a). Viscoelastic material property of the cartilage rings is an important feature that allows rings to resist deformation in spite of changes of intrathoracic pressure which occur during respiration. It is a term used to describe materials that display both viscous and elastic deformation and thus exhibiting time dependant strain behaviours and stress-stiffening (Bartlett et al., 2016). It is governed by the biphasic composite structure of cartilage where collagen fibers (Solid) entraps large aggregates of hydrophilic GAGs (viscous) (Rains et al., 1992). On which the viscoelastic response results

from the frictional interactions between solid and viscous phases (Butler et al., 2000).

In vivo tracheal rings are exposed to both sustained loads that result from contraction of the trachealis muscle during steady breathing or higher magnitude transient loading rising from coughing or other situations resulting in maximum respiratory flow (Boazak and Auguste, 2018). The response of cartilage to these type of deformation is dependent on its viscoelastic properties (Safshekan et al., 2017b, Rains et al., 1992, Boazak and Auguste, 2018).

In light of these fundamental concepts, this study has prioritised and targeted characterising the viscoelastic properties as a relevant new measure to reflect mechanical stability of tracheal cartilage post decellularisation. In literature, viscoelastic properties studies of tracheal tissues have considered examining the time dependant (tube law) of trachea as whole or focused on tracheal mucus with very rare recent studies available that have investigated this property (Safshekan et al., 2017a, Safshekan et al., 2017b) on native human trachea.

In this thesis Dynamic Mechanical Analysis (DMA) was used to assess viscoelastic properties of native and decellularised tracheal scaffolds. DMA is an automated technique that applies sinusoidal (periodic) force or strain and report material response and mechanical properties as a function of temperature or frequency. DMA is wildly used for characterisation of non-biological materials such as polymers and plastics (Yamashita et al., 2001) and several reports have documented its use in biomechanical characterisation of other biological tissues for example: myocardial tissues (Ramadan et al., 2017), bladder (Barnes et al., 2015) and articular cartilage (Lawless et al., 2017). However, its use in tracheal mechanical evaluation in general and in tracheal bioengineering has not been described yet.

3.1.1 Research aims and objectives

The aim of the work presented in this chapter is to evaluate biochemical and biomechanical structural integrity of the tracheal scaffolds following vacuum assisted decellularisation technique (VAD) (Lange et al., 2015). The highlight of this study is to assess mechanical viscoelastic properties of tracheal cartilage using Dynamic Mechanical Analysis (DMA) as a new tool of mechanical characterisation of tracheal tissue.

Objectives:

1. To evaluate efficacy of cellular clearance post VAD decellularisation.
2. To assess the structural integrity and Extracellular Matrix (ECM) components of decellularised trachea scaffolds
3. Biomechanical evaluation of both tensile and dynamic viscoelastic properties of VAD decellularised tracheal scaffolds.

3.1.2 Experimental approach

The study involved a comparative assessment of the chemical and biomechanical characteristics of decellularised tracheal scaffolds in relative to native trachea. Paired samples of native and decellularised trachea were produced by dividing intact native trachea in to equal halves, with one half undergoing VAD decellularization process. Native trachea served as a matched control. All grafts remained in tubular form during decellularization and were not cut or divided into smaller pieces.

Two sample types were investigated:

1. Adult porcine tracheae were procured commercially and were decellularised by previously described Vacuum Assisted Decellularisation (VAD) method (Lange et al., 2015) as detailed in materials and methods section. Throughout this thesis, porcine tracheae were used to test, establish, and validate methods. Porcine trachea is a widely used large animal model for tracheal research that has comparable morphology and physiology to human (Goh et al., 2018, Murison et al., 2009).

2. Adult human tracheae from cadaveric donors procured by the National Health Service Blood and Transplant (NHSBT) team with appropriate consent, following the current clinical practice for non-living tissue retrieval in the U.K (HTA license 1108). Ethical approval was obtained through the National Research Ethics Committee (REC reference: 11.LO.1522). Human tracheae were decellularised following the same VAD decellularisation protocol by the NHSBT team.

Paired tracheal samples were assessed for:

1- The gross macroscopic appearance and structure.

2- Histoarchitecture and cellular clearance

3- Quantitative and qualitative assessment of ECM components.

4- Mechanical evaluation of tracheal cartilage using:

   i) Uniaxial tensile test

   ii) Dynamic mechanical analysis (DMA) of the viscoelastic properties as detailed in chapter 2.

3.2 RESULTS

3.2.1 Macroscopic evaluation of tracheal scaffolds

Porcine tracheal scaffolds post decellularisation retained the macroscopic structure of the native tissue. Decellularised scaffolds appeared de-coloured (White) and cartilage rings were visible and maintained an open lumen and resisted collapse under light pressure (Figure 3.1). There was no observed statistical difference in the internal diameter (Id) and the External diameter (Ed) of both sagittal and coronal planes post decellularisation as shown in (Figure 3.2). Similarly, examination of human tracheal scaffolds post decellularisation revealed retention of the macroscopic structure of the native tissue (Figure 3.3). interestingly, it was also noted that the colour of human decellularised scaffolds varied between white and brownish grey as shown in (Figure 3.3, C, D). This finding could be attributed to insufficient washing of blood from tissue pre-decellularisation.

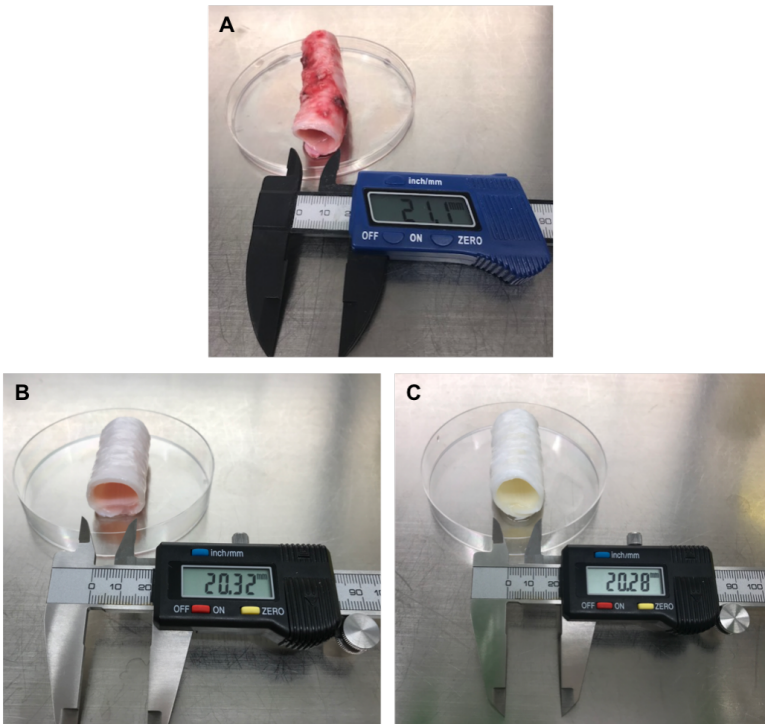

Figure 3.1: Macroscopic view of porcine trachea pre and post decellularisation.

Native trachea after harvest (A), Native trachea after PBS rinses and removal of excess tissue (B), and decellularised trachea (C).

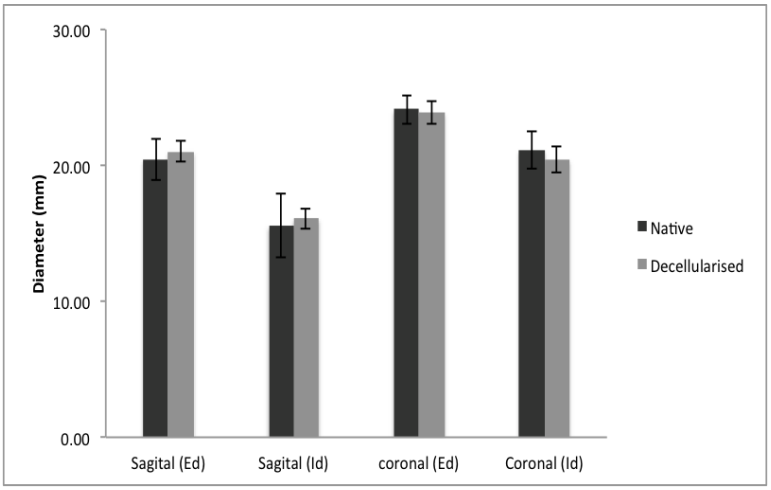

Figure 3.2: Average Internal diameter (Id) and External diameter (Ed) of porcine trachea pre and post decellularisation.

No difference observed in diameter (sagittal and coronal planes) between native and decellularised trachea. Values represent mean ± SD, N=8.

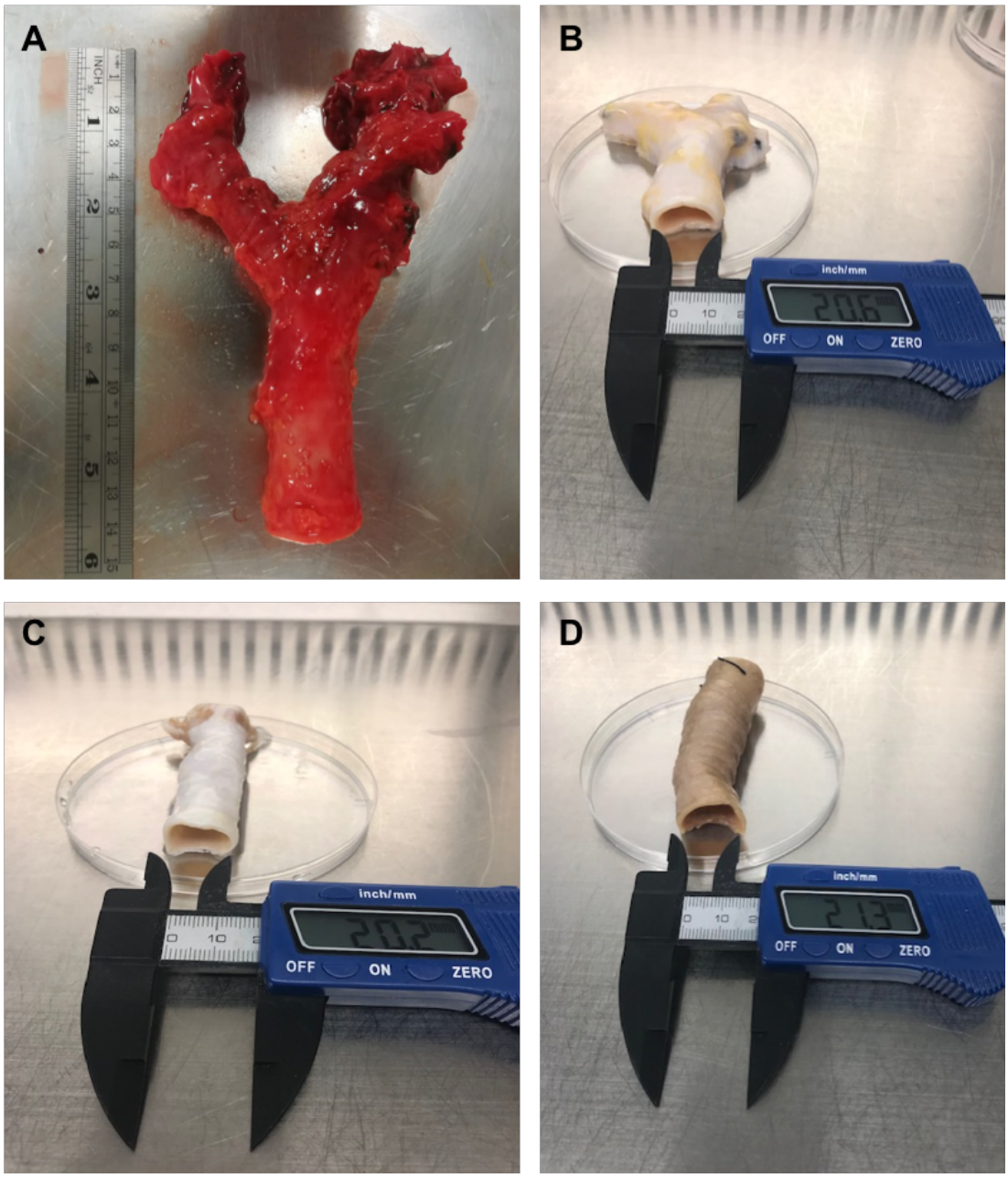

Figure 3.3: Macroscopic view of human trachea pre and post decellularisation.

Native human trachea after harvest (A), Native trachea post PBS rinses (B) and decellularised trachea (C, D). Sometimes, human tracheae appear brownish in colour post decellularisation (D).

3.2.2 Assessment of cellular clearance and histoarchitecture

The efficacy of cellular clearance post decellularisation was assessed mainly by two criteria: (1) absence of visible nuclear material on tissue sections stained with haematoxylin and eosin (H&E) and 4′, 6-diamidino-2-phenylindole (DAPI) immunofluorescent staining; and (2) quantification of double-stranded dsDNA using NanoDrop (ND1000.USA) spectrophotometer.

3.2.2.1 Haematoxylin and eosin (H&E) staining of native and decellularised trachea

Histological examination using H&E staining of porcine samples as shown in (Figure 3.4) demonstrated that native trachea (Figure 3.4, A-C) displayed the typical tracheal histoarchitecture of a pseudostratified ciliated epithelium (mucosal layer) and a submucosa containing mixed glands and smooth muscle (Figure 3.4, A), a hyaline cartilage and an outer adventitia (Figure 3.4, C). The cellular components were clearly visible in all layers and stained blue. Following decellularisation process, tissue sections (Figure 3.4, D- F) appear to retain the overall histoarchitectural organisation: mucosa, submucosa, hyaline cartilage, and adventitia (Figure 3.4, E). there appears to be a complete clearance of intact nuclear materials from luminal epithelium (mucosa) and the outer adventitia, however nuclear materials remained within the cartilaginous layer (Figure 3.4, F). Occasional nuclei were also observed within the submucosal gland (Figure 3.4, D).

In human tracheal samples subjected to VAD, H&E stained sections as shown in (Figure 3.5) revealed similar findings. The overall histoarchitectural organisation of trachea post decellularisation was preserved (Figure 3.5, E) and decellularised tissue sections displayed a complete loss of nuclear material from luminal epithelium (mucosa), submucosa (Figure 3.5, D) and outer adventitia. But nuclei were still observed within the more dense hyaline cartilaginous layer (Figure 3.5, F).

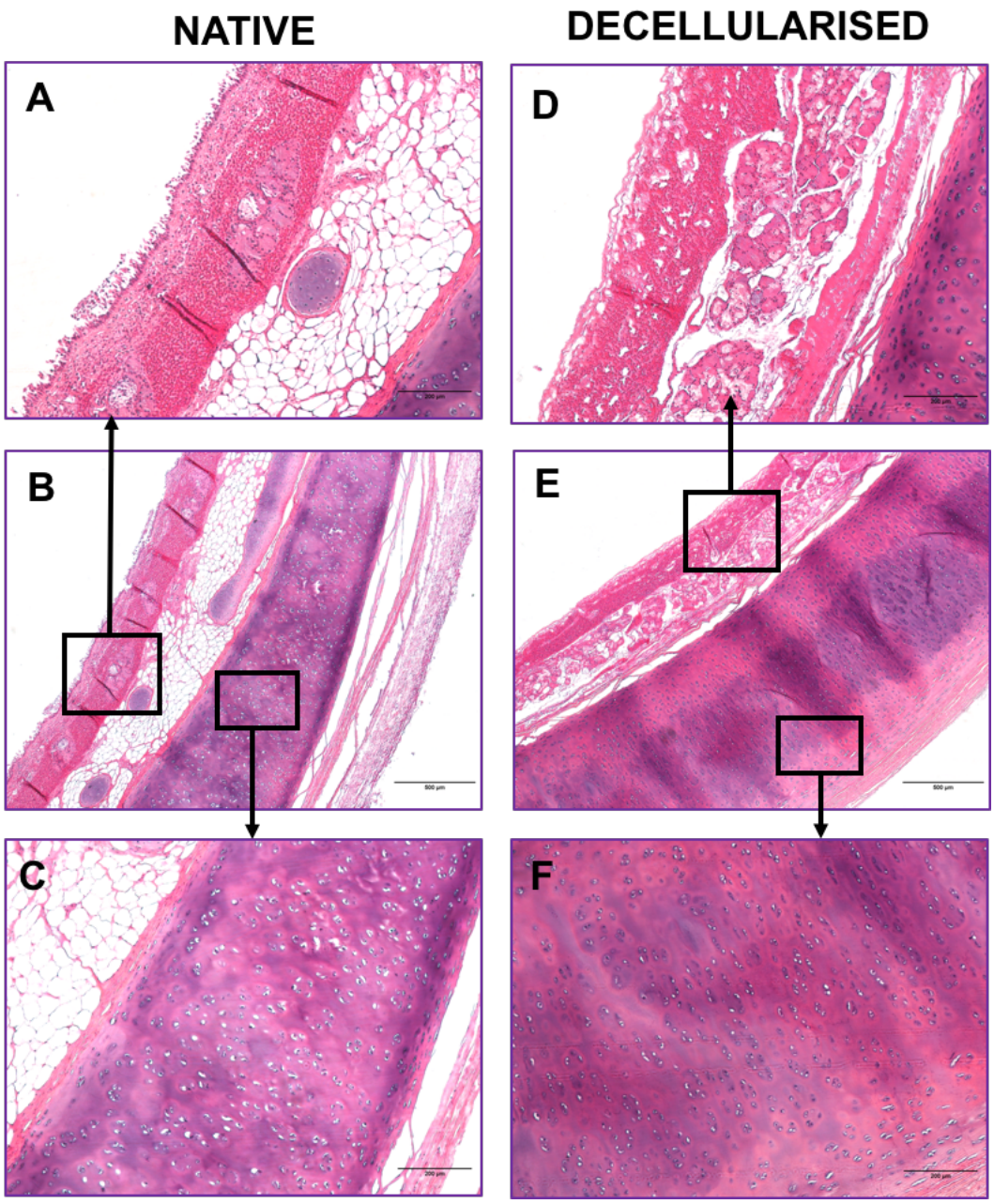

Figure 3.4: Haematoxylin and eosin (H&E) staining of native and decellularised porcine trachea.

Native trachea (A, B, C), displays a pseudostratified ciliated epithelium with submucosal gland (A), and hyaline cartilage (C). In the decellularised trachea (D, E, F), there appears to be a complete loss of the epithelium but nuclear materials were still present in submucosal glands (D). The nuclear material remains within the hyaline cartilage (F). Scale bar (B, D) X4 magnification = 500 μm, (A, C, D, F) X10 magnification, scale bar =200μm.

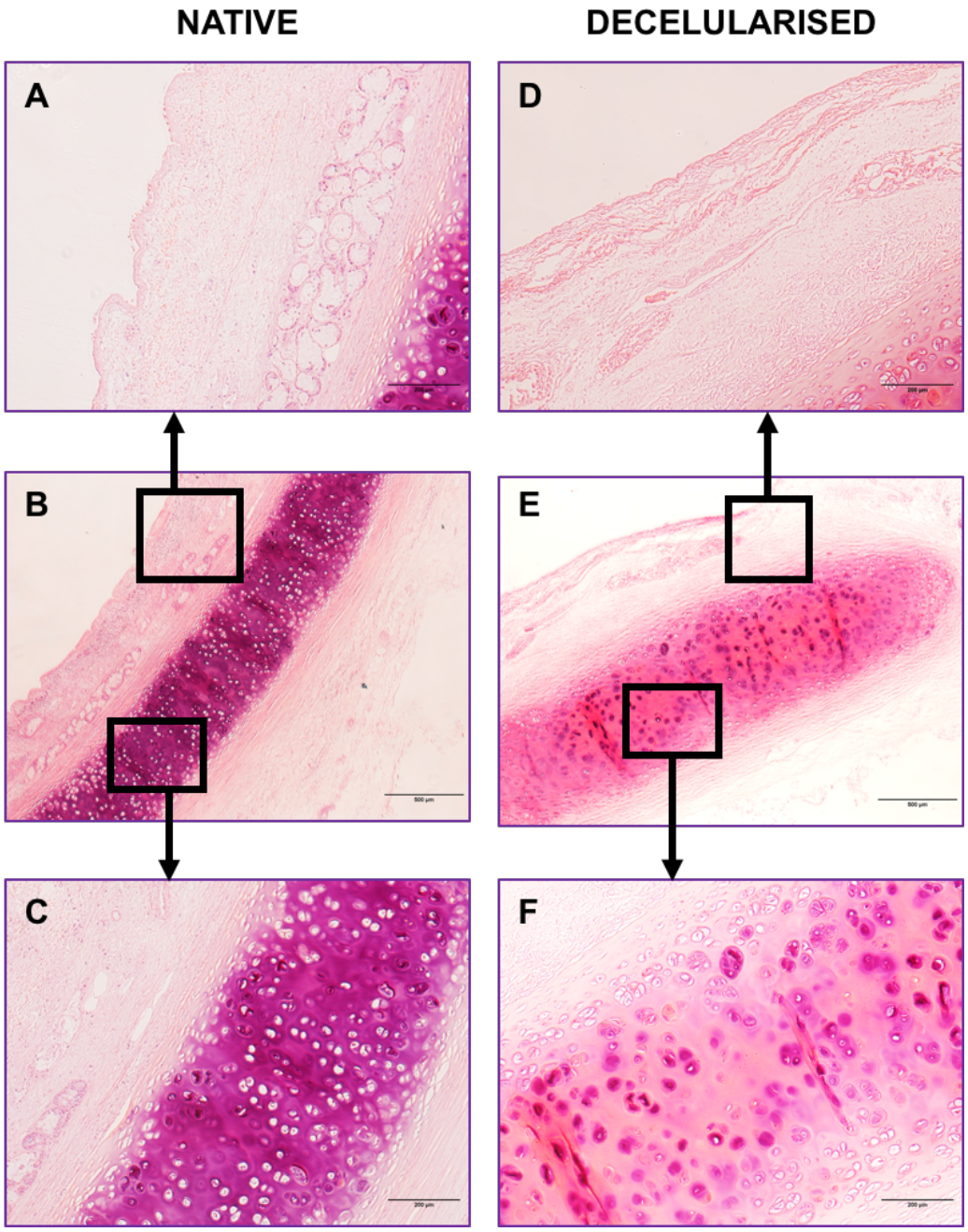

Figure 3.5: Haematoxylin and eosin (H&E) staining of native and decellularised human trachea.

Native trachea (A, B, C), displays a pseudostratified ciliated epithelium submucosal gland (A), and hyaline cartilage (C). Decellularised trachea (D, E, F), there appears to be a complete clearance of the epithelium and cells in submucosal layer (D). The nuclear material remains within the hyaline cartilage (F) . (B, D) X4 magnification, Scale bar = 500 μm, (A, C, D, F) X10 magnification, scale bar = 200μm.

3.2.2.2 DAPI immunofluorescence staining

DAPI immunolabelling was used to label residual dsDNA materials for both porcine and human tracheal samples as shown in (Figure 3.6) and (Figure 3.7) respectively. The results are consistent with our H&E staining findings.

The staining revealed absence of nuclear materials in the epithelium (mucosa) and confirmed that the localisation of residual nuclear materials in the decellularised group was predominantly in hyaline cartilage and it was also noted that nuclear materials were still detected in submucosa and in particular within submucosal glands (Figure 3.6, C, D) and (Figure 3.7, C, D).

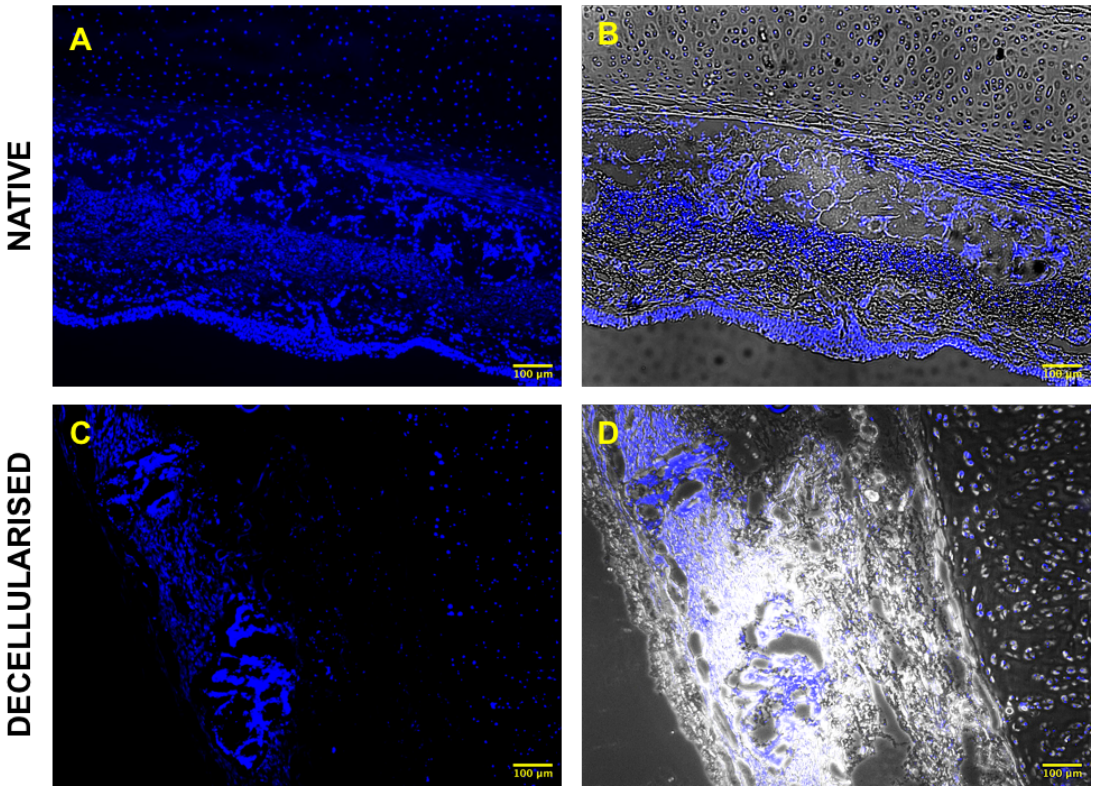

Figure 3.6: DAPI immunostaining for residual DNA materials in porcine trachea samples.

Native trachea sections (A, B) show positive DAPI staining in mucosa, submucosa, and cartilaginous layer. Decellularised sections demonstrate loss of nuclear staining in mucosa but maintenance of nuclear staining within cartilage and occasionally within submucosal glands (C, D). Scale bar= 100μm, B and D represent fluorescent image overlay on bright field view of tissue section.

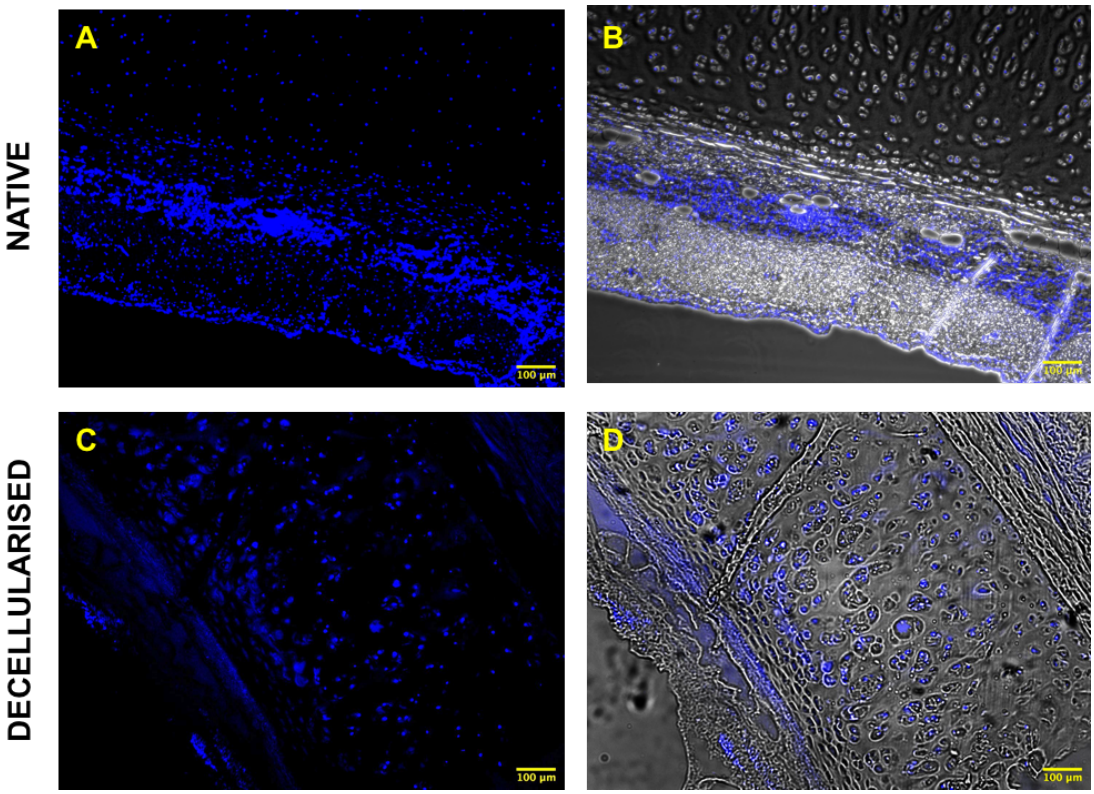

Figure 3.7: DAPI immunostaining of residual nuclear materials in human tracheal samples.

Native trachea sections (A, B) show typical nuclear staining in mucosa, submucosa, and cartilaginous layer. Decellularised sections display loss of epithelia in mucosa but nuclear staining is still evident within cartilage layer and occasional DNA smear over ECM in submucosal layer (C, D). Scale bar =100μm, B and D represent fluorescent image overlay on bright field view of tissue section.

3.2.2.3 Total dsDNA level in native versus decellularised scaffolds

Quantitative analysis of dsDNA in porcine tracheal samples revealed a significant reduction of total DNA level post decellularisation as shown in (Figure 3.8, A, B). The amount of DNA level in decellularised tracheal scaffolds was 210 ± 71 ng/mg of dry tissue weight, $P \leq 0.0001$ compared to native tissue level of 1052 ± 260ng/mg dry tissue weight.

Turning now to total DNA level in decellularised human tracheal scaffolds as displayed in (Figure 3.9, A, B), a significant reduction ($P \leq 0.0001$) on total DNA was also confirmed, the mean total DNA of decellularised tissue was 24.15 ± 19.70 ng/mg dry tissue weight compared to native tissue level of 393.8± 162.4ng/mg. Interestingly human residual DNA level was much lower than detected in porcine decellularised scaffolds.

Taken all together these findings suggest that VAD decellularisation protocol was able to significantly reduce total DNA level in decellularised scaffolds, yet prominent intact nuclei were still visualised in the tissue mainly within the hyaline cartilage and sometimes within the submucosa in addition to that nuclear materials were still seen smeared over submucosal layer. Efficiency of nuclear clearance was also found to be variable between pig and human tracheal tissues.

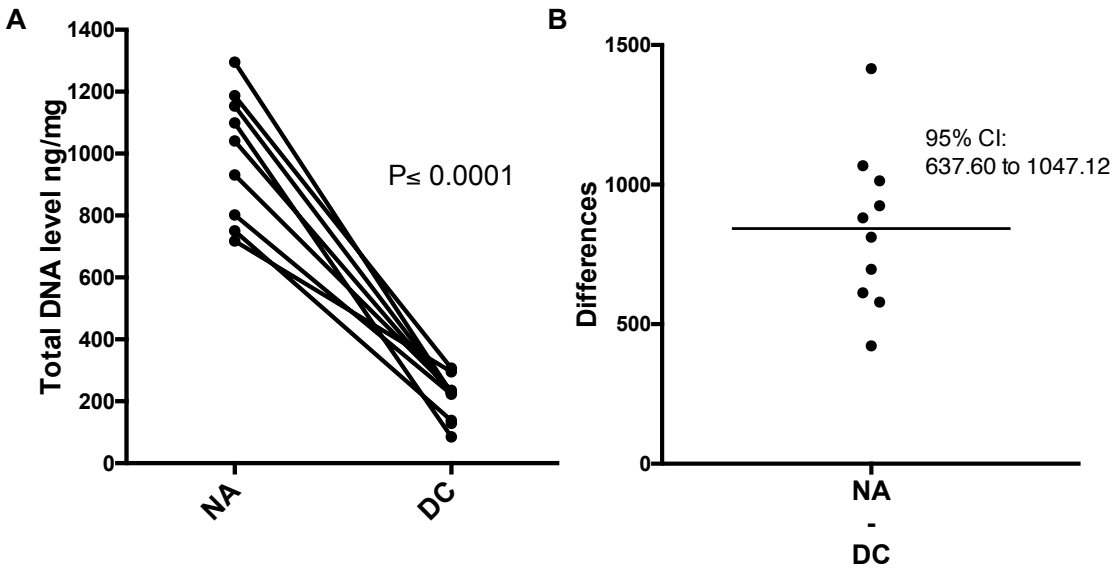

Figure 3.8: Quantification of total dsDNA level in native and decellularised porcine trachea.

There is a significant reduction in total DNA content post decellularisation. Residual DNA level in decelluarised tissues was 210 ± 71 ng/mg of dry tissue weight. P≤ 0.0001. Values are Mean ± SD. N=10. (B) represents the differences between pairs and shows the 95% confidence interval (CI) of the differences between means.

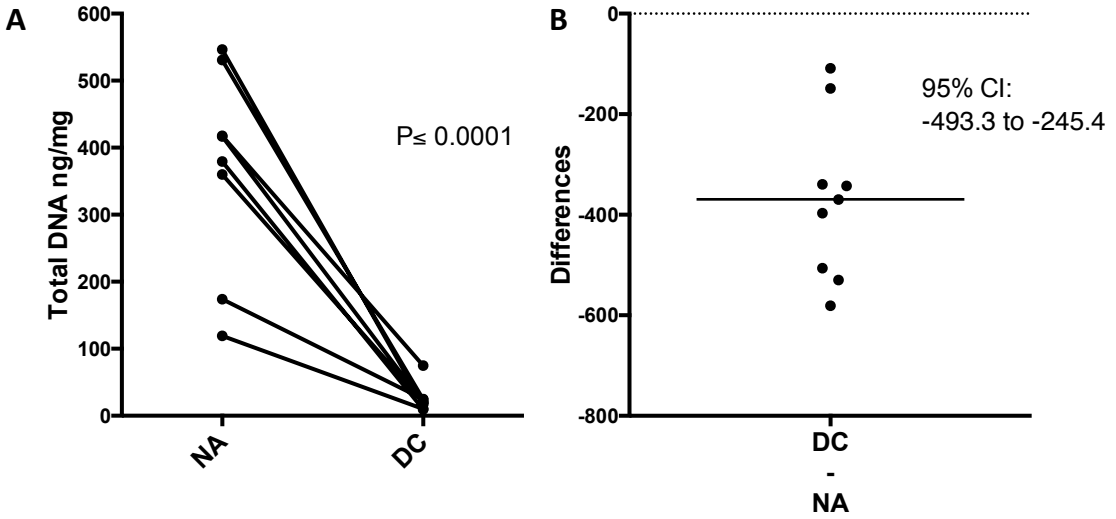

Figure 3.9: Quantification of total dsDNA level in native and decellularised human trachea.

There is a significant reduction in total DNA content post decellularisation. Total DNA level in decelluarised tissues was 24.15 ± 19.70 ng/mg of dry tissue weight. P≤ 0.0001. Values are Mean ± SD. N=9. (B) represents the differences between pairs and shows 95% confidence interval (CI) of the differences between means.

3.2.3 Quantitative and qualitative assessment of extracellular matrix (ECM) components

3.2.3.1 Assessment of collagen level

Quantification of total collagen in decellularised porcine tracheal scaffolds indicated that there was no statistical difference between native and decellularised tissues as shown in (Figure 3.10), the collagen level in native tissue was 70.67± 13.83 µg/mg compared to 77.31± 14.29 µg/mg in decellularised tissue. Histochemical staining with picrosirius red (Figure 3.11) revealed an intense pink-red staining within mucosa, submucosa and adventitia indicating retention of fibrillar collagen I and collagen III. A lighter diffuse pinkish staining of cartilaginous layer was also noted, this could be a result of the non-specific staining of other proteins within the ECM. Retention of collagen was further confirmed with specific immunostaining of collagen II as displayed in (Figure 3.12).

Similarly, quantification of total collagen in human tracheal scaffolds revealed no significant difference between native and decellularised samples (Figure 3.13). Collagen level in decellularised scaffolds was (292.9 ± 98.85) versus (233.8 ± 127.1). Picrosirius red staining displayed a similar pattern of porcine data showing a strong pink-red staining of collagen I and collagen III, specifically within Mucosa, submucosa and adventitia and a more lighter staining of the cartilaginous layer, these were all retained post decellularisation (Figure 3.14).

Collagen II was also preserved post decellularisation as evident in (Figure 3.15).

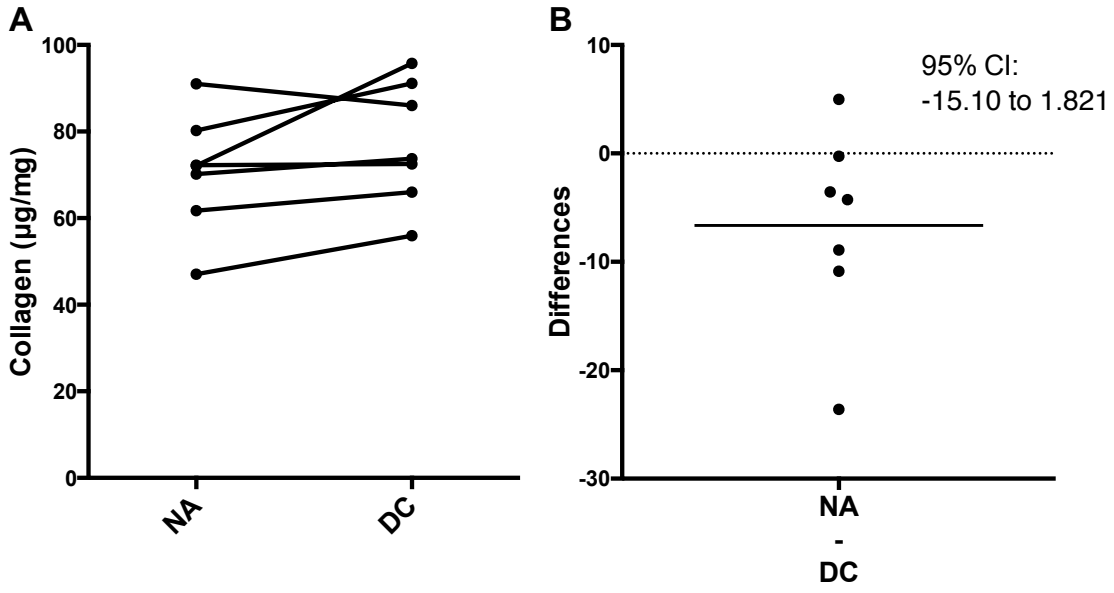

Figure 3.10: Total collagen level in native and decellularised porcine trachea.

Results showed no significant difference in the total collagen content between native and decellularised trachea. N=8. (B) represents the differences between pairs and shows 95% confidence interval (CI) of the differences between means.

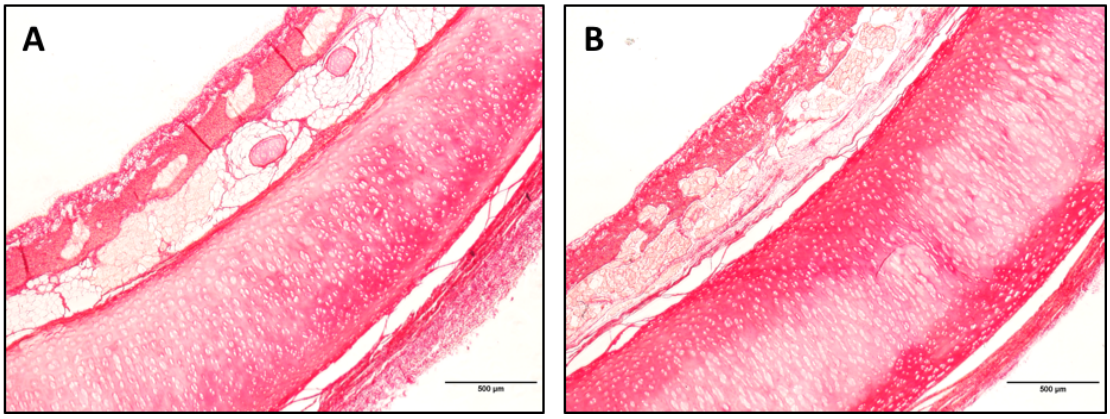

Figure 3.11: Picrosirius red staining of native and decellularised porcine trachea.

(A) native trachea, (B) decellularised tracheal scaffolds. A positive red staining is observed in mucosa, submucosa, and adventitia with a lighter diffuse staining in the hyaline cartilage. Scale bar =500µm

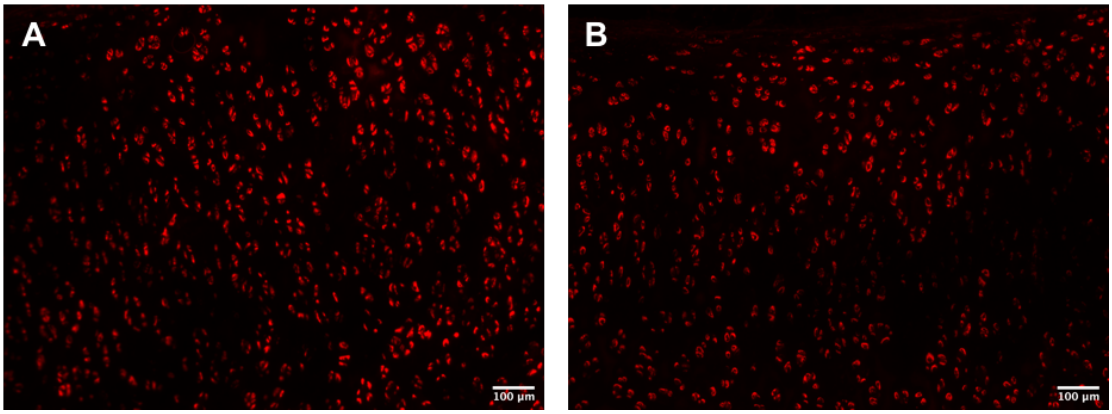

Figure 3.12: Immunostaining of collagen II in native and decellularised porcine trachea.

A) Native trachea, (B) decellularised trachea. Collagen II staining was preserved post decellularisation. Scale bar =100μm.

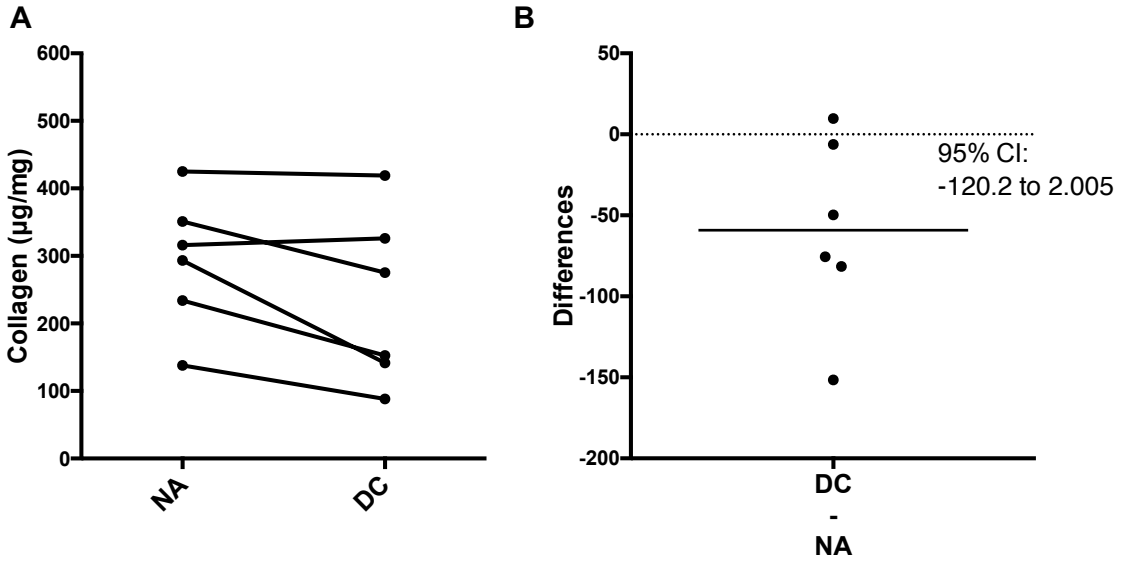

Figure 3.13: Total collagen level in native versus decellularised human trachea.

Graph shows no statistically significant difference in total collagen content between native and decellularised trachea. N= 6. (B) represents the differences between pairs and shows 95% confidence interval (CI) of the differences between means.

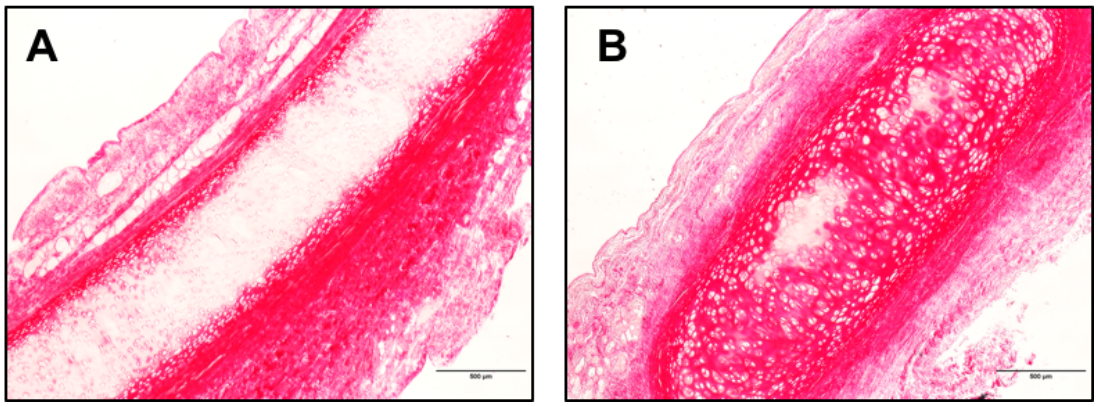

Figure 3.14: Picrosirius red staining of native and decellularised human trachea.

(A) Native trachea, (B) decellularised. In native and decellularised trachea positive strong pink-red staining is detected within (mucosa, submucosa, and adventitia) . A dispersed staining pattern is seen in the decellularised scaffolds hyaline cartilage layer. Scale bar =500μm.

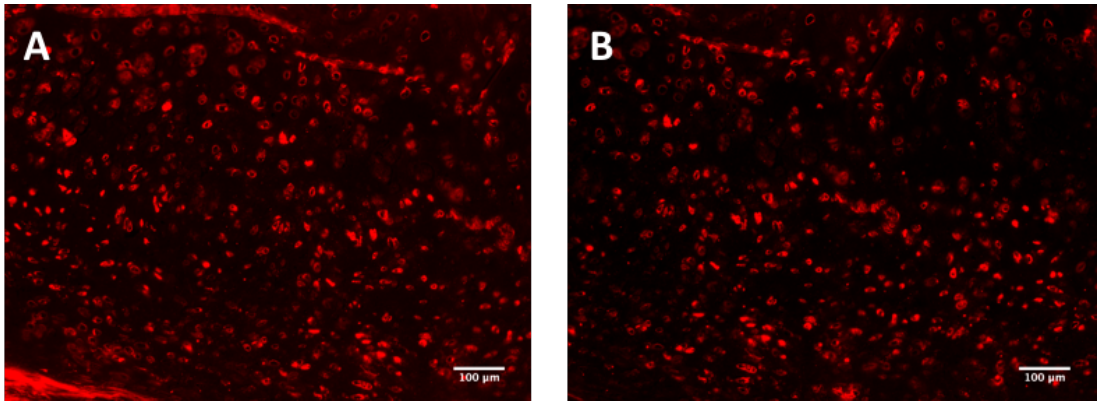

Figure 3.15: Immunofluorescence staining of collagen II in native and decellularised human trachea.

(A) native trachea, (B) decellularised tracheal scaffold. Collagen II was preserved post decellularisation. Scale bar=100μm.

3.2.3.2 Assessment of sGAG level and glycoproteins

Quantitative measurement of sulphated glycosaminoglycan and glycoproteins in porcine tissue showed no detectable difference post decellularisation process as indicated in (Figure 3.16, A & B). The sGAG level in decellularised scaffolds was 97± 15 µg/mg and 88.1± 24 µg/mg in native tissue.

Special histochemical staining for sGAG and proteoglycan confirmed our findings and showed retention of sGAG and proteoglycans post VAD , where : safranin O staining shows a deep red staining of cartilaginous layer (Figure 3.17, A & B), toluidine blue staining revealed a deep violet metachromatic staining (Figure 3.17, C & D) and a strong pink PAS staining is detected within cartilaginous layer (Figure 3.17, E & F). This staining pattern was conserved post decellularisation.

Turning now to human tissue samples, the examination of total sGAG and proteoglycan level revealed similar results, no statistically significant difference between native and decellularised tissue was observed as shown in (Figure 3.18, A & B). The mean sGAG level in native tissue was 49.48 ± 15.13 and 41.71 ± 15.92 in decellularised tissue. Histochemical staining of human tissue samples (Figure 3.19) confirmed conservation of sGAG and proteoglycan post decellularisation. Safranin O showed maintenance of the deep red staining within the cartilaginous layer, mucosa, and submucosa (Figure 3.19, A & B). In addition to conservation of the positive toluidine blue and PAS staining of decellularised tissue sections (Figure 3.19, C, D, E, F).

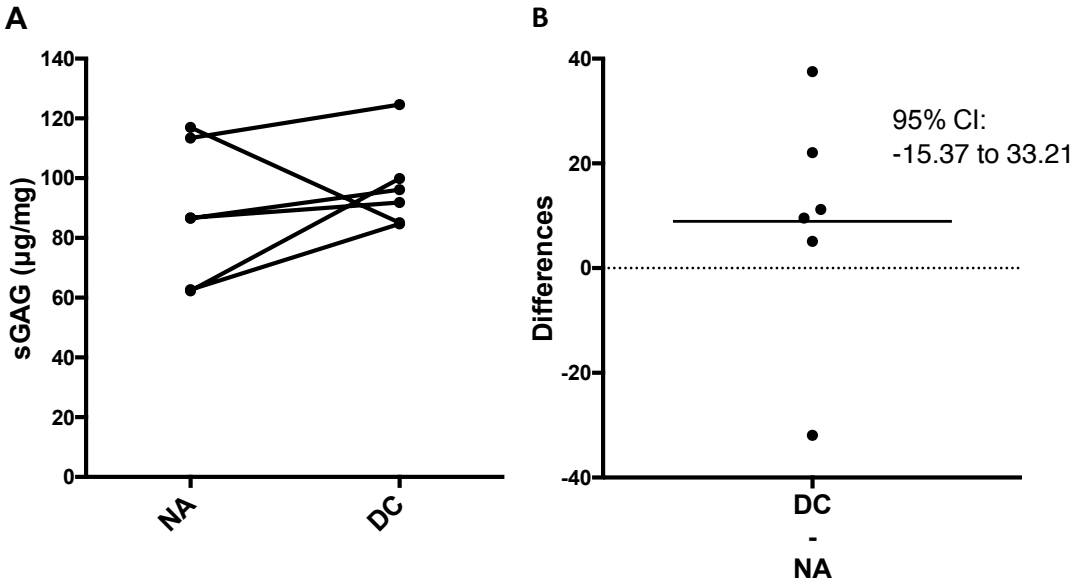

Figure 3.16: sGAG level in native and decellularised porcine tracheal scaffolds.

Results showed no significant difference in the total collagen content between native and decellularised trachea. N=6. (B) represents the differences between pairs and shows 95% confidence interval (CI) of the differences between means.

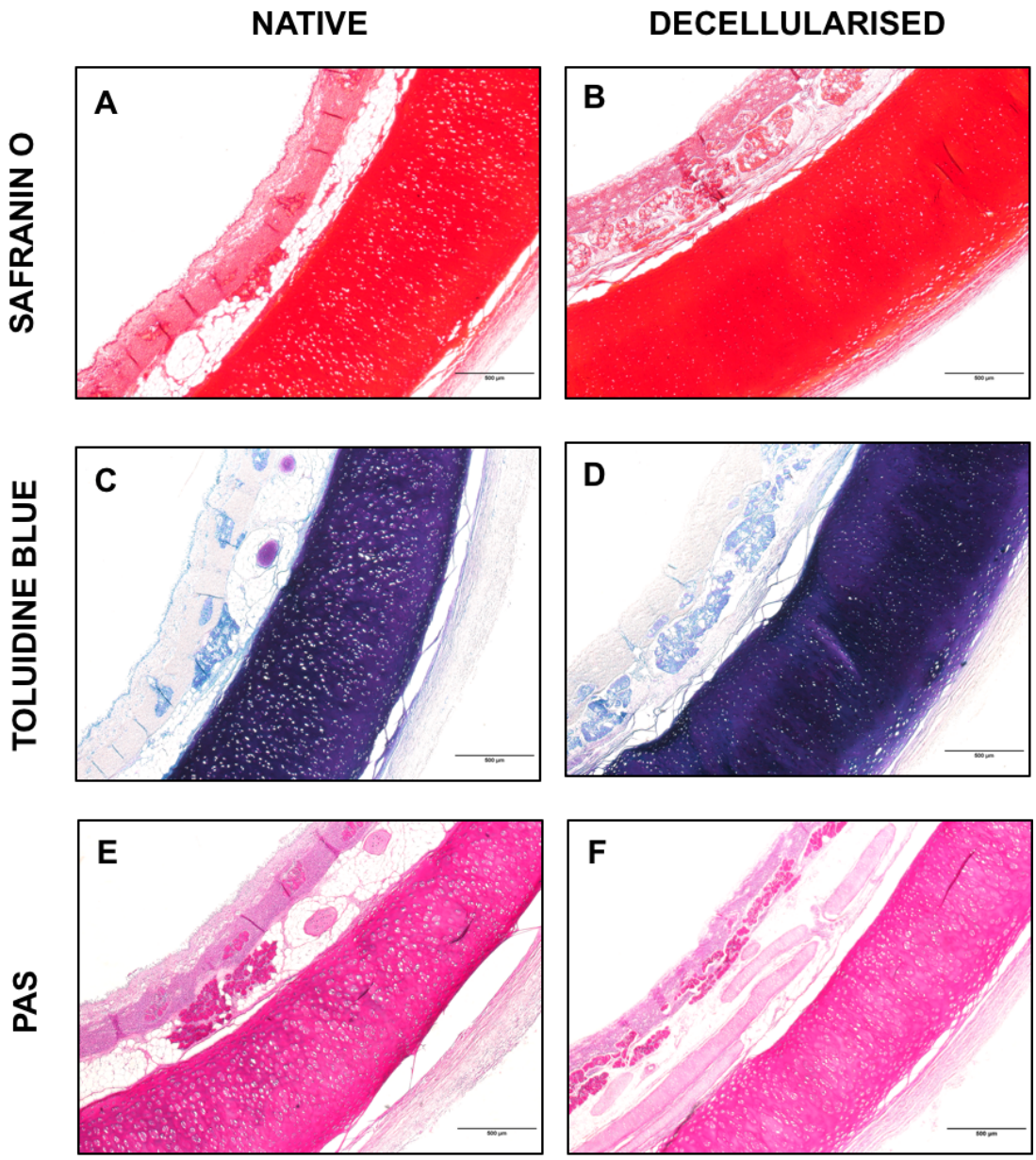

Figure 3.17: Histochemical special stains for sGAG and proteoglycans in porcine native and decellularised tissue.

Safranin O staining of native (A) versus decellularised (B) scaffolds. Toluidine blue staining of native (C) and decellularised (D) tracheal tissue. Periodic Acid Schiff (PAS) staining of native (E) and decellularised trachea (F). Scale bar=500μm.

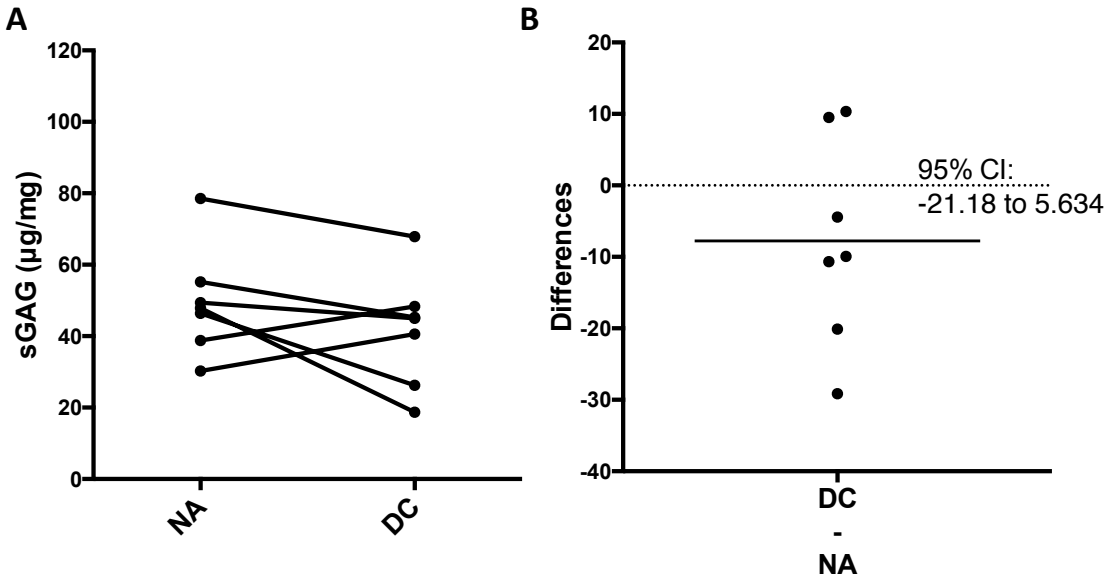

Figure 3.18: sGAG and proteoglycan level in human native and decellularised tracheal scaffolds.

Results showed no significant difference in the total collagen content between native and decellularised trachea. N=6. (B) represents the differences between pairs and shows 95% confidence interval (CI) of the differences between means.

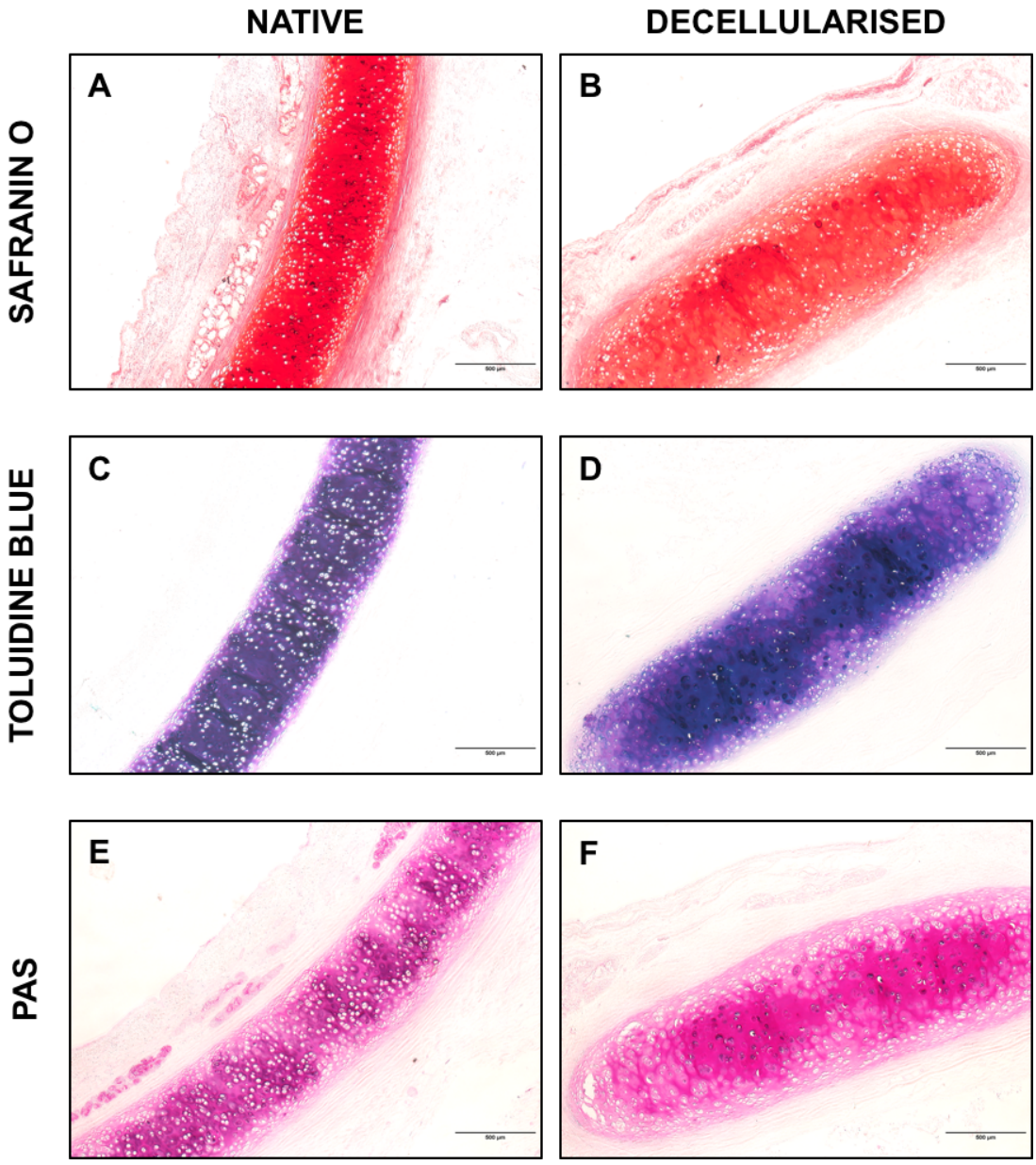

Figure 3.19: Histochemical special stains for sGAG and proteoglycans in human native and decellularised tissue.

Safranin O staining of native (A) versus decellularised (B) scaffolds. Toluidine blue staining of native (C) and decellularised (D) tracheal tissue. Periodic Acid Schiff (PAS) staining of native (E) and decellularised trachea (F). Scale bar=500μm.

3.2.3.3 Immunofluorescence Staining of Key ECM components (Elastin, laminin, collagen- IV, and fibronectin)

Immunofluorescence staining was used to assess the retention of several important structural ECM components post decellularisation process. Figure 3.20 and Figure 3.21 present the staining patterns observed post VAD in both porcine and human tissue groups respectively. What stands out in both figures, is the overall disrupted reduced expression of elastin (Figure 3.20, A ,B & Figure 3.21, A, B), laminin (Figure 3.20, C, D & Figure 3.21, C, D) and collagen IV (Figure 3.20, E, F & Figure 3.21, E, F) compared to native tissue. However, fibronectin expression pattern appears to be preserved (Figure 3.20, G, H & Figure 3.21, G, H). Semi quantitative analysis of samples expression pre and post decellularisation was not performed because of our inability to standardise the exposure time during image acquisition due to high variability of autofluorescence between different samples.

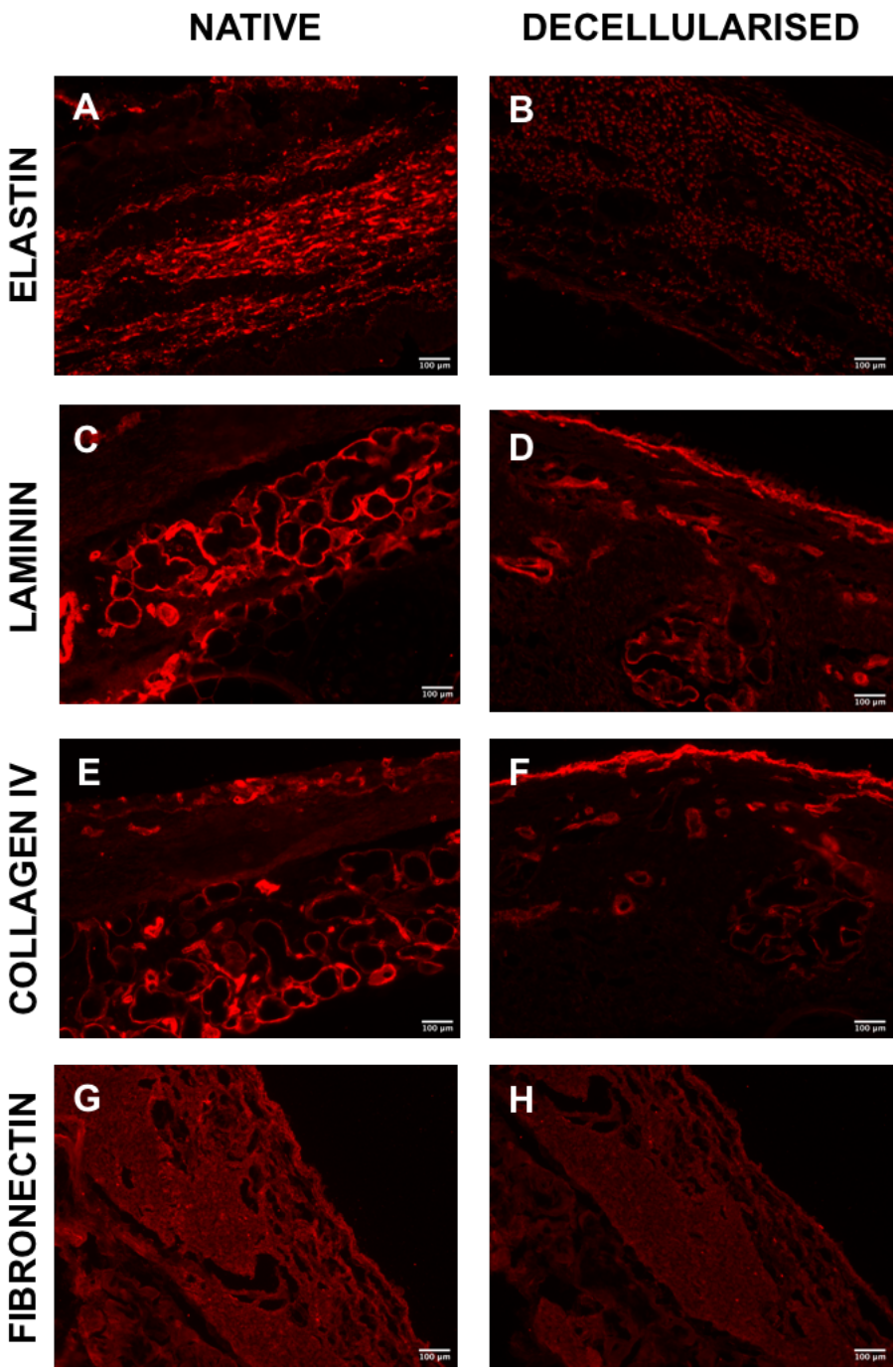

Figure 3.20: Immunofluorescence staining of key ECM components in porcine tracheal tissue.

Immunostaining of elastin (A,B), laminin (C,D), collagen IV (E,F) was localised within mucosa and submucosa and demonstrated reduced expression compared to native tissue. Fibronectin staining (G,H) showed retention of fibronectin post decellularisation. Scale bar=100μm.

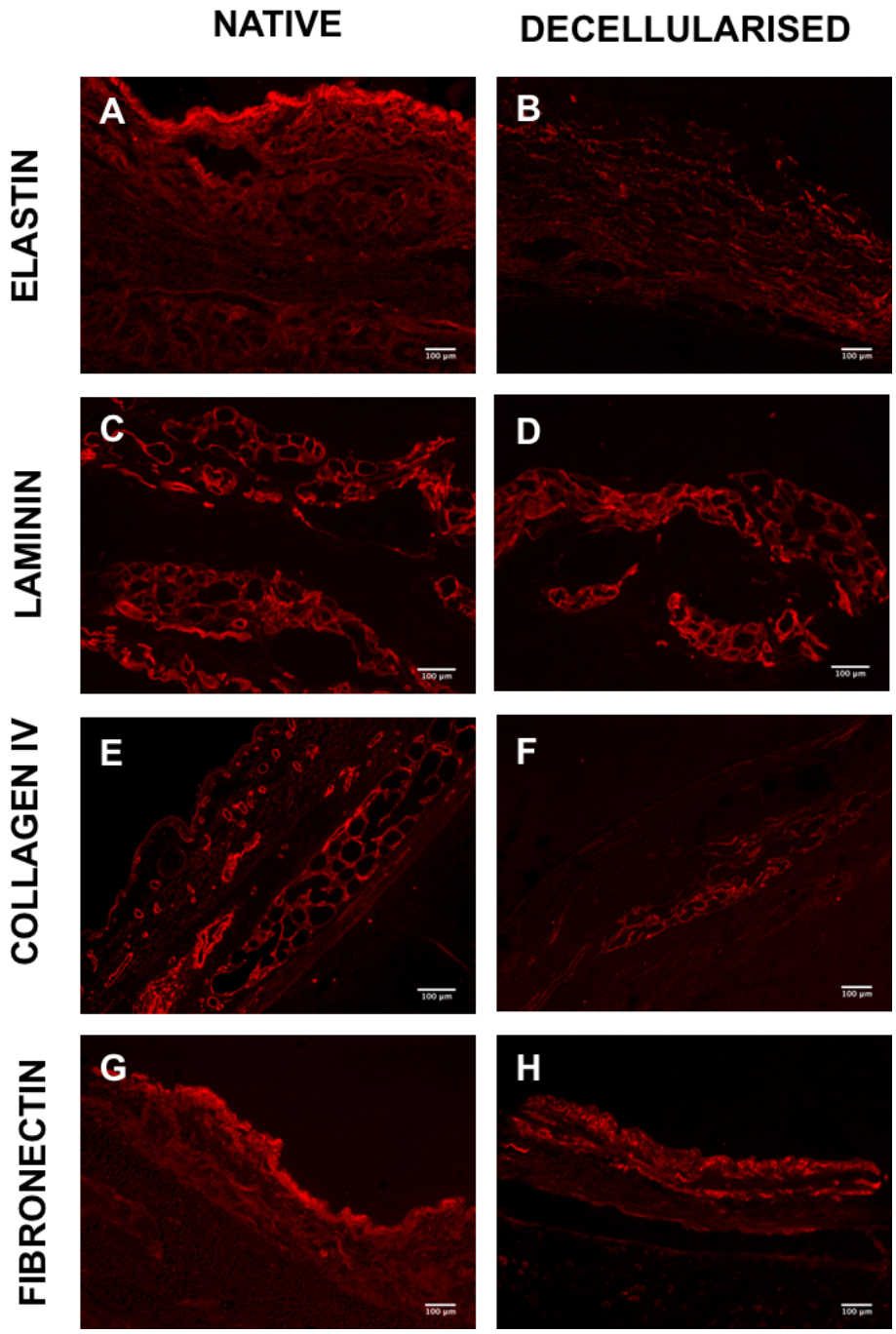

Figure 3.21: Immunofluorescence staining of key ECM components in human tracheal tissue.

Immunostaining of elastin (A,B), laminin (C,D), collagen IV (E,F) was localised within mucosa and submucosa and demonstrated reduced expression compared to native tissue. Fibronectin staining (G,H) showed retention of fibronectin post decellularisation. Scale bar=100μm

3.2.4 Biomechanical assessment of decellularised scaffolds

3.2.4.1 Uniaxial tensile test

A conventional uniaxial tensile test was used to determine the tensile strength of tracheal cartilaginous rings as an indicator of the mechanical strength post decellularisation. The test was performed on dumbbell shaped samples (20x2mm) taken from the cartilage rings and stretched circumferentially until failure. The force- displacement curves obtained were then used to derive stress-strain curves for all samples as detailed in chapter 2. Stress strain curves displayed the typical non-Hookean response of soft biological tissues (Herman, 2016). As shown in (Figure 3.22) three main phases were noted, (1) the toe region denoting the un-crimping of tangled collagen fibres as a result of the stress applied, (2) the linear region, where collagen fibres aligned in the direction of stress and stretch in a linear fashion, this phase is elastic and reversible. The final phase (3) where the macro-failure and rupture of fibers occur. Indeed, it was observed during the test that breaking point of most samples did not happen in the middle of the specimen as expected and mostly was localised near the grips side. Moreover, due to the composite non-homogenous nature of the trachea, the breaking observed in most cases was as a result of breaking and sliding of outer layers first due to applied stress and not the breaking of cartilage layer itself. This observation is clearly illustrated in (Figure 3.23, A &B). Therefore, the ultimate tensile strength data will be mainly representing maximum force required to break the outer layer rather than the breaking of the cartilage.

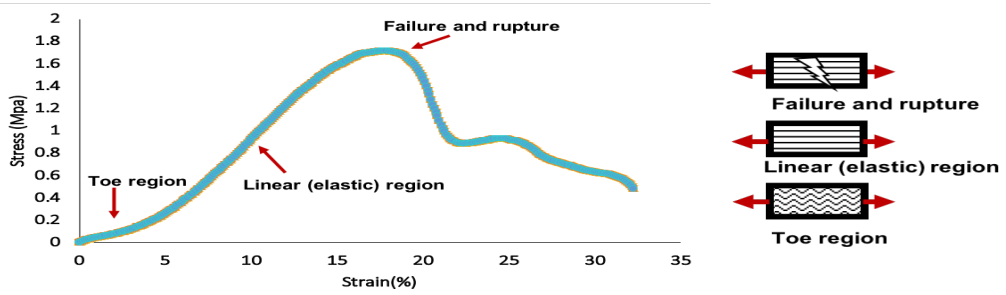

Figure 3.22: Representative stress-strain curve of tracheal cartilage response during uniaxial tensile test.

Red arrows depict three distinct regions of tissue non-Hookean behaviour: toe deformation, linear (elastic) deformation and the complete failure phase (plastic deformation).

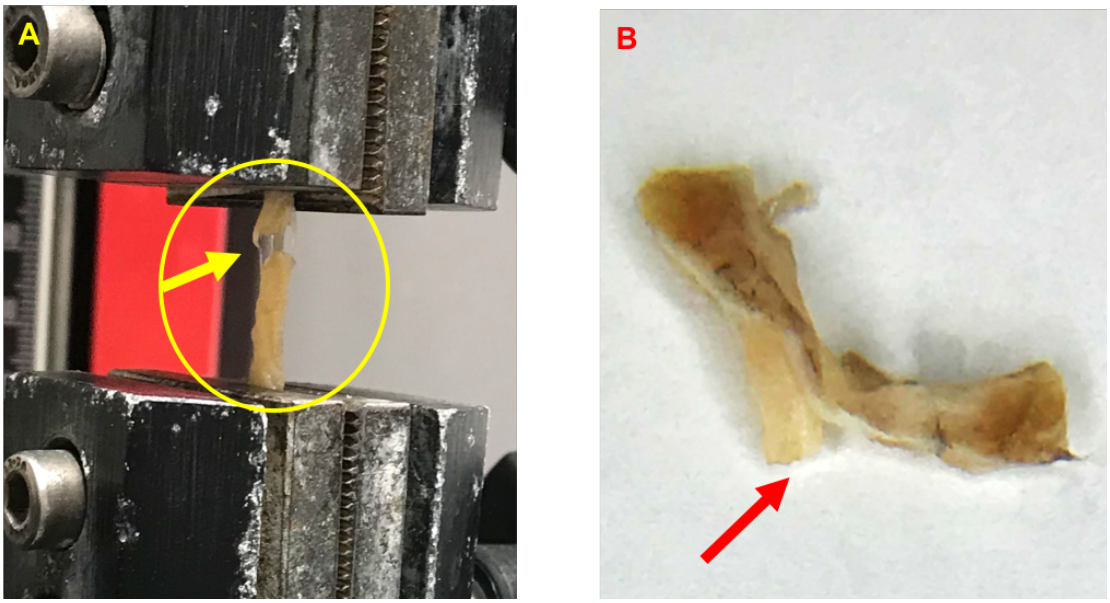

Figure 3.23: Failure and rapture mode of tracheal samples during uniaxial tensile test.

(A) shows failure occurring sometimes near grip side, (B) shows breaking of outer layer and not the entire structure.

Table 3.1 and Table 3.2 below show the mean tensile properties calculated from stress- strain curves of native and decellularised tracheal scaffolds of both porcine and human samples. The Young's (tensile) modulus was determined by calculating the slope of the linear region of stress-strain curves at 10% strain, ultimate tensile strength and ultimate percent elongation represents the maximum stress required to rupture the sample and the maximum degree the sample is stretched before it ruptures respectively.

Statistical comparison of native and decellularised porcine samples demonstrated that there is no significant difference in tensile properties post VAD as shown in (Figure 3.24). Likewise, paired t- test analysis of tensile properties of human native versus decellularised scaffolds (Figure 3.25) revealed no significant difference between the two groups.

Table 3.1: Tensile properties of native and decellularised porcine trachea.

Values represent mean ± SD, n=10.

	Young Modulus (MPa)	Ultimate tensile stress (MPa)	Ultimate strain %
Native (NA)	0.151 ± 0.039	2.072 ± 0.039	21.69 ± 4.947
Decellularised (DC)	0.179 ± 0.050	2.838 ± 1.237	23.35 ± 4.713

Table 3.2: Tensile properties of native and decellularised human trachea.

Values represent mean ± SD, n=6.

	Young Modulus (MPa)	Ultimate tensile stress (MPa)	Ultimate strain %
Native (NA)	0.0705 ± 0.037	1.975 ± 0.9679	21.07 ± 4.175
Decellularised (DC)	0.05855 ± 0.040	1.488 ± 0.6592	23.92 ± 4.490

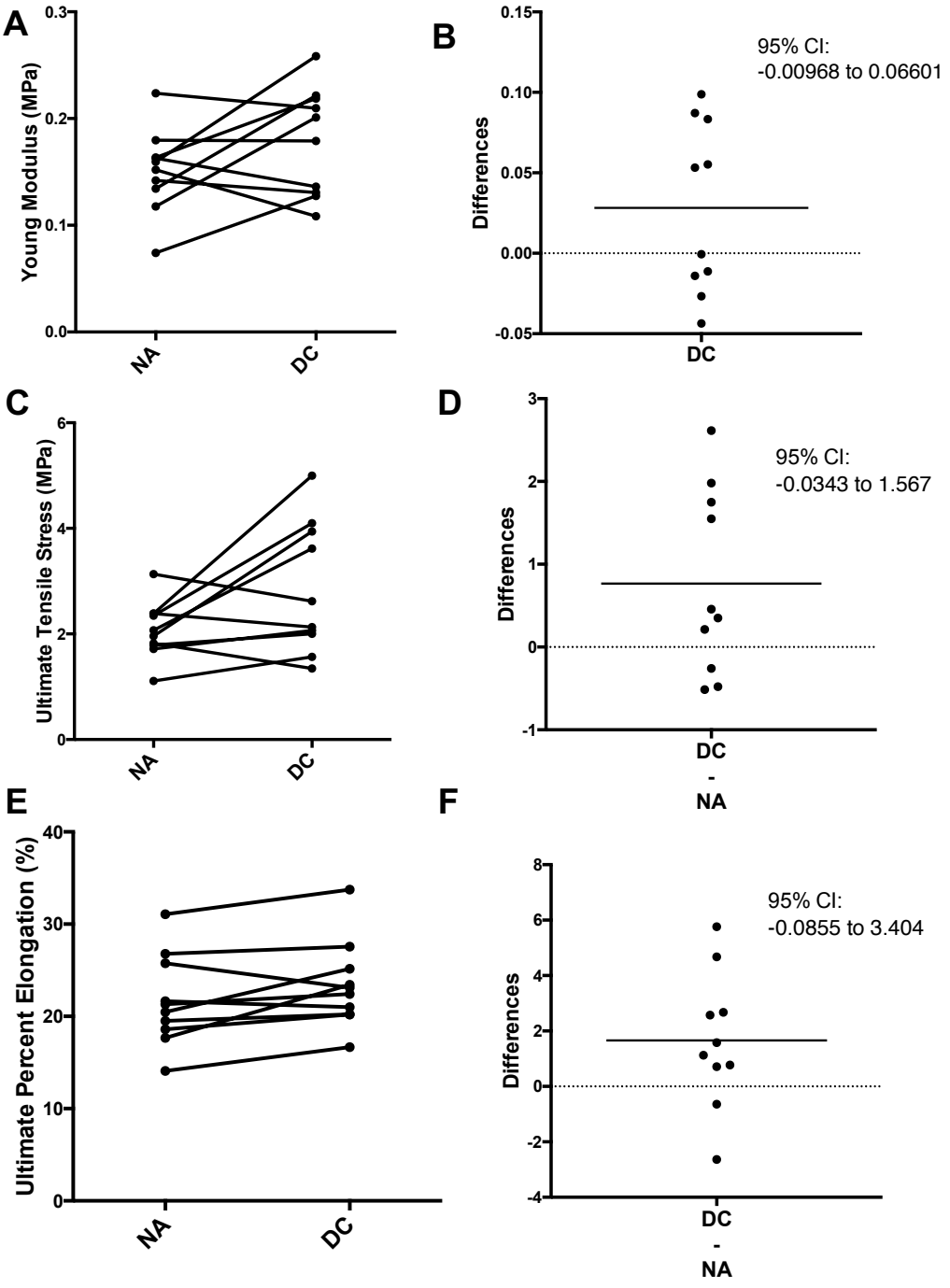

Figure 3.24: Uniaxial tensile test of native versus decellularised porcine trachea.

Results shows that there is no significant difference between Young's modulus (A, B), ultimate tensile strength (C, D) and ultimate percent elongation (E, F) between native and decellularised scaffolds. n=10, (B, D, F) represent the differences between pairs and show 95% confidence interval (CI) of the differences between means.

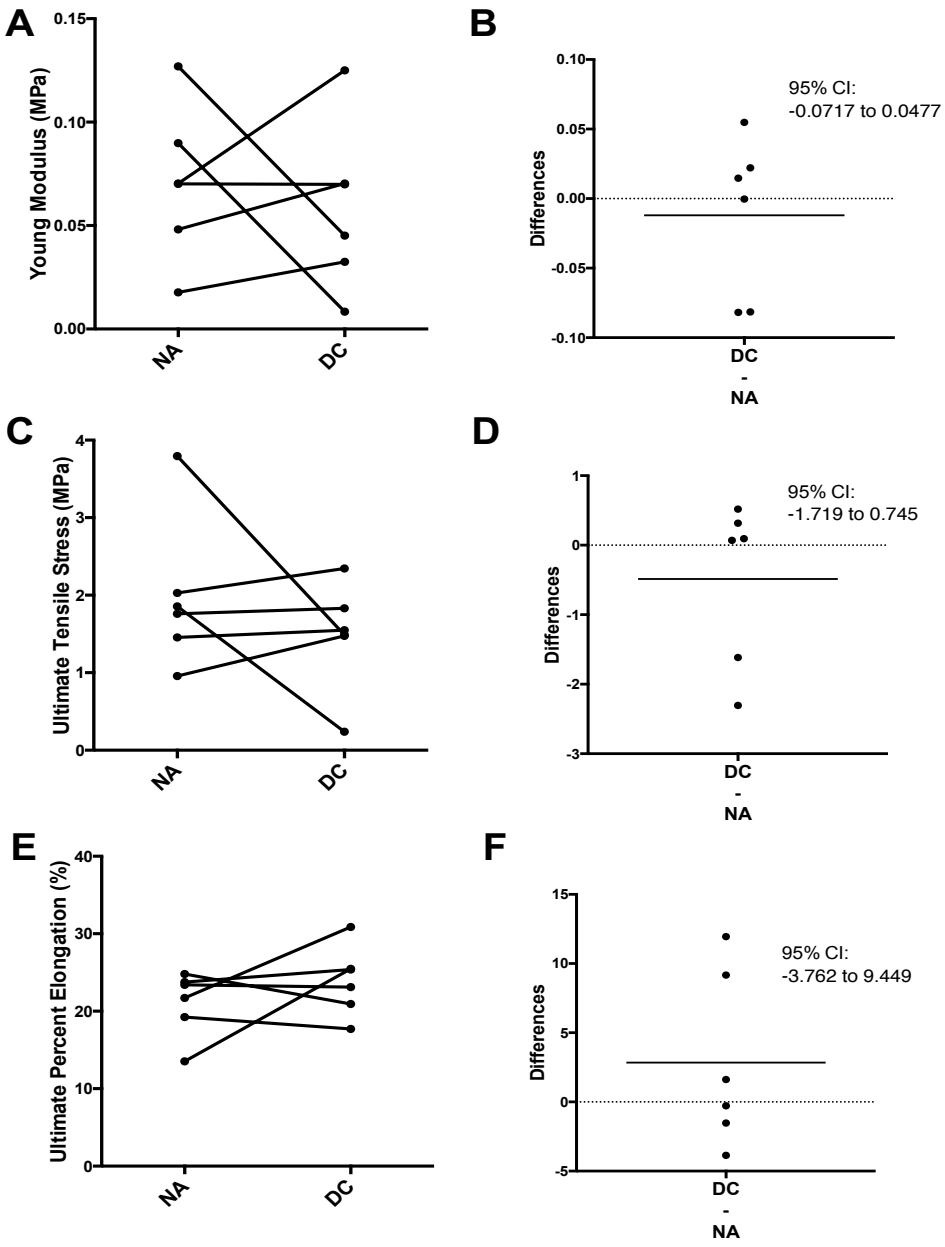

Figure 3.25: Uniaxial tensile test of native versus decellularised human trachea.

Data indicate that there is no significant difference between Young's modulus (A, B), Ultimate tensile strength (C, D) and ultimate percent elongation (E, F) between native and decellularised scaffolds. n=10, (B, D, F) represent the differences between pairs and show 95% confidence interval (CI) of the differences between means.

3.2.4.2 Dynamic Mechanical Analysis (DMA)

In this study, Dynamic mechanical analysis (DMA) was utilised to characterize and assess retention of the viscoelastic mechanical nature of tracheal cartilage pre and post decellularisation. Native and decellularised samples where tested by a physiologically tailored frequency sweep test, at a range of frequencies (0.1 Hz -1 Hz). This range correlates to human breathing rates of (10-60 breathes/minute) and covers the range of normal and high breathing rates.

DMA analysis of native and decellularised tracheal cartilage of both porcine (Figure 3.26) and human (Figure 3.27) tissues revealed that the tissues were viscoelastic throughout the frequency range tested. The samples displayed the storage modulus M' that represents the elastic-like component, Loss modulus M'' that represents viscous-like component, Complex modulus M* and tan delta which represent a measure of internal friction of the material.

What stands out from the graphs with a visual assessment is that there was no difference in the viscoelastic response curves of native and decellularised scaffolds for both porcine (Figure 3.26, A, C, E, G) and human samples (Figure 3.27, A, C, E, G). Semi quantitative and statistical comparison of Area Under the curves (AUC) confirmed that there is no significant difference between native and decellularised porcine (Figure 3.26, B, D, F, H) and human samples (Figure 3.27, B, D, F, H).

Looking at porcine data (Figure 3.26, A, C, E), it can be seen that storage modulus was higher than loss modulus and ranged between (1.8-2 MPa), while loss modulus ranged between (0.2-0.4) MPa. Overall, at 10% strain, storage modulus, loss modulus and complex modulus shows a constant trend with a slight increasing trend starting from (0.85-1) Hz. Likewise, human samples dynamic properties (Figure 3.27, A, C, E) shows also a higher storage modulus ranging between (1-1.5) MPa compared to a loss modulus ranging from (0.1-0.2) MPa. However, unlike porcine samples, the storage modulus, loss modulus and complex modulus remain relatively constant at all frequencies tested.

Nonetheless, the tan delta remains relatively constant for both porcine and human samples (0.1-0.15) indicating that the storage and loss modulus are increasing at the same proportions.

It can also be drawn from the dynamic properties of both porcine and human samples, that the porcine tissue acts as a stiffer elastomer as compared to human samples. This difference is seen through a storage modulus of approximately (1MPa) larger, a loss modulus of (0.1MPa) larger and a (1MPa) larger complex modulus.

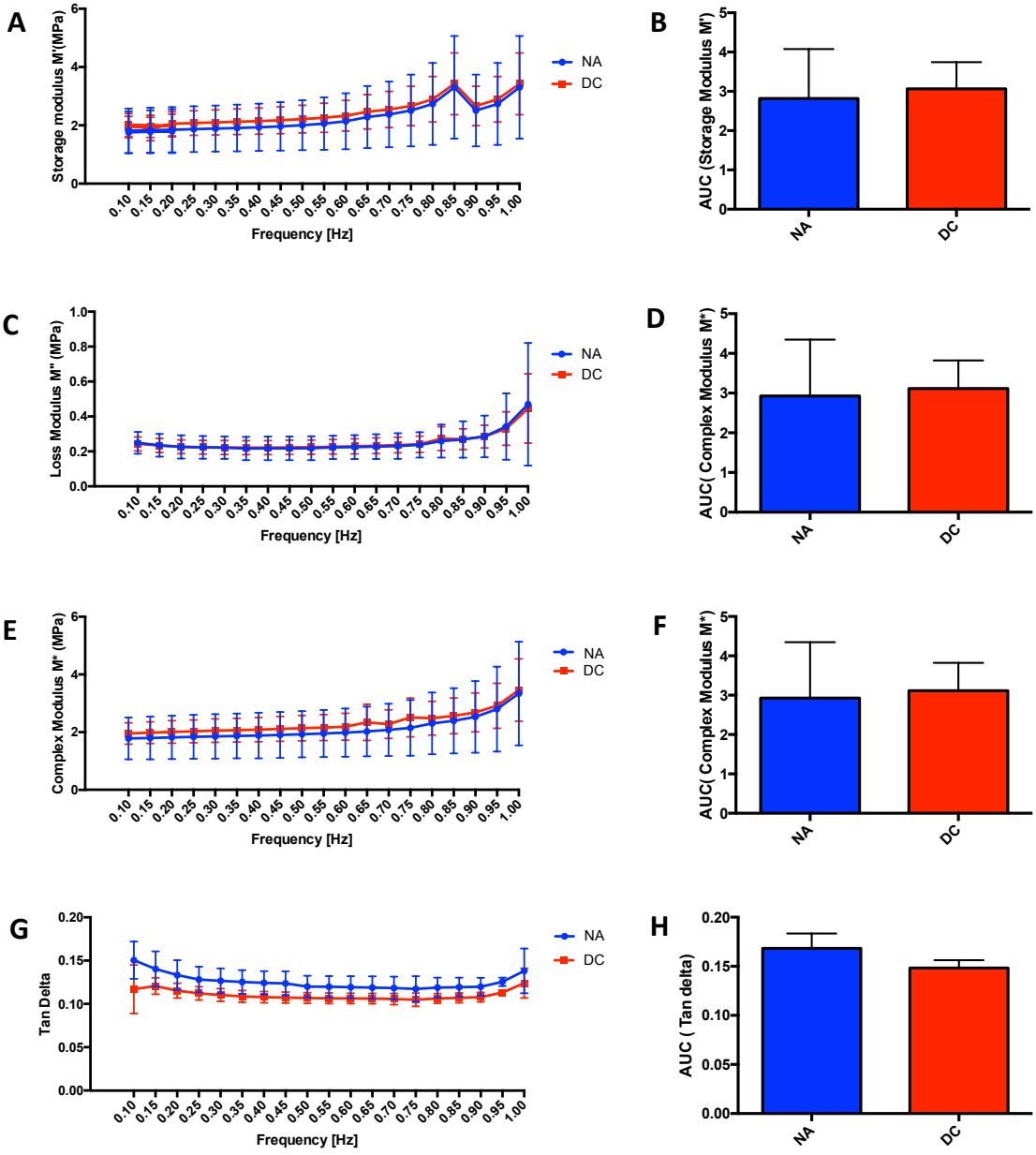

Figure 3.26: DMA analysis of porcine native and decellularised trachea with varying frequency.

(A) storage modulus, (C) loss modulus, (E) complex modulus, (G) tan delta. Error bars represent standard deviation n= 6. Bar graphs (B,D,F,H) represents t test comparison of area under the curves (AUC). Data show no significant difference on viscoelastic measures of native and decellularised scaffolds.

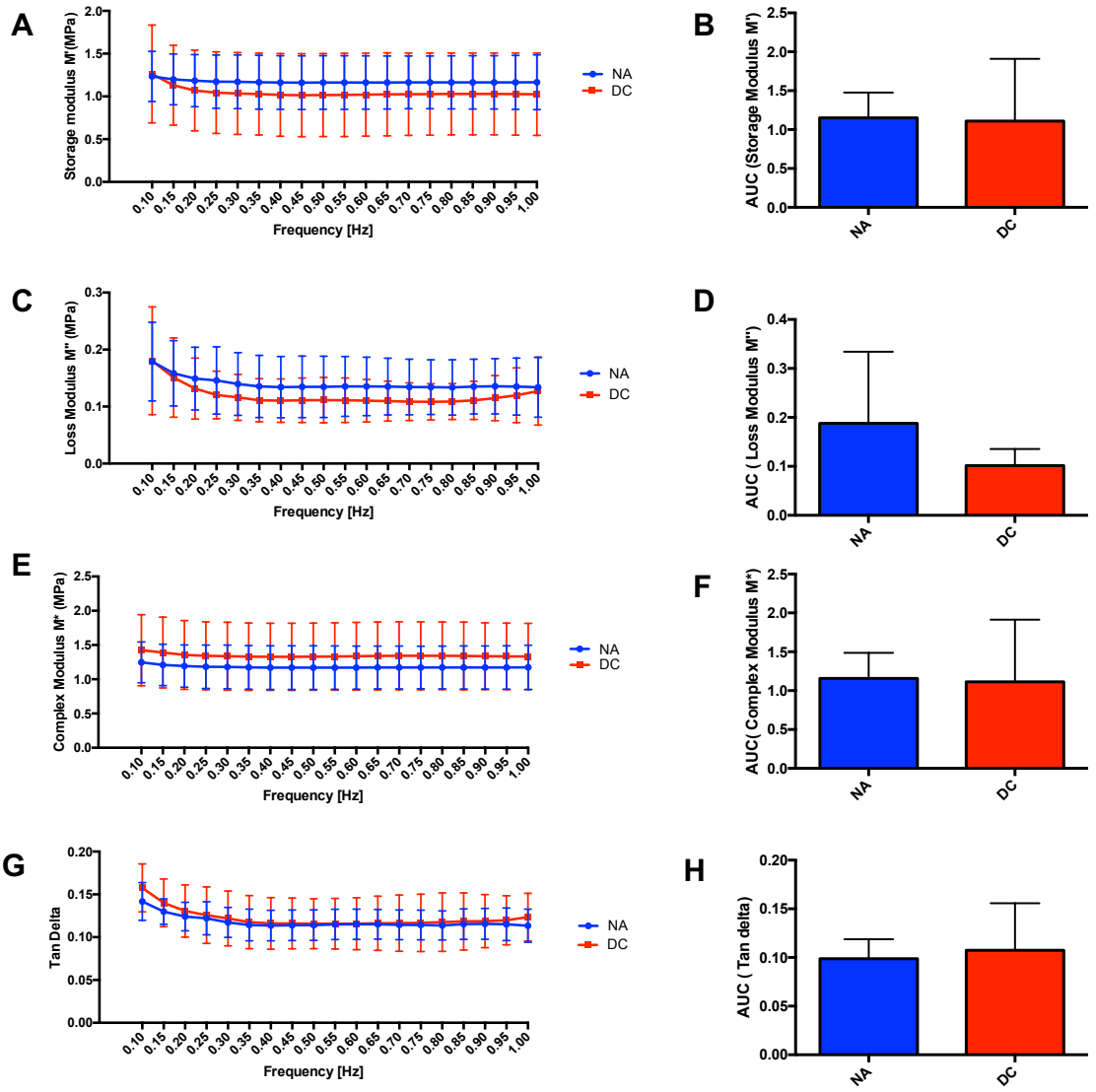

Figure 3.27: DMA analysis of human native and decellularised trachea with varying frequencies.

(A) storage modulus, (C) loss modulus, (E) complex modulus, (G) tan delta. Error bars represent standard deviation, n=6. Bar graphs (B,D,F,H) represents t test comparison of area under the curves (AUC). Data show no significant difference on viscoelastic measures of native and decellularised scaffolds.

3.3 Discussion

The concept of tissue decellularisation to create biocompatible scaffolds for tissue regeneration implies creating a balance between efficient removal of cellular and nuclear materials, maintenance of the native three-dimensional architecture and preservation of the ECM composition, biologic and mechanical integrity (Gilbert et al., 2006). An initial objective of this project was to provide a comprehensive evaluation of whether the composition, structure, and mechanics of tracheal scaffolds are altered as a function of VAD decellularisation.

This study demonstrated that post VAD there was an overall preservation of the macroscopic and microscopic layers structure of tracheal tissue for both porcine and human samples. To assess whether an efficient decellularisation was achieved, cellular contents were evaluated by H&E, DAPI nuclear staining and quantification of total dsDNA level.

Judging by H&E and DAPI staining, porcine and human decellularised tissue sections demonstrated complete removal of epithelial layer and nuclear clearing of cellular content from the outer adventitia and partially from submucosa. However, the protocol was unable to adequately clear cellular materials from the cartilaginous layer and sometimes within submucosal glands. Moreover, residual DNA materials were still seen smeared over ECM fibers in submucosal layer. In fact, this observation has been reported elsewhere and have been attributed to the sticky nature of DNA that make its removal a challenging task (Gilbert et al., 2006, Keane et al., 2012, Partington et al., 2013). Further research is required to determine if extra DNase enzymatic steps or extra washing steps are required to facilitate removal of these fragments.

Although our decellularisation protocol was essentially the same as that used and developed by Lange and colleagues in 2015 (Lange et al., 2015, Butler et al., 2017a) where they have reported complete removal of all chondrocytes within cartilaginous layer and a significant reduction of the total DNA to 36.83 ng/mg for pig scaffolds and less than 50 ng/mg for human decellularised scaffolds. Contrary to expectations, our findings did not support their reports to some extent and shows that the VAD protocol decellularised tracheal outer layers while only devitalising the cartilaginous layer. Nevertheless, the results presented in this

study are in keeping with previous studies of trachea decellularisation with similar detergent enzymatic/ no vacuum-based protocols (Conconi et al., 2005, Macchiarini et al., 2008, Go et al., 2010, Haykal et al., 2012, Partington et al., 2013) where complete removal of chondrocytes was not achieved. In fact, this is not a surprising finding for cartilage-based tissues decellularisation such as (articular cartilage), that present a challenge for complete decellularisation due the dense nature of ECM and lack of interconnectivity of cartilage compared to other connective tissues (Sun et al., 2018, Sutherland et al., 2015).
While the development of the VAD protocol represented a purposeful attempt to improve delivery of decellularisation reagents through introducing negative pressure (vacuum). One would argue, that cartilage by nature is highly compact hydrated matrix that has evolved to resist collapse under pressure. Whilst the protocol may have expedited the nuclear clearance from outer layers (less dense), vacuum might not be ideal for cartilage nuclear clearance. Moreover, there is a considerable literature of cartilage decellularisation which have reported the use of high positive pressure instead of negative pressure to improve nuclear clearance efficiency (Hiemer et al., 2016, Huang et al., 2017), with a reported risk of disruption of mechanical stability that should be carefully accounted for with such approach (Gilbert et al., 2006, Huang et al., 2017). Hence, the utility of vacuum/no vacuum approach should be further investigated and probably an incorporation of positive pressure or perfusion-based protocol would be beneficial.

Total quantification of DNA revealed a significant reduction of DNA level post VAD for both porcine and human samples. Interestingly, total DNA level of human sample group was below 50ng/mg dry tissue weight, hence meeting the minimum criteria of DNA level indicative of efficient decellularisation that was proposed by (Crapo et al., 2011). On the other hand, porcine data did not meet this criterion despite being significantly reduced. Notwithstanding these findings that might indicate that VAD achieved more efficient nuclear clearing in human and not pigs tracheal samples, we believe that our findings of both human and pig samples are comparable. This is because a careful analysis of DNA level of both human and pig data pre and post VAD shows a relatively similar nuclear clearance efficiency being (80% and 90% for porcine and human samples respectively)

denoting a reduction from (1052 ± 260 to 210 ± 71 ng/mg) for pig samples and from (393.8 ± 162 to 24.15 ± 19,70 ng/mg) for human sample group. This suggests that VAD clearing efficiency was relatively the same for both tissues and that the difference observed was attributed to the difference in initial DNA level in native porcine and human tracheal tissue. In other respects, comparison of total DNA level between our study and (Lange et al., 2015) findings should be interpreted with caution due to the methodology they used to normalise data. As in this study sample dry weight was used while they have used wet tissue weight. Indeed, in a separate early optimisation study a comparison of wet versus dry weight normalisation was conducted and have found a 3.5-fold reduction of the total DNA post decellularisation when wet tissue weight was used compared to dry weight.

It is worth noting that the quest to meet Crapo *et al* residual DNA criteria for tracheal decellularisation is probably not justified. this is because the criteria were based upon phenomenological review of findings related to several decellularisation studies that covers a broad spectrum of tissues where an *in vivo* constructive remodelling response has been observed. However, tracheal decellularisation studies comprised only 2 % of their reviewed studies, in addition none of the quoted tracheal studies addressed constructive remodelling with regards to residual DNA content. It is important to bear in mind that the suggested criteria merely reflect a selected group of studies where tracheal tissue decellularisation studies were poorly represented.

Moreover, the clinical relevance for achieving complete nuclear clearance would appear to be minimal in trachea, more specifically within the tracheal cartilage, owing to the dense avascular nature of it that physically protects chondrocytes from circulating T lymphocytes and natural killer NK cells and so making it immune-privileged to a large extent (Benders et al., 2013). This was supported by a wealth of literature (Ghanavi et al., 2012, Jin et al., 2007, Sutherland et al., 2015, Bolano and Kopta, 1991, Arzi et al., 2015), for example clinical results using cadaveric osteochondral allografts showed that there was a 60-95% success rate defined by graft survival and patient evaluations (Revell and Athanasiou, 2009). Moreover, proof of concept trials of decellularised tracheal scaffolds have demonstrated a minimal immune response to constructs despite presence of

residual chondrocytes in the cartilage layer (Macchiarini et al., 2008, Hamilton et al., 2015, Gonfiotti et al., 2014, Elliott et al., 2012).

Although, Sufficient removal of residual cellular and DNA materials is a primary requirement for a successful decellularisation to avoid adverse host responses *in vivo (Badylak and Gilbert, 2008, Gilbert et al., 2009, Zheng et al., 2005).* On which recent studies have shown that residual cellular materials in scaffolds might lead to scar formation deriving an M1 macrophage proinflammatory phenotype (Brown et al., 2009, Keane et al., 2012) while efficiently decellularised scaffolds show appropriate constructive remodelling responses and demonstrated skewing the immune response towards an anti- inflammatory M2 macrophage polarisation (Badylak et al., 2011, Keane et al., 2012, Fishman et al., 2013, Agrawal et al., 2012). On the other hand, many commercially available decellularised products have been demonstrated to have residual DNA fragments (Badylak and Gilbert, 2008, Gilbert et al., 2009).

All of that had led to the hypothesis that a threshold level of residual DNA materials exist bellow which a constructive remodelling response will be the main response (Morris et al., 2017). Therefore, Crapo *et al* criteria was meant as a bench mark to aid studies and the level of minimal residual DNA within ECM (Crapo et al., 2011) will definitely vary depending on the tissue type, characteristics, and degradation rate. Therefore, further research is required to elucidate if there is a threshold level for DNA to avoid deleterious responses within the tracheal tissue and this criterion has yet to be established. In fact, residual DNA is not the sole dominant of immune response to decellularised scaffolds and other important components within decellularised scaffolds or released after implantation such as: mitochondria, membrane associated phospholipids (Crapo et al., 2011),damage associated molecular patterns (DAMPS) like heat shock proteins and high mobility box group 1(HMGB1) , all are involved in the host immune response to scaffolds (Morris et al., 2017, Wiles et al., 2016). This is currently an active area of tissue engineering research (Wiles et al., 2016). It is worth noting that our study did not investigate retention of MHC-I and II as it was mainly focused on structural integrity of VAD decellularised scaffolds.

The second aim of this chapter sought to assess retention of major ECM matrix structural proteins and some functional components post VAD. The ECM is a

highly specialised substrate consisting of a complex mixture of structural and functional bioactive molecules that assume different roles, ranging from defining the functional organ architecture to providing cues to guide cell attachment, differentiation and proliferation (Gattazzo et al., 2014, Badylak et al., 2009).

Collagens, GAGs, and proteoglycans are the core structural components of ECM. The functional coupling of them defines the mechanical resilient properties, as well as regulating cells adhesion, providing support and mediating direct tissue remodelling (Frantz et al., 2010). In this study quantitative evaluation of collagens demonstrated no significant difference post VAD for both human and porcine tracheal scaffolds. Special histochemical staining of collagen I and III using picrosirius red also confirmed overall retention of collagens. It is worth pointing out that the specificity of picrosirius red staining would have been much enhanced if polarised light microscopy was used instead of bright field examination, because it allows discrimination of collagen I and III. Hence, providing better assessment of collagens network organization. However, access to polarised light microscope was not available in this study. Moreover, immunofluorescence staining of collagen II, the most dominant collagen type in tracheal cartilage revealed preservation of it post VAD. These results are in agreement with previous studies that utilised the same VAD protocol (Lange et al., 2015, Butler et al., 2017a). While the majority of studies in the field have focused on measuring the overall retention of collagens, an interesting complementary assay will be to determine the degree of collagen degradation or destruction as a result of decellularisation by probably performing collagen cross linking analysis in the tissue (Kindt et al., 2000).

Another vital component of ECM which have been investigated in this study is GAGs. GAGs are extremely hydrophilic molecules that entrap water and bind other Growth factors ,it assume highly extended conformations and they have a wide variety of functions that reflect their unique buffering , hydration, binding and maintenance of pressure resistant viscoelastic properties of tissues (Frantz et al., 2010, Sun et al., 2018). In addition, increasing evidences indicated that they provide chondro-inductive cues in cartilage (Caliari and Harley, 2014, Yang et al., 2008, Zhang et al., 2009) and their loss leads to increasing stiffness and loss of viscoelastic properties (Rains et al., 1992, Roberts and Pare, 1991, Azhim et al., 2013, Benders et al., 2013).

In this study comparison of sGAG level pre and post VAD revealed no significant difference between native and decellularised scaffolds for both human and porcine samples. The retention of GAG and proteoglycans was further confirmed with special staining with safranin O, toluidine blue and PAS staining. Retention of sGAG levels obtained in this study were in agreement with previous studies using vacuum assisted approach (Lange et al., 2015, Butler et al., 2017a). However, it was contrary to other DEM/no vacuum approaches that reported reduced GAG post decellularisation (Partington et al., 2013, Haykal et al., 2012).

Other functional ECM components were investigated in this study, these included: fibronectin and laminin that aid recellularization by promoting cell adhesion, migration and differentiation (Herard et al., 1996, Simon-Assmann et al., 2011, Ruoslahti, 1984, Durbeej, 2009, Hocking and Chang, 2003, Morrissey and Sherwood, 2015). Studies have showed that laminin is important in promoting polarity in newly formed epithelial tissues as well (Morrissey and Sherwood, 2015). Elastin that plays a role in the elastic recoil of the tissue during breathing, and Collagen IV that maintains basement membrane mechanical stability (Tanjore and Kalluri, 2006, Morrissey and Sherwood, 2015). Immunofluorescence staining in this study demonstrated retention of fibronectin but there was an overall reduced disrupted expression of laminin, elastin, and Collagen- IV in both human and pig scaffolds. A study by (Partington et al., 2013) using DEM/ no vacuum protocol have demonstrated retention of laminin and fibronectin. On the other hand, studies on tracheal decellularisation using VAD protocol (Butler et al., 2017a, Lange et al., 2015, Kutten et al., 2015) did not investigate retention of these molecules and our study suggested reduced expression of these vital components that are necessary for cell adhesion and recellularisation. These findings highlight the importance of investigating the effect of vacuum/no vacuum approach further. It is worth stressing that ECM scaffolds are highly complex and contain many bioactive molecules like growth factors and adhesion molecules that are necessary to promote constructive remodelling and aid tissue recellularisation and vascularisation. hence a comprehensive biochemical assessment of decellularised scaffolds should assess their retention post decellularisation. In tracheal decellularisation few

studies using DEM protocol have reported the retention of the angiogenic factor bFGF (Conconi et al., 2005, Baiguera et al., 2010b). But, this chapter was mainly focused on structural and mechanical stability and therefore growth factors were not investigated, thusly future research should establish their preservation post VAD.

The central aim of this chapter was to provide mechanical characterisation of VAD decellularised scaffolds. The main physiological function of trachea is maintenance of an open airway resistant to collapse during breathing. Therefore, any tissue engineered replacement will need to be mechanically stable and resistant to collapse from time of implantation.

Although cartilaginous rings, annular ligaments and trachealis muscle are the main structural components that contribute to mechanical functions of trachea making it longitudinally flexible while laterally rigid (Boazak and Auguste, 2018), This study have mainly focused on characterising the mechanical properties of tracheal cartilaginous rings due to their vital role in maintaining patency of the airway. That said we were unable to mechanically evaluate other tracheal components due to unsuitability of pig samples having a very small trachealis muscle and annular ligaments and the limited human samples supplied.

In the present work uniaxial tensile test was initially used to evaluate VAD decellularised tracheal scaffolds. The uniaxial tensile test is one of the most commonly used methods to evaluate mechanical properties of tracheal tissues. Circumferential tracheal specimens from tracheal cartilaginous rings were stretched until failure. The results of this study showed that there was no significant difference between tensile (Young's) modulus, ultimate tensile strength, and ultimate percent elongation between native and decellularised tracheal scaffolds of both porcine and human samples. The data reported in this study are in line with other VAD studies (Lange et al., 2015, Butler et al., 2017a) that investigated tensile properties demonstrating that post decellularisation no significant difference was observed in tensile properties. But there was a striking difference in the values of tensile properties reported in comparison to other studies, for example the Young's modulus in this study ranged between (0.7-0.1

MPa) compared to other studies (Lange et al., 2015, Butler et al., 2017a) were it ranged between (1-25 MPa). In fact, this large range of differences was still observed in studies using uniaxial tests for tracheal tissues (Ajalloueian et al., Partington et al., 2013, Lange et al., 2015, Go et al., 2010, Hoffman et al., 2015). These differences could be attributed to the differences in sample sizes, experimental setup due to differences in measurement methods and interindividual variations (Boazak and Auguste, 2018). Moreover, a study by (Aoki and Moriya, 2018) have highlighted the same issue and reported that despite there are more than 180000 published studies on mechanical evaluation of tracheal tissue, it is however challenging to compare data from different studies due to the broad variation in tensile properties obtained even within the same species as result of differences in sample size, preparation and testing setup and the way data are reported. Therefore, published tensile data should be interpreted with extreme caution when comparing different findings.

Whilst, uniaxial tensile testing can give some basic useful information about overall maximum tensile strength of the tissue and may be useful in creating computational injury models, it might not be the ideal test to reflect the complex physiological mechanical properties of the tracheal cartilage. This is because it is unlikely that the tracheal cartilage will encounter a high strain to failure during normal physiological loading. Moreover, the test is limited in predicting only the linear solid-like (elastic-like) mechanical properties of tissues at low deformations (Rains et al., 1992, Suki, 2014). But, tracheal cartilage like other biological tissues displays a non-linear anisotropic properties (Teng et al., 2008, Teng et al., 2012). In fact , a study by (Teng et al., 2009a) that have simulated the collapse behaviour of trachea using simplified linear assumption have demonstrated that this assumption have led to big deviations in predicting the tracheal compliance.
Given all that, tensile testing technique needs to be standardised to allow useful, meaningful interpretation of findings and allow valid comparison among studies. One possible solution could be formulating a standard test method for tensile properties of tracheal tissue similar to the Standard Test Method for Tensile Properties of Plastics of the American Society for Testing Materials that is normally used when testing synthetic or hybrid biomaterials (D638-02a, 2003). Biomechanical experts could help define main guidelines for testing that involves

a standard sample size, gripping technique, tensile mode that focus on exploring stiffness at low strains (quasi-static loading), in addition stressing the importance of reporting rate and magnitude of strain alongside modulus values for more meaningful interpretation and to better reflect the strain dependant modulus nature of tracheal cartilage.

A central goal of this chapter was to explore new measures that could better determine mechanical stability of tracheal tissue post decellularisation. The study prioritised investigating viscoelastic properties of the cartilaginous rings and the rational of choosing this measure has been detailed in this chapter introduction. To achieve this, Dynamic mechanical analysis (DMA) was used as a tool to design a mechanical test that is physiologically – tailored to breathing frequencies (01-1Hz) as detailed in Chapter 2. This range was intended to span over a range of both normal and abnormal breathing rates of (10 - 60 breath /minutes).
Results demonstrated that porcine and human native and decellularised samples were viscoelastic over the frequency range tested by displaying storage modulus M' (denoting elastic component) and a loss modulus M" (denoting the viscous component) of the tissue.

Comparison of the dynamic viscoelastic spectrum revealed that there was no statistically significant difference in dynamic mechanical properties between native and VAD decellularised scaffolds for both porcine and human samples. These finding are in good agreement with our findings that shows preservation of collagens and GAGs level post decellularisation and it indicate maintenance of structural and mechanic al stability.

DMA data for both porcine and human samples showed that the storage modulus M' (which represents the elastic properties of tracheal cartilage) was higher than the loss modulus M'' (which represents the viscous properties of the tissues) and tan delta which is a measure of energy efficiency was less than <1, these findings demonstrate the elastomeric nature of the tissue (being more elastic than viscous) (Ramadan et al., 2017). Elastomers are rubber- like materials characterised by excellent shock absorbent properties and high resilient . These findings accords with previous studies demonstrating the elastomeric nature of a similar hyaline tissue type like articular cartilage (Herman, 2016). These data can be used as useful aids for researchers developing analogue materials for tracheal tissue. Moreover, these results are of physiological relevant as they allow deeper understanding about tracheal ring response to various conditions. For example, our DMA analysis at low strain of 10 % strain that is deemed philological showed a relatively constant response in in the frequency range tested (0.1-1Hz) with a slight increase near 1Hz in pig samples. This reflects, the cartilage ability to adapt its constituents' materials and minimise damage with increasing frequency through a balance of elastic and viscous components (Lawless et al., 2017). Other potential applications of these findings, include using viscoelastic properties to aid computer simulations like Finite Element Analysis (FEA) or Computer Fluid Dynamics (CFD) modelling of trachea (Barnes et al., 2015). Furthermore, the data also demonstrated an analogy in response curves between pig and human samples, as well as showing that the storage and loss modulus of human samples are around half the respective values in the porcine samples. With a proviso of multiple of two, porcine tracheal cartilage can be used as a model to predict dynamic behaviour of human tracheal cartilage.

To the best of our knowledge this is the first study that have investigated the viscoelastic mechanical properties of tracheal tissue utilising DMA analysis.
This study has investigated viscoelasticity as a new useful parameter to inform about tracheal mechanical status, in addition we have explored a new tool (DMA analysis) to mechanically characterize tissues for tissue engineering applications. DMA analysis provides reliable non-destructive approach (Bartlett et al., 2016) of testing mechanical properties of tissue engineered constructs using simplified

loading configuration. It has many advantages over other methods such as: using relatively small size specimens and this is extremely important with paucity of natural tissues for clinical applications (Yamashita et al., 2001) and is desirable for quality validation studies. Moreover, it allows precise control of strain over a range of strain values and a number frequencies and thus allowing accurate characterisation and facilitate modelling of viscoelastic properties of tissues (Bartlett et al., 2016, Yamashita et al., 2001). In addition to that, physiological conditions can be closely simulated with different loading configuration like bending, stretching and compression and it can also be accurately replicated compared to conventional stress relaxation and creep testing methods (Burton et al., 2017).

It is worth highlighting that mechanical assessment in this study provides only information about the mechanical stability and the initial functional status of tissues and it does not inform about durability of the scaffolds. Whilst durability assessments like fatigue testing, provides vital information about retention of device function under constant loading and over extended periods of time and is used with prostheses and stents developments. In tissue engineering durability assessment might take a whole new exciting definition that is different from the conventional mechanical approach for other devices. On which *in vivo*, the continues remodelling through the complex dynamic reciprocal interactions between ECM microenvironment and cells is what determine tissue haemostasis and any possible abrasions. Therefore, durability in tissue engineering will be the ability to remodel or derive constructive remodelling that will lead to TE scaffold integration as a functional tissue. Overall, Long-term success of tissue engineered products will depend on many complex variables that need to be thoroughly investigated like scaffold degradation rates, ability of cells to produce sufficient matrix, and also on the ability of the new tissue to respond appropriately to normal loading conditions upon implantation. And determining what derives constructive remodelling.

3.4 Conclusion

In conclusion, the results of this study have demonstrated that VAD protocol was able to preserve the overall macro and micro architecture of tracheal tissue. In addition, VAD protocol was able to decellularise the outer layers of tracheal tissue while only devitalising the cartilaginous layer on which residual nuclear materials were still seen post decellularisation. However, results of total DNA level revealed a significant reduction of DNA post decellularisation in both human and pig samples, where only human samples show a DNA level of >50ng/mg. Results also shows that the total level of collagen and GAGs post VAD was maintained. Nevertheless, it has demonstrated disrupted reduced expression of laminin, elastin and collagen IV and a preservation of fibronectin for both human and pig samples. Mechanical characterisation using uniaxial tensile tests and DMA analysis of the viscoelastic properties demonstrated the maintenance of mechanical properties post VAD.

The highlight of the study was that it presented a new approach and a new measure of testing mechanical properties by investigating the dynamic viscoelastic properties of tracheal scaffolds using DMA analysis. It was determined that such a technique can produce repeatable and consistent data. And can be used as an additional quality measure of decellularised scaffolds.

4 Improvement of MSC Cell Seeding Efficiency

4.1 Introduction

Efficient and successful incorporation of cells within scaffolds is a central component of constructing tissue engineered grafts, with an ultimate aim in assisting constructive remodelling or rebuilding a functional tissue replacement. Hence optimisation of reliable and reproducible cell seeding techniques, coupled to the utilisation of reliable objective measures to evaluate seeding efficiency, are fundamental requirements for the development of any tissue engineered graft regardless of the tissue scaffold type or the cell type used.

The choice of the optimal seeding strategy is highly dependent on the cell type used, scaffold type and its properties as well as on the target end goals of the clinical applications. Despite the current progress in cell-seeding techniques, there is an identified need for further investigation of the process of cellularisation in terms of seeding efficiency and efficacy to allow evidence-based selection of the optimal seeding methods and choice of the best cells-scaffold combination (Badylak et al., 2011, Villalona et al., 2010).

In tracheal bioengineering, the target criteria for an ideal tissue engineered replacement are: maintenance of biomechanical durability, supporting a functional mucosal epithelial barrier, rapid vascularisation to help cells survival and integration to achieve bio-functionality. Therefore, the choice of cells used for recellularisation echoed these criteria. On which the most widely used cell types for recellularisation in tracheal bioengineering are (1) Chondrocytes with the aim to regenerate cartilage, (2) epithelial cells to recreate the epithelial sheet barrier of native airway, and (3) MSCs, for their anticipated role in promoting constructive remodelling and tissue integration by either differentiating or through their immunomodulatory and trophic factors.

The most common technique of seeding cells in tracheal TE is static passive cell seeding. This technique denotes the process of drop seeding cell suspension onto the scaffold surface (luminal or abluminal sides depending on cell type) and allowing cells to sit relatively undisturbed to maximise cells attachment and permeation (Godbey et al., 2004). This step is followed by cultivation in media in specially designed bioreactors for a variable length of time under either static conditions or under dynamic movement of the graft, media or both (Batioglu-Karaaltin et al., 2015, Kunisaki et al., 2006, Lee et al., 2002, Fuchs et al., 2003, Lin et al., 2009, Gray et al., 2012, Elliott et al., 2017, Macchiarini et al., 2008). Yet, numerous studies in the field of tissue engineering have reported the shortcoming of passive seeding technique, being the least efficient in terms of cells retention and often yielding heterogenous results (Wendt et al., 2003, Dunkelman et al., 1995, Davisson et al., 2002, Pazzano et al., 2000, Raimondi et al., 2004, Kim et al., 1998, Haykal et al., 2014b). Despite being the most widely used technique of seeding, its efficiency has been limited by many variables such as initial cell density, seeding volume, scaffold biomaterial properties, cell type and scaffold geometry (Patel et al., 2016).

In tracheal bioengineering there is a lack of studies in the field that have investigated the seeding process or attempted to understand critical variables related to seeding techniques like seeding density or scaffolds properties that are necessary to achieve a seeding success. For example, in studies using bone marrow derived MSCs the seeding density varied largely between $1x10^6$/ml to $5x10^{10}$/ml (Maughan et al., 2017). Furthermore, preclinical and clinical data regarding cell seeding efficiency have mainly relied on qualitative outcome measures of cells retention like histology with no quantitative assessment of cells retention, survival and proliferation (Haykal et al., 2014b, Maughan et al., 2017). Moreover, there is rarely a mention of blinding approach to demonstrate the presence or absence of cells. This made comparison among studies a challenging task.

That said, improving cell seeding efficiency and its reproducibility in tracheal bioengineering remains a key variable for optimisation and improvement, on which the quality of this step will affect the downstream investigations and the manufacturing process for clinical translation.

As the main theme of this thesis is the investigation of the interaction of MSCs with the decellularised scaffolds. The central aim of this chapter was to try improve passive cell seeding technique of MSCs on DC tracheal scaffolds to facilitate close assessment of MSCs interaction with the underlying matrix and evaluate their survival and spatial distribution. Indeed, the motivation behind the work of this chapter started with the continuous failure to achieve a reproducible seeding outcome despite the large number of repeats. Not to mention the tubular geometry of DC scaffolds that have complicated passive seeding of MSCs and caused more cells to runoff.

In order to improve our seeding process. We started exploring what condition might prevents the cells from running off the scaffolds. Tracheal scaffolds are maintained fully hydrated in PBS pre-seeding. The liquid layer spreading across the surface reduces the friction of the surface causing it to become more slippery. So, we hypothesised that if we removed excess moisture from the scaffolds surface by partially drying them, friction will increase and so will limit runoff and ultimately improve passive cells delivery to the tubular tracheal scaffolds. The process of surface drying will be done taking the advantage of the natural evaporation process. And since the evaporation rate depend on the degree of saturation of air above the wet surface. We propose that performing this step in a humidified CO_2 incubator, where evaporation rate is kept minimal to ensure gentle and better control on the degree of scaffolds dehydration. And this will avoid introducing adverse dehydration damage to the scaffolds.

4.1.1 Research aims and objectives

The aim of the work presented in this chapter is to improve passive cell seeding efficiency of MSCs into DC tracheal scaffolds and to assess cytocompatibility of the scaffolds and cell survival and interactions.

Objectives:

- Testing the hypothesis that partial surface dehydration (PSD) of DC tracheal scaffolds in a CO_2 incubator will improve passive cell seeding efficiency (CSE) of MSCs on DC tracheal scaffolds.
- Investigation and assessment of cell's viability, proliferation, attachment, and spatial distribution on DC tracheal scaffolds

4.1.2 Experimental approach

Umbilical cord MSCs (UC-MSCs) were used for seeding VAD decellularised porcine scaffolds in this chapter. The experimental work of this study involved three main parts as outlined in the schematic diagram bellow (Figure 4.1):

Part 1: The study started by testing if introducing the additional PSD conditioning step to remove excess moisture of scaffolds prior to cells seeding will have an adverse effect on scaffold structure. The duration of PSD step was first determined by incubating n=12 punch biopsies in 6 well plate in CO_2 incubator and determining relative water loss at different time points by measuring sample weight. Then the time point that represent 10-20 % water loss was used to evaluate effect of PSD on scaffolds structure in comparison to control (unconditioned) and biosafety cabinet conditioned scaffolds. Scaffolds were evaluated using SEM imaging and fiber diameter analysis to inspect for adverse dehydration damage.

Part 2: The experimental work in this part involved deriving an initial cell seeding density to be used for the following seeding experiments using a basic MTT assay. Then it involved testing the effect of scaffold PSD conditioning in improving cell seeding efficiency (CSE). A blinded experiment with three independent operators was conducted, where they were instructed to seed MSC cell-suspension into both PSD conditioned scaffolds versus control DC tracheal scaffolds. Then assessment and comparison of CSE was based on dsDNA quantification assay of cells runout as detailed in chapter 2 and finally assessment of cells retention by H&E and PKH26 immunofluorescence staining.

Part 3: The experimental work in this part involved a thorough assessment and evaluation of MSCs seeded on DC scaffolds. Assays included: assessments of viability, metabolic activity, and cell proliferation. SEM was used to evaluate cell attachment and scaffold structure. Then an optical clearing protocol was developed to facilitate assessment of cells distribution and infiltration in whole mount punch biopsies of Zs.green transduced cells using multiphoton microscopy.

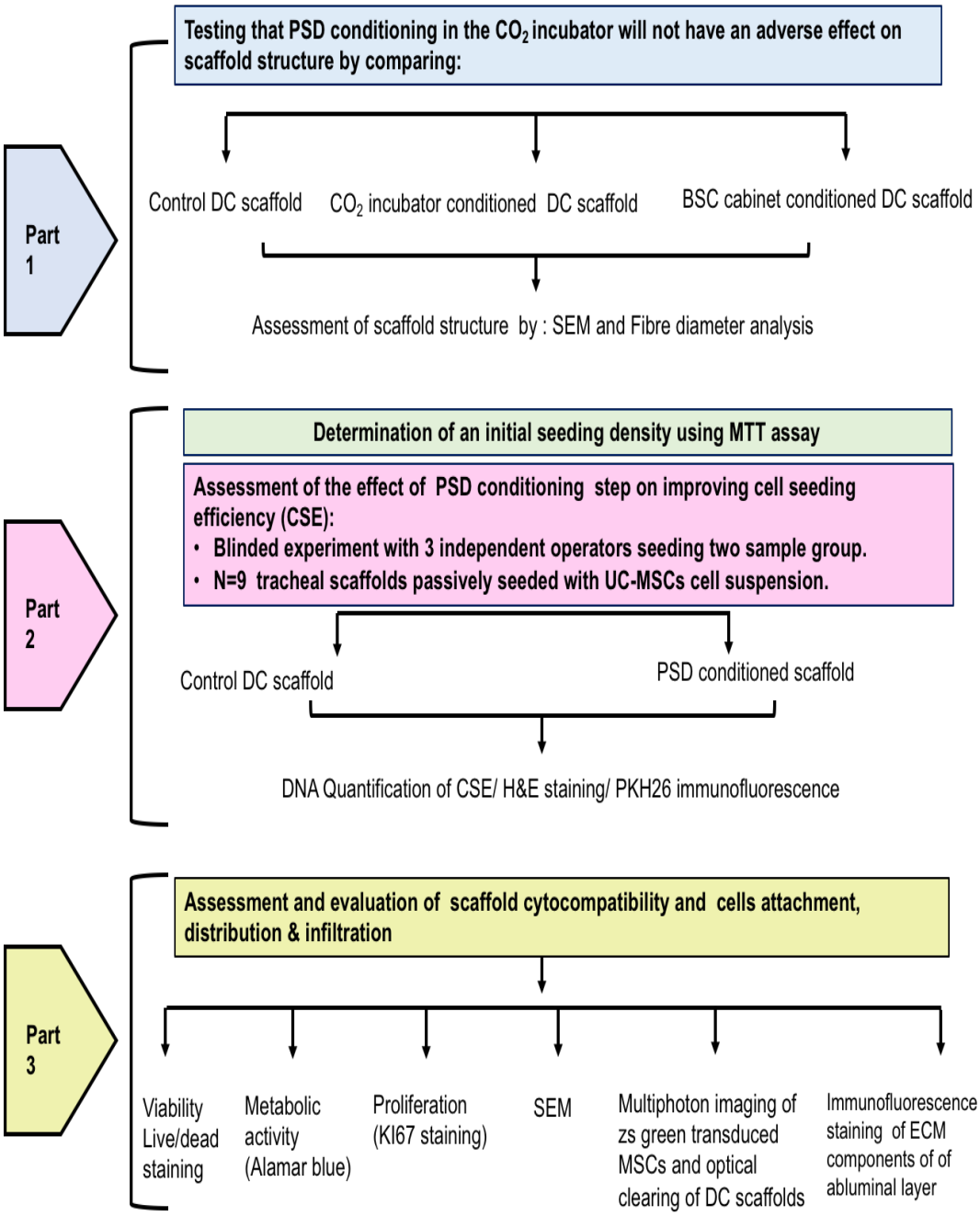

Figure 4.1: Schematic outline of the experimental approach.

4.2 Results

4.2.1 MSCs characterisation and immunophenotyping

Characterisation of MSCs prior to seeding into DC tracheal scaffolds proved that cells conformed to the ISCT minimal recommended criteria for identification of MSCs (Dominici et al., 2006a). Results on (Figure 4.2) shows the FMO controls that were used to confirm compensation. As displayed in (Figure 4.3), cells demonstrated the typical in vitro culture features as plastic adherent spindle shaped cells (Figure 4.3, A). Flowcytometric analysis of cell surface antigen expression demonstrated that 95% of the cells expressed the antigens CD105, CD73, and CD90 with the same cells lacking (2% positive) expression of CD45, CD34, CD14, CD19, and HLA-DR. The trilineage *in vitro* differentiation potential of cells to adiopogenic, chondrogenic and osteogenic potential have been conducted and confirmed by Dr. Ben Weil from the CCGTT facility.

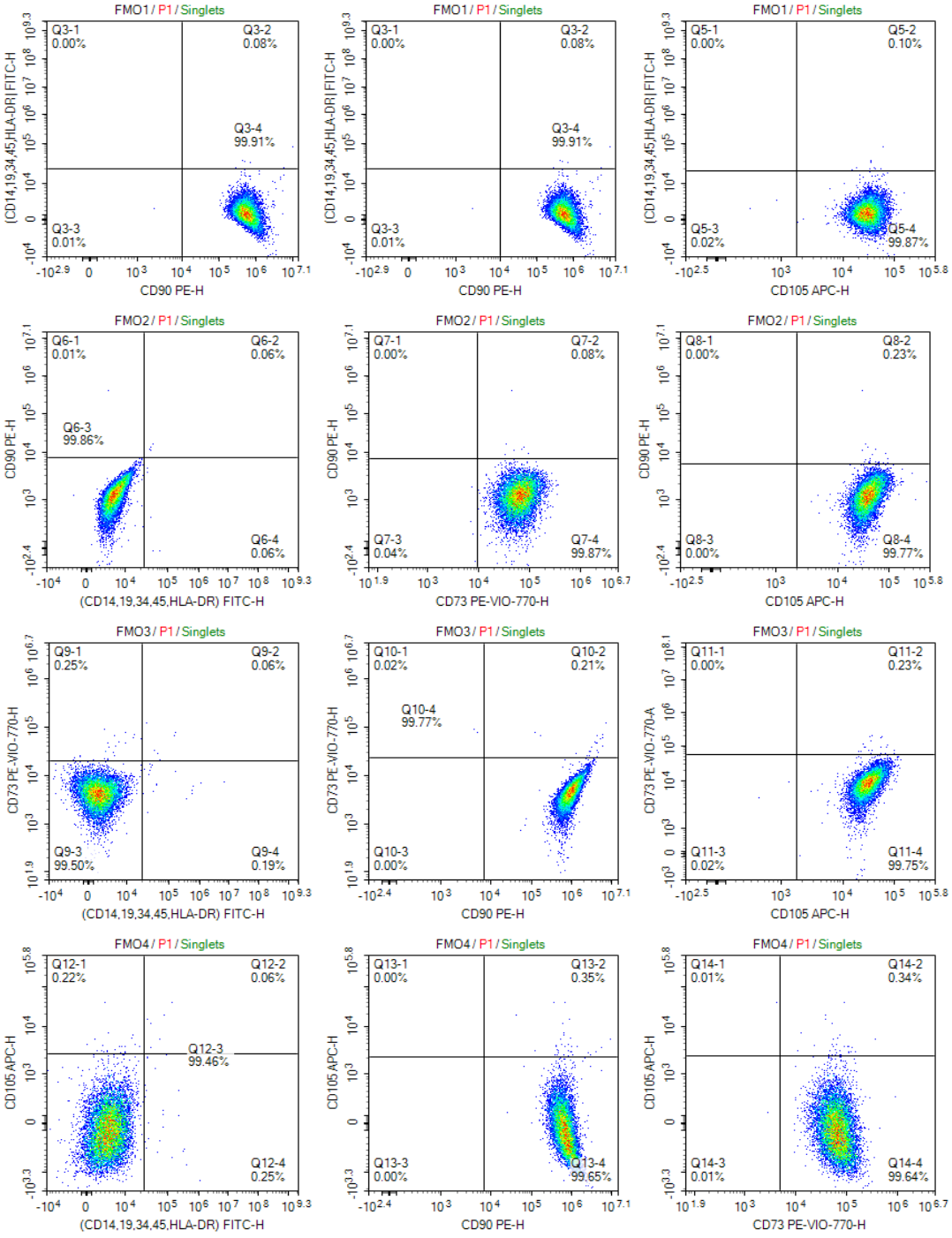

Figure 4.2: FMO controls (Fluorescence- Minus One controls) panel for MSC immunophenotyping.

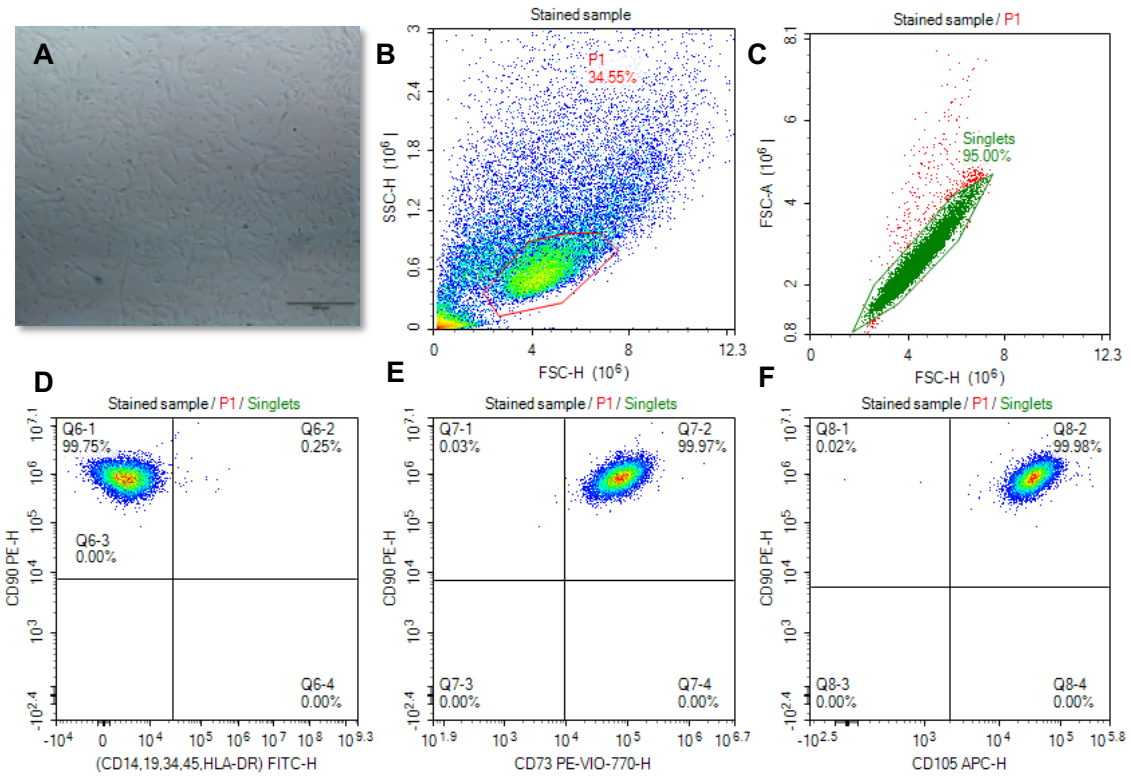

G

Parameter	Specification	Results
CD45+CD34+CD14+CD19+HLA-DR+	<2%	0.25%
CD105+	>95%	98.98%
CD90+	>95%	99.75%
CD73+	>95%	99.97%

Figure 4.3: MSCs characterisation and Immunophenotyping.

UC-MSCs in culture displaying adherent spindle shaped cells (A), flowcytometric analysis of UC-MSCs (B-G), demonstrated that 95% of cells population expressed: CD105,CD90 and CD73 while showing negative expression (<2%) for CD45,CD34,CD14,CD19 and HLA-DR. Scale bar= 500μm.

4.2.2 Testing the effect of partial surface dehydration (PSD) step on decellularised tracheal scaffold structure.

The following set of experiments aimed to initially determine the duration of partial surface dehydration (PSD) conditioning step carried out in the CO_2 incubator versus conditioning in a biological safety cabinet (BSC conditioned) relative to control scaffolds (unconditioned). This was followed by investigating whether introducing this step pre-seeding will have an adverse effects on the DC scaffolds structure.

4.2.2.1 Determination of the duration of the PSD conditioning step.

Samples from DC tracheal scaffolds were conditioned in a CO_2 incubator using the designated seeding plates during which weight and percentage water loss was calculated. As shown in Figure 4.4, A &B there was a gradual decrease in water content of the DC tracheal scaffolds with time. 80% water loss was recorded after 24 hours incubation. It was decided to test sample quality at a time range between (30 min to 4hrs), denoting 10-20% water loss to confirm that no adverse changes are caused by this additional step.

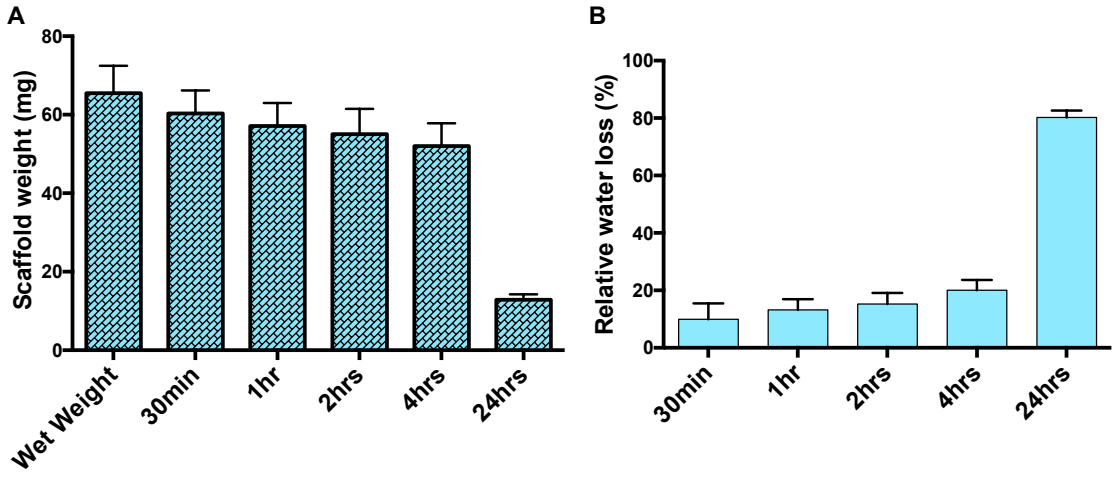

Figure 4.4: Relative water loss from DC scaffolds during CO_2 incubator conditioning at different time points.

There appear to be a gradual reduction in sample weight with time (A). Relative water loss from scaffold was calculated and showed a gradual increase with incubation time (B). n=12. Values represent mean±SD.

4.2.2.2 Assessment of the structural integrity of DC scaffold.

Scanning electron microscopy (SEM) was used to observe any adverse structural damage resulting from the PSD conditioning of DC tracheal scaffolds in the CO_2 incubator versus the biological safety cabinet (BSC-conditioned) relative to control DC scaffold (unconditioned). It is worth noting that different samples at (30min, 1hr, 2hrs, 4hrs) were sent for imaging, however due to a complete failure of SEM facility only one time point was tested and was chosen to be at 4hrs as it denoted an extreme case condition.

As can be seen from (Figure 4.5), the PSD conditioned scaffolds in the CO_2 incubator (Figure 4.5, C&D) displayed relatively similar morphological features to the control (unconditioned) DC scaffolds with borderline reduction in the open spaces between fibres (Figure 4.5, A&B). This is suggestive that conditioning in the CO_2 incubator did not adversely alter the morphological architecture of the scaffolds. On the other hand, looking at BSC-conditioned scaffolds (Figure 4.5, E&F), there appear to be a striking change on DC scaffolds structure displaying a compacted (flattened) fibre network morphology in contrast to the open fibre network architecture that is observed in the control scaffolds. Moreover, the images show that there was some swelling or fiber enlargement observed on the BSC conditioned scaffolds as compared to the DC control scaffold (Figure 4.5, F). In our opinion, this is unlikely to be a swelling of the fibres but rather the result of several fibres compacting together making the fibres appear swollen.

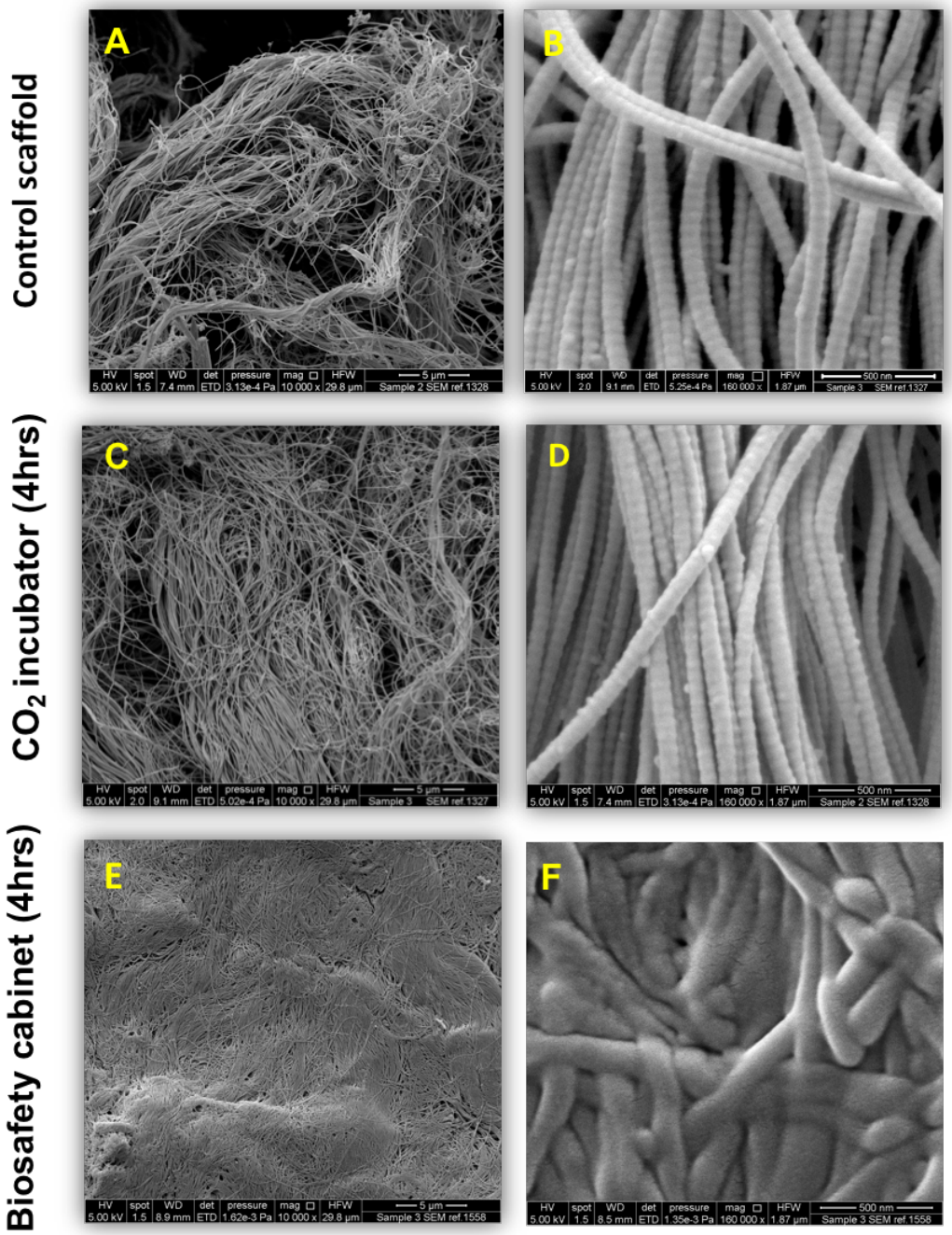

Figure 4.5: SEM micrographs of DC tracheal scaffolds comparing different pre-seeding partial surface dehydration (PSD) conditions.

Control DC scaffold (A, B) showing an open fibre network architecture, CO_2 incubator conditioned scaffolds (C, D) displaying a relatively similar appearance as control scaffolds. Biosafety cabinet conditioned scaffolds (E, F) displaying a compacted architecture with enlarged fibres appearance indicating a dehydration damage (E). Scale bar=5um (10000X) for (A, C, F), and 500nm (160000X) for (B,D, F).

4.2.2.3 Fibre diameter analysis post PSD conditioning

Fibre diameter analysis was conducted from the SEM images at each condition with the aid of Fiji image analysis software. Statistical analysis of the calculated fibre diameter (n=60) was done using one-way ANOVA.

As shown in (Figure 4.6) the results confirmed that there is no statistical difference observed between scaffolds conditioned in the CO_2 incubator and control scaffolds. The mean fibre diameter was 84.94 ± 8.64nm and 84.76 ± 8.22nm for control scaffolds and CO_2 incubator conditioned scaffolds respectively as shown in (Table 4.1). The data also revealed that there is a significant difference in fibre diameter ($P \leq 0.0001$) between the BSC-conditioned scaffolds and the CO_2 incubator conditioned scaffolds as well as the control scaffolds. The mean fibre diameter of BSC conditioned scaffolds was 122.40 ± 44.13nm.

Taken as a whole, evidence from these experiments appear to indicate that the additional PSD conditioning step in the CO_2 incubator did not cause detrimental damage to the structure of the DC scaffolds and can be introduced pre-seeding in contrast to BSC conditioned scaffolds that revealed the appearance of a dehydration damage.

These initial experiments had helped us define a safety range between (30 min to 4hrs) for the PSD incubation time in the CO_2 incubator. This range is specific to size of the seeding plate used. Based on these data it was decided to use a duration of 1-2 hrs PSD conditioning in the CO_2 incubator as a pre-seeding step.

Table 4.1: Descriptive statistics of fibre diameter analysis of different PSD conditions.

	MAX (nm)	MIN (nm)	Mean ± SD (nm)
DC scaffold	103.90	65.69	84.94 ± 8.64
CO_2 incubator (4hrs)	100.60	63.02	84.76 ± 8.22
Biosafety cabinet (4hrs)	260.40	57.89	122.40 ± 44.13

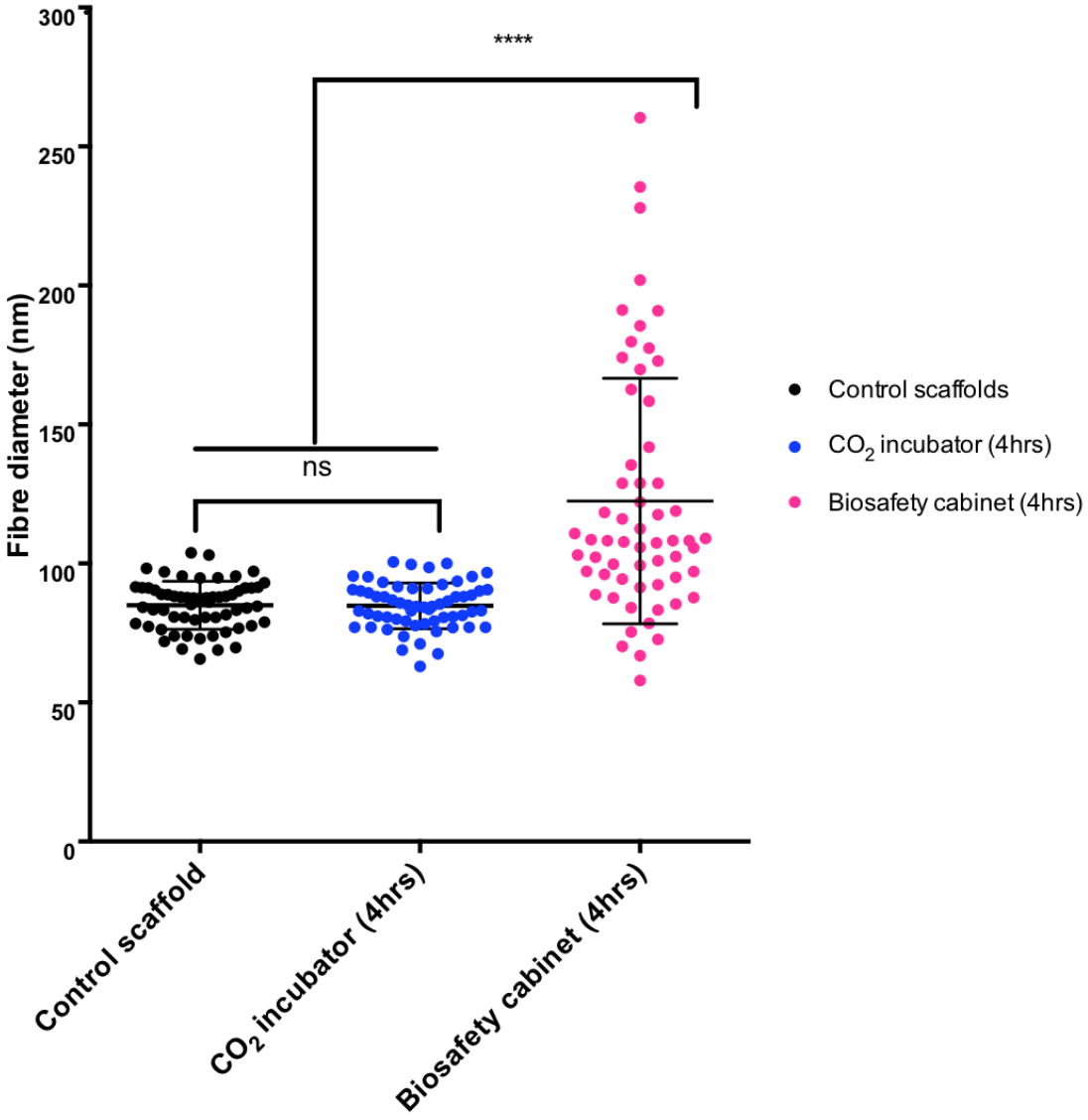

Figure 4.6: Statistical comparison of fibres diameter between different PSD conditions.

Results show that there is no statistical difference observed between CO_2 incubator conditioned scaffolds and control scaffolds whereas, there is a significant difference in fibres diameter between biosafety cabinet conditioned scaffolds and the control scaffold as well as CO_2 incubator conditioned scaffolds. Data were analysed using One-way ANOVA statistical test, n=60, $P \leq 0.0001$. Values represents mean±SD.

4.2.3 Estimation of an initial cell seeding density using MTT assay.

As previously discussed, there is no clear agreement on the cell seeding density used for recellularisation in tracheal bioengineering. This experiment aimed to derive a rough estimate of MSC seeding density as a starting point of experimentation. Estimation of a working cell seeding density was achieved by exploiting the advantage of an MTT (3-(4,5-dimethylthiazol-2-yl)-2,5-diphenyl tetrazolium bromide) reagent that is normally bioreduced by metabolically active cells to form a coloured insoluble formazan precipitate that can be visually inspected. Hence, it was used to guide selecting the seeding density that gives the best cell coverage of the tracheal DC scaffolds. A visual assessment of results displayed in (Figure 4.7) revealed that a seeding density of $500X10^3/cm^2$ to $1x10^3/cm^2$ gave a complete uniform coverage of the scaffold surface. It was decided to select $500X10^3/cm^2$ as a starting seeding density for experimentation in this study. Solubilising the blue formazan precipitate from the decellularised scaffolds to quantitate absorbance using spectrophotometry proved to be challenging and was not successful.

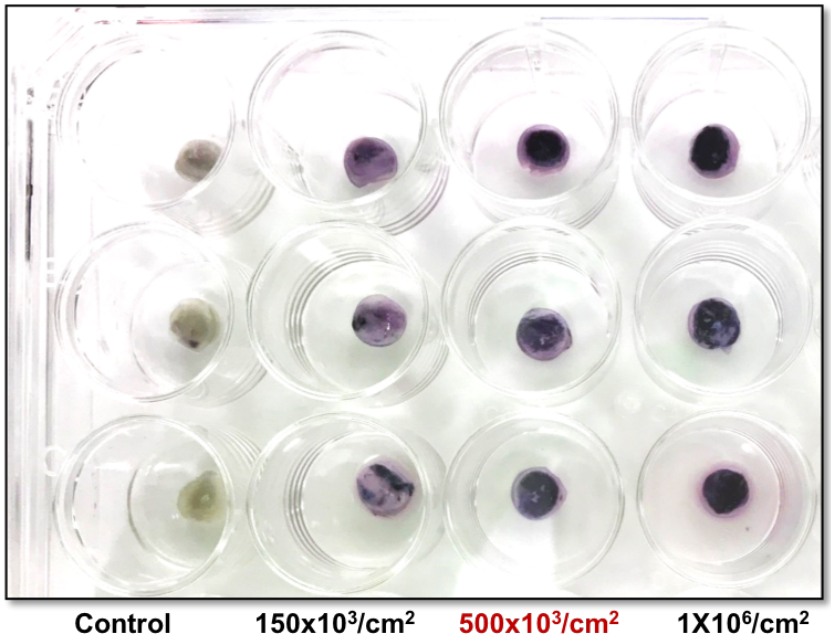

Figure 4.7: MTT assay for MSC seeded scaffolds.

Representative image of MTT assay on MSC- seeded DC tracheal scaffolds (6mm punch biopsies) at different seeding densities. n=3.

4.2.4 Assessing the effect of partial surface dehydration (PSD-conditioning) step in improving cell seeding efficiency (CSE).

Cell retention was quantitated using Quant-iT Picogreen dsDNA assay as detailed in chapter 2. The cell seeding efficiency (CSE) was calculated as the percentage of the amount of DNA of the unattached cells in the medium to the amount of DNA of cells initially seeded to the DC tracheal scaffolds.

As shown in (Figure 4.8), comparison of the cell seeding efficiency (CSE) between the tracheal scaffolds that were PSD-conditioned in the CO_2 incubator and the control DC scaffolds (unconditioned) using unpaired t-test revealed that there is a statistically significant difference between both groups $P \leq 0.001$. The most remarkable finding that emerged from the data is the improvement of CSE and most importantly the consistency on the PSD conditioned scaffold group. The mean CSE was (96.46% $\pm$1.710). On the other hand, the data demonstrated that the control (unconditioned) group displayed a variable CSE values denoted by the higher standard deviation, on which mean CSE was (79.09 $\pm$ 9.091).

Qualitative inspection of cell retention on scaffolds using H&E staining and immunofluorescence staining of PKH26 labelled cells as displayed in (Figure 4.9, A-D) confirmed the retention of more cells in the PSD-conditioned scaffolds group in comparison to control scaffold group.

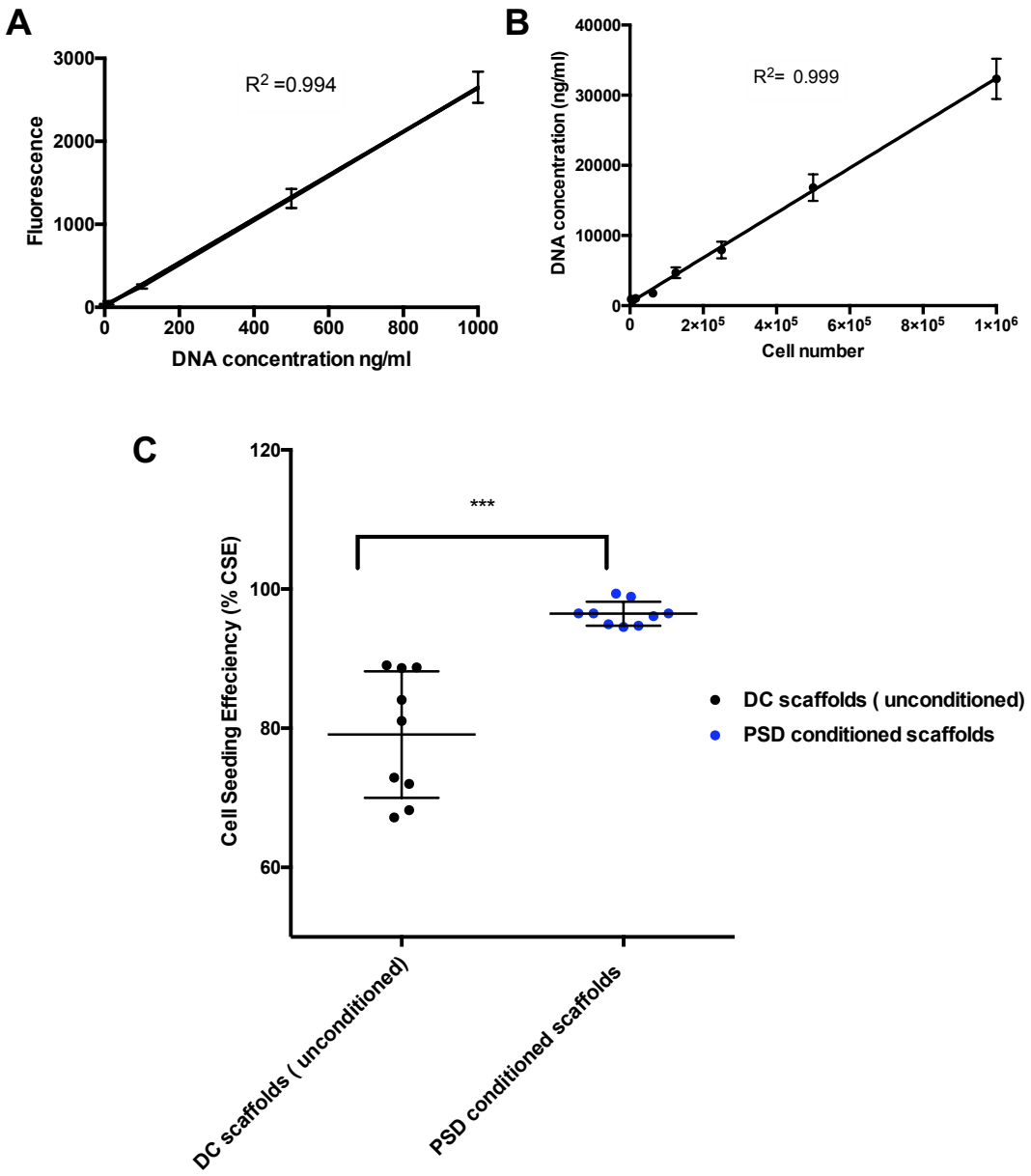

Figure 4.8: Comparison of cell seeding efficiency (CSE) between PSD conditioned and control (unconditioned) scaffolds.

(A) DNA standard calibration plot, (B) standard curve of cell number versus DNA concentration. The graph shows a significant difference (***P≤0.001) between both groups (C). Data were analysed using unpaired t-test, n= 9, values represents mean±SD.

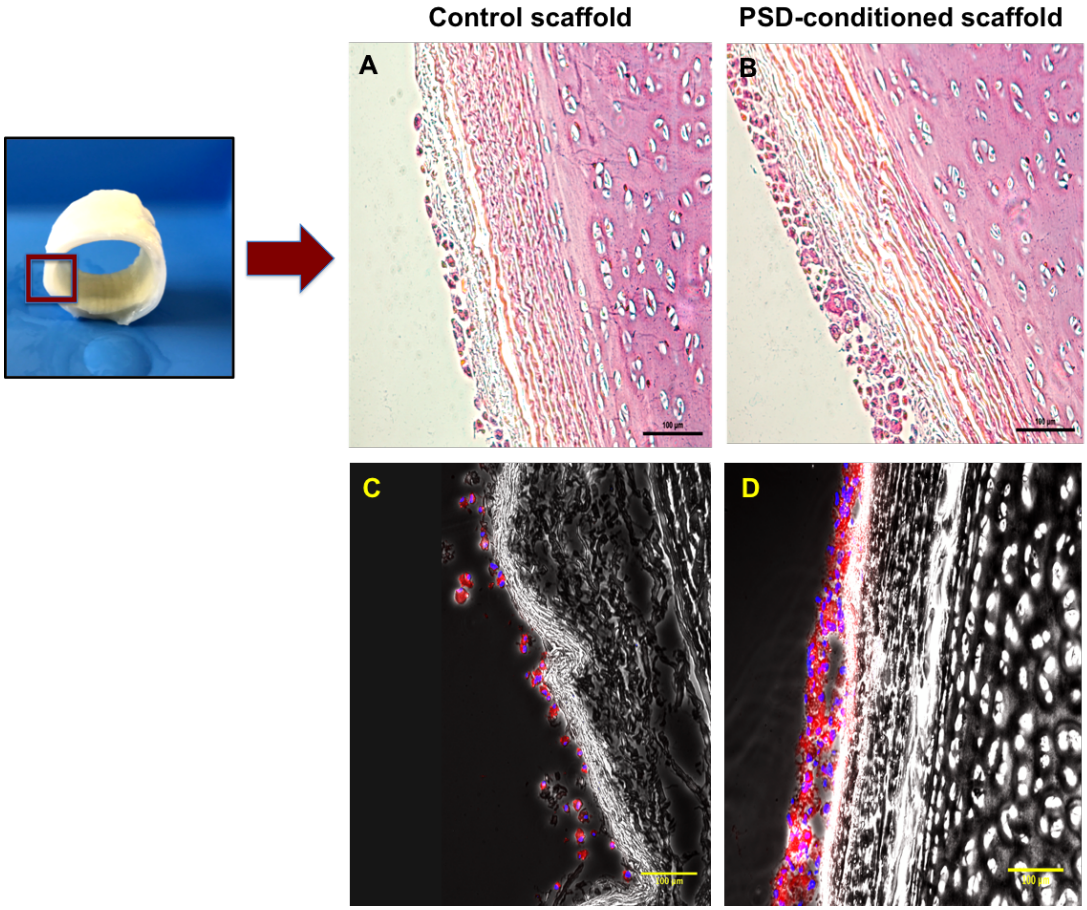

Figure 4.9: Comparative assessment of (CSE) of PSD-conditioning versus control scaffolds.

More cells appear to attach to PSD-conditioned scaffolds (B,D) compared to unconditioned control scaffolds (A,C).Scale bar = 100μm. Haematoxylin and eosin (H&E) staining (A,B), PKH26(red) and DAPI(blue) immunofluorescence imaging (C,D).

4.2.5 Assessment of cell viability and metabolic activity

4.2.5.1 Live dead staining

Cell viability was determined by simultaneous staining of whole mount punch biopsies of cell-seeded scaffolds with Hoechst 33342 as a live stain and ethidium homodimer-1(EthD-1) as a dead cell indicator. Confocal microscope (Leica SP8 laser scanning confocal microscope) was used to image samples. Z-stacked images were captured and evaluated at different time points: 3 days, 7days and 14 days of culture. Fiji image analysis software was used to quantitate the percentage of living cells.

Visual inspection of the cell viability images (Figure 4.10, A-C) have demonstrated an overall maintenance of viable cells throughout 14 days of cultivation. On day 3, a mixed population of live and several dead cells were observed, while at day 7 results show an absence of dead cells. However, on day 14, the presence of dead cells was observed again.

Statistical analysis using one-way ANOVA of the percentage cell viability as displayed in (Figure 4.11) revealed that there is a significant difference ($P \leq 0.001$) in cell viability between day 3 and day 7. At day 3 the percentage viability was (50.01 $\pm$0.617)% compared to (94.97$\pm$3.605)% at day 7. There was also a significant difference between day 7 and day 14 ($P \leq 0.0001$) showing a decrease of percentage cell viability to (56.49 $\pm$4.406)%.

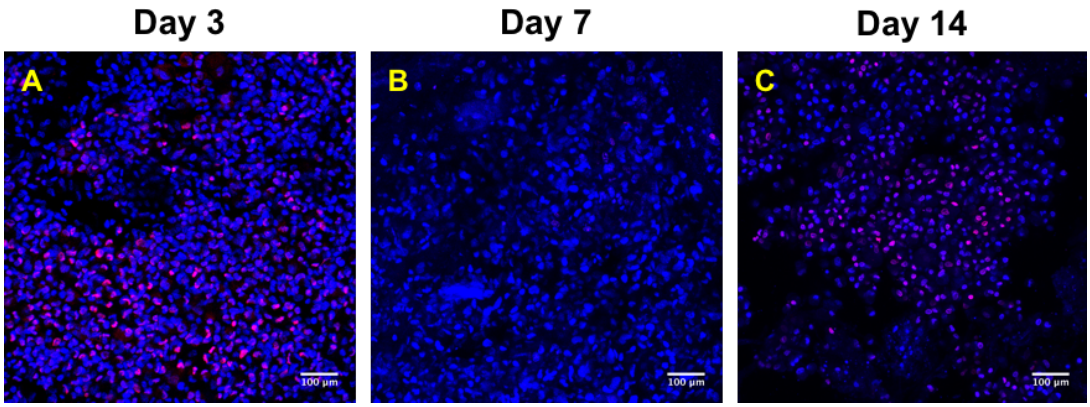

Figure 4.10: Assessment of cells viability using live/ dead staining.

Representative maximum intensity projection images of Hoechst 33342 (Blue=live) and ethidium homodimer-1(EthD-1)(Magenta=dead) staining. (A) day 3, (B) day 7, (C) day 14.

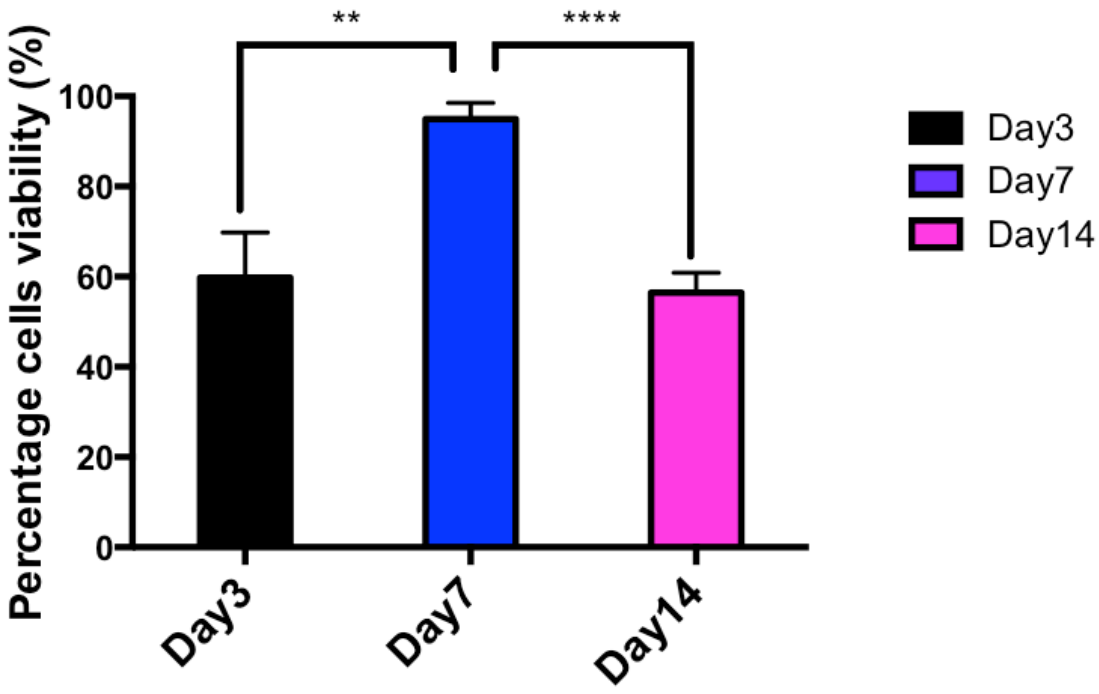

Figure 4.11: Percentage of viable cells on decelluarised tracheal scaffolds at different time points.

One-way ANOVA showing a significant difference in percentage cell viability between day 3 and day and also between day 7 and day 14. n = 6, Error bars represent mean±SD, (**≤ P0.01, **** P≤0.0001).

4.2.5.2 Assessment of metabolic activity

Two commercially available kits were used to assess the metabolic activities of cells seeded on tracheal scaffold; **MTT** tetrazolium reduction assay (Sigma) and **Alamar blue** quantification assay (Biorad). MSCs were seeded into 6mm punch biopsies of DC tracheal scaffolds at a cell seeding density of $500X10^3/cm^2$.

As previously described, the MTT assay allowed only qualitative assessment of cell activity that reduced MTT reagent forming blue formazan precipitate. But the quantification of assay results could not be done, due to failure to lyse the formazan precipitate from the tracheal scaffolds.

Alamar blue was also tried and the results showed that the linear limit of the standard curve of MSCs was at 60,000 cells and no linear correlation could be established at our high cell density range. Macroscopic observation of Alamar blue redox reaction on cell seeded scaffolds at $500X10^3/cm^2$ (Figure 4.12, A, B) showed that the extent of Alamar blue reduction reaction denoted by the colour change from blue to pink was variable among the different scaffolds on day 1 and no reliable correlation could be established due to saturation, in addition to that there was high variability between replicates. This has indicated that probably the high cell seeding density of our model is affecting the assay detection sensitivity. Therefore, on a parallel experiment Alamar blue assay was repeated on scaffolds seeded with a lower seeding density of $35X10^3/cm^2$ denoting seeding $10X10^3$ cells per scaffold (6mm punch biopsy). Fluorescent intensity was measured at different time points. Results demonstrated a trending increase on Alamar blue reduction (Figure 4.13).

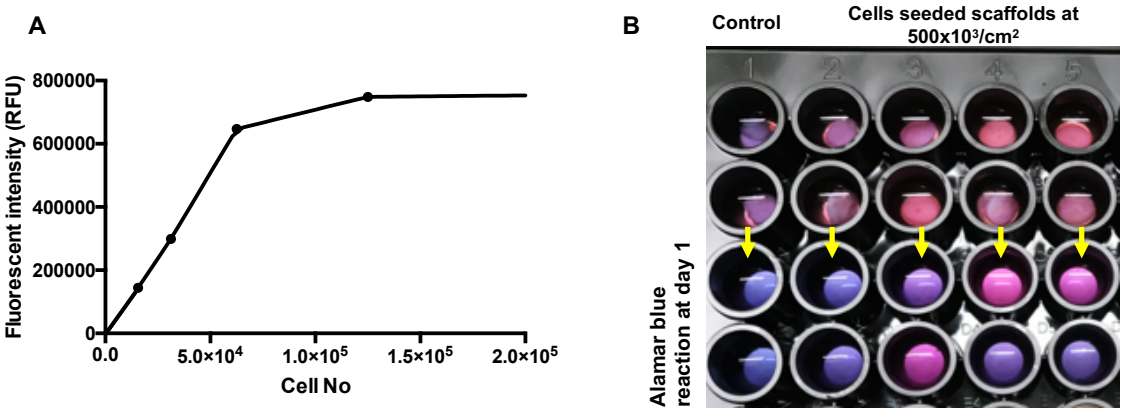

Figure 4.12: Alamar blue reduction on DC scaffolds seeded at 500x10^3 /cm^2

(A) Standard curve shows saturation at 60,000 cells, (B) variable Alamar blue reduction observed at seeded DC scaffolds.

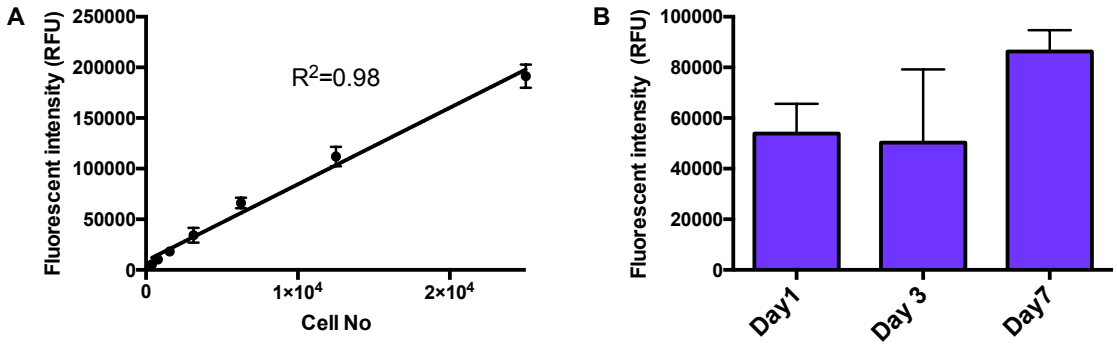

Figure 4.13: Alamar blue reduction on DC scaffolds seeded at low seeding density.

Reliable correlation could be established when seeding cells at low seeding density (35x10^{3}cells/cm^2). One-way ANOVA shows no significant difference observed of cells metabolic activity at 7 days of culture. n = 6, values represent mean±SD.

4.2.6 Assessment of cells proliferation

Immunofluorescence staining of proliferation marker KI67 was used to assess cells proliferation on decellularised tracheal scaffolds. Confocal microscope (Leica SP8 laser scanning confocal microscope) was used to image samples. Z-stacked images were captured and evaluated at different time points: 3 days, 7 days and 14 days of culture.

As shown in (Figure 4.14), KI67 staining results revealed localisation of several cells expressing positive KI67 staining (red) at day 3 (Figure 4.14, A&B) and at day 7 (Figure 4.14, C&D) However at day 14 of culture rare cells expressing KI67 were observed.

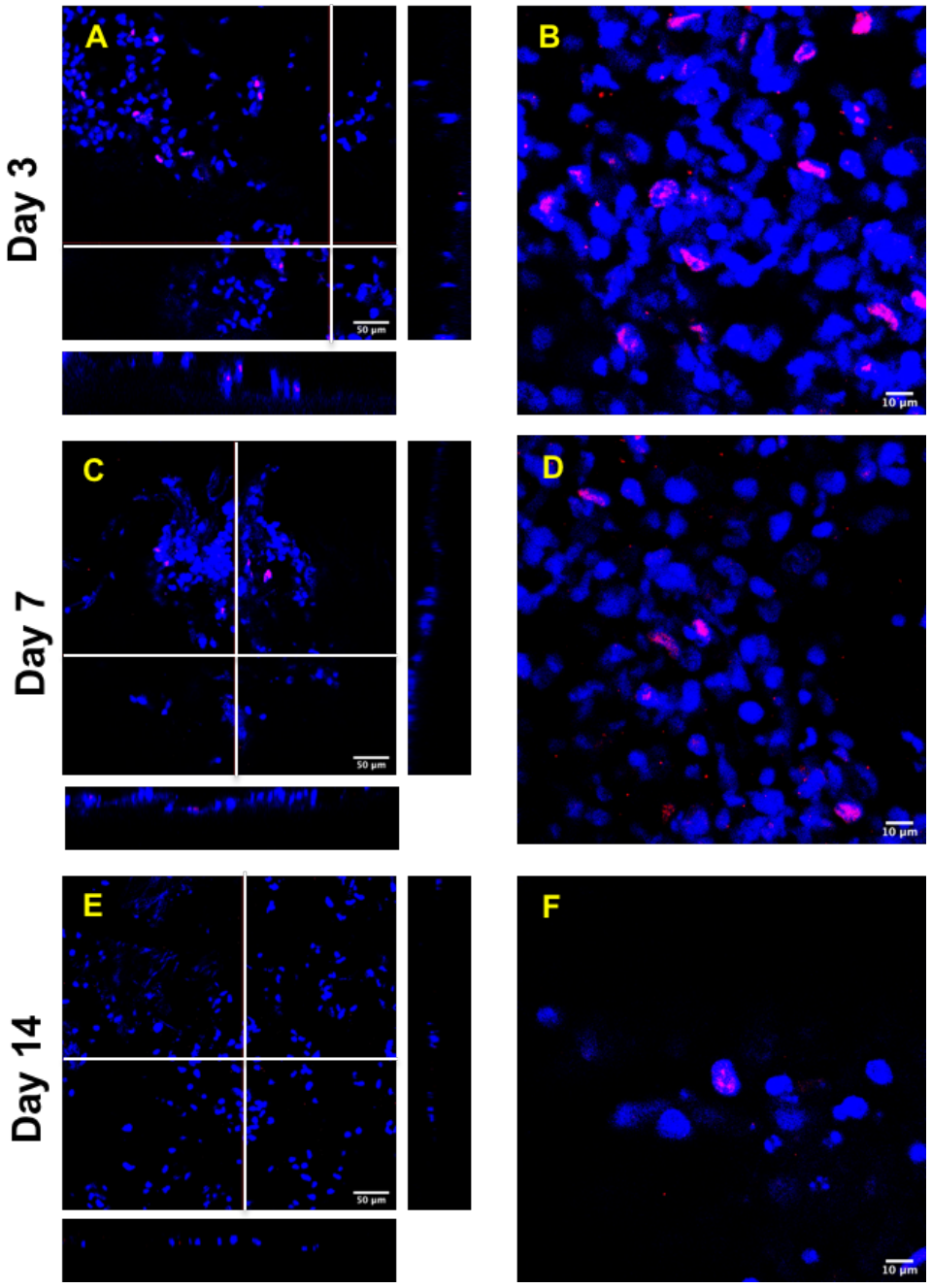

Figure 4.14: Assessment of cells proliferation with KI67 immunofluorescence staining.

Assessment of cells proliferation with KI67 immunofluorescence staining. Double-fluorescent image of Ki67 immunolabeling (red) and DAPI (blue) nuclear staining. Images shows localisation of KI67 staining (red) in several cells during day 3 and day 7. At 14 days, rare KI67 positive cells were observed. Scale bar for (A, C, E) = 50 µm, for (B, D, F)=10µm.

4.2.7 SEM evaluation of DC tracheal scaffolds microstructure

Scanning electron microscopy (SEM) was used to provide insights about the overall microstructural characteristics of the DC tracheal scaffolds and its effect on re-seeding technique. As can been seen in (Figure 4.15, A-D), the DC tracheal scaffolds display the typical microarchitecture of native trachea having three main layers, mucosal, hyaline cartilage layer and outer adventitia. A visual inspection of the images reveal that the outer adventitial layer consist of two layers: an outer layer displaying a more open loose fibres and an inner denser layer (Figure 4.15, B). The middle layer of the trachea consisted of more densely packed fibres with lacunae that lack interconnectivity (Figure 4.15, C). In contrast, the inner most luminal layer consist of a more open fibre structure (Figure 4.15,D) compared to the hyaline cartilage.

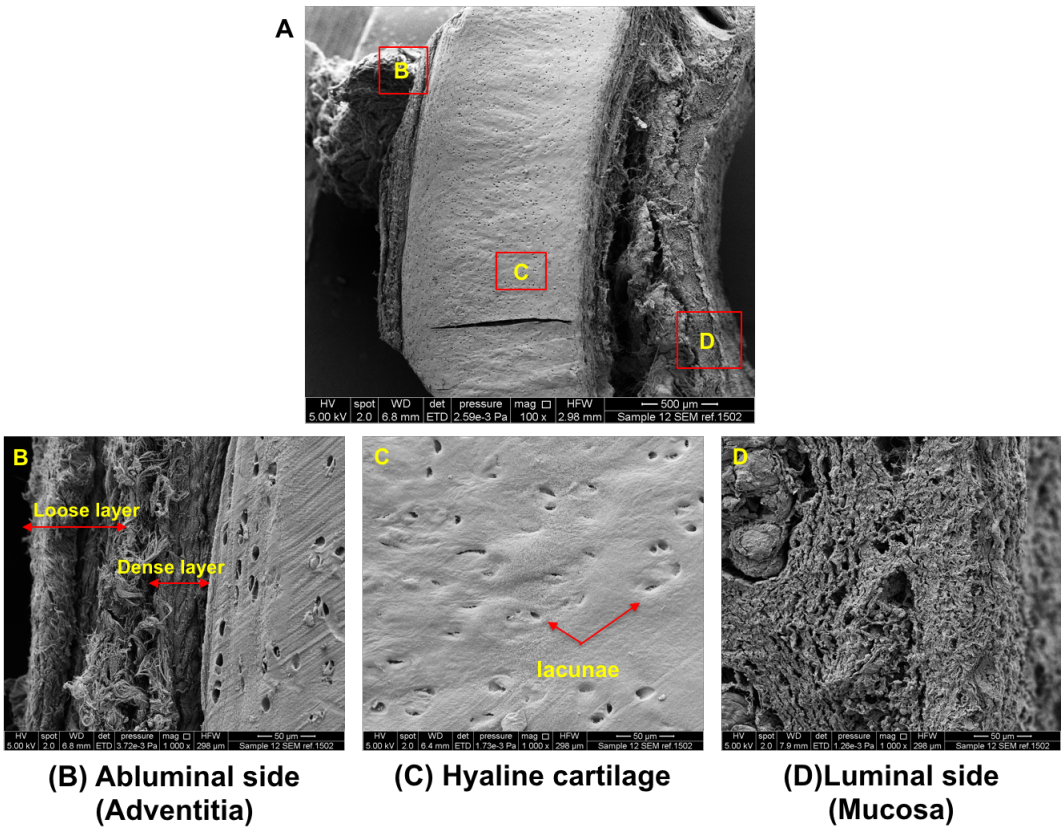

Figure 4.15: Cross sectional SEM micrographs of DC tracheal scaffolds. (A) cross section of DC tracheal scaffold, (B) abluminal side of trachea showing adventitia, (C), Hyaline cartilaginous layer, (D) Luminal mucosal side of DC scaffold. Scale bar for A=500μm, for (B-D)=50μm.

4.2.8 SEM evaluation of MSCs seeded decellularised tracheal scaffolds.

SEM was used to evaluate overall cell attachment and morphology to DC scaffolds over 7 days. It can be seen from (Figure 4.16), that MSCs seeded on DC tracheal scaffolds (abluminal side) were found to display two distinct morphology, a flat morphology spreading over the scaffold surface (Figure 4.16,B,C), or a round cell morphology (Figure 4.16,D,E). Observation of cells after 7 days in culture has demonstrated that cells remain attached while still maintaining the same mixed morphological pattern, this is displayed in (Figure 4.17).

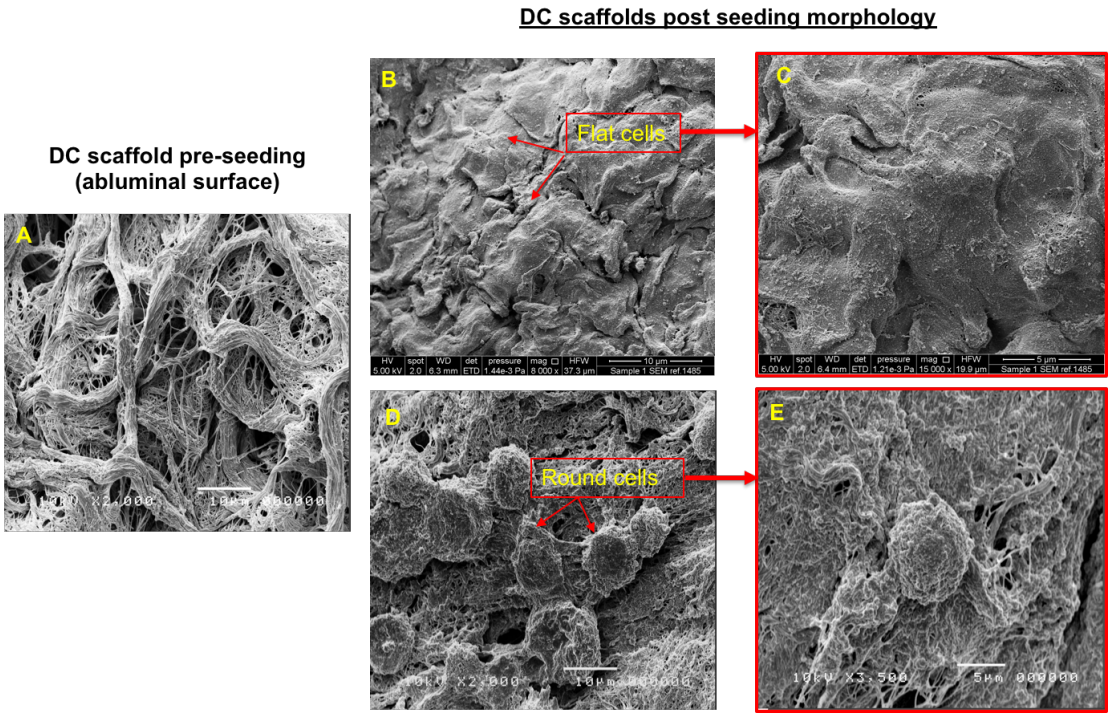

Figure 4.16: Representative SEM micrographs of MSC seeded into DC scaffolds at 3 days of culture.

(A) DC scaffold pre-seeding. Two cell morphology pattern were observed, a flat spread cell morphology (B,C), and a round cell morphology (D,E). Scale bar for (A,B,D)=10μm, for (C,E)=5μm.

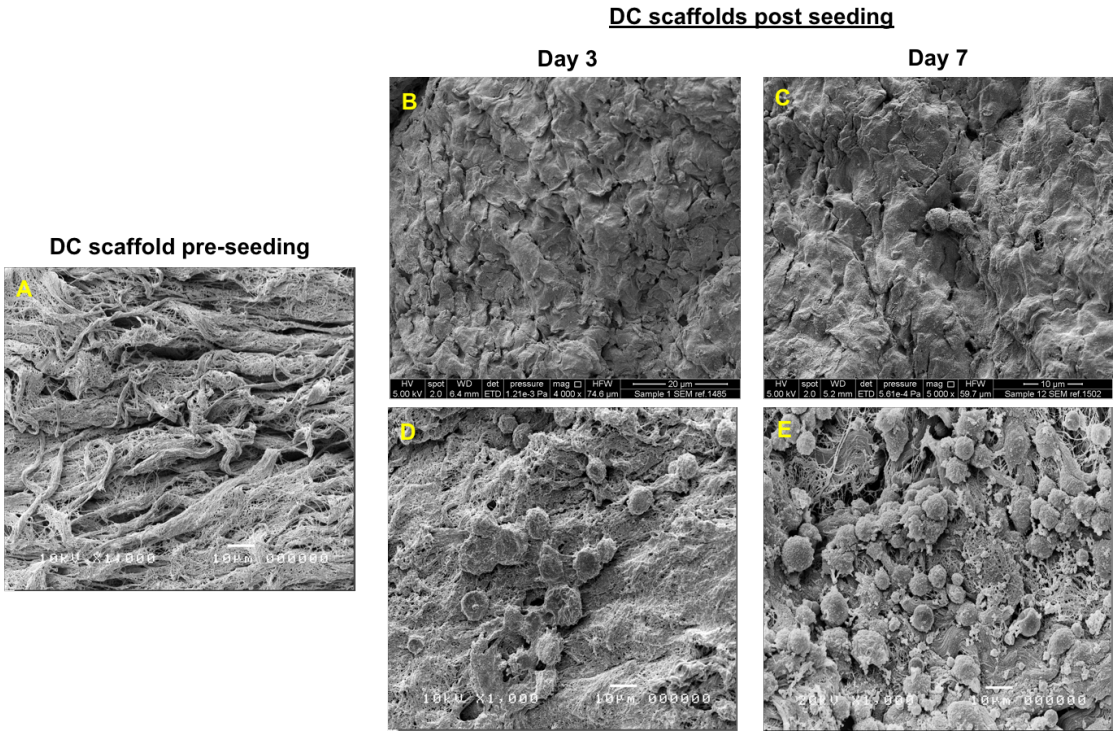

Figure 4.17: SEM micrographs of MSCs seeded into DC scaffolds at 7 days of culture.

(A) DC scaffold pre-seeding. (B, D) cells at day 3 showing round or flat cell morphology, (C, E) cells at day 7 showing flat or round cell appearance. Scale bar for (A, C, D, E)=10μm and for (B)=20μm.

4.2.9 Development of optical clearing protocol.

To aid a more representative assessment of cells localisation and infiltration in the intact volume the DC tracheal scaffolds. MSCs were transduced with Zs.green fluorescent reporter gene to facilitate studying cells localisation on DC scaffolds. Then a compatible BABB based optical clearing protocol was developed and optimised as detailed on chapter 2 to allow deeper visualisation of cell distribution and infiltration using multiphoton microscope (Leica SP8 laser scanning confocal microscope).

4.2.9.1 Zs.green lentiviral transduction of UC-MSCs

Lentivirus particles expressing Zs.green florescent protein were used to transduce UC-MSCs using an optimised laboratory protocol. Optimisation to determine optimal multiplicity of infection (MOI) was conducted by Dr. Antonio Di Rocco and Zs.green expression stability was confirmed over three weeks. Optimal MOI of 6 was found to provide effective and stable fluorescent labelling of UC-MSCs. As shown in (Figure 4.18, A, B), successful Zs.green transduction was achieved and 98.25% of UC-MSCs confirmed expression of Zs.green relative to negative control. Expression was further confirmed with the bright green fluorescent cells observed with fluorescent microscopy imaging of transduced cells (Figure 4.19).

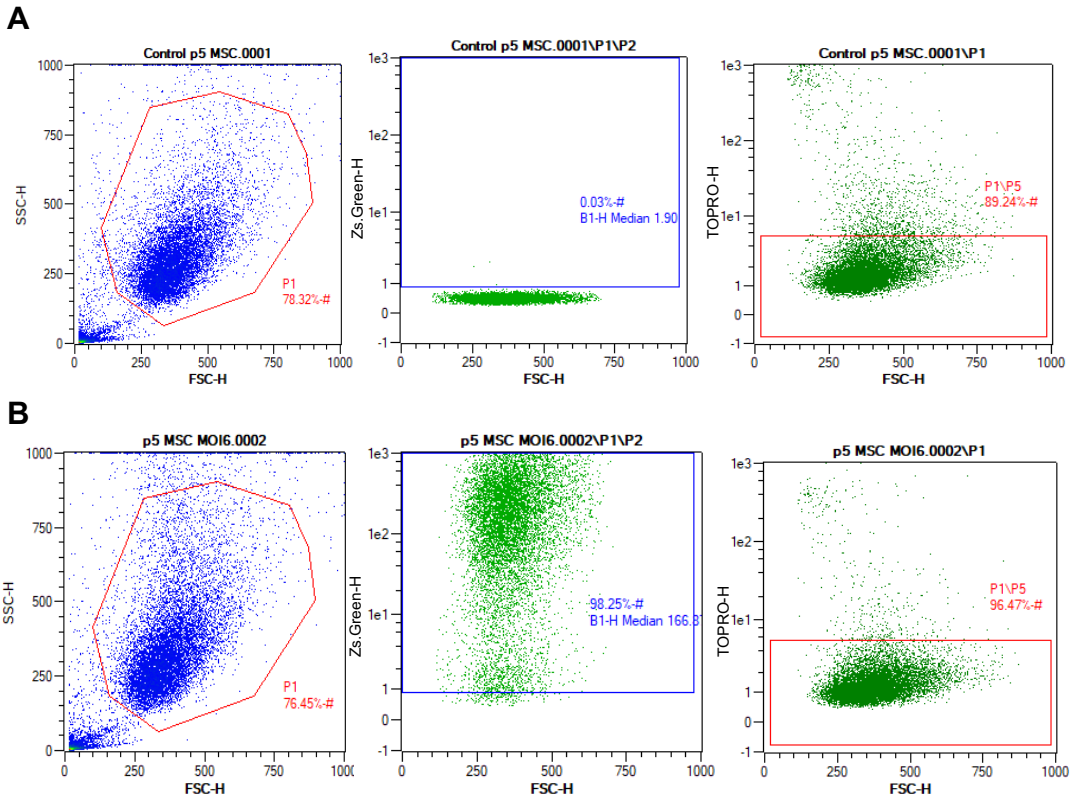

Figure 4.18: Flowcytometric assessment of Zs.green lentiviral transduction of UC-MSCs.

unlabelled control cells scatter plots showing negative expression for Zs.green and Topro (A), (B) are scatter plots of Zs.green transduced cells showing 96.47% of cells expressing Zs.green and are negative for Topro indicating viability.

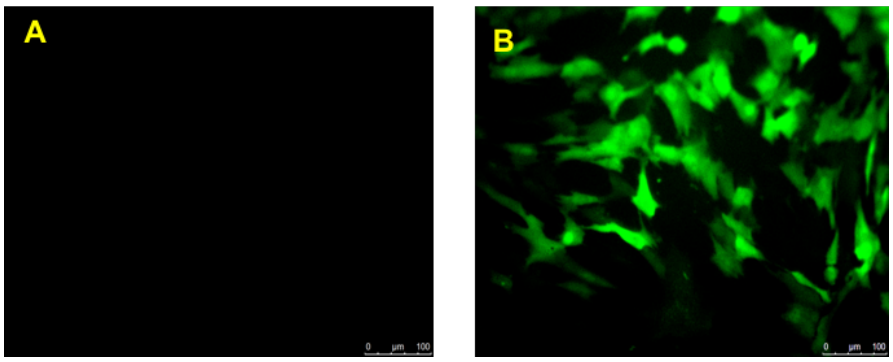

Figure 4.19: Fluorescence imaging of Zs.green transduced MSCs.

(B) shows bright green fluorescent signal of transduced UC-MSCs compared to unlabelled cells (C). Scale bar=100μm.

4.2.9.2 Optical clearing of seeded DC tracheal scaffolds

4.2.9.2.1 Macroscopic evaluation of BABB clearing protocol

BABB based protocol was used to optically clear DC tracheal tissue. As shown in (Figure 4.20). The specimens became notably more transparent and at a macroscopic level the light transmission was enhanced as evidenced by the appearance of the grid pattern placed behind the specimen. The overall macrostructure of the DC scaffold was also preserved.

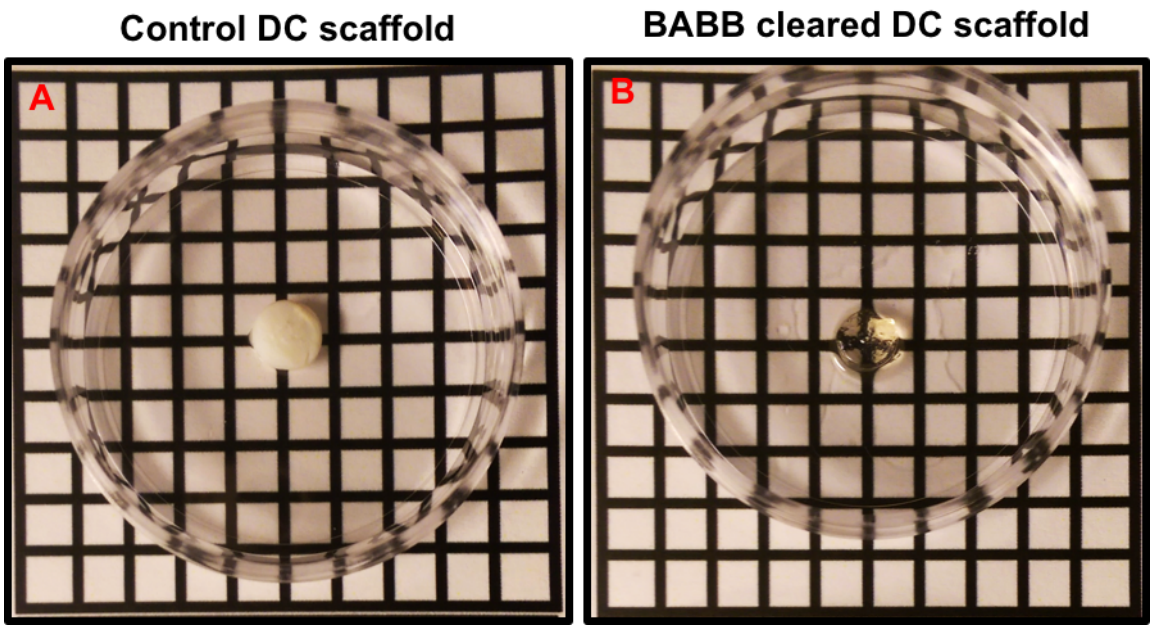

Figure 4.20: BABB optical clearing of DC tracheal scaffolds.

(A) control DC scaffold, (B) BABB cleared DC scaffolds. Punch biopsy diameter size= 6mm.

4.2.9.2.2 Microscopic evaluation of BABB clearing protocol

Comparative assessment of the utility of BABB clearing in improving imaging penetration was conducted using multiphoton microscopy (Leica SP8 laser scanning confocal microscope). Z stacks were processed and rendered using IMARIS image processing software.

Looking at (Figure 4.21), it can be seen that optical clearing of MSCs seeded scaffold has enhanced 3D volume visualisation to 4-folds (Figure 4.21, C, D) relative to control (non-cleared) scaffolds (Figure 4.21, A, B). The green fluorescent cells were imaged on the scaffolds with a reference to scaffold autofluorescence signal. It is worth noting that with BABB clearing, an imaging depth of 800μm (8-10 folds) could be reached but acquisition was stopped as no green signal was detected. Overall, we report an expedited 3-4 hours total processing time of optical clearing coupled to multiphoton imaging that allowed a more spatial survey of the 3D volume of the scaffold as opposed to conventional methods.

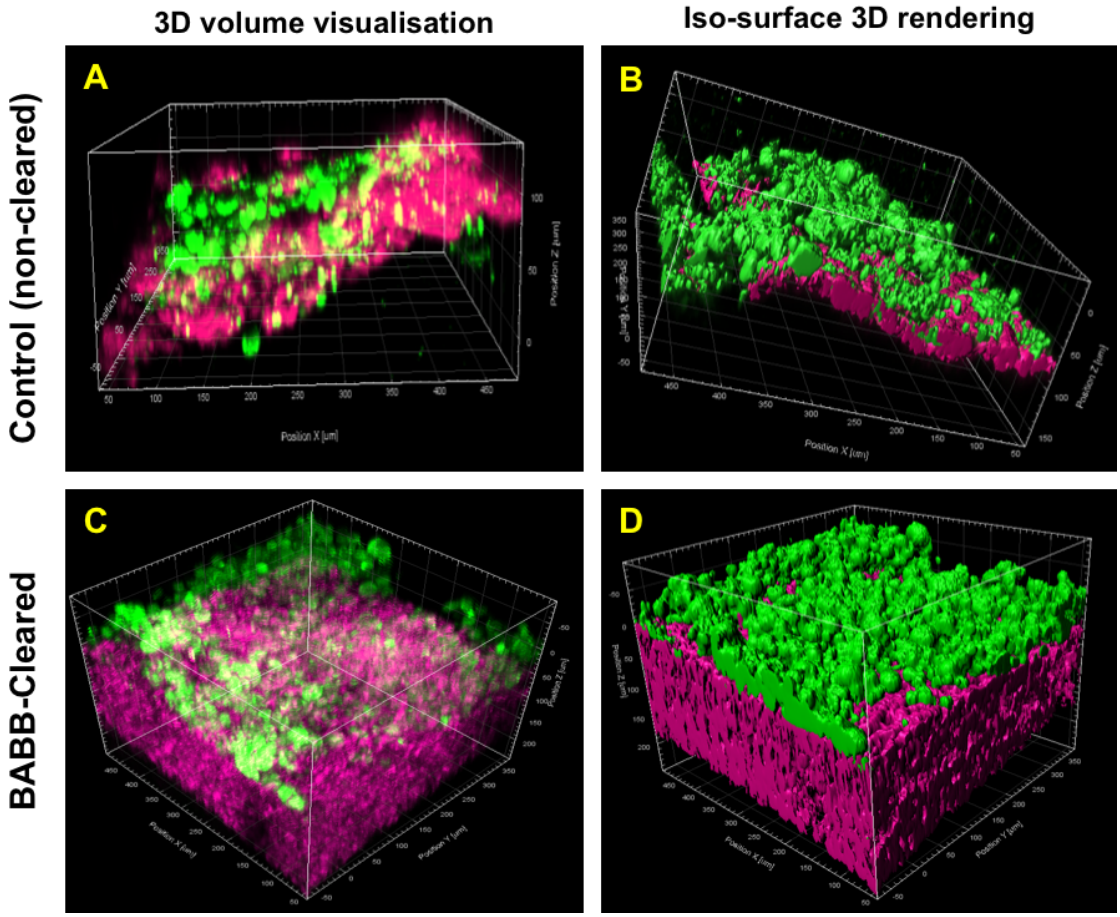

Figure 4.21: Microscopic evaluation of BABB optical clearing protocol.

In control (non-cleared) scaffold (A, B) imaging depth was approximately less than 50μm. Following BABB optical clearing imaging depth was improved to approximately 250 μm (C, D). Z stacks were rendered in 3D using IMARIS. Major tick grid lines = 50μm. (C& D) are IMARIS iso-surface rendering images of both (A, C).

4.2.10 Assessment of MSCs distribution and infiltration

Zs.green transduced MSCs-seeded scaffold were optically cleared and then imaged using multiphoton microscopy at 3 days and 7 days of cell culture to examine cells distribution and infiltration.

As can be seen in (Figure 4.22), optical clearing coupled with multiphoton imaging allowed the investigation of a significant amount of tissue as well as providing a more intuitive view of seeded cells distribution. Over 7 days of culture, cells appear to display two different morphological features, the typical fibroblastoid spindle shape of MSCs and sometimes display a rounded cell morphology (Figure 4.22, E,F). This finding is in line with SEM imaging results.

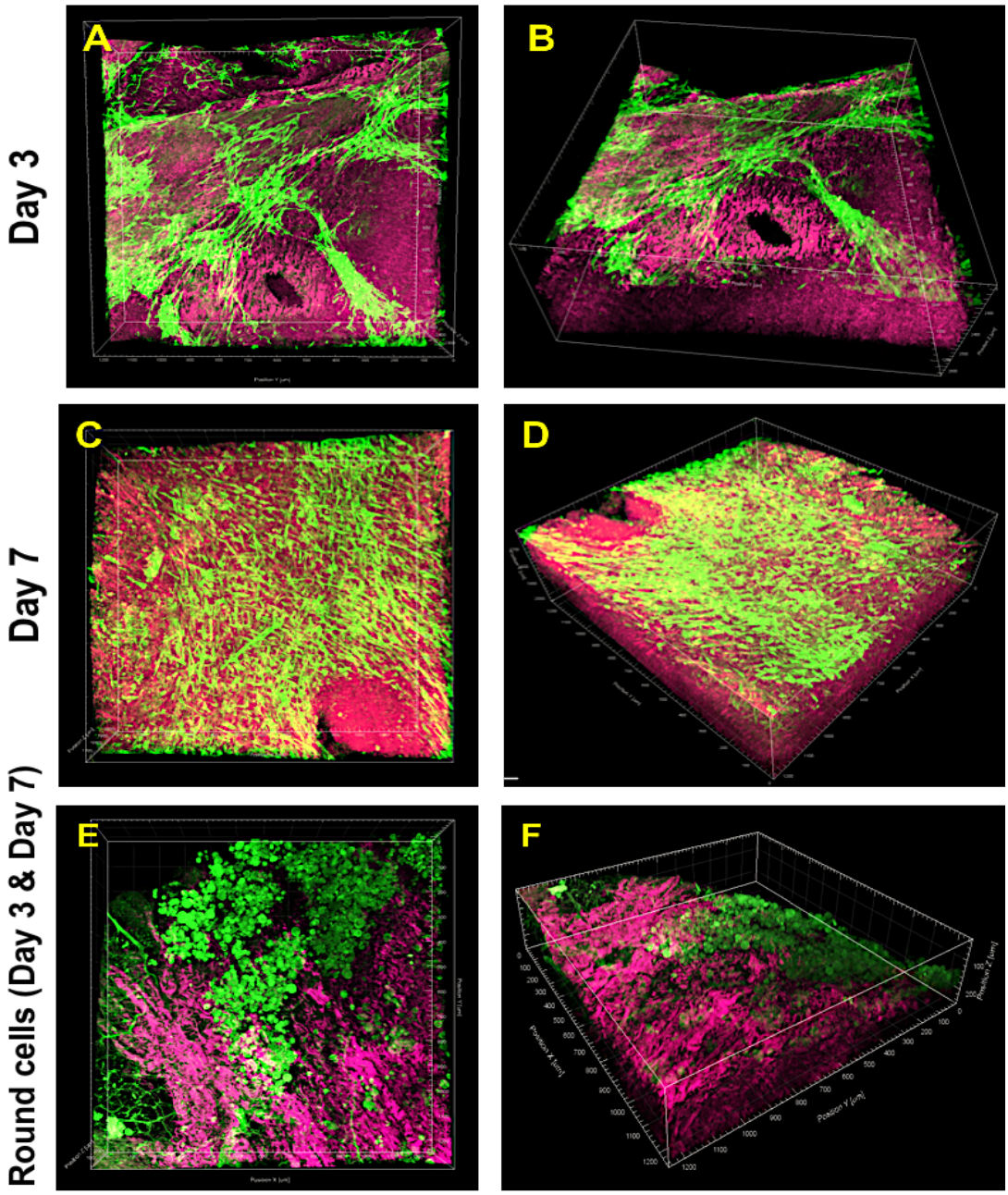

Figure 4.22: Assessment of cell distribution of Zs.green transduced UC-MSCs on DC tracheal scaffold.

(A, B) show Zs.green transduced cells (green) seeded on DC scaffolds (Magenta) at 3 days and at day 7 of culture (C, E), the cells displayed the typical spindle shape morphology of cells forming a layer covering the scaffold.(E, F) representative image of occasions when a round cell morphology was also observed on day 3 or day 7.(A, C, E) represent maximum intensity projection acquisition, (B, D, F) represent 3D volume rendering. Major tick line=50μm.

Assessment of cells infiltration revealed that over 7 days cells attach as a layer covering the DC scaffolds (Figure 4.23, A, B), however when examining infiltration by inspecting different optical sections of several 3D volume stacks (n=10), cell infiltration was only observed within the upper adventitial layer at an estimated mean depth of (127.56± 17.90μm) as clearly illustrated in (Figure 4.23, A, B, C). This was also seen in tissue sections of scaffolds seeded with prelabelled PKH26 cells (Red) as shown in (Figure 4.24).

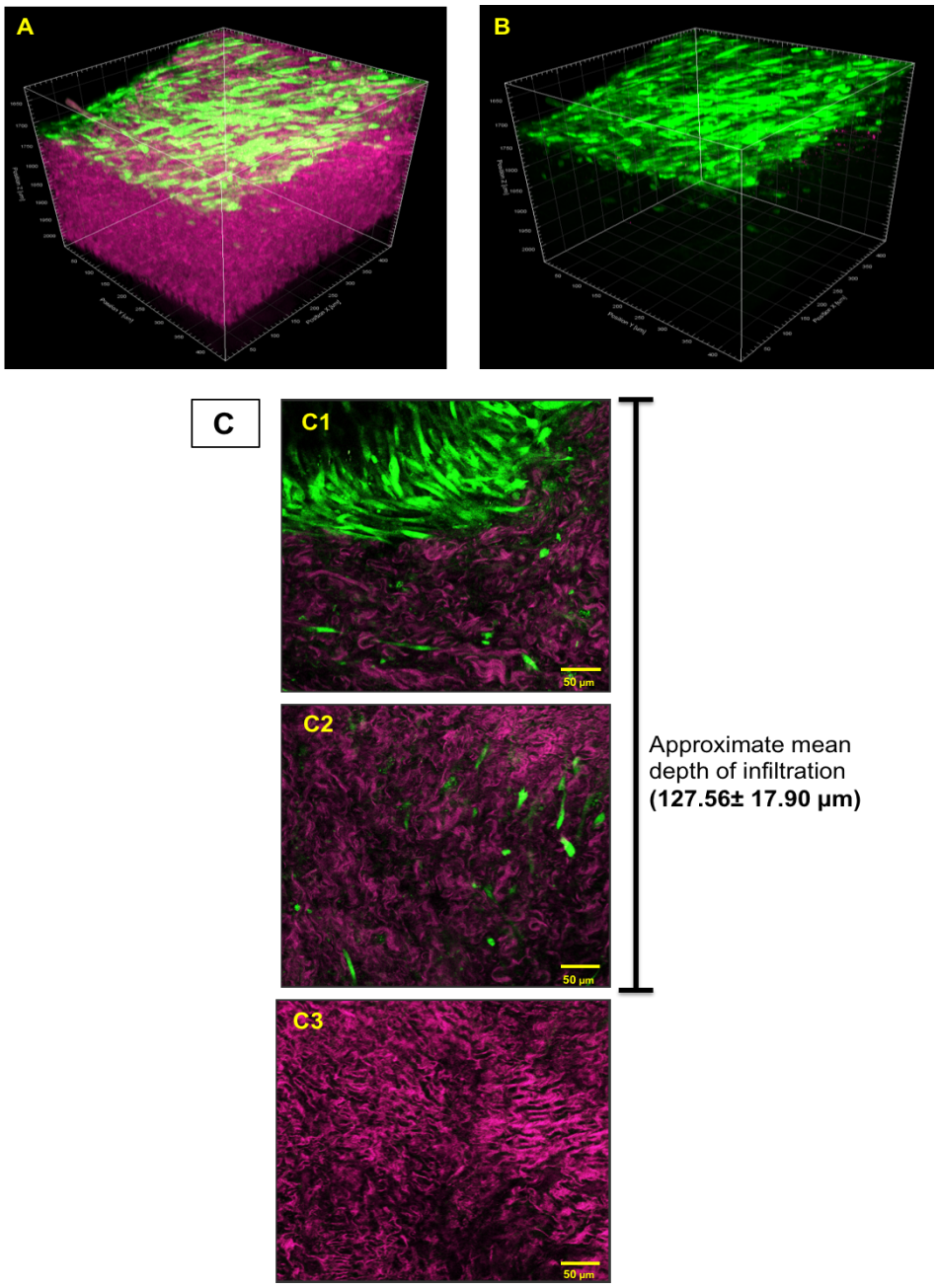

Figure 4.23: Assessment of cells infiltration of on representative 3D volume images.

3D volume image of cell-seeded scaffolds (A), (B) represent image A after removing scaffold fluorescence. Both (A & B) showing cells forming a layer covering the scaffold surfaces with no deep infiltration at 7 days, (C) is a representative cross optical-section view showing cells infiltration within the upper loose layer (C1, C2) at an approximate mean depth of 127.56±17.90µm and no cells were observed in the more dense matrix layer (C3). Scale bar=50µm.

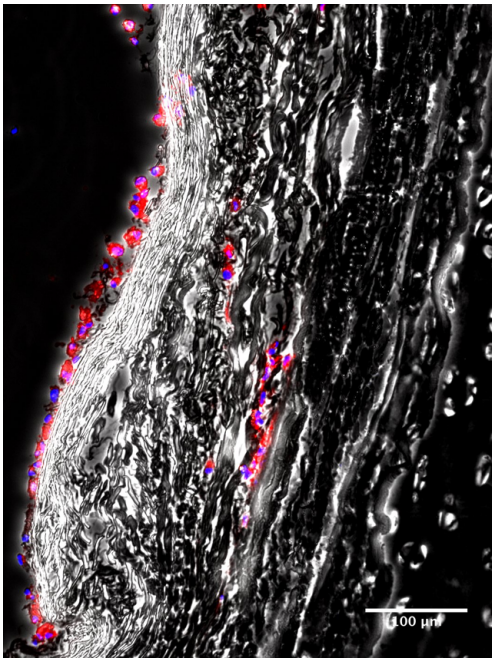

Figure 4.24: Assessment of cells infiltration in PKH26 prelabelled seeded scaffolds.

Cells appear to infiltrate within the upper adventitial layer. Scale bar= 100µm.

An interesting observation was also noted by visually inspecting different acquired 3D volume stacks and analysing many single optical sections as illustrated in (Figure 4.25), It was noted that when cells attach to the upper loose matrix (adventitia), they assume the spindle shape and seem to attach better covering the scaffolds (Figure 4.25, B) while if they are seeded on areas where only the dense collagen matrix is exposed, they appear to undertake the round shape morphology (Figure 4.25, D).

To further investigate this, we explored the expression of several ECM components that are known to support cells attachments by immunofluorescence staining as shown in (Figure 4.26), these are: collagen I, laminin and fibronectin. Results revealed that DC scaffolds that had an intact adventitia matrix expressed collagen I, laminin, and fibronectin (Figure 4.26, C-G). However, scaffolds that lack this layer showed no collagen I and laminin expression and had faint expression of fibronectin (Figure 4.26, D, F, H).

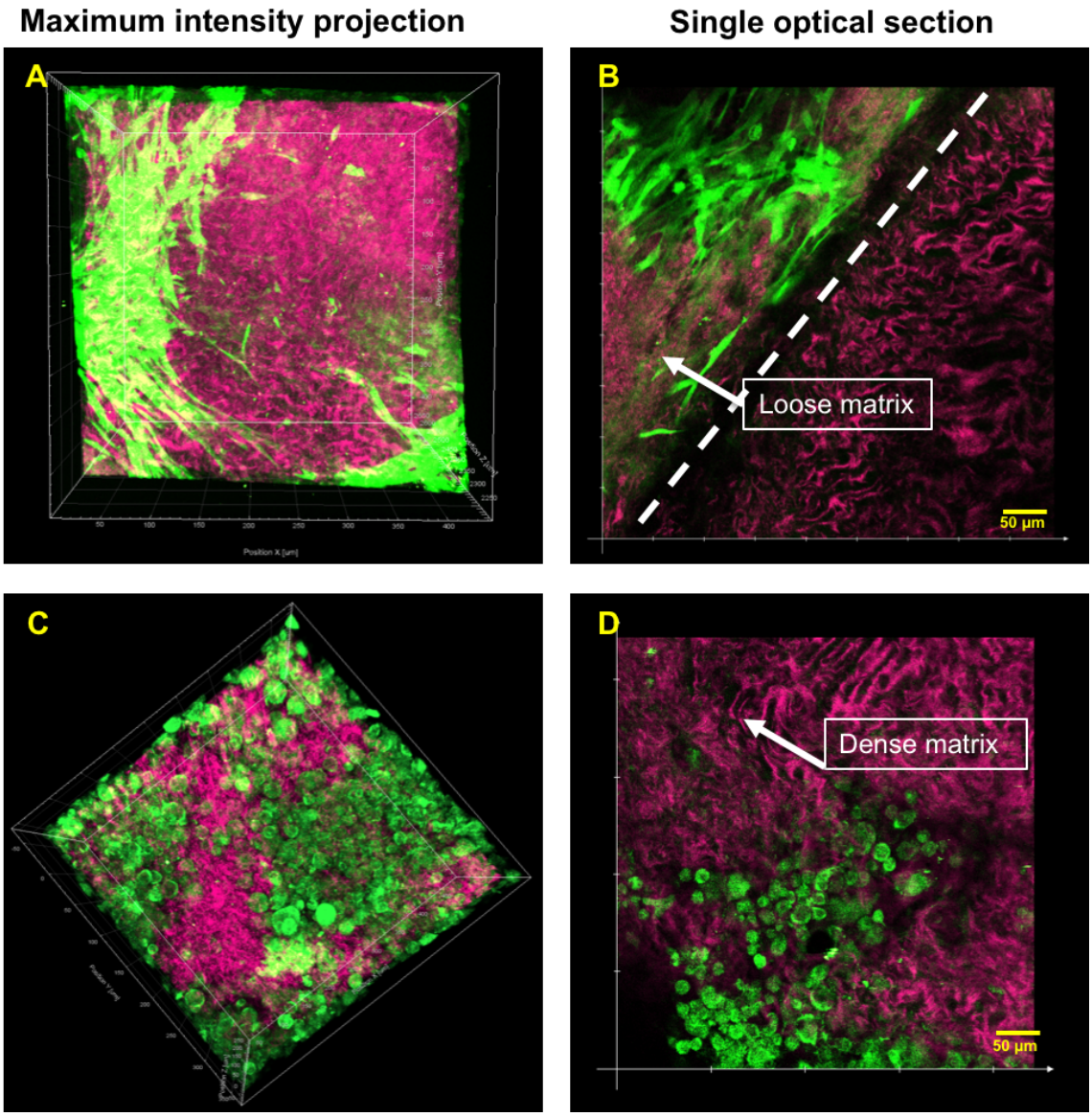

Figure 4.25: Visual inspection of shape of cells and their associated matrix. Maximum projection image of cells seeded scaffolds displaying spindle shape cells (A), (B) An optical section that reveal the presence two type matrix denoted by dotted line, an open loose matrix where cells are attached and looked spindle shaped. Maximum intensity projection of cells seeded scaffold showing round shaped cells (C). Single optical section showing round cells on dense collagen matrix (D). Scale bar=50μm.

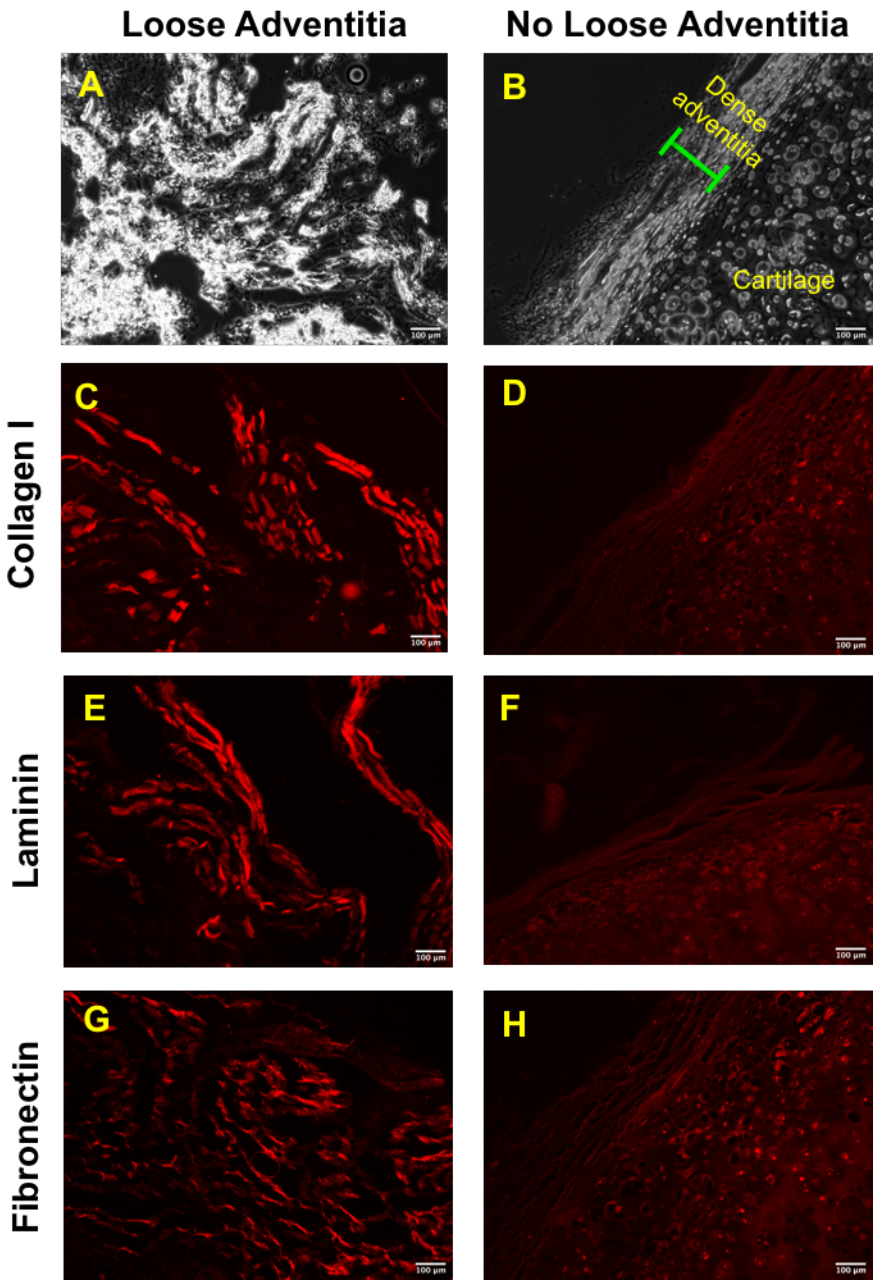

Figure 4.26:. Immunofluorescence staining of tracheal abluminal side comparing key ECM components between DC scaffolds with adventitial layer versus scaffolds lacking the adventitial layer.

Bright field images showing scaffold with intact upper adventitia layer (A) versus scaffolds with no loose adventitia (B). Scaffolds with intact adventitia display positive expression of collagen I (A), laminin (E) and fibronectin (G). While scaffolds with no loose adventitia demonstrate loss of collagen I (D), laminin (F) expression and reduced fibronectin expression (H). Scale bar= 100μm.

Fiji image analysis software was used to try estimate cell surface coverage area, two different seeding densities were compared 150x10^3 cells/cm^2 versus 500x10^3/cm^2 at 3 days of culture. Results revealed that at 500x10^3 cells/cm^2, the percentage cell coverage area was significantly higher showing a mean of (67.50± 6.716)% compared to the seeding density of 150x10^3 cells/cm^2 that showed a mean of (40.40 ±4.009)%. The results suggest that our cell seeding density displayed more surface cell coverage of the DC scaffolds.

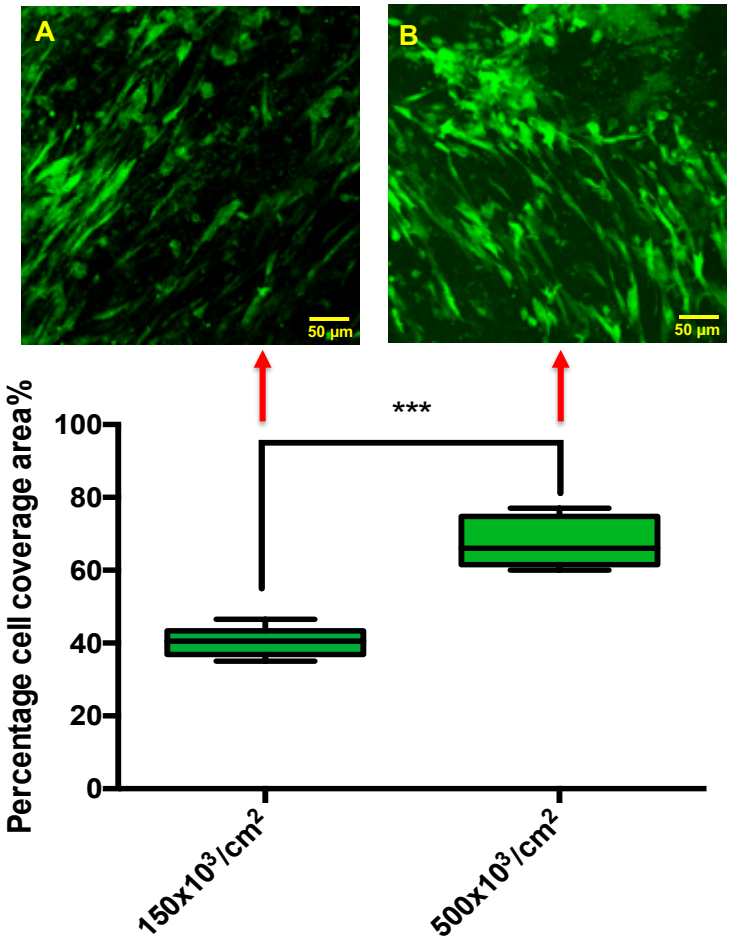

Figure 4.27: Comparison of percentage cell coverage area of seeded DC tracheal scaffolds.

Paired t-test comparison between different seeding densities. There is a significant increase in percentage cell coverage area difference between the two seeding densities. n=6. P≤0.001. Values represents mean ± SD.

4.3 Discussion

Cell seeding is a vital step in tissue engineering. The quality of this step will determine the level of cells incorporation on these TE constructs and consequently affects their anticipated role in promoting tissue functionalisation and constructive remodelling. Therefore, a desirable seeding technique needs to: achieve high seeding efficiency, cause minimal damage to cells while insuring homogenous distribution, as well as insuring reproducibility with minimal time and technical requirements (Soletti et al., 2006).

Passive cell seeding is the most common method of seeding cells in tracheal bioengineering, however considerable reports in literature have reported low cells seeding efficiency (10%-75%) and low cells penetration (Villalona et al., 2010, Song et al., 2018). Our own experience with passive seeding MSCs on decellularised scaffolds have supported these reports.

Therefore, one of the central aims of this chapter was initially to improve passive cells delivery of MSCs on DC tracheal scaffolds, and then to investigate closely cytocompatibility, cells spatial distribution and behaviour. All of which aim to provide some basic understanding and draw some useful clues that could help establish a better manufacturing process.

In order to improve passive cell seeding efficiency of DC tracheal scaffolds, it was hypothesised that partial surface dehydration (PSD) of the DC scaffold will help improve cells retention when passively drop-seeding cells on the surface of the scaffold. PSD is aimed to increase friction on the surface of the scaffolds, hence minimising runoff during the seeding process. In contrast to wet surfaces that are slippery by nature as a result of the low friction. It was proposed to perform the step in a CO_2 incubator, as it will provide a more controlled environment that by default maintain evaporation to the minimum and thus dehydration will be more controlled and temperate. Therefore, the initial part of this study aimed to test the above hypothesis.

As a first step towards this aim, experiments were conducted to determine the duration of PSD conditioning step and the effect of it on the scaffold quality, i.e., how long the DC scaffolds can be safely conditioned in the CO_2 incubator before an adverse dehydration damage occurs?

To address this question, the percentage water loss relative to sample wet weight at different time points during 24 hours incubation in a CO_2 incubator have been determined initially. The results demonstrated that between 30 minutes to 4 hours of incubation approximately 10-20% of water is lost from the DC scaffolds. Then SEM imaging and fibre diameter analysis were conducted on representative scaffolds at 4 hours to determine the effect of this additional step on the scaffold structure and inspect for dehydration damage. The results revealed that PSD conditioned samples in the CO_2 incubator maintained a relatively similar fibre network architecture displaying only a borderline reduction in the open spaces between fibres in comparison to control (unconditioned) DC scaffolds. Moreover, fibre diameter analysis demonstrated no observed statistical difference in fibres diameter compared to control scaffolds. On the other hand, samples conditioned under (BSC) cabinet displayed a compacted fiber network morphology with a complete loss of the open spaces between fibres and showed an enlarged swollen fibres appearance. In addition to that, statistical analysis of fibres diameter have shown a significant difference in contrast to control and CO_2 incubator conditioned samples.

As predicted, these data provided evidence that PSD conditioning can be performed in a CO_2 incubator without causing detrimental damage to the scaffold surface architecture. Moreover, it suggests that conditioning under a biosafety cabinet (BSC) appear to be more aggressive, evidenced by the appearance of signs of dehydration damage in the scaffolds. That said, these experiments provided an estimated safe range of incubation duration where samples can be PSD conditioned with minimal dehydration damage. It was decided to use a one-hour PSD conditioning step in the CO2 incubator pre-seeding in all the following experiments. It is noteworthy to know that this range is specific to the size and the slit area of the seeding plate used and should be optimised accordingly if the seeding chamber changed.

However, another problem was faced prior to starting experimentation, which is the lack of an agreed cells seeding density for MSCs in the field of tracheal bioengineering (Maughan et al., 2017). Therefore, to derive an initial (working) seeding density, an MTT assay was utilised to estimate a seeding density that gives the best cell coverage of the DC scaffold. The MTT assay was used because it has an advantage, that when applied to metabolically active cells it will be reduced to form blue formazan precipitate that can be visually inspected. So, a range of densities between $150x10^3$ -$1x10^6$ cells/cm^2 was compared, and the results showed that at a seeding density of $500x10^3$-$1x10^6$ cells/cm^2, full coverage of the scaffolds surface was attained. Therefore, it was decided to adopt $500x10^3/cm^2$ as an initial (working) seeding density in this study.

In fact, the utilisation of an MTT assay to provide immediate decision with regards to verification of seeding in scaffolds has been used in many studies (Sherwood et al., 2002, Zund et al., 1999). For example, Jungebluth *et al*. used a modified one-hour MTT protocol coupled to DAPI stained cell counting to verify seeding prior to transplantation. In this study the authors used mathematical modelling to develop a colorimetric scale bar that can predict cell coverage of the tracheal scaffolds prior to transplantation (Jungebluth et al., 2013, Philipp et al., 2014).

But contrary to their findings calorimetric quantitation of MTT results was not achieved in our study because lysing of the formazan precipitate from the DC tracheal scaffolds proved difficult. This discrepancy could be attributed to the difference in reagent used for solubilisation of formazan precipitate, in their study they used a modified 10% SDS in 0.01 HCL lysing solution, while in our study the kit was found to be based on the original protocol developed by (Mosmann, 1983) that uses acid isopropanol.

Overall the use of macroscopic (visual) MTT evaluation in this study had served the purpose and offered a practical simple solution to help define an initial working seeding density as a starting point for experimentation. It is important to stress that this derived seeding density must not be considered as an optimal density at this stage. This is because cell seeding density is a complex parameter that is affected by many other variables such as: scaffold permeability, structural and biomaterial properties, and should be finetuned in light of information about these microscopic interactions.

But results from this experiment suggests that the seeding density that ensure uniform delivery and cell coverage is in the range of > $150x10^3$ and $\geq$ $500x10^3$. This experiment was also conducted on punch biopsies of DC tracheal scaffolds to eliminate the tubular geometrical effect on the results.

Overall, these experiments helped set the stage to test our hypothesis that PSD conditioning of DC scaffold will improve cell seeding efficiency (CSE). For this purpose, a blinded multiple operator experiment was conducted to compare CSE of PSD conditioned scaffolds group to control DC scaffolds (unconditioned) after 24 hours cultivation of cell seeded scaffolds.

As hypothesised, the results showed that there was a significant increase in the cells seeding efficiency (CSE) in the PSD conditioned group compared to control (unconditioned group). The mean CSE reported was (96.46% $\pm$1.710) for PSD conditioned group and (79.09 $\pm$ 9.091) for the control group. The most interesting finding that emerged from the data was the improvement of consistency and reproducibility of the CSE despite the multiple operators as denoted by low standard deviation in the PSD conditioned group. These results were further confirmed by H&E staining and PKH26 immunofluorescence staining of seeded scaffolds, which showed retention of more cells within the PSD group relative to the control group.

Efficient cell seeding must also preserve cells viability and avoid damage as much as possible. Moreover, cell damage might change the environment of the medium and might eventually affect other cellular interactions (Adebiyi et al., 2011). Therefore, cell viability assays were conducted to confirm the effect of our modified seeding technique.

Live/ dead staining and quantification of the percentage cell viability demonstrated maintenance of cell viability over 14 days of culture. The data showed that there was a significant increase in the ratio of live cells between day 3 and day 7 from 60% to 94.97% then the ratio of viable cells decreased at day 14 to 56.49%. The cells ratio obtained on day 3 is probably representing the mixture of both attached and un-attached (dead) cells. But owing to the limitation of the quantitation method being only a percentage ratio of live to dead cells, the observed increase in the ratio on day 7 is not likely reflecting an increase on the number of viable cells but could be reflecting the cytocompatibility of the scaffold where attached cells remain viable. Also, the drop of viability on day 14 could be attributed to either overcrowding that lead to cell death or it could be a natural progression of cell cycle.

Taken together we have described PSD conditioning as a new step pre-seeding that have proved to significantly improve the passive CSE of the DC tracheal scaffolds. The main strength of this study is blinding that confirmed improvement of reproducibility, as this is a highly desirable feature of a successful seeding technique.

In fact, it was not possible to compare our CSE findings with the published studies in tracheal TE seeding that have employed similar or other seeding methods like perfusion seeding or vacuum seeding (Haykal et al., 2014b, Chiang et al., 2016). This is because, these studies have often relied on qualitative assessment on CSE such as: histology and SEM. This highlights the need to have a unified quantitative assessment method for reporting CSE to allow reliable comparison among different cell seeding techniques.

It is worth noting that in our study we have utilised an indirect DNA based quantification CSE. Whilst several studies have considered direct DNA quantification methods of CSE a more realistic estimate of the cells ending up in the scaffolds (Impens et al., 2010). Trying direct quantification of DNA to reflect CSE in our study was not possible due to the inhomogeneous nature of the tracheal scaffolds and the variability of residual DNA within the decellularised scaffolds, so normalisation and reliable quantification proved difficult. Nevertheless, the CSE was confirmed by our ability to reproducibly detect cells in whole mount and tissue sections in contrast to our previous attempts prior to introducing PSD conditioning step.

The modified method offers a simple, time and cost-effective method of attaining reproducible CSE of tracheal grafts. Although dynamic seeding techniques like perfusion seeding have been reported to give higher seeding efficiency to some degree in other models of tissue engineering (Li et al., 2014), these methods are still complex techniques that require lengthy culture periods and are labour-intensive. Moreover, they depend on the durability of the scaffolds and the biomaterial properties. In addition to that dynamic systems might cause cell damage as a result of shear stress (Li et al., 2014, Impens et al., 2010).

An interesting piece of information that we came across during our project which supports our approach, was when we found out that Prof. Anthony Atalla's group at Wake forest Institute for regenerative medicine, have been blotting the surface of their scaffolds prior to seeding to reduce moisture and enhance cells retention (Dr.Hadi Mirmalek Sani, 2017, Personal communication). We believe that we have provided a safe sterile method of surface drying that can be clinically translated. Indeed, our modified seeding technique has been clinically translated in to a GMP manufacturing process of a compassionate case (MHRA/MIA (IMP)11149) of decellularised tracheal scaffold seeded with BM-MSCs, where the PSD conditioning step have been scaled to the size of the GMP seeding bioreactor. The operators observed during the seeding process, the reduction of cells runoff. Moreover, DAPI staining of the seeded tracheal scaffolds pre-implantation have revealed successful cell delivery.

Turning now to the second part of the study, which aimed to investigate scaffolds cytocompatibility, cells proliferation, infiltration and distribution.

Alamar blue assay was used as a quantitative assessment of metabolic activity. The results revealed that the linear limit of the assay was at 60000 cells and no reliable linear correlation for quantitative measurement of cell numbers could be established within the range limit of our seeding density of $500x10^3$ cells/cm^2. So due to saturation the results were sometimes off scale the linear limit of the assay. It was also observed by inspecting for the colour change, that cell seeded scaffold had variable reduction pattern for Alamar blue reagent from no reaction to bright pinkish colour change. However, when seeding density was reduced to fall within the liner limit of the assay, Alamar blue reduction was apparent and was reliably quantitated.

The results demonstrated no significant different on cells metabolic activity over 7 days of culture despite the trending increase observed. These results substantiates previous findings in literature that have reported a limitation of Alamar blue responsiveness to high cell numbers, on which the correlation of viable cell numbers to the rate of Alamar blue reduction deviates from linearity at high cell densities (Uzarski et al., 2017, Rampersad, 2012). Whilst Alamar blue is one of the highly referenced substrates for metabolic activity and quantitative estimation of cell numbers as a non-invasive assay that provides time course measurements, its applicability for accurate quantification is highly affected by the assay conditions. For example, high cells density, lower Alamar blue working volume or longer incubation times all of which may lead to depletion of Alamar blue pool (Uzarski et al., 2017). Moreover, Alamar blue might be irreversibly reduced by cells to a colourless non-fluorescent by-product (hydroresurofin) rather than the fluorescent (resurofin), hence leading to underestimation of the actual cell number (O' Brien et al., 2000, Zalata et al., 1998, Uzarski et al., 2017). Other factors that might affect Alamar blue sensitivity include other non- specific interactions with assay chemistry that may cause false positive or false negative results, such as presence of foetal bovine serum (FBS) that might quench fluorescent signal (Rampersad, 2012).

In light of this, our results demonstrated the unsuitability of Alamar blue for quantitative estimation of cells number and metabolic activity in the density range of our seeding technique. Also, the observation of variable reduction intensity of Alamar blue on different cell seeded scaffolds might reflect variable cell attachment affinity to the underlying ECM, or reduced metabolic activity due to high cell numbers on the limited scaffold space or it might also reflect suboptimal assay conditions.

In this context it is important to mention some successful application of Alamar blue in tissue engineering literature where Alamar blue reduction was used in a perfusion system to monitor cell viability and proliferation of re-reendothelialised decellularised lung scaffolds (Ren et al., 2015, Tapias et al., 2015). These studies were interesting in that, reduction standard curves were optimised based on cells to medium ratios instead of absolute counts in order to reflect alamar blue activity in the large volume of media used the bioreactor system. In their study it was clearly stated that they have observed saturation of the standard curves at high density of $500x10^3$/ml and their reported cell seeding density was within the linear limit of the assay. These finding supports our findings in this study.

In fact, the use of metabolic based assays like MTT or Alamar blue to reflect cell numbers have always been critiqued in tissue engineering literature, because these assays mainly correlate to cellular activities that fluctuates with time and are affected by many other variables. For example, the test cannot differentiate between cells that are actively dividing and cells that are quiescent and so might incorrectly overestimate numbers (Ng et al., 2005, Impens et al., 2010). Moreover, even when predicting cell viability, a reduction of cell viability could either be a result of cytotoxic effect or might also indicate suboptimal assay conditions (Rampersad, 2012).

Then the proliferation of UC-MSCs on DC tracheal scaffolds was also evaluated by immunofluorescence staining for the proliferation nuclear antigen KI67 over 14 days of culture. The expression of KI67 has been widely used in routine pathological investigations as a proliferation marker (Li et al., 2015). It is present in the nucleus of all active phases of cell cycle (G1,S,G2 and M) but not those in

quiescent phase (G0) (Scholzen and Gerdes, 2000). Our results demonstrated positive staining of KI67 between day 3 and day 7 indicating cytocompatibility of the scaffolds to support cells proliferation. However, on day 14 occasional to no KI67 expression was observed, reflecting reduced proliferative capacity of cells that might be attributed to progression of cell cycle to the resting state or senescence. These findings are in line with our live/ dead viability results that showed drop of cell viability on day 14 to 50%.

Then the study focused in investigating the attachment, spatial distribution, and infiltration of MSC on DC tracheal scaffolds. As a start, SEM imaging was utilised to illustrate the microscopic 3D architectural structure of DC tracheal scaffolds. In this chapter we revisited the assessment of the scaffold structure from the aspect of its implication in cells seeding. Whilst the scaffold composition and its material properties determine the cells ability to attach and the overall cytocompatibility, the scaffolds microstructural properties like porosity plays key roles in determining cells infiltration capabilities (Perez and Mestres, 2016, Patel et al., 2016).

In our study SEM micrographs revealed that the outer abluminal layer, (adventitia) consist of two layers, an outer loose layer showing an open loose fibres appearance and an inner denser matrix. This two-layer pattern was clearly defined to be near the annular ligaments and tend to be obscured away from it (Ohkimoto et al., 1997). Then the hyaline cartilage layer display a compacted dense fibres with lack of interconnectivity between chondrocytes lacunas. The innermost layer appeared to have an open fibre appearance in comparison to the hyaline cartilage.

This clearly highlights the typical complex inhomogeneous microstructure of the trachea and how it can hinder passive incorporation of cells within its entire depth. This is particularly true within the dense hyaline cartilage. Indeed, a wealth of studies have demonstrated the challenges in incorporating cells in to cartilage type tissue due to its nanopore dense ECM structure and lack of interconnectivity (Xu et al., 2017, Gong et al., 2011). This sheds light in one of the limitation encountered when seeding natural DC scaffolds that have predefined matrix architecture unlike synthetic scaffolds where pore size can be easily controlled

during manufacturing to facilitate cells incorporation (Vitacolonna et al., 2013). Additionally, even the measurement of porosity to draw expectation with regards to cells incorporation is a challenging task. Because natural tissues cannot withstand the drying procedures used with conventional porosity measurement (Majda et al., 2017).

Based on that, our study aimed to investigate the degree of cells infiltration post passive seeding within the upper adventitia and the annular ligaments that are structurally less dense than the hyaline cartilage. Initially MSCs attachment to the DC tracheal scaffolds was evaluated with SEM over 7 days of culture. The cells remained attached to the scaffolds over 7 days of culture. But, interestingly cells were found to display two distinct morphologies. Either flat cells that spread covering scaffolds surface or sometimes appear as round cells. This could be a manifestation of the ECM microenvironment effect on cells behaviour.

The ECM microenvironment is a complex dynamic substrate that interact with cells and provides various physical and biochemical cues that orchestrate cells attachment, morphology, proliferation, commitment and survival (Watt and Huck, 2013, Gattazzo et al., 2014). For example, (Engler et al.) have demonstrated in his studies how MSCs sense matrix stiffness and transduce this in to morphological changes and lineage commitment . On which MSCs on stiffer matrices that mimic striated muscle elasticity (Elasticity $_{muscle}$ 8–17 kPa) displayed a spindle-shaped cells similar in shape to myoblasts, while MSCs cultured on more stiffer matrices that mimic collagen of osteoid (Elasticity $_{muscle}$ 25–40 kPa) displayed polygonal osteoblastic morphology (Engler et al., 2006, Engler et al., 2004). Other ECM cues involve topographical features of the matrix, for example on topographical features that restricted the spreading of MSCs and promoted elongated morphologies, MSCs assumed osteogenic differentiation (Fiona and Wilhelm, 2013). Another central element is the ECM structural and adhesive components, such as collagen, fibronectin, elastin etc. These components serve many functions including influencing cells adhesion, morphology, fate and stability. For example, absence of epithelial cells adhesion will induce cell death by apoptosis (Anoikis) (Grossmann, 2002), or culturing chondrocytes on collagen type I may induce their dedifferentiation (Nehrer et al., 1997). With regards to our

findings, cells were seeded on scaffolds that possess predefined complex characteristics in addition to the effect of decellularisation process that might have altered or removed certain cues and therefore further investigation will be needed decrypt these micro interactions and its implications.

Then the final part of this study, sought to develop an understanding about the spatial distribution, organization and infiltration of MSCs when passively seeded on DC tracheal scaffolds. As the tissue engineering field continues to progress with the development of large complex tissue engineered constructs. There is a need to develop tools that allows interrogation of large volumes of tissue and exploration of the spatial interactions between scaffolds and seeded cells. The standard method in tissue engineering mainly rely on the use of histological sectioning, this technique is time consuming and requires laborious sectioning. In addition to that it only provides a two-dimensional (2D) snapshot of the constructs that fail to reflect cells distribution and interactions. Other methods like MRI, μCT scan, are not cost effective and lack resolution (Vielreicher et al., 2013). Whilst laser scanning fluorescence microscopes (confocal and multiphoton microscopy, MPM) can solve this problem because they employ optical sectioning for the creation of 3-dimensional (3D) volume imaging with improved depth. Yet, their imaging depth depends on tissue transparency and is limited by the high light scattering that results from thick opaque tissues to less than 100μm (Vielreicher et al., 2013, Silvestri et al., 2016).

Herein we describe the use of optical clearing technique coupled to fluorescently labelled reporter (Zs.green) UC-MSCs and multiphoton imaging to visualise cell seeding distribution and infiltration. Optical clearing is a technique that denotes transformation of an opaque tissue to transparent by matching the refractive indices of its components by immersing them in specialised reagents. In fact, tissues are opaque because there is a mismatch between the refractive index of the dry components (protein, lipids) relative to its water content, which ultimately cause more light scattering leading to the perceived tissue opacity (Silvestri et al., 2016). The technique has been mainly used in the field of embryology and neurology (Calve et al., 2015), but recently many studies started to use it in adult

tissues like lung (Scott et al., 2014), heart (Moy et al., 2013) and peripheral nerve (Jung et al., 2014).

In this study we have optimised a BABB (benzyl alcohol : benzyl benzoate) based optical clearing protocol that rendered the sample transparent within 10 minutes while preserving the overall macrostructure. The comparison between non-cleared versus cleared specimens revealed an improved 3D volume imaging depth of 4 to 10 folds. Even the overall processing and acquisition time was approximately 3 hours in contrast to conventional histological sectioning. It is worth mentioning that with this protocol the entire depth could have been imaged but our focus was to acquire where the cells are attached and expected to infiltrate.

By visually inspecting 3D volume imaging of seeded decellularised scaffolds, cells were found to be attached on the DC scaffold over 7 days of culture, however a similar finding to SEM results have been noted, where cells either displayed the typical fibroblastoid spindle shape morphology and spread over the entire scaffolds surface or sometimes where found to display round shape morphology. The assessment of infiltration revealed that the cells mainly remained as a layer covering the scaffolds over 7 days of culture, however penetration was sometimes observed within the upper adventitial layer at an approximate depth of 127.56 ± 17.90 μm. It is possible that owing to static culture setup that cells layered on the surface where nutrient and oxygen supply are abundant or it could also indicate that cells penetration is limited to the upper loose layer only. Future work should aim to compare static culture to dynamic culture and inspect for cells infiltration.

Then, we have taken the advantage of the improved 3D volume resolution and queried closely many optical sections of the acquired 3D volume stacks and noticed a specific pattern related to cells morphology. It was apparent that when cells are attached on the loose adventitia, the cells assumed a fibroblastoid spindle shape morphology. However, when the cells were laying on the dense matrix or exposed collagen matrix, they assumed the round morphology. So, we sought to investigate this further.

As discussed earlier, the ECM physical and biochemical cues interact with cells and influence cells behaviour including shape, attachment, proliferation and fate. MSCs are anchorage dependent cells (Salzig et al., 2016). Their adhesion to ECM is mediated mainly by transmembrane heterodimeric integrin receptors that bind specific adhesive ligands such as (fibronectin, collagen, laminin) forming their focal adhesion complexes (Salzig et al., 2016). This mediates signalling that induces modification in cell morphology and will direct crucial downstream functions such as growth, behaviour and their subsequent fate (Barthes et al., 2014, Hynes, 2002). The maintenance of strong adhesion and spreading is required for cell proliferation (Salzig et al., 2016). Moreover, MSCs fibroblastic morphology have been found to strongly correlate with their actin cytoskeleton organization and the distribution of their focal adhesion points (Yin-Ping et al., 2016).

That said, and based on our results, we hypothesised that cells that displayed spindle spread morphology are cells that have found a niche to adhere to the matrix, whereas cells that were round in shape failed to attach due to lack of their corresponding docking ligands. Therefore, we have investigated the presence of several known adhesive ligands of MSCs including: Collagen I, laminin and fibronectin (Zwolanek et al., 2015, Salzig et al., 2016) and compared between both type of scaffolds: the scaffolds that maintained intact adventitia layer versus the scaffolds that lost it.

Immunofluorescence staining revealed an interesting difference in composition between both scaffolds, where scaffolds with intact adventitia confirmed expression of collagen I, laminin and fibronectin. On the other hand, scaffolds with no adventitia showed a lack of collagen I and laminin expression as well as borderline fibronectin expression. These finding support our hypothesis and suggests that MSCs attach better and display the typical morphology when seeded on tracheal DC scaffolds where the adventitia layer is preserved.

These results correlates with (McKee and Chaudhry) study, that have shown that when UC-MSCs were grown in (Dex-SH/PEG-4 Acr) scaffolds that lack collagen I, they did not show significant proliferation and did not display fibroblastoid morphology. However, when, collagen I was added to scaffolds, MSCs adhered better and displayed the typical fibroblastic morphology as well as had a higher proliferative rate (McKee and Chaudhry, 2017). This might highlight a role of collagen I and laminin in promoting better cell attachment to DC scaffolds. Each tissue consist of unique ECM components, the differences in ECM components may be selectively responsible for triggering tissue specific cell responses. Moreover, studies have revealed that cells follows specific ligand priority while still capable of binding to more than one ECM ligands (Schlie-Wolter et al., 2013). For example, fibroblast were found to respond better to fibronectin (Schlie-Wolter et al., 2013). Another study has also found that MSCs display improved adhesion when plated on collagen I matrix (Chinnapaka et al., 2015). While these cell: ECM interactions are complex and not fully understood, the development of a basic understanding of these interactions and tissue composition will have an immense impact on improving cells seeding protocols for tissue engineering applications.

Taken together these data suggest that, adventitia might contain abundant anchorage sites that may improve MSCs attachment to DC tracheal scaffold. The adventitia fibrous bundles join the connective tissue of the annular ligaments (Ohkimoto et al., 1997) and these are the target sites when passively seeding MSCs on tracheal scaffolds. But we are unaware of any studies that have investigated the components of these layers. It is worth noting also that during our process of decellularisation the first step has been the dissection and removal of excess tissue covering the trachea, so probably this layer was compromised during this process and then it is followed by the decellularisation process. Therefore, the final DC product had heterogenous areas that maintained this layer. Future work should aim to thoroughly investigate its components and characterise its properties and its role in improving cells attachment and on cell fate.

In a parallel experiment, we have attempted to investigate cell coverage area in a micro-level comparing two cells seeding density $150x10^3$ cells/cm^2 to our seeding density of $500x10^3$ cells/cm^2. The percentage cell coverage area of random locations of cells seeded scaffolds was estimated using FIJI image analysis software. The results showed that the seeding density of $500x10^3$ cells /cm^2 displayed a significantly higher percentage surface coverage area compared to $150x10^3$ cells /cm^2. However, these results must be considered with caution, given that our previous data that have indicated that cells attachment is variable on the DC tracheal scaffolds that display heterogenous attachment sites. Although it is possible using multiphoton imaging to inspect for increasing fluorescent intensity and correlate it with cells proliferation but, we could not standardize microscope setting as scaffolds did not have uniform surfaces and setup was adjusted as needed for samples imaging. Future work should aim to take an advantage and optimise new tools like fluorescent life cells imaging, or oxygen saturation measurements(Westphal et al., 2017) in order to reflect cells growth and proliferation in these complex TE constructs.

As can be seen from all these findings, multiphoton imaging of optically cleared DC scaffolds seeded with Zs.green transduced cells offered a viable method that can be applied in tissue engineering and circumvent many of the obstacles faced with conventional methods. For example, it allows visualization of significantly greater amount of tissue in less time compared to conventional methods. Additionally, it allowed probing spatial distribution of both cells and tissue engineered constructs structure in all three dimensions. Moreover, it has increased assessment efficiency of tracheal construct as it helped us highlight area of interest and special patterns associated with cells /scaffolds interactions. However, one identified limitation with the use of BABB clearing reagent is being a toxic aggressive organic solvent that dissolve plastic and glue and must be handled with extreme care, in addition to that no objective lens available in the market that can be immersed on it and require the use of special chamber slides (Silvestri et al., 2016). Therefore, future work should aim to optimise and use other clearing agents. Indeed, in a parallel study where we attempted to tattoo seed tracheal scaffolds and inject seeding, the technique proved helpful in

demonstrating effect of seeding technique on which its showed destruction of the matrix due to random tattoo machine needle hits while it still showed cells penetration and therefore this technique can be useful when comparing different seeding techniques especially with TE constructs where deep infiltration of cells is possible.

4.4 Conclusion

The data in this chapter demonstrate the effectiveness of our modified passive seeding protocol that incorporates a partial surface dehydration (PSD) step prior to seeding for DC tracheal scaffolds in improving cell seeding efficiency (CSE) of UC-MSCs. This study also warrants the need of a unified tool to evaluate seeding efficiency to allow comparison among studies.

Despite its exploratory nature, this study offers insight to the importance of exploring the role of scaffolds ECM components in supporting and improving cells adhesion and integration. Our study suggested that maintenance of the adventitial layer may improve cells attachment and future work should aim to confirm this finding. The study also highlighted the challenges in monitoring cells growth Kinetics and proliferation using conventional methods and stresses the need to explore and introduce new tools that help probe the complex cell scaffolds interaction. We have also introduced the use of fluorescently labelled reporter cell line coupled to optical clearing and multiphoton imaging to facilitate exploring cells spatial distribution and localisation. This study also demonstrated the complex structure of the trachea that hampers deep infiltration of cells and requires a careful selection of the optimal seeding techniques. In this thesis the focus was the investigating MSCs/scaffold interaction as we hypothesised that MSCs play a supportive role in constructive remodelling of the TE constructs and therefore achieving deep cellular infiltration might not be necessary. However, if the aim was to functionalise cartilage layer of the scaffolds using chondrocytes then may be a dual seeding technique is more relevant, like micro injection of the cartilage rings as a possible interesting direction. The optimal seeding technique and the optimal seeding conditions are yet to be defined.

5 Chapter 5: Optimisation of RNA extraction from MSCs seeded into decellularised tracheal scaffolds

5.1 Introduction

Gene expression analysis of cell seeded scaffolds can provide valuable information about cellular responses to the tissue engineered microenvironment. Isolation of high-quality RNA, (intact, free of impurities) is a key prerequisite for a successful functional genomic study. Despite it being one of the basic techniques in research, development of RNA extraction protocols for cell seeded scaffolds remains a difficult task that requires excessive optimisation. Indeed, in tracheal bioengineering, there is almost no published gene expression data available. This could be reflecting the complexity encountered conducting such analysis.

There is a general consensus that the isolation of high-quality RNA is more problematic than the extraction of DNA. This is due to the presence of 2'-hydroxyl groups in RNA which act as nucleophiles making it more susceptible to degradation by RNases enzymes (Lavoie and Abou Elela, 2008). RNases are the bane of any extraction process because of their abundant spread in nature and the difficulty faced to destroy or remove them completely. Moreover, other contaminants like salts and proteins may interfere with efficiency of the extraction process and compromise its quality. Although many RNA extraction protocols have been developed and many kits are commercially available and routinely used to purify RNA from different cell lines and tissues, preparing high-quality RNA from certain tissues and scaffolds remains challenging. This is especially true with fibrous tissues and tissues rich in protein, DNA and nucleases and they require more manipulation and extensive optimisation for RNA isolation. Cartilage based tissues are considered one of the difficult tissues with regards to isolation of RNA due to their low cellularity and abundance of dense ECM components (Ruettger et al., 2010, Le Bleu et al., 2017, Lee et al., 2015).

Furthermore, detailed RNA extraction methodological protocols are highly under recorded in literature and most publications do not describe adequately key details used to extract RNA (Bustin et al., 2013).

The choice of an RNA isolation method is dependent on many factors, such as tissue or scaffold type, composition, size, mechanical properties, charge and cell density (Yu et al., 2013).

One of the main aims of this thesis is the investigation of gene expression profile of MSCs seeded onto DC tracheal scaffolds. The work presented in this mini chapter reports the work undertaken to establish a reproducible RNA extraction protocol from UC-MSCs seeded onto DC tracheal scaffolds.

5.1.1 Research aims and objectives

The central aim of this chapter is to extract high quality RNA from UC-MSCs seeded on decellularised tracheal scaffolds that is suitable for downstream genomic analysis (RNA sequencing and RT-PCR).

Objectives:

1. Establishment of reproducible RNA extraction protocol from UC-MSCs seeded DC tracheal scaffold that yields high quality RNA.
2. Extraction of RNA from UC-MSCs seeded human DC scaffolds to be used for downstream RNA sequencing and RT-PCR analysis.

5.1.2 Experimental approach

The experimental work in this chapter involved two main parts as displayed in (Figure 5.1)

PART1: the work in this part involved a comparative assessment of four different RNA extraction methods based on yield and purity of RNA using nanodrop spectrophotometer. With the aim of selecting and adopting the RNA extraction method that will give the highest yield and purity, then assessment of RNA integrity of the best extraction method was done to confirm suitability for downstream analysis. UC-MSCs seeded on porcine scaffolds (n=7) were used for this study. All RNA extraction methods involved a genomic DNA elimination step prior to analysis. The methods were:

Method (A): Based on cryopulverisation of cell seeded scaffolds (6mm biopsies followed by Qiazol reagent separation and RNeasy column-based purification (Qiagen)

Method (B): Based on initial cell detachment from DC scaffolds using TryplE (Gibco) followed by column-based extraction using (Acturus, Picopure Kit).

Method (C): Based on direct lysis of cells on DC scaffolds using TRizol reagent (Invitrogen), followed by conventional TRizol extraction methods.

Method (D): Based on initial cell scraping and detachment in RNA protect reagent (Qiagen) followed by column-based extraction using (Acturus, Picopure kit).

PART 2: The experimental work in this part involved seeding UC-MSCs on human cadaver DC tracheal scaffolds supplied by NHSBT (REC:11/LO/1522). Then at 3 days of culture, RNA was extracted from cell seeded scaffolds (n=5) and control cells pre-seeding (n=3). Then yield and purity were measured using nanodrop spectrophotometer before samples were sent to the UCL Genomics Platform at Institute of Child Health (ICH) for RNA integrity assessment and for downstream analysis.

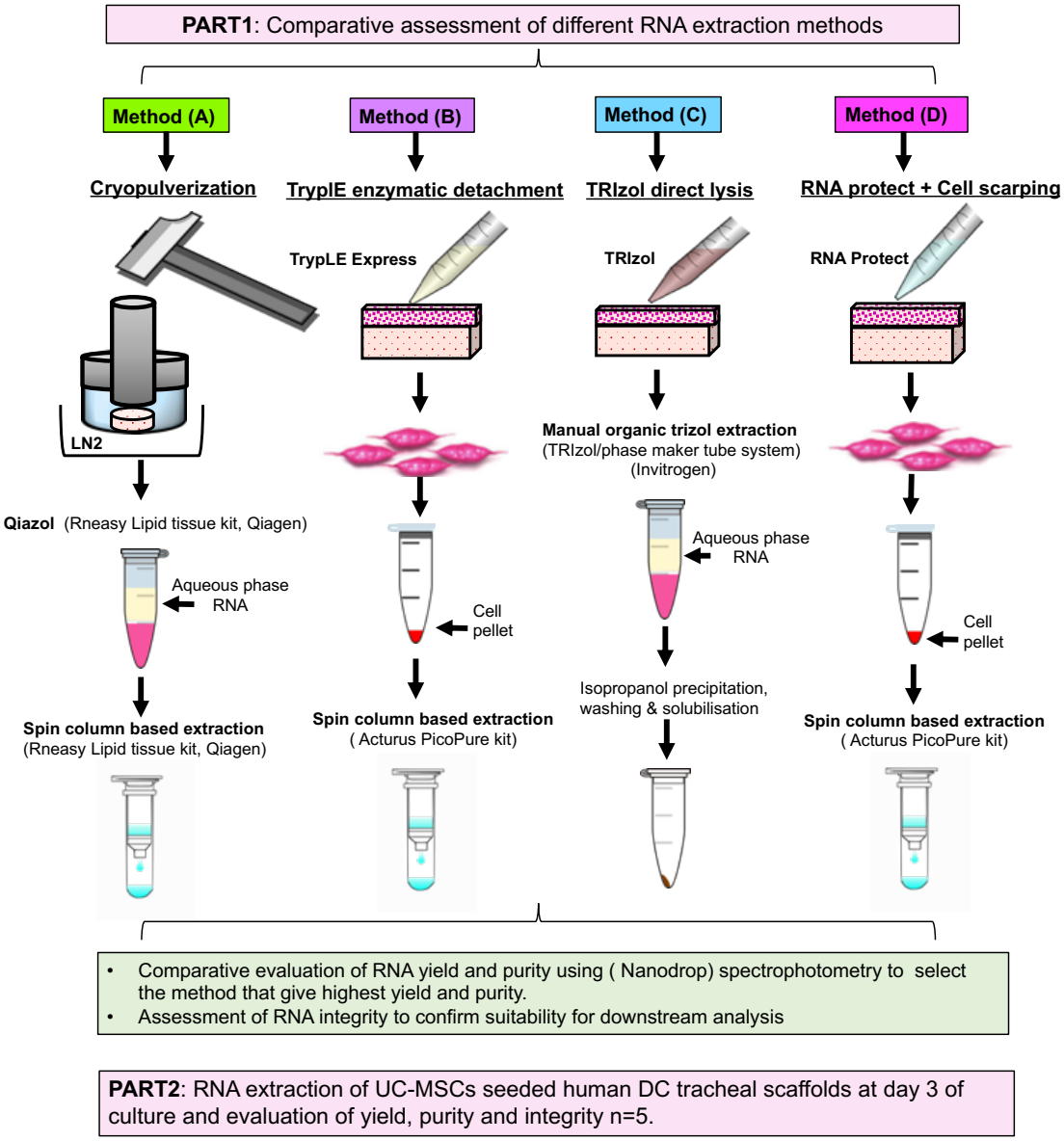

Figure 5.1: Schematic diagram of the different RNA extraction methods.

The diagram shows four extraction techniques (A, B, C, D) and the overall steps involved.

5.2 Results

5.2.1 Comparative assessments of different RNA extraction methods

A range of RNA extraction methods have been compared for the extraction of high-quality RNA from UC-MSCs seeded DC tracheal scaffolds. The extracted RNA was evaluated initially in terms of yield and purity using Nanodrop spectrophotometer (ND1000; NanoDrop Products, Wilmington, USA). Then RNA integrity (RIN) assessment using Agilent 2200 bioanalyzer (Agilent technologies) was used for confirmation of RNA quality.

5.2.1.1 RNA yield and purity

Analysis of RNA yield recovered when comparing the four methods revealed that there was a significant difference in RNA yield ($P \leq 0.001$) between method (D) which is based on cell detachment and scraping in RNA protect followed by column-based purification, and method A and B and C as shown in (Figure 5.2). One-way ANOVA statistical analysis of RNA purity shows a significant difference ($P \leq 0.001$) of the absorbance 260/280 ratio (Figure 5.3, A) between method D and method A, B and C, on which method D absorbance 260/280 ratio fall within the acceptable purity target range of (1.8-2.1). While method A, B and C showed low absorbance 260/280 ratio of approximately ≤ 1.6. The absorbance 260/230 ratio showed lower values in all extraction methods (Figure 5.3, B) less than the acceptable range of (2-2.2). This is normally attributed to presence of other contaminants like glycoproteins.

Overall the data demonstrated that method D was able to recover highest yield and most pure RNA compared to other methods (A, B and C). The mean RNA yield extracted using Method D was (160.60 ± 119.4) ng/μl in 20 μl total volume. It can also be noted that there was a high variability among values obtained for RNA yield with method (D) denoted by the high standard deviation where we find values being either on the high side or in the lower side, this might be reflecting the variable cell attachment affinity to the DC ECM matrix. Table 5.1shows the respective mean ± SD values of RNA yield and purity in all methods tested.

It is worth noting that method (C) and (A) that involved the use of trizol reagent showed phenol contamination denoted by the presence of an absorption peak at 270nm. However, the attempts to clean up RNA using both Zymo-spin clean and concentrate kit did not improve the purity of the extracted RNA.

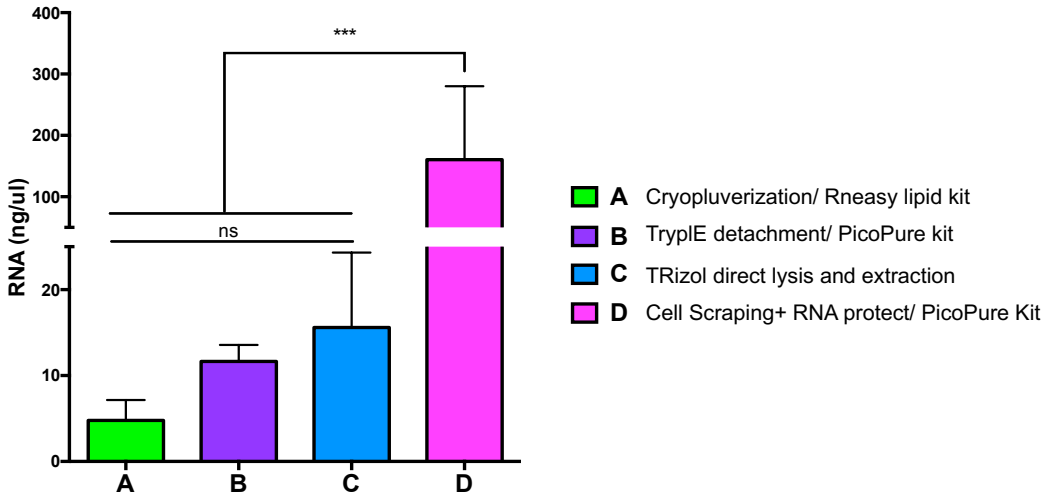

Figure 5.2: Comparative assessment of RNA yield from different RNA extraction methods

Kruskal-Wallis test statistical analysis showed a significant ($P \leq 0.001$) higher RNA yield obtained with Method (D) in comparison to Method (A, B and C). Values represent Mean±SD, n=7.

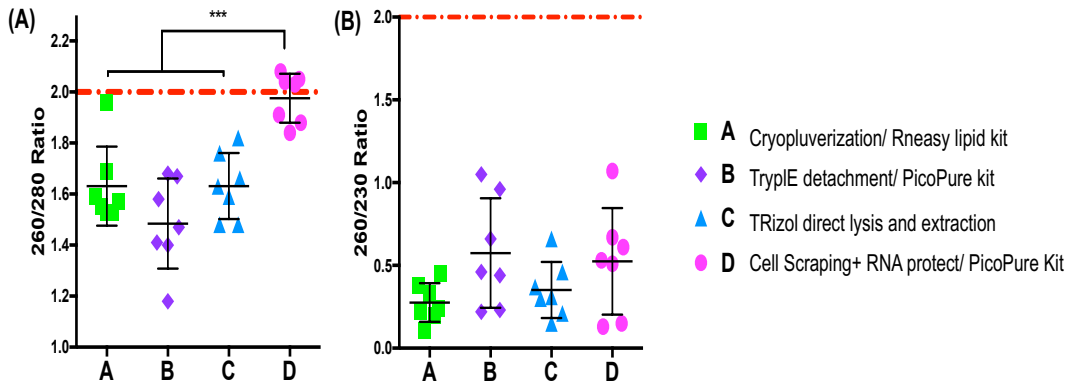

Figure 5.3: Comparative assessment of RNA purity of different extraction methods.

(A) shows one-way ANOVA statistical analysis of the absorbance 260/280 ratio of the different extraction methods, results show a significant difference (P≤0.001) between Method (D) and method (A, B &C). Method (D) appear to meet the target range of (1.8 - 2.1) unlike method (A, B, C). (B) shows the absorbance 260/230 ratio of RNA extracted from all methods. All methods show reduced 260/230 ratio compared to the target ratio of (2 - 2.2). Values represent mean ±SD, n=7. The red dotted line marks the expected target absorbance ratio of 2 for both 260/280 and 260/230 ratios.

Table 5.1: Mean RNA yield and purity measures from comparative RNA extraction analysis.

Values represents Mean ± SD, n=7

Method	RNA yield (ng/µl)	260/280 ratio	260/230 ratio
Method (A)	4.787 ± 2.360	1.631 ±0.129	0.276 ±0.117
Method (B)	11.64 ± 1.926	1.484 ± 0.176	0.574 ± 0.331
Method (C)	15.59 ± 8.719	1.631 ± 0.129	0.351 ± 0.169
Method (D)	160.60 ± 119.4	1.976 ±0.0961	0.524 ± 0.322

5.2.1.2 RNA integrity

Based on the above results, RNA samples recovered using method (D) were further analysed for RNA integrity to detect for any RNA degradation and to confirm quality and suitability for use in downstream analysis. RNA integrity was determined using Agilent 2200 bioanalyzer (Agilent technologies) that measures 28S/18S ribosomal RNA (r RNA) ratios and then calculates the respective RNA integrity number (RIN) to reflect the overall RNA quality. Results confirmed that the extracted RNA had an RNA integrity number (RIN) above > 7 as recommended for RNA seq analysis and RT-PCR. Results are displayed in (Figure 5.4).

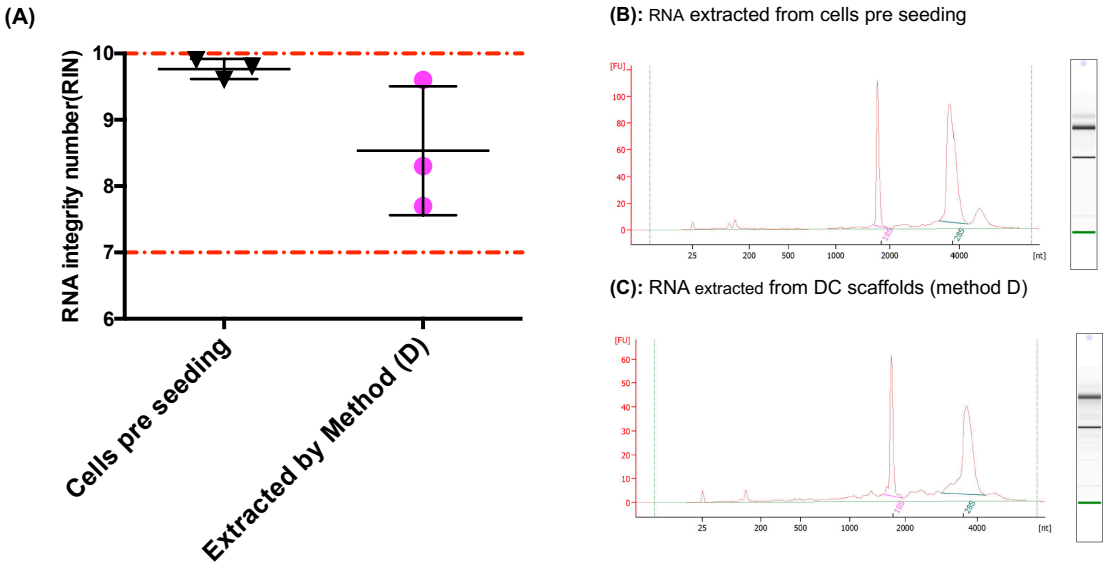

Figure 5.4: Assessment of RNA integrity of RNA recovered from extraction method (D)

(A) statistical analysis using unpaired t test revealed that there is no significant difference observed in RNA integrity between RNA obtained from DC scaffolds using method (D) and cell control. Overall RNA integrity number (RIN), was within the acceptable RIN range (7-10) suitable for RNA seq analysis. (B &C) show representative images of rRNA peaks, 18S and 28S as displayed by Agilent 2200, bioanalyzer on both sample groups. Values represent mean ±SD, n=3. The red dotted line marks the acceptable range of RNA integrity number (RIN between 7-10).

5.2.2 Extraction of RNA from MSCs seeded into DC tracheal scaffolds.

Decellularised human scaffolds (n=5) were seeded as previously described in chapter 2. Then method (D) was adopted as an extraction protocol of RNA from tracheal seeded scaffolds. Then yield, purity and integrity were measured prior to RNA seq analysis.

Results showed that the mean RNA yield recovered from seeded DC scaffolds was (131.6 ± 147.1)ng/μl (Figure 5.5, A). A highly variable RNA yield was observed as indicated by the high standard deviation similar to finding obtained during optimization of extraction protocol experiments.

Then the assessment of RNA purity (Figure 5.5, B) in comparison to RNA extracted from cells pre-seeding revealed that the absorbance 260/280 ratio was within the acceptable range indicative of purity (1.8-2.1), however the absorbance 260/230 ratio (Figure 5.5, C) was significantly less than the expected range (2 - 2.2) in the RNA extracted from DC seeded scaffolds ($P \leq 0.001$). This is normally attributed to presence of other contaminants like glycoproteins, however in practice it does not normally interfere with downstream analysis as per manufacturer's recommendation. Finally, assessment of RNA integrity in both groups (Figure 5.5, D) demonstrated that the RNA integrity number (RIN) was within the acceptable range (7-10) indicative of good RNA integrity suitable for downstream analysis.

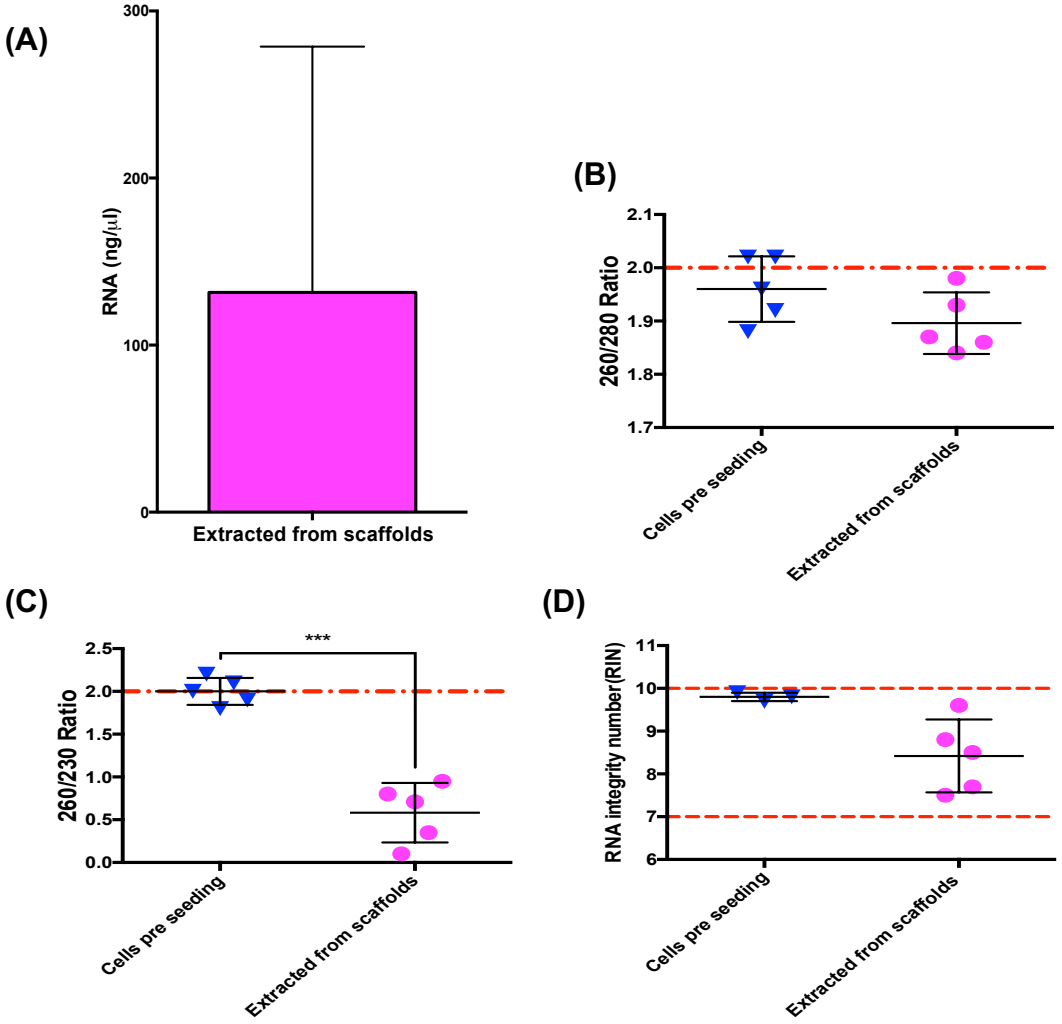

Figure 5.5: Assessment of yield and quality of RNA extracted from MSCs seeded into human scaffolds.

(A) RNA yield extracted from seeded scaffold was sufficient for downstream analysis showing a mean of (131.6 ± 147.1) ng/µl. Comparison of RNA purity and integrity between RNA extracted from seeded scaffolds and from cells pre-seeding revealed: (B) absorbance 260/280 ratio of both group showing that it meets the acceptable range of (1.9- 2.1). (C) absorbance 260/230 ratio of both groups showing a significant difference in ratio with scaffold group failing to meet cut-off point of 2 ($P \leq 0.001$). (D) assessment of RNA integrity showing that both groups meet the acceptable RIN range of (7-10). Values represent mean±SD, n=5 in (A, B, C), n=3 versus 5 in (D). The red dotted line marks the acceptable range or cut-off point of each outcome measure.

5.3 Discussion

With regards to this part of the thesis, we aimed at extracting RNA from seeded DC scaffolds and several methods have been compared. It was initially attempted to cryopulverise biopsies of seeded scaffolds prior to purification with RNeasy column-based kit (Qiagen) (Method A). While cryogenic grinding is a common practice for extracting RNA from tissue matrices (Yu et al., 2013), this method failed to recover enough and pure RNA. In fact, the low yield can be explained by the low cell to scaffold ratio, given that cells only occupy the surface of scaffolds as confirmed from our work in chapter 4 and the method is actually limited to grinding small size tissue pieces. Therefore, to improve yield, larger pieces of tissue would need to be pulverized and this is technically challenging. Moreover, the harsh homogenization used to break the dense rigid matrix structure of the tracheal scaffolds might contribute to the reduced RNA quality by releasing endogenous RNases (Le Bleu et al., 2017, Yu et al., 2013). It is worth noting that, immediate thawing of the grinded tissue occurred during transfer from the cryopulveriser to microtubes due to room temperature and this may have caused increased degradation.

Therefore, taking the advantage of cells growing on the surface of scaffolds, we sought to use methods that detach or directly lyse cells from scaffolds to minimize scaffold interference. When using an enzymatic detachment method with TryplE Express dissociation reagent (Invitrogen) followed by column-based purification (PicoPure, acturus) (Method B), the results did not improve as well and the low yield and quality were still persistent. This could be explained by the fact that TryplE Express has been actually optimized to adherent cells on plastic flasks and a stronger formulation may be required to detach cells from scaffolds. Indeed, we have used a (1X) TryplE Express formulation. Other possible explanation of this could be the presence of RNases (endogenous and exogenous) during the detachment process prior to cell lysis for extraction. Exogenous RNases represent a threat at this stage as no RNase inactivation reagent is yet introduced to cells and RNases have the ability to enter cells by endocytosis, thus it might cause degradation of RNA even before the cells lysis step has started (Chao and Raines, 2011). Exogenous RNases are either present within the scaffolds or

within the TryplE Express reagent which might contain traces of RNases, as manufacturers may not have tested this product grade for the presence of nucleases. In fact, an interesting study by (Vrtačnik et al.) has suggested that the presence of RNases contamination in Trypsin reagents used could be responsible for the observed degradation of RNA (Vrtačnik et al., 2014). Moreover, enzymatic detachment process may damage cell surface proteins leading to the activation of cell stress inducible endogenous RNases causing subsequent degradation of RNA (Nicholson, 2001).

Then we opted for a direct lysis method that is based on using TRIzol (Invitrogen) followed by manual precipitation in isopropanol (Method C). Although TRIzol reagent is one of the most commonly used methods to isolate high yield quality RNA and has many advantages including strong denaturation of RNases, superior cell lysing capabilities, and can be used at scalable volumes to isolate RNA. Yet, it did not improve RNA yield and quality in our study. This could be attributed to the nature of DC scaffolds that are composed of a highly cross-linked ECM containing high concentration of proteoglycans and polysaccharides. In fact, many studies have demonstrated that high concentration of proteoglycans and polysaccharides interfere with TRIzol based method extraction, as they physically entrap RNA during centrifugation to the discarded phase leading to a low RNA yield (Lee et al., 2015, Wang and Stegemann, 2010, Ogura et al., 2015). In addition to that, small polysaccharides fragments may also precipitate with RNA reducing its purity (Ogura et al., 2015). It is worth noting that during this study phenol carryover was also encountered and was not improved despite using the Zymospin clean and concentrate kit. Taken together, it was apparent that extra modifications and cleaning steps are required to improve the outcome. Indeed, several modifications of TRIzol method have been suggested to resolve this issue and some showed improved RNA yield and quality. For example, a study by (Chomczynski and Mackey) have reported improved yield and quality by modifying of the TRIzol protocol using a mixture of isopropanol and high salt solution containing (0.8 M sodium citrate and 1.2 M NaCl) instead of isopropanol only during RNA precipitation in proteoglycan rich rat liver and aorta (Chomczynski and Mackey, 1995). Others have suggested the use of high salt solutions like cetyltrimethylammonium bromide (CTAB) instead of guanidinium

thiocyanate-based TRIzol reagent as salts help dissolve polysaccharides (Ogura et al., 2015, Chang et al., 1993).

The final method that have been investigated (method D), is based on cell detachment by scraping in RNA protect reagent (Qiagen) followed by spin column purification using Picopure kit (Acturus). RNA protect is a stabilization reagent that is manufactured by Qiagen. It is formulated to protect and stabilise nucleic acids from degradation mainly in cell suspensions similar to RNA later that is used for tissue RNA stabilisation. RNA protect can be used also to detach and stabilise adherent cells from culture flasks without the need for cell dissociation step pre-processing using reagents like trypsin. In fact, the rational of trying this reagent to detach cells from tracheal DC scaffolds, was that we were looking for a reagent that can detach cells while providing immediate stabilisation of RNA in one go. However, as per manufacturer's information's this reagent have never been tested on 3D scaffolds.

Interestingly, our results have shown a significant ($P \leq 0.001$) recovery of a higher RNA yield that meet the acceptable RNA quality criteria in terms of purity and integrity in comparison to the previous methods used (A, B and C). On which the mean RNA yield extracted using Method D was (160.60 ± 119.4) ng/μl with 260/280 ratio of (1.8-2.1) and an RNA integrity of more than > 7. The results have also demonstrated a low 260/230 ratio of less than 2, this can be attributed to the presence of contaminants. For example, glycoproteins tend to co-purify with RNA because of their size and their high negative charge (Gehrsitz et al., 2001). Other contaminants include guanidine thiocyanate, a salt that absorbs at 220-230nm and is normally presents in high concentration in lysis buffers used with RNA extraction kits. But no consensus exists on the lower limit of 260/230 ratio and in practice it does not normally interfere with downstream analysis especially with acceptable RNA yield. This has been confirmed by manufacturer's (Qiagen) and by seeking expert's advice (Tony Brooks, personal communication, July, 2018) and (Patricia de winter, personal communication, May, 2017).

It is worth noting that during RNA extraction optimisation, RNA later (Qiagen) was tried to stabilise the tissue pre -processing, but it was noted that scaffolds float despite submerging them in the reagent that do not appear to penetrate the tissue. This could be related to the specific gravity of the reagent and suggests that it might not be an ideal reagent to stabilise tracheal DC scaffolds.
Overall, we have established a less exhaustive method for extracting high quality RNA suitable for our target downstream genomics analysis.
With the completion of this, the experiments proceeded by seeding MSCs on human DC tracheal scaffolds and then extracting RNA from the seeded scaffolds after 3 days of cultivation using our developed protocol. The results confirmed the optimisation result. The mean RNA yield was (131.6 $\pm$ 147.1) ng/μl, with an absorbance 260/280 ratio of 1.8-2.1 and an RNA integrity number RIN more than 7. All extracted samples were frozen at -80 ready for downstream analysis.

It was also noted that there was a high standard deviation when inspecting RNA yield during both the optimisation process and the final extraction experiments using method D. This might be reflecting a variability on the number of cells attached to scaffolds possibly relating to cells affinity to attach to the underlaying matrices. The technique we have described has a limitation as it is only applicable to cells attaching on the surface of the DC scaffolds. That said, another viable RNA isolation method that can be helpful with cells seeded scaffolds, is laser capture microdissection (LCM) method. Although it not readily available in every laboratory setup and can be an expensive option, but it can be used to specifically select region of interests while excluding ECM components that can interfere with analysis.

5.4 Conclusion

The Lack of a reproducible protocol to extract high-quality RNA directly from the cell seeded scaffolds hinders efficient application of functional genomics analysis. In this mini chapter we have devised a reproducible RNA isolation protocol for extracting intact high-quality RNA from MSCs seeded into DC tracheal scaffold.

6 Differential gene expression analysis of MSCs seeded into DC tracheal scaffolds

6.1 Introduction

The use of Mesenchymal stromal cells (MSCs) in regenerative medicine and tissue engineering applications has expanded exponentially during the last decades as a promising therapeutic tool. Their charm has increased by our ever-expanding knowledge of their special biological characteristics, these include their multilineage differentiation potentials to multiple cell lineages. Another feature is their dramatic homing capabilities to tumour and pathological or injury sites. In addition to that, MSCs secrete a plethora of biologically active factors including cytokines, chemokines, growth factors and miRNAs that have profound effects on the local cellular dynamics (Liang et al., 2014, da Silva Meirelles et al., 2009, Murphy et al., 2013). There is a general consensus that their paracrine signalling is a critical player that orchestrates their therapeutic effects (Murphy et al., 2013) . Their therapeutic effect have been classified to six main categories: (1) support of growth and differentiation of local stem and progenitor cells, (2) immunomodulation by interaction with immune cells and inflammatory factors,(3) angiogenesis,(4) anti-scaring, (5) anti-apoptosis and (6) chemoattraction (Bai et al., 2016, da Silva Meirelles et al., 2009). Moreover, MSCs are a technically feasible cell source that is relatively easy to isolate and expand and can be readily isolated from different tissues, such as bone marrow, umbilical cord, Wharton jelly, adipose tissue, amniotic fluid and many more. In addition to that MSCs are thought to be immune evasive compared to other cell types (James et al., 2014). All these characteristics have made them an attractive source in tissue engineering applications. Indeed, the implantation of TE constructs elicit an inflammatory immune response analogous to a physiological wound healing response that could lead to either implant failure or engraftment depending on the succession and the balance of the inflammatory process (Morris et al., 2017, Crupi et al., 2015, Badylak and Gilbert, 2008). In this context the use of MSCs becomes an interesting strategy owing to their unique features that could help

creating a pro-regenerative, immunomodulatory environment that could drive the inflammation process towards constructive tissue remodelling(Crupi et al., 2015).

In tracheal bioengineering, MSCs are one the most commonly employed cell types for cellularization of tracheal scaffolds (Maughan et al., 2017). The rationale of using MSCs in tracheal bioengineering has been to benefit from their anticipated role in promoting tissue repair and remodelling. Variable MSC types have been used in tracheal tissue engineering studies that ranged from bone marrow, amniotic and adipose tissue derived cells (Chiang et al., 2016). The cells were also applied in various ways ,where some groups have focused on *in vitro* maturation of chondrocytes from MSC cultures for scaffold seeding (Go et al., 2010, Fuchs et al., 2003, Macchiarini et al., 2008), others have seeded only MSCs to scaffolds (Kim, 2013, Clark et al., 2016, Wood et al., 2014). Another strategy involved co-seeding MSCs with other cell types like chondrocytes or epithelial cells (Haykal et al., 2014b, Jungebluth et al., 2012, Go et al., 2010, Elliott et al., 2012). But there is still no agreement on the best cell combination for seeding tracheal scaffolds.

Notwithstanding the small-scale studies, increasing data from preclinical studies on the use of MSCs in tracheal bioengineering support the favourable effect of using these cells in improving graft integration, vascularisation and epithelialization (Clark et al., 2016, Batioglu-Karaaltin et al., 2015, Gray et al., 2012). For example, Suziuki *et al* compared the effect of incorporating adipose derived MSCs on bioengineered collagen sponge graft to repair tracheal defects in rats and reported that the MSCs seeded group had improved vascularization and had an accelerating generation of epithelium within 14 days of implantation compared to the control, non-seeded group (Suzuki et al., 2008). Another study by Haykal *et al* that co- seeded MSCs and epithelial cells on decellularised scaffold in a heterotopic pig model, have demonstrated an immunomodulatory response showing increased infiltration of T regulatory cells in comparison to control DC scaffolds (Haykal et al., 2013). Moreover, co-seeding MSCs with chondrocytes on biodegradable synthetic scaffolds displayed increase and homogenous ECM deposition and improved rigidity in contrast to controls (Tsao et al., 2014).

A systemic review by Jakonsen *et al* of preclinical studies investigating the effects of MSCs in tracheal tissue engineering demonstrated a general agreement among studies suggesting enhanced epithelialization of grafts when incorporating MSCs, but owing to the considerable variations in study design, species and methods the results were difficult to integrate in to a clear coherent conclusions (Jakobsen et al., 2017). Moreover, no human trials studies investigating the effect of MSCs in airways have been conducted yet (Jakobsen et al., 2017). In fact, the preclinical and clinical literature in tracheal TE comprises a heterogenous mix of experimental designs and outcome measures that have mainly relied on qualitative measures like endoscopic observation, inspection for gross complication to evaluate cells retention, fate and contribution (Maughan et al., 2017). Moreover, the investigation of the effect of DC scaffolds on MSCs cellular behaviour as well as cellular responses have been largely overlooked in tracheal bioengineering studies.

We and others have used MSCs for recellularization of decellularised, cadaveric donor tracheal scaffolds in several clinical compassionate cases of airway tissue engineering for stenosis (Elliott et al., 2017, Hamilton et al., 2015). However, the role of these cells in the engineered airway remains controversial. It is unclear yet whether the observed improvement is a result of direct cell engraftment and retention or because of release of trophic factors. Other studies showed that MSCs fail to persist long term after implantation, hence it was hypothesised that signals released by cells might provide stimulus for regeneration by immune modulation and recruitment of host cells (Casey et al., 2014).

That said, the relevance, contribution, and fate of these cells as well as cell scaffold interaction in airway tissue engineering remain fundamental research questions that need to be addressed. Therefore, this chapter aim to investigate the *in vitro* MSCs differential gene expression when seeded on DC tracheal scaffolds in order to reflect their cellular activities.

Transcriptome analysis (RNA sequencing) will be used to aid identification of differential gene expression and will help provide valuable information and

insights about cells biological behaviour, and consequently will improve our understanding of their potential benefits.

Since our inhouse protocol is based on cultivating autologous MSCs for 3 days on cadaver DC tracheal tissue prior to implantation, the study will focus in exploring differential gene expression at 3 days of culture using high throughput RNA sequencing (RNA seq) followed by RT-PCR. It is worth noting that UC-MSCs have been used throughout this project as an alternative source of BM-MSCs, this is because they were a cost effective readily available source for this study. UC-MSCs also have many advantages including higher proliferative capacity and expandability compared to BM-MSCs. Moreover, they do not express MHC class II and costimulatory molecules CD80 and CD86, thus making them a promising source for allogenic transplantation(Bai et al., 2016)

6.1.1 Research aims and objectives

The central aim of this chapter is to investigate differential gene expression of MSCs seeded on decellularised human tracheal scaffolds with a specific focus on trophic bioactive factors produced by MSCs and of relevance to tissue remodelling and integration.

Objectives:

3. Investigation of global differential gene expression of MSCs seeded on human decellularised tracheal scaffolds at day 3 of culture prior to implantation using high throughput RNA sequencing (RNA seq).
4. Investigating the presence of transcripts of known trophic bioactive molecules produced by MSCs relevant for tissue engineering applications. These associated with: ECM remodelling, anti-scaring, anti-apoptotic, chemoattraction, immunoregulatory and supportive factors.
5. Confirmation of RNA seq data with RT-PCR.

6.1.2 Experimental approach

The work in this chapter involve RNA sequencing for differential gene expression of MSCs seeded human DC tracheal scaffolds at 3 days of culture. The workflow is illustrated in (Figure 6.1) bellow.

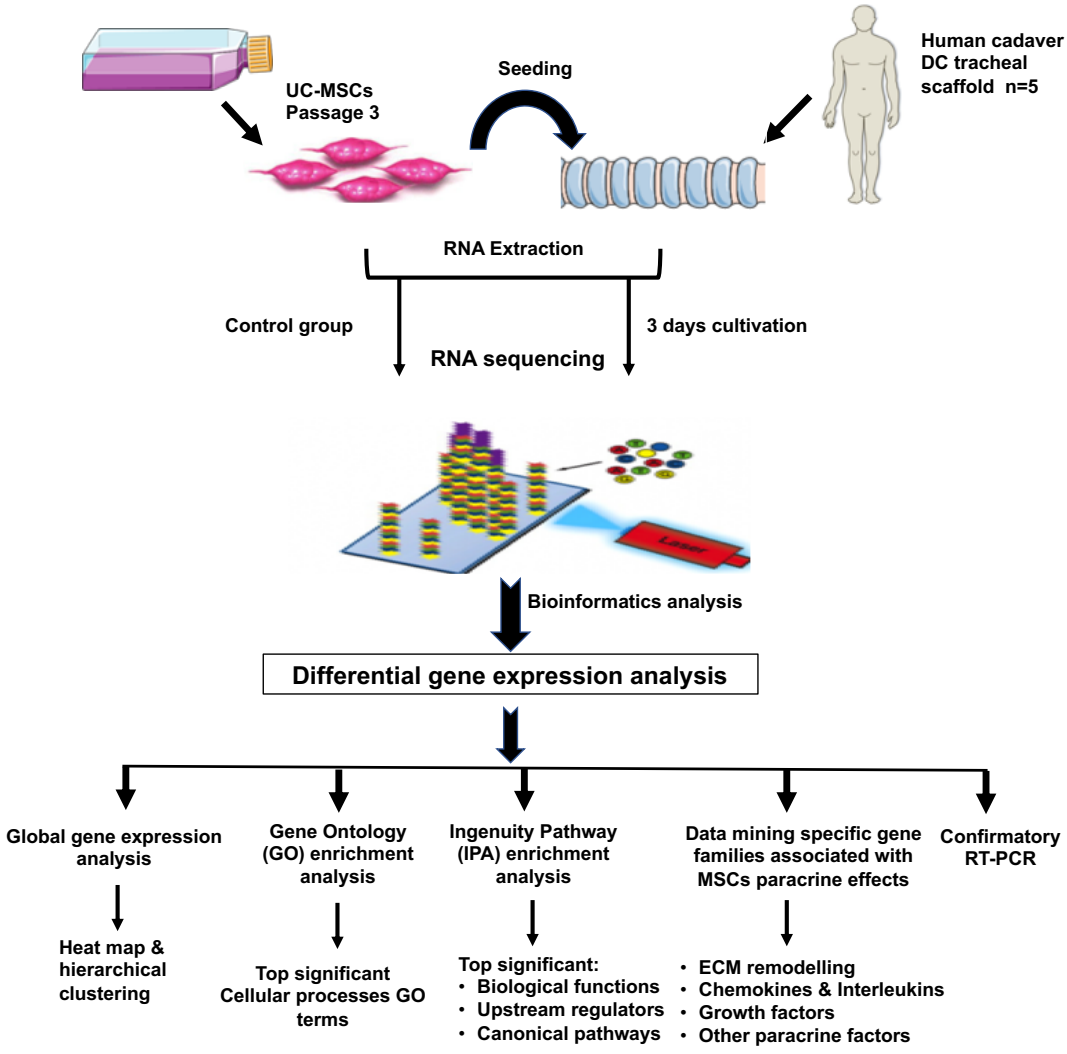

Figure 6.1: Schematic diagram of the experimental design and workflow of the differential gene expression analysis of MSCs seeded on human DC tracheal scaffolds.

6.2 Results

6.2.1 Comparative transcriptome analysis using expression profiling RNA sequencing (RNA seq)

6.2.1.1 Differentially expressed genes (DEGs)

For this study RNA sequencing (RNA seq) was conducted on RNA extracted from UC-MSCs seeded on to DC scaffolds (3D) on day 3 of culture (n=5) in comparison to UC-MSCs prior to seeding to DC scaffolds (n=3) as a control. The aim was to find features that are differentially expressed in cells seeded on DC scaffolds versus control. Normalization and differential expression analysis were carried out using the Bioconductor package SARTools, using a DESeq2 model and package and all annotation and sequence were obtained from Illumina,iGenomes,(http://emea.support.illumina.com/sequencing/sequencing_software/igenome.html). A list of differentially expressed genes was created by considering exclusively a significant threshold of $P \leq 0.05$, and each differential gene expression was presented as a fold change (FC) relative to control followed by the adjusted P value (corrected P value by Benjamini-Hochberg, BH procedure to control for false positive discoveries).

6.2.1.2 Hierarchical clustering and total number of differentially expressed genes (DEGs)

Prior to starting analysis, a visual representation of gene expression was created using a heat map and hierarchical clustering graph (Figure 6.2) in order to assess heterogeneity of sample groups and to reveal the hidden structure of gene expression profile across samples while ordering them based on similarities. In the heat map, rows represent genes and columns represent the different samples. All rows are scaled based on a Z-Score which is calculated using the following formula; (gene expression value in sample of interest - mean expression across all samples) / Standard Deviation. The Z score will reflect every gene variable expression a cross all samples and then colour coded as upregulated (red colour gradient) and downregulated (green colour gradient). The organization and length of the branches within the associated dendrograms reflect the similarity in gene expression profiles between each of the samples and between each gene.

As show in (Figure 6.2) when inspecting gene expression across all sample groups, control samples appear to have a concordant expression pattern as expected. This pattern of expression is different from samples of cells grown on 3D decellularised scaffolds. However, remarkably, variable expression pattern was observed within the 3D samples group showing two distinct gene expression patterns that were denoted as 3D-1 and 3D-2 subgroups. Interestingly it was found that the 3D-1 sample group corresponds to DC scaffolds that had an intact adventitial layer, while 3D-2 sample group correspond to DC tracheal scaffolds that lacked the loose adventitial layer.

A volcano plot as shown in (Figure 6.3) was also used to visualise differential gene expression between cells on DC scaffolds (3D) versus control, the scatter plots revealed the presence of many significantly ($P \leq 0.05$) differentially expressed genes (Upregulated and downregulated) between groups.

Overall, there was a total of 5687 (3204 upregulated, 2483 downregulated) differentially expressed genes (DEGs) between cells grown on 3D (All) and control. Deferential gene expression analysis was also conducted on the subgroups identified 3D-1 and 3D-2 in comparison to control in order to further analyse and understand their pattern of expression. The total number of DEGs was calculated and is displayed on (Table 6.1). When specifically analysing the DEGs between subgroups and control, results shows that there was 7751 and 9539 DEGs in 3D-1 and 3D-2 subgroups respectively.

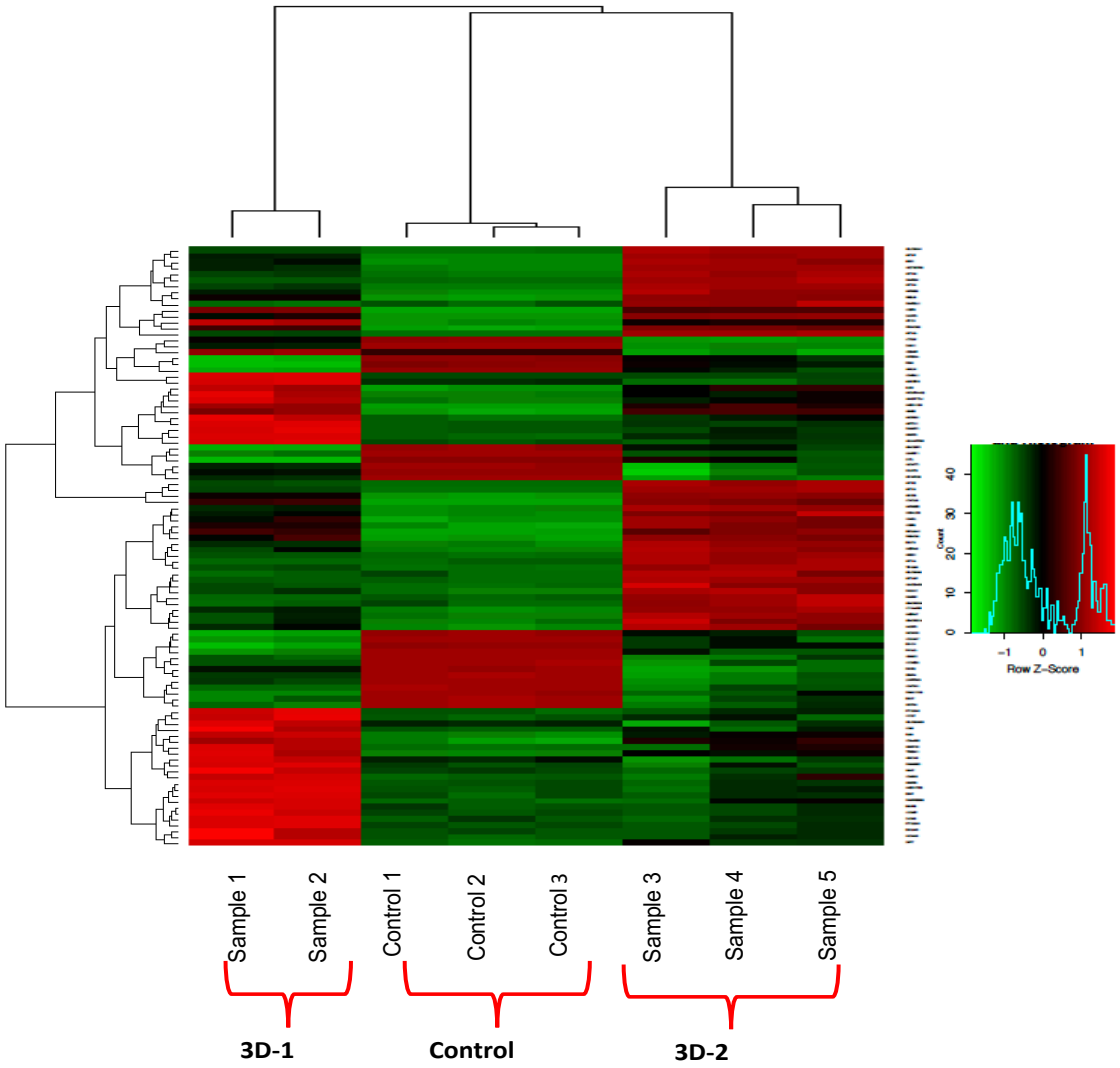

Control: UC-MSCs pre seeding.

3D-1: UC-MSCs on DC scaffolds with intact adventitia.

3D-2 : UC-MSCs on DC scaffolds lacking loose adventitia.

Figure 6.2: Heat map and hierarchical clustering of the top differentially expressed genes.

Rows represent genes, columns represent different samples. Colours reflect Z score indicating the magnitude of relative expression of a particular gene across samples, on which brighter red corresponds to increased expression and darker green corresponds to reduced expression. The top x axis dendrogram reflect similarities between different samples while the left Y axis represent gene clustering dendrogram. Z-Score is calculated using the following formula; (gene expression value in sample of interest) - (mean expression across all samples) / Standard Deviation.

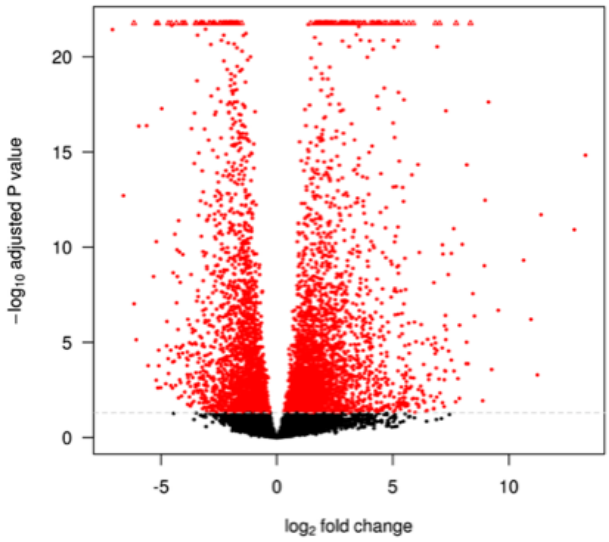

Figure 6.3: Volcano plots of differentially expressed genes.

Differential gene expression of all samples extracted from all seeded DC scaffolds (3D -All). Scattered points represent genes. The x axis represents the log2 fold change denoting the ratio of the difference of expression between test sample and control, y axis is -log10 adjusted P ratio which represent the probability that a gene has a statistical significance in its differential expression. Red points represent genes that are significantly upregulated (> 0 log2 fold change) and downregulated (< 0 log2 fold change).

Table 6.1: Number of differentially expressed genes (DEGs) for each comparison considering a significance level of ($P \leq 0.05$)

	Total number	Upregulated	Downregulated
3D (All) vs control	5687	3204	2483
3D-1 vs control	7751	3925	3826
3D-2 vs control	9539	4540	4999

To further analyse the data sets, a more stringent threshold was defined to select only for the most significant DEGs. Therefore, it was decided to filter data sets and only consider differentially regulated genes that show ±1.5 log2 fold change (plus sign indicates upregulation, minus sign indicates downregulation) and an adjusted P value of ≤ 0.001. The total number of DEGs per each group considering the more stringent cut-offs is displayed in the table below.

Table 6.2: Total number of differentially regulated genes considering a significance threshed of P≤ 0.001 and a log2 fold change of ± 1.5.

	Total number	Upregulated	Downregulated
3D (All) vs control	1737	1089	648
3D-1 vs control	2821	1209	1612
3D-2 vs control	2145	1203	942

6.2.2 Functional gene ontology (GO) enrichment analysis and top differentially regulated genes

Gene set ontology (GO) enrichment analysis was performed on the different groups. The analysis is based on classifying gene sets and inferring their biological functions based on the predefined gene ontology classification terms (Cellular process, molecular functions, and cellular component). The gene ontology consortium (http://www.geneontology.org) is a worldwide consortium that defines ontologies to annotate the biological knowledge we have or predicted for a given gene function. It allows defining the cellular and biological functions dominating the DEGs sets and as also help elucidate if the associated DEGs has some coherent functional signal. And then it will identify overrepresentation of gene ontology terms in the gene set to reflect the most significant functional profile that describe the DEGs data set.

GOrilla web-based application (Eden et al., 2009) was used as a tool to perform the GO enrichment analysis. For this study GO enriched terms related to biological process were only considered with an enrichments P value of ($\leq$0.01). Figures corresponding to the GO enrichment analysis for each group are displayed bellow. The top regulated genes (highest log2 fold change) were also defined per each DEGs gene set.

6.2.2.1 GO enrichment analysis and top regulated genes for 3D (All) versus Control.

GO analysis of the overall biological profile of the genes differentially expressed in UC-MSCs post seeding in to DC scaffolds (3D All) as shown in Figure 6.4 revealed that the upregulated DEGs (Table 6.3, A) showed significantly enriched biological processes related mainly to zinc ion homeostasis, detoxification and detoxification of inorganic compounds, cellular response to cadmium ions, regulation of cellular response to stimulus, cytokine mediated signalling pathways and signal transduction.

On the other hand, GO analysis of the downregulated DEGs (Table 6.3, B) showed that the most significant cellular processes were mainly related to regulation of signalling receptor activities, DNA replication initiation, activation of MAPKK activity, regulation of cell migration and cellular response to endogenous stimulus.

The top ten DEGs with the highest log2 fold change are shown in (Table 6.3), as can be seen from the table, the top upregulated genes include 5 genes that belong to the metallothionine gene family (MT1G, MT1H, MT1M, MT1JP and MT1F), and 2 genes (HSPA7, HSPA6) of the heat shock proteins family HsP70. The list also includes IL24 gene (encodes for interleukin 24 of the IL10 interleukin family) and DPT that encodes for the ECM matrix protein (dermatopontin). Whilst the top downregulated genes included: Epidermal growth factor (EGF), Bone morphogenic protein 4 (BMP4), Myopalladin (MYPN), contactin1 (CNTN1) and Cyclin E2 (CCNE2).

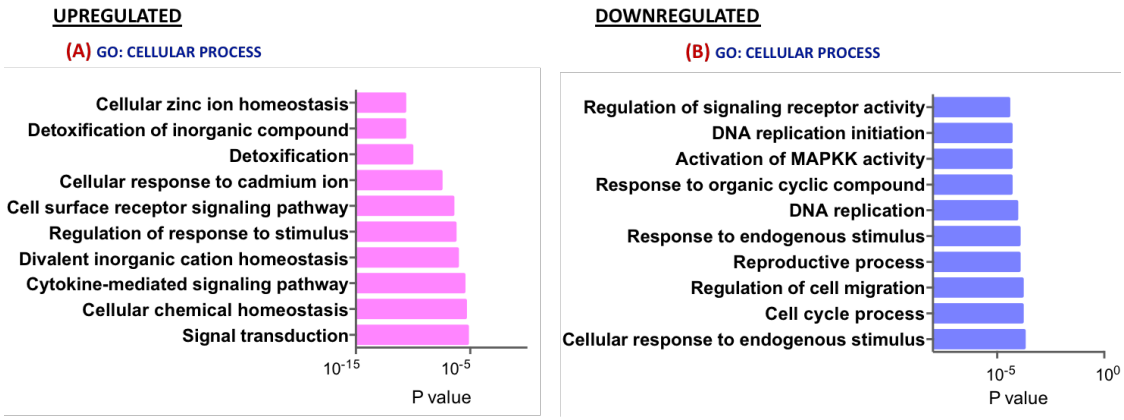

Figure 6.4: Gene ontology enrichment analysis of highly regulated genes associated with MSCs on 3D (All) versus control group.

Bar charts represents the most significant top GO terms associated with biological process (A, upregulated) and (B) downregulated. Enrichment P value ≤0.01.

Table 6.3: Top regulated genes in 3D(All) versus control group.

Upregulated	Log2 FC	Downregulated	Log2 FC
MT1G	13.293	MYPN	-7.089
MT1H	12.812	LINC00707	-6.621
MT1M	11.384	CNTN1	-6.165
DPT	11.225	E2F2	-6.16
HSPA7	10.949	FAM111B	-6.068
IL24	8.943	CCNE2	-5.958
RGCC	9.54	EGF	-5.62
MT1JP	9.257	C7orf69	-5.558
MT1F	9.123	BMP4	-5.323
HSPA6	8.978	ZCCHC5	-5.206

Note: (FC) Fold change

6.2.2.2 GO enrichment analysis and top differentially regulated genes for 3D-1 subgroup versus control group.

Go enrichment analysis of 3D-1 versus control subgroup (Figure 6.5, A) revealed that the most significant upregulated GO cellular processes were involving: regulation of cellular signalling activity, cell-cell signalling, cytokine mediated signalling pathway, cell surface receptor signalling pathway, cellular response to chemical stimulus, extracellular matrix disassembly, collagen metabolic process and extracellular structure organization. With regards to the downregulated DEGs (Figure 6.5, B), the top significant GO cellular processes were related to regulation of cell cycle process, regulation of mitotic cell division, regulation of mitotic nuclear division, microtubule-based process, and regulation of chromosome segregation.

The top differentially expressed genes within this subgroup are listed on (Table 6.4), where the top upregulated DEGs include: DPT(encodes for the ECM matrix protein dermatopontin), KCNJ6 (encodes for a G protein of the inward rectifier potassium channels), IL24, EHF(encodes for ETs homologous transcription factor characterised by epithelial specific expression), CHI3L1(encodes for chitinase-30-like 1 glycoprotein), C2CD4A (encodes for calcium dependant domain containing protein4A), ANGPTL4 (encodes for angiopoietin-like 4) and CLEC18B (encodes for mannose receptor binding protein). The top downregulated genes include: MCM10 (encodes for minichromosomal maintenance protein), E2F2 (encodes for E2F2 transcription factors, EXO (encodes for exonuclease 1) and ANLN which encodes for actin-binding protein.

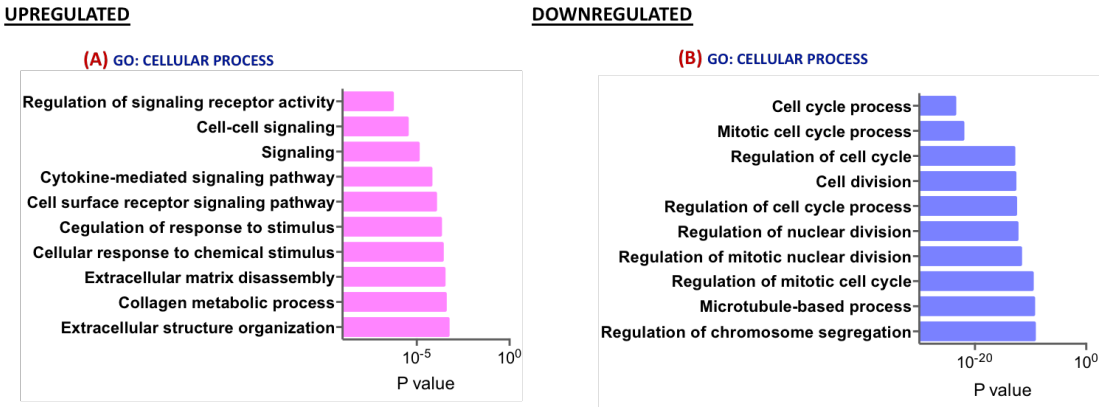

Figure 6.5: Gene ontology enrichment analysis of highly regulated genes associated with 3D-1 subgroup versus control.

Bar charts represents the most significant top GO terms in biological process category. (A) represent GO enrichments of upregulated genes, (B) represents GO enrichment of downregulated genes. Enrichment P value ≤0.01.

Table 6.4: Top differentially regulated genes on the 3D-1 subgroup.

Upregulated	Log2 FC	Downregulated	Log2 FC
DPT	12.523	FAM111B	-11.675
KCNJ6	10.18	PLCE1-AS1	-8.702
IL24	10.163	MCM10	-8.58
TREM1	9.562	SPC25	-8.18
CHI3L1	9.557	E2F2	-7.781
C2CD4A	9.393	KIF20A	-7.737
HSD11B1	9.24	EXO1	-7.709
EHF	9.059	SPC24	-7.521
ANGPTL4	8.8	ESCO2	-7.403
CLEC18B	8.8	ANLN	-7.373

Note: (FC) Fold change

6.2.2.3 GO enrichment analysis and top differentially regulated genes for 3D-2 subgroup versus control group.

As shown in (Figure 6.6), GO enrichments analysis of the 3D-2 subgroup versus control demonstrated that the most significant cellular processes terms within the upregulated DEGs set (Figure 6.6, A) involved, cellular zinc ion homeostasis, detoxification of inorganic compounds, response to zinc ions, detoxification of copper ion, cellular transition metal ion homeostasis, cellular response to cadmium ions and detoxification. When inspecting top enriched cellular process GO classification of downregulated genes (Figure 6.6, B), the most significant processes involved: cell-cell adhesion, biological adhesion, positive regulation of collagen biosynthetic process, regulation of signalling receptor activity, positive regulation of collagen metabolic process and G-protein coupled receptor signalling pathway.

The top DEGs with the highest log2 fold change are shown in (Table 6.5). Results revealed that most of the upregulated genes belong to the metallothionine gene family including (MT1G, MT1H, MT1M, MT1JP, MT1F) and shows 2 heat shock protein HSp70 encoding genes (HSP7 and HSPA6), it also includes RGCC (encodes for regulator of cell cycle protein). The downregulated genes include, PKP2 (encodes for plakophilin-2), BMP4(bone morphogenic protein), PTPN20 (encodes for protein tyrosine phosphatase), KIAA1161 (encodes for myogenesis regulating glycosidase), MIR614 (micro RNA 614)

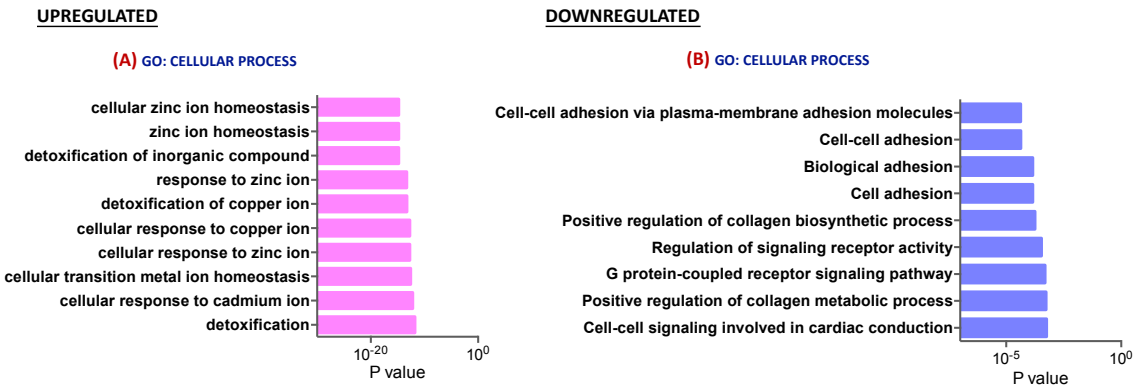

Figure 6.6: Gene ontology enrichment analysis of highly regulated genes associated with 3D-2 versus control group.

Bar charts represents the most significant top GO terms in biological process and molecular functions categories. (A, B) represent GO enrichments of upregulated genes, (C, D) represents GO enrichment of downregulated genes. Enrichment P value ≤0.01.

Table 6.5: Top differentially regulated genes on the 3D-2 vs control group.

Upregulated	Log2 FC	Downregulated	Log2 FC
MT1G	14.026	PKP2	-9.867
MT1H	13.38	BMP4	-7.931
MT1M	12.258	LRRTM3	-7.646
HSPA7	11.676	LINC00707	-7.401
C11orf96	11.293	PTPN20	-7.225
RGCC	10.284	KIAA1161	-7.201
MT1JP	9.999	ZNF439	-7.167
MT1F	9.819	MIR614	-7.156
HSPA6	9.719	MYPN	-7.136
RN7SK	9.258	SLC27A2	-6.84

Note: (FC) Fold change

6.2.2.4 Unique DEGs corresponding 3D-1 and 3D-2 subgroups.

In order to further elucidate the differences between cells differential expression within the DC tracheal scaffolds subgroups (3D-1 and 3D-2) and to identify unique genes expressed exclusively in each subgroup, a 2-way Venn diagram was drawn from upregulated (Figure 6.7, B) and down regulated genes (Figure 6.8, B) from 3D-1 and 3D-2 subgroups. Then lists of unique DEGs were further analysed for the most significant GO cellular processes terms (enrichment P value $\leq$ 0.01). The results demonstrated that there were 617 and 1151 unique upregulated DEGs present within the 3D-1 and 3D-2 subgroups respectively (Figure 6.7,B). In the 3D-1 subgroup the most significant upregulated GO cellular process terms (Figure 6.7, A and C) were found to be related to cell- cell signalling, Signalling, extracellular matrix organization and ECM structure organisation. While in the 3D-2 subgroup, upregulated GO terms were related to zinc ion homeostasis, protein hetrotetramerization and gene silencing.

With regards to unique downregulated DEGs in 3D-1 and 3D-2 subgroups (Figure 6.8, B), data showed that there were 447 and 1407 unique downregulated DEGs in 3D-1 and 3D-2 subgroups respectively. The most significant upregulated GO cellular processes in 3D-1 unique gene list (Figure 6.8, A) were found to be involved in cell cycle process, mitotic cell cycle process, regulation of mitotic nuclear division and cell division. On the other hand, GO cellular process terms associated with unique downregulated DEGs in 3D-2 subgroup (Figure 6.8, C) mainly involved cell-cell adhesion, biological adhesion, and cell adhesion.

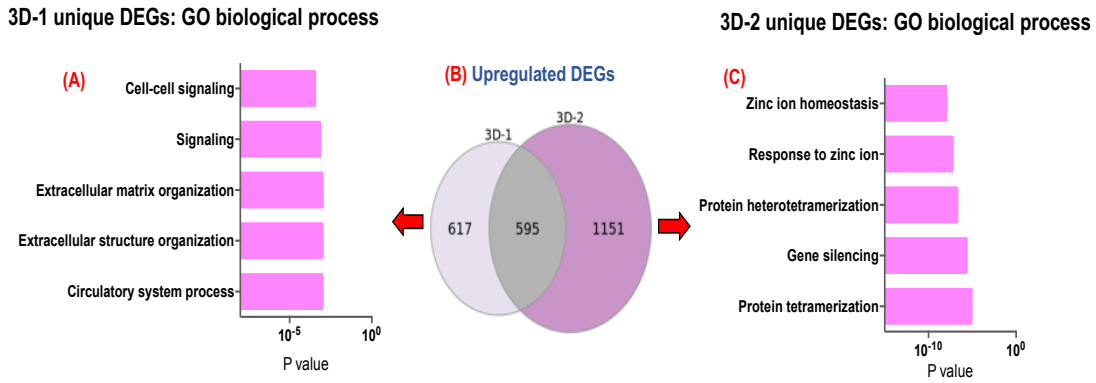

Figure 6.7: Unique upregulated DEGs gene ontology enrichment in 3D-1 and 3D-2 subgroups.

Venn diagram (B) shows that there are 617 and 1151 unique upregulated DEGs present within the 3D-1 and 3D-2 subgroups respectively. The unique list of genes was analysed for the most significantly GO cellular processes terms corresponding to 3D-1 (A) and 3D-2 (C) subgroups. GO enrichment P value ≤0.01.

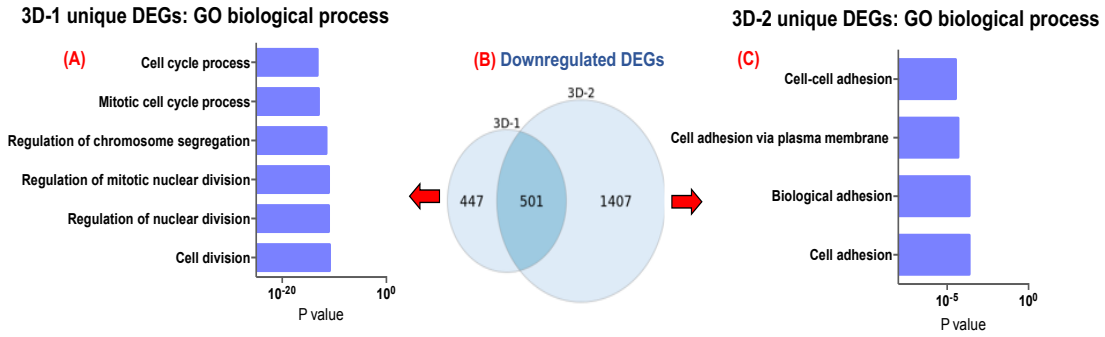

Figure 6.8: Unique downregulated DEGs gene ontology enrichment in 3D-1 and 3D-2 subgroups.

Venn diagram (B) shows that there are 447 and 1407 unique downregulated DEGs present within the 3D-1 and 3D-2 subgroups respectively. The unique lists of genes were analysed for the most significantly GO cellular processes terms corresponding to 3D-1 (A) and 3D-2 (C) subgroups. GO enrichment P value ≤0.01.

6.2.3 Pathways enrichment analysis

DEGs data sets were further analysed and interpreted using Ingenuity Pathway analysis (IPA) software. The IPA analysis is based on mapping the observed gene expression change on our data set to what is known in literature in the Ingenuity knowledge base. Then it was used to identify upstream regulators causing the gene expression changes, biological functions and relevant canonical pathways enriched in the data set. In addition to that it will predict the direction of the change observed in the data set weather it is activated or inhibited and present it statistically as a Z score considering a score of ± 2 as a significant prediction. IPA enrichment and comparative analysis was conducted and the top significant biological functions, upstream regulators and canonical pathways were identified for 3D-All, 3D-1 and 3D-2 subgroups and presented as a heat map as shown in (Figure 6.2).

By inspecting the heat map (Figure 6.9) it can be seen that there is an overall maintenance of cellular homeostasis and an activation of several biological functions related to homing of cells, chemotaxis, migration and activation of cells and leukocytes. Moreover, the data demonstrate a favourable activation of angiogenesis markers.

Interestingly when comparing 3D-1 and 3D-2 subgroups, variable cellular responses were enriched supporting the observed differential behaviour of UC-MSCs on the different matrices of the tracheal scaffolds. On which cellular functions involving chemotaxis, homing, leukocytes and mononuclear leukocytes migration and movement and respiratory system development were only activated on 3D-1 subgroups while it was lacking in 3D-2 subgroup.

However, 3D-2 subgroup shows distinct activation of autophagy and metabolism of reactive oxygen species biological functions.

Potential upstream regulators were also identified by analysing linkage to DEGs. IPA consider transcription factors and any gene or molecule that has been observed to affect gene expression (Krämer et al., 2014).

The top activated upstream regulators in our data set have been found sharing a common role in controlling genes involved in pro-inflammatory response and immune cells trafficking (macrophages and neutrophils). These included: TNF, IL1B, NFKB, RELA, NFkB complex, INFG, INFA2, TLR3. In addition to that,

NUPR1 have been also identified as an upstream regulator, NUPR1 is a pleotropic stress gene that is involved in cytoprotective autophagy, apoptosis, and cell survival.

When inspecting IPA enriched pathways, analysis revealed activation of many signalling pathways and the top activated pathways included: Dendritic cell maturation, Oncastatin M signalling, Role of IL17F in inflammatory airway disease, acute phase response signalling, p38 MAPK signalling, IL6 & IL8 signalling, INF signalling, HMGB1 signalling and TREM1 signalling. Interestingly EIF2 signalling pathway seem to be only activated in 3D-2 subgroup.

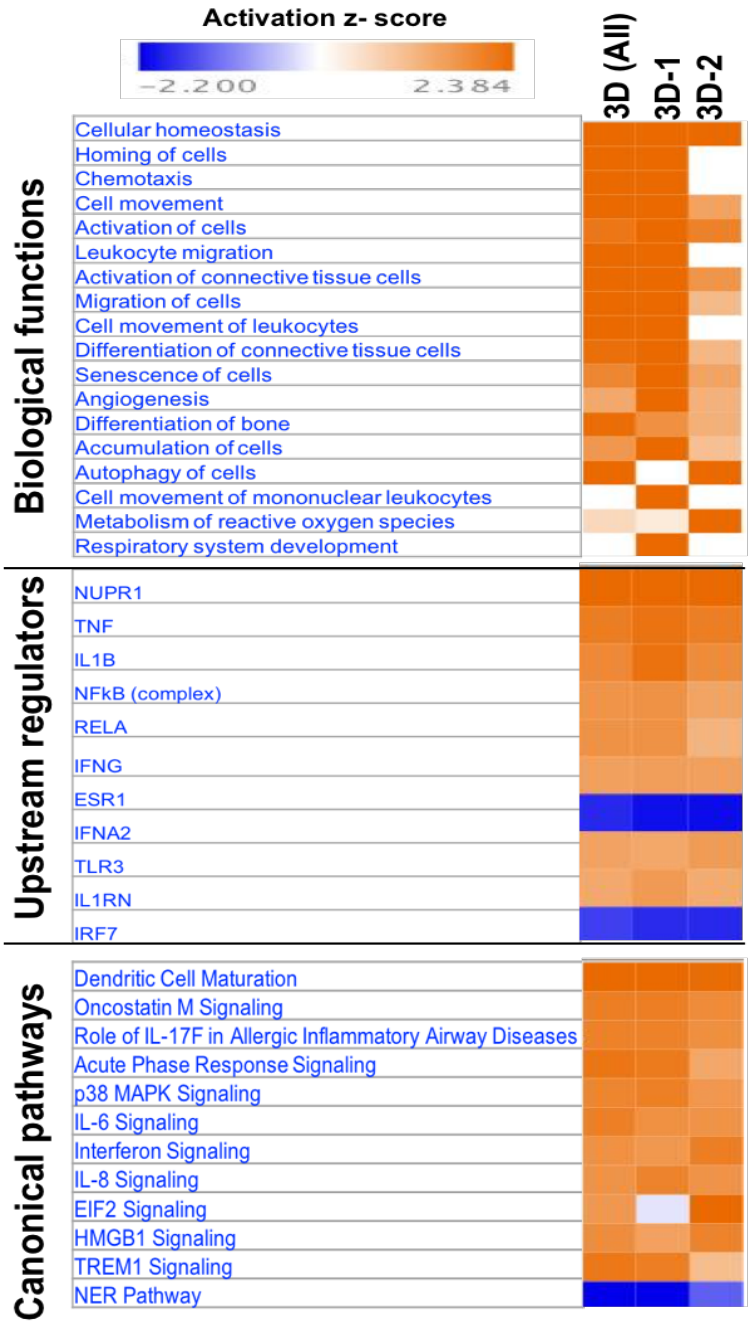

Figure 6.9: IPA comparative analysis of DEGs data sets.

The heat map shows and compare the top biological functions, upstream regulators and canonical pathways enriched in DEGs of the 3D (All) group, while specifically comparing the 3D-1 and 3D-2 subgroups gene expression patterns. Z score denotes direction of the change (Orange: Activated, Blue: inhibited, White: no change).

6.2.4 Gene families of selected bioactive factors mediating MSCs paracrine therapeutic effects.

The data set was specifically investigated for the differential expression of selected gene sets representing known bioactive factors produced by MSCs. These factors were known from literature to mediate MSC therapeutic activities and tissue repair and are of relevance in tissue engineering applications. The selected gene families included factors associated with ECM remodelling, anti-fibrotic, anti-scarring, anti-apoptotic, chemoattraction, supportive and immunomodulatory effects. However, it was decided to group them based on their type for simplification as many factors overlap multiple therapeutic effects and fall under multiple categories. The gene families assigned were:

1. ECM remodelling
2. Chemokines and interleukins
3. Growth factors (A)
4. Growth factors (B)/ adhesion and other paracrine factors.

A visual representation of DEGs for each gene family was created using Heat maps and hierarchical clustering and a summary of DEGs and the corresponding fold change was also listed in tables.

6.2.4.1 ECM remodelling gene family

This gene family correspond to genes associated with ECM and ECM remodelling. The analysis of DEGs revealed the presence of many regulated genes that belong to ECM remodelling family, they were displayed in (Table 6.6) and visualised using heat map (Figure 6.10). The regulated genes observed included:

1. **Metalloproteinases (MMPs)**: which are proteolytic enzymes mainly involved in ECM remodelling.
2. **Adamalysins**: which are a family of proteinases that include ADAMs (disintegrin and metalloproteinases) that act as shedases that cleaves transmembrane protein ectodomains, and ADAMTS which are secreted proteinases with thrombospindin type-I-like repeats.
3. **Metalloproteinases inhibitors**: tissue inhibitors of metalloproteinases (TIMPs) act by inactivating MMPs, ADAMs, ADAMTS to balance ECM degradation
4. **Other ECM proteins**

Overall UC-MSCs grown on DC tracheal scaffolds (3D-All) appear to upregulate MMP1, MMP3, MMP10, MMP14, ADAMTS5 and TIMP1. With regards to ECM proteins upregulation of COL6A1, COL6A2, COL7A1, COL18A1, COL27A1 and DPT was also observed. The data also shows downregulation of COL1A1.

Remarkably when closely inspecting regulated gene expression within subgroups 3D-1 and 3D-2 (Figure 6.10), 3D-1 appear to actively upregulate more transcripts involved in ECM remodelling. Such as, MMP2, MMP8, MMP12, MMp13, ADAM8, TIMP2, TIMP3. In addition to that 3D-1 subgroup demonstrated upregulation of more ECM proteins these including, COL10A, COL14A, COL15A, COL24A and Elastin (ELN). While in 3D-2 subgroup a downregulation of ADAM1A, ADAM9, ADAM10, ADAM19, ADAMTS15 and MMP16 was observed.

Table 6.6: Differentially regulated genes corresponding to ECM remodelling gene family and their associated log2 fold change with an adjusted P value of (≤0.001).

Category	Gene ID	Log2 fold change/ P adjusted ≤ 0.001		
		3D (All)	3D-1	3D-2
Metalloproteinases	MMP1	5.022	5.894	3.764
	MMP2		3.143	
	MMP3	7.406	8.747	2.334
	MMP8		7.235	
	MMP10	7.272	8.444	4.172
	MMP12		6.682	
	MMP13		5.148	
	MMP14	1.952	2.282	1.69
	MMP16			-1.842
Adamalysins	ADAM8		3.784	
	ADAM1A			-4.369
	ADAM9	-3.048		-4.869
	ADAM10			-2.805
	ADAM19			-2.313
	ADAMTS5	4.536	5.816	
	ADAMTS15			-5.574
Metalloproteinases inhibitors	TIMP1	2.852	2.84	2.861
	TIMP2		2.237	
	TIMP3		1.543	
Extracellular matrix	COL1A1	-2.546	-1.467	-4.498
	COL6A1	1.855	2.068	1.695
	COL6A2	3.007	2.971	3.031
	COL7A1	5.011	5.247	4.829
	COL10A1		5.876	
	COL15A1		3.685	
	COL14A1		2.776	
	COL18A1	1.756	1.884	1.667
	COL27A1	1.643	1.742	1.561
	COL24A1		3.615	
	ELN		5.033	
	DPT	11.225	12.523	

*Note: Grey cells, represent DEGs that did not pass cut-off range of ±1.5 log2 FC, P adjusted value= 0.001.

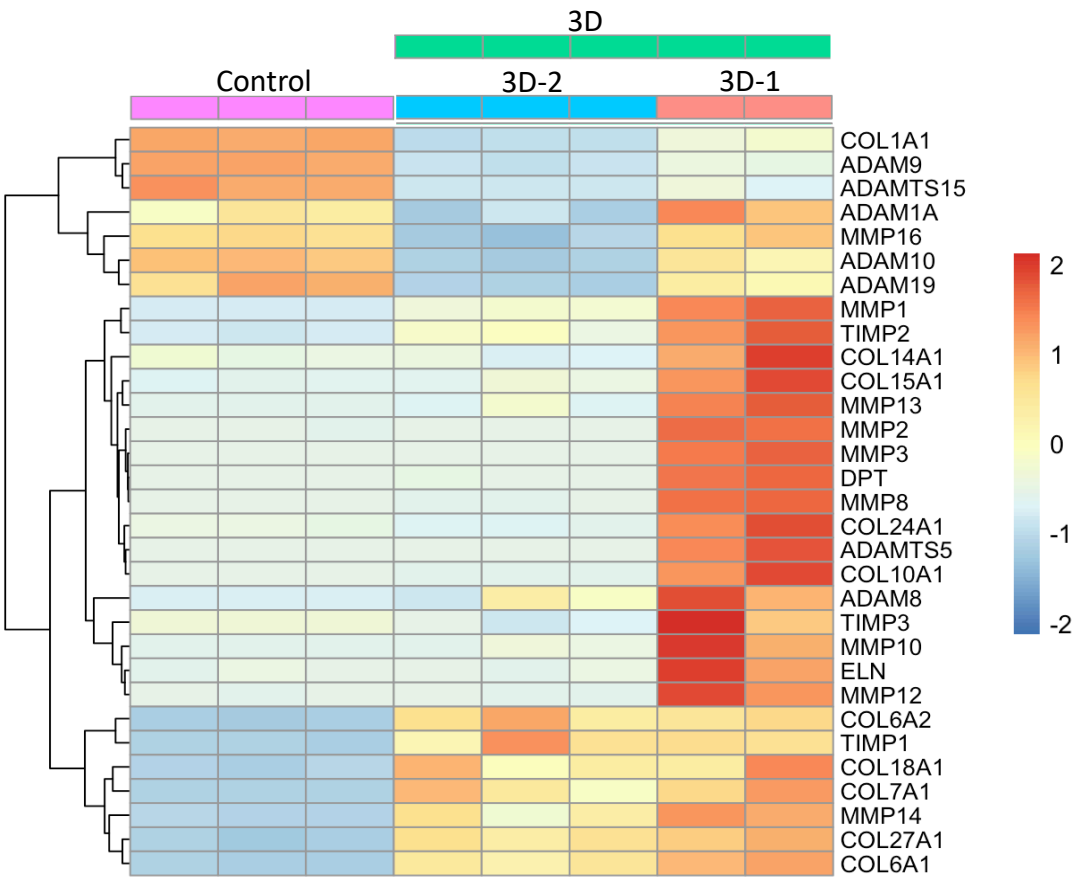

Figure 6.10: Heat map of differentially expressed genes associated with ECM remodelling.

Rows represents genes, columns represent different sample groups. Color scale reflect Z score indicating the magnitude of relative expression of a particular gene across sample groups, on which graded orange corresponds to upregulation and graded blue corresponds to downregulation, Pale yellow represent no change. The left Y axis shows gene clustering dendrogram. Control= UC-MSCs pre-seeding, 3D= UC-MSCs grown on DC tracheal scaffolds, 3D-1= DC scaffolds with intact adventitia, 3D-2= DC scaffolds lacking Loose adventitia.

6.2.4.2 Chemokines and Interleukins gene family

Transcriptome analysis demonstrated that UC-MSCs seeded on DC scaffolds appear to upregulate many chemokines and interleukins in comparison to control group as shown in (Table 6.7) and (Figure 6.11). Overall, the upregulated chemokines included: CCL2, CCl7, CCL20, CXCL2, CXCL3, CXCL5 and CXCL8. The upregulated interleukins included: IL1A, IL1B, IL1RN, IL6, IL11, IL15, IL15RA, IL23A, IL24, IL32, IL33, IL34, IL4I1. However, when inspecting for differences in gene expression between 3D-1 and 3D-2 subgroups, a similar expression pattern to the observed with ECM remodelling gene family was noted, in which cells grown on 3D-1 DC scaffolds upregulate more transcripts compared to 3D-2 subgroups. The upregulated genes included: CCL2, CCL7, CCL20, CxCL1, CXCL6, IL19, IL34, LIF and IL4R. Whilst cells grown on 3D-2 showed downregulation of CXCL12.

Table 6.7: Differentially regulated chemokines and interleukins and their associated log2 fold change with an adjusted P value of (≤0.001).

Category	Gene ID	Log2 fold change/ P adjusted ≤ 0.001		
		3D (All)	3D-1	3D-2
chemokines	CCL2	1.581	2.132	
	CCL7	4.715	5.971	
	CCL20	3.591	4.499	
	CXCL1		3.245	
	CXCL2	4.344	3.886	4.586
	CXCL3	4.442	4.394	4.473
	CXCL5	3.149	4.159	1.590
	CXCL6		3.156	
	CXCL8	5.484	4.699	5.840
	CXCL12			-3.906
Interleukins	IL1A	2.842	2.69	2.934
	IL1RN	4.002	4.678	3.229
	IL1B	3.536	3.689	3.424
	IL6	3.939	4.802	2.778
	IL11	4.324	5.017	3.570
	IL15	2.042	1.747	2.214
	IL15RA	3.271		3.718
	IL19		8.19	
	IL17RC			2.212
	IL23A	2.596	2.619	2.584
	IL24	8.943	10.163	5.737
	IL32	4.147	3.294	4.510
	IL33	6.085	7.031	4.567
	IL34	5.091	4.553	
	IL4I1	5.245	5.651	4.916
	LIF		1.972	
	IL4R		2.083	

*Note: Grey cells, represents DEGs that did not pass cut-offs range of ±1.5 log2 Fold Change, P adjusted value= 0.001.

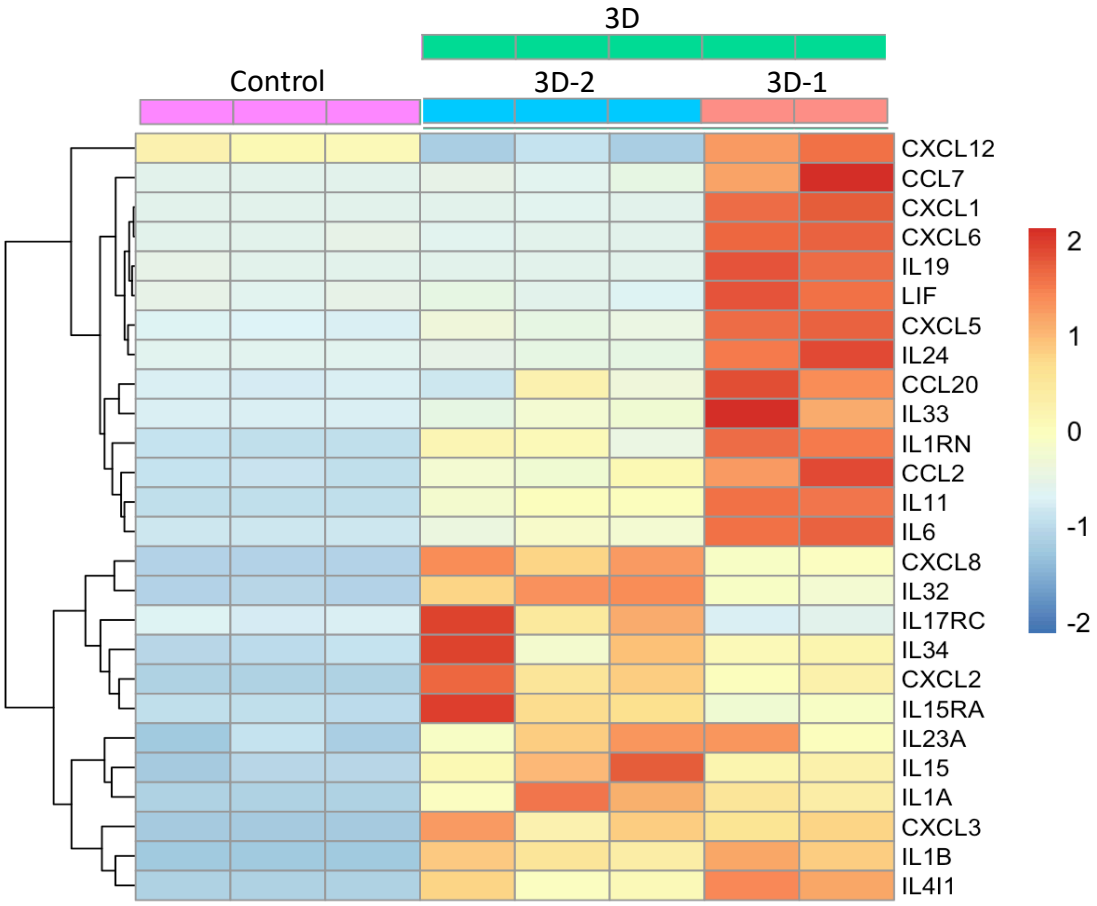

Figure 6.11: Heat map of differentially expressed chemokines and interleukins.

Rows represents genes, columns represent different sample groups. Color scale reflect Z score indicating the magnitude of relative expression of a particular gene across sample groups, on which graded orange corresponds to upregulation and graded blue corresponds to downregulation, Pale yellow represent no change. The left Y axis shows gene clustering dendrogram. Control= UC-MSCs pre-seeding, 3D= UC-MSCs grown on DC tracheal scaffolds, 3D-1= DC scaffolds with intact adventitia, 3D-2= DC scaffolds lacking Loose adventitia.

6.2.4.3 Growth factors (A) gene family

This gene family included transcripts of growth factors belonging to: Transforming growth factor beta super family (TGF-β), Epidermal growth factors (EGF), Fibroblast growth factors (FGFs) and Insulin -like growth factors (IGFs). As displayed in (Table 6.8) and heat map (Figure 6.12), there was an upregulation in TGFB1, GDF15, FGF18, IGFBP4 and IGFBP7. On the other hand, a downregulation was noted in BMP4, EGF, FGF1, FGF5.

When inspecting gene expression within the subgroups 3D-1 and 3D-2, cells grown on 3D-1 Dc scaffolds showed upregulation of more genes in comparison to 3D-2, these included: TGFBI, BMP1, BMP2, GDNF, FGF11, IGF2 and IGFBP5.

Table 6.8: Differentially expressed growth factors A and their associated log2 fold change at P value ≤0.001.

Category	Gene ID	Log2 fold change/ P adjusted ≤ 0.001		
		3D All	3D1	3D2
TFG superfamily	TGFB1	1.975	1.7	2.166
	TGFB2	-3.081	-2.076	-4.579
	TGFBI		1.741	
	BMP1		1.226	
	BMP2		5.937	
	BMP4	-5.323	-4.411	-7.931
	GDNF		2.639	
	GDF15	4.936	4.7	5.078
EGF	EGF	-5.62	-5.659	-5.652
FGF	FGF1	-2.942	-3.577	-2.629
	FGF2			-1.341
	FGF5	-1.796	-1.639	-1.902
	FGF7			-3.242
	FGF11		4.546	
	FGF18	6.22	5.626	6.591
IGF	IGF2		1.755	
	IGFBP3		1.15	-2.299
	IGFBP4	1.89	1.81	2.866
	IGFBP5		5.403	-1.485
	IGFBP6			2.516
	IGFBP7	2.526	1.468	2.114

*Note: Grey cells, represents DEGs that did not pass cut-off range of ±1.5 log2 Fold Change, P adjusted value= 0.001.

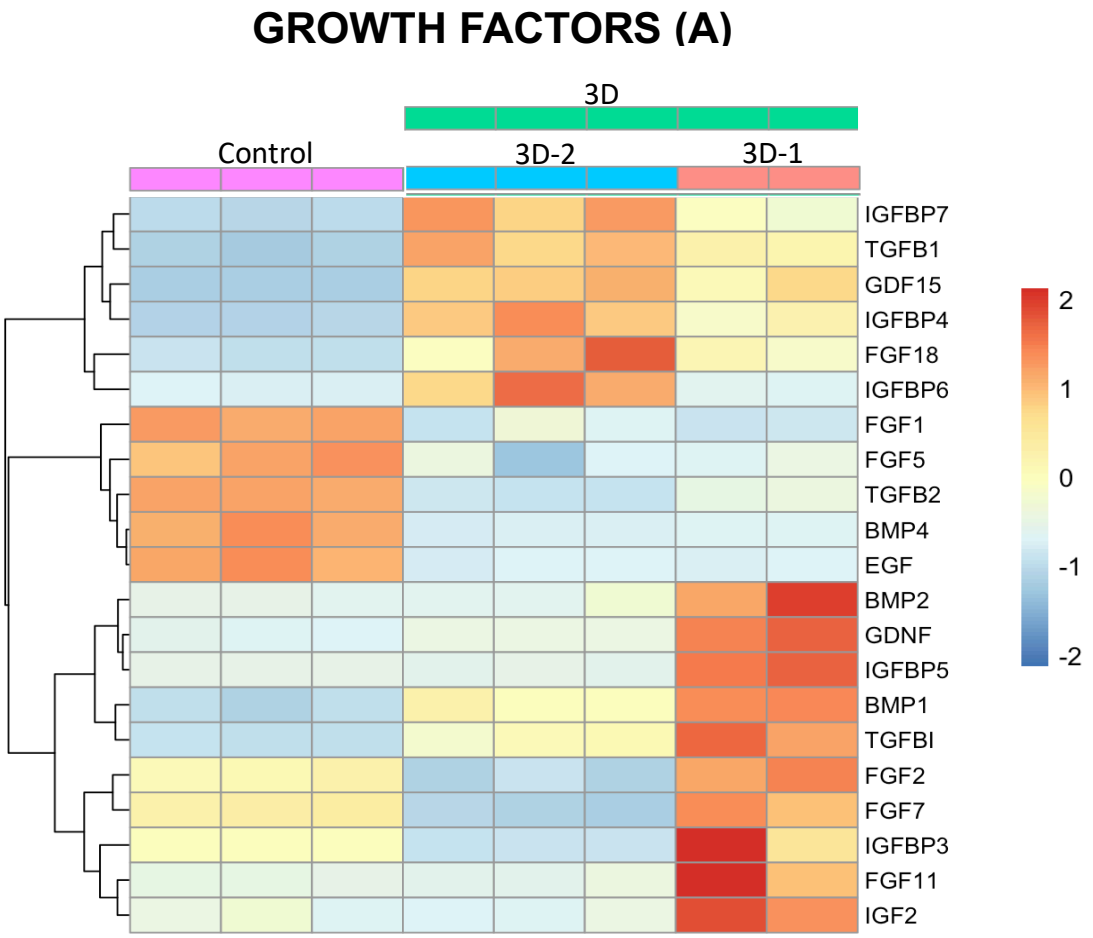

Figure 6.12: Heat map of differentially expressed growth factors A.

Rows represent genes, columns represent different sample groups. Color scale reflects Z score indicating the magnitude of relative expression of a particular gene across sample groups, on which graded orange corresponds to upregulation and graded blue corresponds to downregulation, Pale yellow represents no change. The left Y axis shows gene clustering dendrogram. Control= UC-MSCs pre-seeding, 3D= UC-MSCs grown on DC tracheal scaffolds, 3D-1= DC scaffolds with intact adventitia, 3D-2= DC scaffolds lacking Loose adventitia.

6.2.4.4 Growth factors B/ adhesion and other paracrine factors gene family

This gene family involves factors belonging to the: hepatocyte growth factors (HGF), Tumour necrosis factors (TNF), Vascular endothelial growth factors (VEGF), Colony stimulating factors, adhesion molecules and other paracrine factors.

As shown in (Table 6.9) and (Figure 6.13), MSCs on DC tracheal scaffolds showed upregulation of TNFRSF18, VEGFA, VEGFB, CSF2, CSF3, ICAM1, ICAM3, VCAM1, STC1, PTGES,ANGPTL4, ADM, BCL2A1, HLA-A,B,C and showed a downregulation of HGF.

Like the above findings, cells grown on 3D-1 DC scaffolds showed upregulation of more genes compared to 3D-2 subgroup. The genes included: TNFRSF1B, TNFRSF11B, TNFRSF21, VEGFC and HIF3A.

Table 6.9: Differentially expressed growth factors B and their associated log2 fold change at P value ≤0.001.

Category	Gene ID	Log2 fold change/ P adjusted ≤ 0.001		
		3D (All)	3D1	3D2
HGF	HGF	-2.098	-2.4	-1.908
TNF	TNFRSF1B		4.608	
	TNFRSF11B		2.56	
	TNFRSF18	5.079	4.424	
	TNFRSF21		3.418	
VEGF	VEGFA	3.475	4.186	2.651
	VEGFB	2.861	2.533	3.034
	VEGFC		2.204	
Colony stimulating factors	CSF2	7.292	6.061	7.977
	CSF3	7.73	8.253	7.282
Adhesion	ICAM1	4.027	2.107	4.603
	ICAM3	1.85		2.367
	VCAM1	2.095		2.679
Others	STC1	5.122	6.113	3.524
	PTGES	2.003	2.363	1.686
	ANGPTL4	7.527	8.8	4.082
	ADM	2.246		2.655
	BCL2A1	6.84	6.089	7.151
	HIF3A		4.227	
	HLA-A	2.161	2.114	2.19
	HLA-C	2.392	2.378	2.396
	HLA-B	3.01	3.28	2.793

*Note: Grey cells, represents DEGs that did not pass cut-off range of ±1.5 log2 Fold Change, P adjusted value= 0.001.

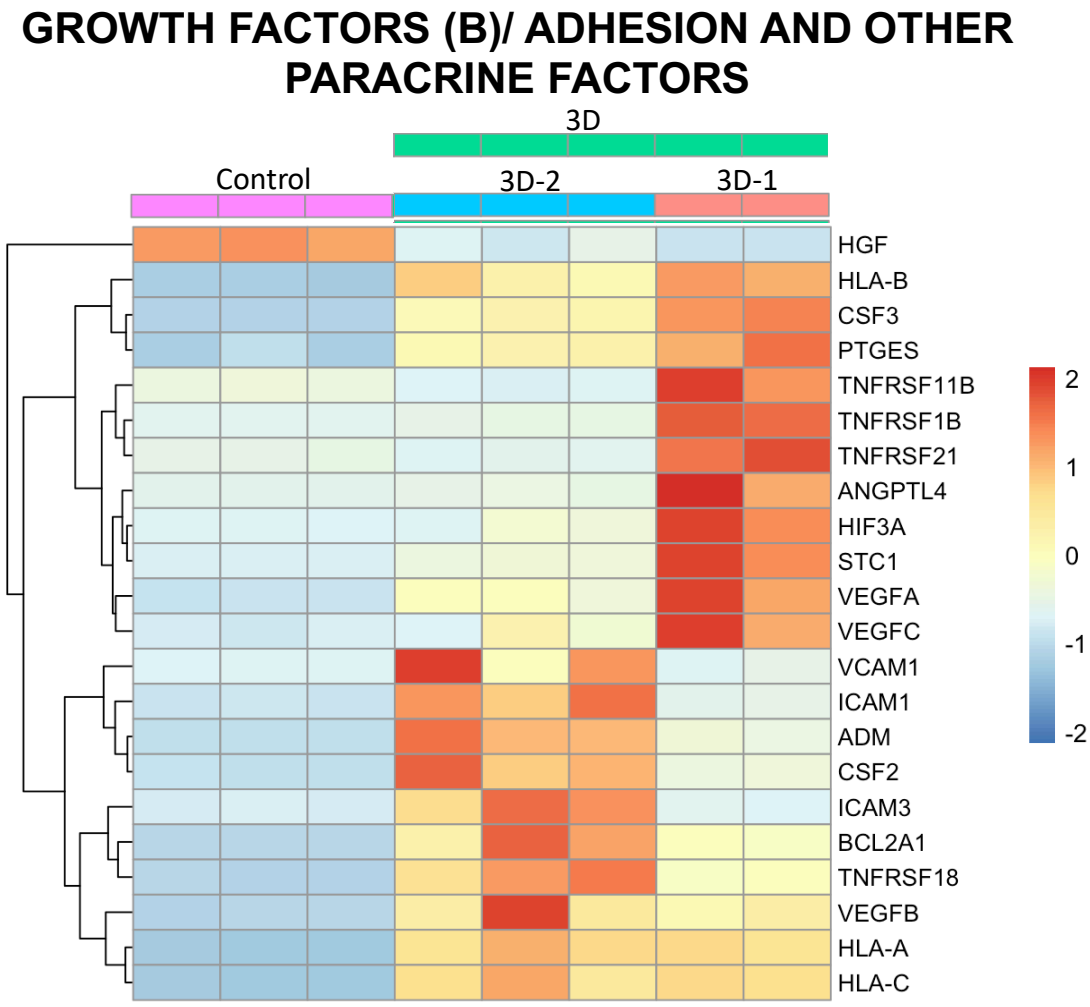

Figure 6.13: Heat map of selected differentially expressed growth factors B, adhesion molecules and other paracrine factors.

Rows represent genes, columns represent different sample groups. Color scale reflects Z score indicating the magnitude of relative expression of a particular gene across sample groups, on which graded orange corresponds to upregulation and graded blue corresponds to downregulation, Pale yellow represent no change. The left Y axis shows gene clustering dendrogram. Control= UC-MSCs pre-seeding, 3D= UC-MSCs grown on DC tracheal scaffolds, 3D-1= DC scaffolds with intact adventitia, 3D-2= DC scaffolds lacking Loose adventitia.

6.2.5 RT-PCR

In order to validate RNA seq analysis, selected DEGs expressions were post-checked using RT-PCR. The results confirmed an upregulation of VEGFA, PTGES (PGE2), CSF2 (GM-CSF) and a downregulation of BMP4. As shown in (Figure 6.14) unpaired t-test statistical analysis was performed comparing gene expression between cells pre-seeding (control) and cells post seeding and data showed a significant upregulation of VEGFA (P≤0.01), PTGES (P≤ 0.05) and CSF2 (P≤0.001) while they show a downregulation of BMP4 (P≤0.0001).

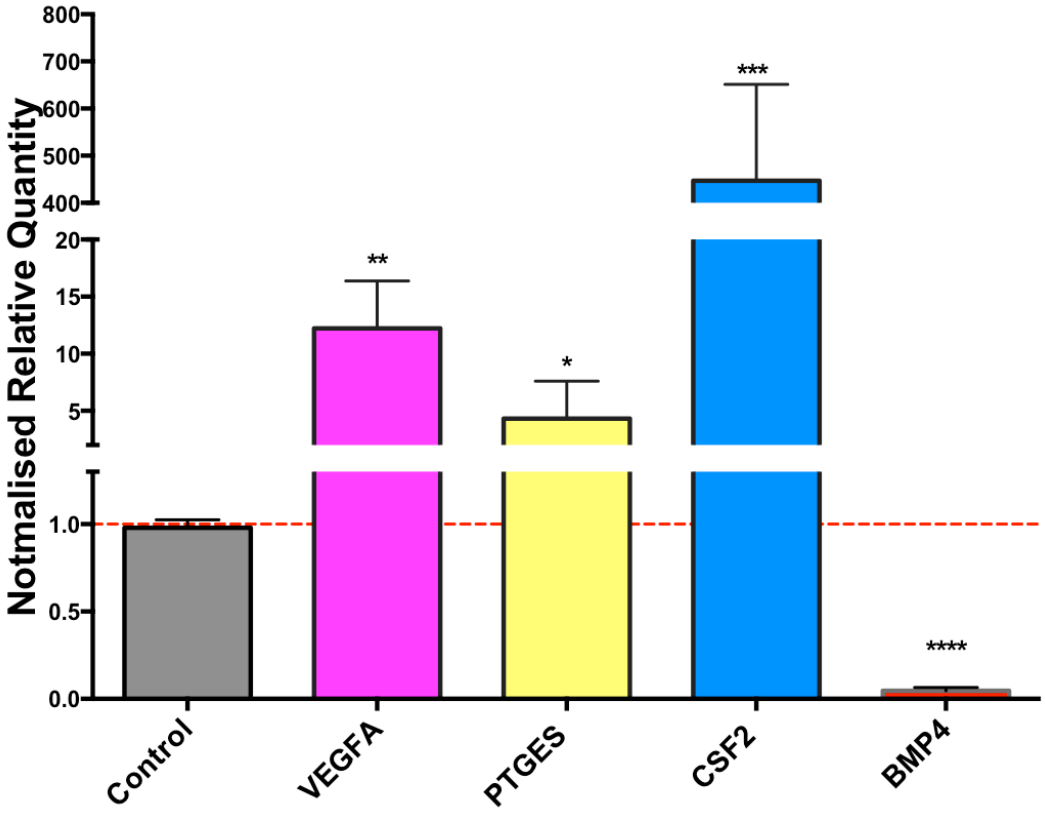

Figure 6.14: RT-PCR post RNA sequencing checking of selected DEGs.
Data shows the normalised relative quantities of VEGFA, PTGES, CSF2 and BMP4 versus control (cells pre-seeding). The analysis confirms a significant upregulation of VEGFA (**=P≤0.01), PTGES (*=P≤ 0.05) and CSF2 (***=P≤0.001) while it shows a downregulation of BMP4 (****=P≤0.0001). Dotted red line marks the control level. Data were analysed using unpaired t-test, values represents mean ± SD, n=5.

6.3 Discussion

Mesenchymal stromal cells are one the most employed cell type for cellularization in tracheal bioengineering. The rational was to leverage their strong immunomodulatory capacity and their paracrine support in creating a constructive environment for remodeling and integration of tracheal constructs. This speculation was taken from plethora of analogous experimental and clinical studies utilising MSCs and demonstrating their beneficial effect. However, the utility of these cells for tracheal tissue engineering has not been fully explored and to date no data are available about the cell's molecular interactions and responses to DC tracheal scaffolds. Therefore, an in-depth knowledge about the cells behavior when seeded onto the bioactive decellularised scaffold compared to tissue culture plastic is one of the fundamental requirements to understand their potential application for tracheal tissue engineering.

The aim of this chapter was to explore differential gene expression profile of UC-MSCs post seeding on to human DC tracheal scaffolds prior to implantation. Transcriptome analysis using RNA sequencing was used as a tool to (1) describe the overall functional and biological processes characterising cellular response on DC tracheal scaffolds and (2) to unravel trophic factors that might play a role in promoting constructive remodelling of bioengineered trachea if any.

Comparative transcriptome analysis between UC-MSCs seeded on human DC tracheal scaffolds at 3 days of culture and cells pre-seeding revealed the presence of numerous differentially expressed genes (DEGs). The total number of DEGs was 5687 (3204 upregulated and 2483 downregulated) at an adjusted P value of ≤ 0.05. But, in order to facilitate bioinformatics analysis and biological interpretation of the data set, a more stringent cut-off filter was defined that selected only the most significant DEGs on which differentially regulated genes that showed ± 1.5 log2 fold change and an adjusted P value of ≤ 0.001 were only considered for further analysis.

However, when the initial data were visually inspected using heat map and hierarchical clustering analysis, a marked observation emerged from the data comparison. Two distinct differential expression profiles in cells seeded onto DC tracheal scaffolds (3D-All) were observed and were denoted as 3D-1 and 3D-2 subgroups for simplification. Interestingly, the 3D-1 subgroup corresponded to gene expression of cells seeded on DC scaffolds that had an intact adventitial layer, while 3D-2 subgroup corresponded to cells seeded on DC scaffolds that lacked the loose adventitial layer. This correlation concurs well with my earlier findings in Chapter 4, on which I reported two distinct morphological patterns , fibroblastoid versus round shaped cells when cells were seeded on DC scaffolds maintaining an intact adventitial layer or seeded on scaffolds that lacked this layer respectively. These findings clearly reflect the impact of the underlying ECM substrate in changing cellular behaviour. Indeed, the effects of the physical and biomechanical ECM cues (stiffness, topography, composition, structure) in controlling cellular responses, morphology, survival, and commitment are well recognised (Watt and Huck, 2013, Gattazzo et al., 2014).

In this regard, the present study focused initially in characterising the differential expression of cells on DC scaffolds considering all samples (3D-All), as well as comparing differences between the identified subgroups (3D-1 and 3D-2) in order to understand the observed difference.

It is worth noting that the cadaver tracheas used in this study, were procured and decellularised by the NHSBT. As previously described, the decellularisation protocol involves dissection of the excess connective tissues prior to decellularisation, during which the loose adventitial layer is randomly and non-uniformly stripped during this step. Thus, the end DC scaffolds we received were variable depending on the operator.

The first part of the study aimed to characterise the overall transcriptome portrait of UC-MSCs seeded onto DC tracheal scaffolds in terms of dominant biological functions and enriched pathways that characterise cellular responses on the DC tracheal scaffolds. Two main bioinformatics analysis tools were employed to aid identification of the underlying functional profile, these are: functional gene ontology (GO) enrichment analysis and Ingenuity pathway IPA enrichment analysis.

Functional gene ontology enrichment (GO) analysis revealed that the overall cellular processes associated with the upregulated DEGs involved generally involved: zinc ion homeostasis, detoxification, regulation of cellular response to stimulus, cytokine mediated signalling pathways and signal transduction. On the other hand, major cellular processes terms associated with the downregulated DEGs involved: DNA replication initiation, activation of MAPKK activity, regulation of cell migration and cell cycle process.

But when performing a GO enrichment analysis for each subgroup separately (3D-1 and 3D-2), cells appeared to display a distinct functional profile. On which in the 3D-1 subgroup, the top upregulated GO terms where associated cellular signalling activities, cell-cell signalling, cytokine mediated signalling, ECM disassembly and collagen metabolic processes, whilst in the 3D-2 subgroup the top upregulated cellular process terms involved zinc ion homeostasis, detoxification of inorganic compound, response to zinc ions and cellular transition metal ion homeostasis. Also, by comparing enriched downregulated GO cellular processes, 3D-1 subgroup showed downregulation of processes involving: cell cycle process, mitotic cell cycle, cell division and nuclear cell division. Interestingly 3D-2 subgroup showed downregulation of cellular process terms related to cell- cell adhesion, biologic adhesion, cell adhesion, regulation of collagen biosynthetic process and regulation of collagen metabolic process. As an additional approach to clarify the differences between 3D-1 and 3D-2 subgroups we utilised Venn diagram overlapping analysis to query GO functional profile of DEGs that were exclusively expressed in each subgroup. The results also confirmed the above analysis and revealed similar enriched GO cellular process terms.

Then the top 10 regulated DEGs with the highest log2 fold change were also defined for the overall data set (3D-All) and for the subgroups (3D-1 and 3D-2). Investigation of these lists revealed an upregulation of many genes that belong to the metallothionine gene family (MT1G, MT1H, MT1M, MT1F and MT1JP) in addition to heat shock protein (HSP70 A family) encoding genes (HSPA7 and HSPA6). These genes were among the highest top upregulated genes in the 3D-2 subgroup but not the 3D-1. This is rather an interesting finding, because these two gene families are stress associated genes that are induced in response to environmental or physiological stress (Ponomarenko et al., 2013, Lynes et al., 2014).

The metallothionines are small metal binding cysteine-rich multifunctional proteins that participate in an array of protective stress responses. They can be induced in response to a large number of molecules and stress conditions, such as metal ions, oxidative stress, cytokines and growth factors, radiation and many other metalloproteins (Ziller and Fraissinet-Tachet, 2018). Therefore, they have been implicated in many interconnected cellular processes. For example: detoxification of heavy metals. In addition to that they play a central role in regulating cellular zinc and copper levels and thus maintaining cellular redox level. They have also demonstrated strong cytoprotective antioxidant activities by acting as potent electrophilic scavengers of free radical (Ruttkay-Nedecky et al., 2013). Metallothionine have the ability to capture hydroxyl radicals 300 times greater than glutathione (Inoue et al., 2009). Moreover, they have been involved in inflammatory response, cell proliferation and differentiation and drug resistance (Inoue et al., 2009, Vignesh and Deepe, 2017, Takahashi, 2012). They are also involved in gene regulation of metalloproteins activities by metal exchanges acting as a post translational modulator (Ziller and Fraissinet-Tachet, 2018). These results are in line with GO enrichment analysis that showed upregulation of terms related to zinc ion homeostasis and detoxification because metallothionines are known regulators of zinc homeostasis acting as zinc storing proteins (Beyersmann, 2002).

With regards to heat shock proteins, they are a set of evolutionary conserved proteins that are induced as a results of cellular stress such as: heat stress, heavy metals, toxins, oxidative stress and hypoxia (Shaik et al., 2017). The HSP70 is an inducible a member of the 70 KDa family and are part of the heat shock response that the cell trigger to reverse the damage caused by stressful conditions. They assume their cytoprotective role by either acting as chaperones to repair denatured and misfolded proteins and as anti-apoptotic molecules and also by regulating signal transduction (Simone et al., 2010).

On the other hand, the examination of the highest upregulated DEGs in the 3D-1 subgroup revealed a distinct list of genes that were mainly associated with signalling or inflammatory response and matrix deposition. For example, IL24, CHI3L1 DPT and ANGPTL4. The IL24 gene encodes for interleukin 24, a pleotropic cytokine of the IL10 family. This cytokine has been demonstrated to play several roles as an immunoregulatory, anti-tumour cytokine and it was also involved in promoting wound healing and tissue remodelling (Persaud et al., 2016). Another highly upregulated DEG is CHI3L1 which encodes for the glycoprotein YKL-40, a secreted family protein that has been implicated in tissue remodelling, angiogenesis, and cell survival (Hoover et al., 2013). Dermatopontin (DPT) is another gene that belong to this list, which encodes for a non-collagenous ECM protein that is involved in multiple activities such as: cell adhesion, modification of newly formed collagen fibrils and have been shown to interact and modify TGF-β bioactivity. (Okamoto and Fujiwara, 2006, Kato et al., 2011). In addition to that other studies have demonstrated DPT involvement in improving wound healing (Kato et al., 2011, Krishnaswamy et al., 2014). Another interesting DEGs in this list was the angiopoietin-like 4 (ANGPTL4) gene which encodes for a glycosylated protein that belongs to a superfamily of secreted proteins that regulate and promote angiogenesis (Mousavizadeh et al., 2016). These results also correlate with GO enrichment analysis that showed that top cellular processes in the 3D-2 subgroup were associated with cell signalling and cytokine mediated signalling.

Taking together, these findings confirms a variable response of cells between the subgroups. It also suggests that cells on the DC tracheal scaffolds, especially on the 3D-2 DC scaffolds may be experiencing a higher cellular stress evidenced by the upregulation of several stress associated genes. Indeed, in a separate analysis I compared differential expression between 3D-2 and 3D-1 subgroup, those genes showed 7-8 times fold upregulation in comparison to 3D-1 subgroup. This is interesting as several studies have found that the synthesis of metallothionines tend to increase serval folds especially in response to oxidative stress (Sato and Bremner, 1993). The upregulation of heat shock proteins and metallothionines genes as well as enrichment of cellular process related to zinc ion regulation and detoxification. And given that metal catalysts are involved in redox cycling, the data might suggest that cells were experiencing oxidative stress. Moreover, studies showed that zinc hinders oxidative process by inducing the expression of metallothionines (Jarosz et al., 2017). Indeed, it is expected that the cells will face an initial culture shock and will activate cytoprotective mechanisms in an attempt to adapt to the new ECM microenvironment and to the culture conditions. But it is difficult to rule out a specific cause of stress in our cells due to the multivariable associated with both ECM scaffolds characteristics as well as the cell culture conditions.

The data also showed that 3D-2 scaffolds appear to experience higher stress than cells in the 3D-1 subgroup. But when correlating this to our previous findings in chapter 4 on which the cells on 3D-2 displayed a round morphology indicating probably less focal adhesion points compared to the spread morphology of cells on the 3D-1 subgroup. Collectively these findings suggest that 3D-1 matrix i.e. DC scaffolds with intact adventitial layer might be providing a favourable less stressful niche for cells compared to scaffolds lacking it. However future work with more samples is needed to confirm this prediction.

I extended the analyses described above by using a complementary Ingenuity pathway (IPA) enrichment and comparative analysis as another tool to characterise the transcriptome profile of UC-MSCs seeded on tracheal DC scaffolds. These analyses identified the major biological functions activated, upstream regulators and enriched canonical pathways representing our DEGs.

The results demonstrated an enrichment and activation of several biological functions such as: cellular homeostasis, chemotaxis, homing of cells, leukocytes migration, angiogenesis, activation, and differentiation of connective tissue cells. Also, the comparative assessment of the subgroups 3D-1 and 3D-2, revealed an overlap in most of the biological functions and showed similar enriched upstream regulators and canonical pathways. Interestingly an activation of distinct biological functions was observed between the 3D-1 and 3D-2 subgroups. On which the activation of chemotaxis, homing, leukocytes migrations and movement functions were only observed in the 3D-1 subgroup. Whilst, in 3D-2 subgroup a unique activation of functions like autophagy and metabolism of reactive oxygen species was detected. This finding lends support to our prediction that cells on 3D-2 matrix show higher signs of cellular stress, in addition to that autophagy is considered another cellular stress adaptation mechanism (Simone et al., 2010).

The top significant activated upstream regulators in our data set have been found sharing a common role in controlling genes involved in proinflammatory response and immune cells trafficking. These included: TNF, IL1B, RELA, NFκB complex, INFG, INFA2. For example, TNF (tumour necrosis factor) is considered a master proinflammatory cytokine that has been shown to regulate many signalling pathways and has a wide range of downstream effects mediating inflammatory response (Jonathan et al., 2019, Aggarwal, 2003).

Other upstream regulators identified were, NFκB and RELA which are members of the inducible nuclear factor κB family that regulate transcription of a vast array of genes involved in regulating cell survival, immune and inflammatory responses (Liu et al., 2017, Martindale and Holbrook, 2002). The activities include: increasing production of proinflammatory cytokines like (IL1A, IL1B, IL6, IL8, IL17), chemokines (CXCL1, CCL2, CCL5) and adhesion molecules (ICAM-1, VCAM-1, MMP, selectin). Moreover, they also regulate genes involved in anti-apoptotic, cell proliferation and differentiation (Liu et al., 2017). In addition to that , NUPR1 have also been identified as an upstream regulator, NUPR1 is a pleotropic stress gene that is involved in cytoprotective autophagy, apoptosis and have been found to mediate pro-survival effect on MSCs (Matsunaga et al., 2019).

IPA analysis showed a series of enriched signalling pathways, for example: Dendritic cell maturation, Oncastatin M signalling, Role of IL17F in allergic inflammatory airway disease, P38 MAPK signalling, IL6 signalling, IL8 signalling, Interferon signalling pathway. Most of the activated pathways were associated with inflammatory responses. For example, IL17F in allergic inflammatory airway disease signalling pathway induces the expression of many pro-inflammatory and neutrophil mobilisation cytokines and chemokines (Hizawa et al., 2006). The interleukin (IL17F) shares strong homology, expression, signalling and functions to IL17. (Chang and Dong, 2009). Also, the P38 MAPK signalling pathway (P38 mitogen activated protein kinase) is considered a key regulator of proinflammatory cytokines biosynthesis and recruitment of leukocytes to sites of inflammations (Herlaar and Brown, 1999, Cuenda and Rousseau, 2007). Another enriched pathway is Oncastatin M signalling pathway. This pathway has been associated with multiple biological and cellular processes including growth, differentiation, inflammation, and angiogenesis (Dey et al., 2013, Lee et al., 2007). It has been found to play an anti-fibrotic effect by attenuating TGFβ activity. In addition to that it have been associated with repair and remodelling during pathological conditions like arthritis (Dey et al., 2013). Interestingly the analysis has demonstrated activation of EIF2 signalling pathway only in the 3D-2 subgroup and not 3D-1. This pathway regulate genes that are involved in

alleviating cellular stress, regulating redox status or alternatively inducing apoptosis (Wek et al., 2006).

Taken as a whole, the IPA analysis predicted activation of many functions related mainly to the enhancement of proinflammatory responses, for example activation and recruitment of mononuclear cells and leukocytes, chemotaxis and also activation of endogenous tissue repair mechanisms like angiogenesis. This proinflammatory activity might have a beneficial effect with respect to MSCs seeded tissue engineered implants. Indeed, the initial proinflammatory response is required for the onset of a proper wound healing and tissue repair (Hübner et al., 1996, Crupi et al., 2015). Moreover, creating an inflammatory environment will allow the close interactions between MSCs and other immune effectors cells. Many reports have demonstrated that MSCs are not immunoregulatory by default on which they require activation (licensing) with proinflammatory signals to activate their immunoregulatory functions ,hence facilitating the switching of the immune response to an anti-inflammatory pro-healing response (Bernardo and Fibbe, 2013, Krampera, 2011). It is worth noting that there is complex cross talk between MSCs, scaffolds microenvironment and immune effector cells as well as many variables that orchestrate the sequence of events that will determine implant engraftment or rejection (Crupi et al., 2015). Furthermore, the mechanisms that governs the pro or anti-inflammatory switch are not fully elucidated. This underlines the importance of more research work to correlate these *in vitro* findings to *in vivo* studies to understand these interactions and derive conclusions with regards to the role the cells play.

Then the second aim of this study focused in exploring the differential expression level of specific gene families associated with MSCs therapeutic outcomes. Besides their multilineage differentiation potentials, the therapeutic benefits of MSCs is largely attributed to their paracrine effects. MSCs secrete many known mediators of tissue repair, healing and regeneration, these include growth factors, cytokines and chemokines. These factors have been found to promote several key biological functions, such as modulating immune response and reducing inflammation (Aggarwal and Pittenger, 2005, English, 2013, Klinker and Wei, 2015), inducing cell migration, proliferation and differentiation, ECM

formation and remodeling (Kuchroo et al., 2015), promotion of angiogenesis (Rehman et al., 2004, Beckermann et al., 2008) and anti-fibrotic and anti-scaring effects (Bai et al., 2016, da Silva Meirelles et al., 2009).

In this regard, the present study investigated the presence of known bioactive molecules that have been compiled from literature and are relevant to tissue engineering application. Among the significantly regulated genes, we investigated four general classes of bioactive factors : (1) factors associated with ECM remodeling, (2) chemokines and interleukins, (3) Growth factors, (4) Adhesion and other paracrine factors. Overall the study revealed an upregulation of many DEGs in those gene families. Many of these differentially regulated genes were associated with inflammation and immune regulation.

It is worth noting that the discussion of all regulated genes and their associated effects is beyond the scope of this thesis, thus, the discussion will give an overall snapshot of the most important gene families and discuses where appropriate selected genes of known role in mediating MSCs therapeutic effects.

The study demonstrated the upregulation of genes associated with many key regulators of ECM remodeling. These included matrix metalloproteinases such as (MMP1,MMP3,MMP10,MMP14), adamalysins like (ADAMTS5) and metalloproteinases inhibiters such as, (TIMP1). They are important player during tissue repair, wound healing, inflammation and regeneration. Matrix metalloproteinases (MMPs) are a major family of proteolytic enzymes that selectively digest ECM components as well as regulating non-ECM molecules like growth factors, chemokines and a variety of enzymes (Stamenkovic, 2003). They are involved in a wide variety of bioprocesses such as digestion of ECM proteins and thus facilitating cellular adhesion, migration, penetration and triggering re-epithelization (Streuli, 1999). Moreover, they have been shown to regulate cell-matrix signaling and cell-cell interaction by mediating the cleavage of several cytokines, chemokines and receptors (Caley et al., 2015, Gill and Parks, 2008). In addition to that they are involved in regulating angiogenesis by activation of proangiogenic cytokines like VEGF and TNFα (Caley et al., 2015,

Almalki and Agrawal, 2016). MMPs degradation of ECM will also expose new recognition sites that can trigger a variety of cellular signals (Streuli, 1999).

Furthermore, the ECM degradation products termed (matricrytpins) are potent bioactive fragments that have been shown to influence cellular behavior during ECM remodeling (Brown and Badylak, 2014). In fact, the release of matricryptic peptides has been shown to enhance migration and proliferation rates of endothelial cells and perivascular stem cells as well as supporting polarization of macrophages to the M2 pro-remodeling phenotype (Londono et al., 2017, Reing et al., 2010). With regard to the Adamalysins, (ADAMS & ADAMTS) they are another family of proteinases and their main function is the cleavage of extracellular domain of cytokines, growth factors, receptors and adhesion molecules by a process termed ectodomain shedding (Bonnans et al., 2014, Gillian, 2008). The activities of MMPS and Adamalysins are tightly controlled by metalloproteinases inhibitors (TIMPs), TIMPs inhibit MMPS in a 1:1 inhibitor to enzyme ratio (Gill and Parks, 2008). Hence the balance of activities of these factors will help exerting anti-fibrotic effects preventing excessive undesired collagen deposition while permitting cells penetration and migration and so promoting tissue repair (Formigli et al., 2015).

When examining ECM deposition, the data show a downregulation of Collagen-I expression (COL1A1), while an upregulation of COL6A1, COL6A2, COL18A1 and DPT. When considering COL6A2 and COL6A2, they encode for collagen VI which play an important role in maintaining ECM integrity by forming a unique microfibrillar network that support cell attachment. It acts as both structural and signaling molecule and regulate fibrogenesis by modulating cell-cell interactions and stimulate MSCs proliferation and prevent apoptosis (Sun and Karsdal, 2016). Also, the upregulated gene COL18A1 encodes for the heparan sulphate proteoglycan which is necessary for the maintenance of basement membrane integrity, moreover it is implicated in regulating cell survival, stem and progenitor cells maintenance differentiation and in inflammation (Heljasvaara et al., 2017). The ECM secreted by MSCs have been found by several studies to play several roles in promoting tissue regeneration by creating a microenvironment that

enhance the cell survival capacity and providing a niche that support their functions (Xinyu et al., 2018).

Then I compared differential gene expression of this gene family between 3D-1 and 3D-2 subgroup, the results showed a great overlap in expression but remarkably, 3D-1 subgroups demonstrated the expression of more genes associated with ECM deposition and remodeling. These genes included: Elastin, COL10A1, COL15A1, COL14, COL24, TIMP2, TIMP3, ADAM8, MMP2, MMP8, MMP12 and MMP13.

While investigating the chemokines and interleukins gene family, the study also revealed the upregulation of many chemokines and interleukins. These factors play vital roles in mediating MSCs therapeutic effects by regulating inflammation, cell differentiation, angiogenesis and migration of other immune effector cells. Chemokines mediate the interaction of MSCs with other immunocompetent cells by recruiting cells in close proximity to MSCs, hence providing a direct cell to cell contact enabling the paracrine immunoregulatory cross talk that could direct the inflammatory response towards healing and tissue repair (Kyurkchiev et al., 2014). The target cells include monocytes, neutrophils, natural killer (NK) cells, dendritic cell (DC), T and B lymphocytes, hematopoietic and endothelial progenitor cells (da Silva Meirelles et al., 2009).

The data showed upregulation of CCL2, CCL7, CCL20, CXCL2, CXCL3, CXCL5 and CXCL8. One of the important chemokines upregulated was CCL2 or alternatively termed monocyte chemoattractant protein-1 (MCP-1). This is a key regulator of monocytes-macrophage system recruitment (Deshmane et al., 2009). It also plays a role in immunomodulation by enhancing apoptosis of T lymphocytes, the apoptotic cells stimulate secretion of TGFβ by macrophages and this supports the generation of regulatory T cells (Tregs) (Akiyama et al., 2012). It also modulates switching T helper cell immune response to Th2 (Long et al., 2000). Moreover, this chemokine mediates MSCs migration to site of inflammation and tissue damage in an autocrine manner (Boomsma and Geenen, 2012). In addition to that CCL2, CCL5, CXCL2, CXCL5, CXCL8 are known as potent promotors of angiogenesis (El Omar et al., 2014, Salcedo et al., 2000).

With regards to interleukins, the study demonstrated an upregulation of many genes encoding interleukins such as (IL1A, IL1B, IL1RN, IL6, IL11, IL15, IL23, IL24, IL32, IL33, IL34 and IL4I1). Many of these genes encode for cytokines that play important roles in regulating the inflammatory immune response. For example: IL6 encodes for interleukin 6 which is pleotropic cytokine that is considered one of the basic cytokines responsible for the immunoregulatory effects of MSCs (Park et al., 2009). It mediates many processes such as, cell survival, apoptosis, proliferation and inflammation. Although it known for its proinflammatory response, a wealth of data has piled up about its function as an anti-inflammatory cytokine (Kyurkchiev et al., 2014, Scheller et al., 2011). For example, it has been found to induce the formation of Th17 cells in the presence of TGFβ and on the other hand it directly inhibits this by inducing the generation of CD8+ FoxP3+ T lymphocytes (Nakagawa et al., 2010). Also, in conjunction with IL1 and TNFα it induces recruitment of neutrophils and the expression of adhesion molecules and also induces the switch from neutrophil to macrophage induced inflammation (Xing et al., 1998).

It was also found that IL6 acts in a complex interaction with IL10 and prostaglandin E2 (PGE2) to inhibit dendritic cell (DC) maturation, and stimulate the formation of tolerogenic DC as well as stimulation of Treg cells (Kyurkchiev et al., 2014). It has also been implicated in the polarization of monocytes towards the desired anti-inflammatory type M2 macrophages in conjunction with PGE2 and IDO (Bernardo and Fibbe, 2013). Also, the results showed upregulation of interleukin 4 induced gene 1 (IL4I1). IL4I1 possess an anti-inflammatory properties by inhibiting proliferation of T cells and has been found to regulate the polarization of macrophages to M2 type macrophages (Yue et al., 2015).

In the context of tissue engineered implants, macrophage polarization has been suggested to be a major determinants of host responses and clinical outcome on which polarization towards an anti-inflammatory M2 type macrophages have been associated with supporting constructive remodeling of the implants (Brown and Badylak, 2014, Brown et al., 2012, Londono et al., 2017).

Another interesting upregulated gene was IL1RN (interleukin 1 receptor antagonist) that function as a competitive inhibitor of the proinflammatory interleukin IL1-A and IL1-B. Whilst IL1A and IL1B might be necessary for the initial stage of tissue repair by mediating inflammatory response, IL1RN is a natural inhibitor to control their activities and hence mediating immunoregulation effect (Jing et al., 2018). Also, it has been found to mediate an anti-inflammatory antifibrotic effects of MSCs in a lung injury model (Ortiz et al., 2007). Again, when comparing gene expression in this gene family between 3D-1 and 3D-2 subgroup, 3D-1 subgroup appears to upregulate more genes in this category as well. These included: CCL2, CCL7, CCL20, CxCL1, CXCL6, IL19, IL34, LIF and IL4R.

With regards to investigating growth factors gene family and other supportive molecules, we report downregulation of BMP4, EGF, FGF5. The data also showed an upregulation of many genes these included: TGFB, GDF15, FGF18, IGFBP4, IGFBP7, VEGFA, VEGFB, CSF2, CSF3, ICAM1, ICAM2, VCAM1, STC1, PTGES (PGE2), ANGPTL4, ADM and BCL2A1. Many of these genes encode for factors that are known as important mediators of MSCs therapeutic activities.

Among this list we note the upregulation of TGFB that encodes for transforming Growth factor beta (TGFβ). This is one of the key immunomodulatory cytokines that is constitutively secreted by MSCs. It is a pleiotropic cytokine with broad immunoregulatory properties and it plays a central role orchestrating the induction and resolution of the inflammatory response as well as induction of immune tolerance (Wahl et al., 2004, Johnston et al., 2016). It has an extensive functions being an instrumental cytokine in every immune system compartment

(Li et al., 2006) for example: it mediates inhibition of T cell proliferation, induction of Treg generation and mediate also suppression of NK cell proliferation (Kyurkchiev et al., 2014).

Another important unregulated transcript is VEGFA and B both encode for vascular endothelial growth factor VEGF. VEGF are principal mediators of angiogenesis as they mediate endothelial cells migration, proliferation, differentiation and survival (Bai et al., 2016). In addition to that, they are involved in mediating recruitment of inflammatory cells and priming of proinflammatory T lymphocytes.

Another upregulated transcript includes the colony stimulating factor encoding genes: CSF2 and CSF3 or alternatively termed GM-CSF (granulocyte-macrophage colony stimulating factor) and G-CSF (Granulocyte colony stimulating factor). They are paracrine growth factor secreted by MSCs that stimulate proliferation and maturation of monocyte-macrophages and granulocytes. In addition to that they are involved in enhancing mobilization of bone marrow MSCs (Kim et al., 2019). These are all important cell population that mediate tissue repair during inflammatory response.

Among the most important trophic factors produced by MSCs that have been found upregulated in the data set was the PTGES gene which encodes for prostaglandin E2 (PGE2). It is a major factor mediating the immunomodulatory competence of MSCs and it acts in both paracrine and autocrine fashion. It affects the activation status, differentiation functions of immune cells. For example, it can inhibit maturation of DC as well as shifting the balance between Th1 and Th2 and also supress NK cells in conjunction with TGFβ (Ma et al., 2013). It is also one of the most potent activators of anti-inflammatory M2 macrophages and hence help in the resolution of inflammation and promotion of constructive remodelling (Bartosh et al., 2013).

Also, the upregulation of ICAM1/ICAM2 genes which encode for the intracellular adhesion molecule-1 and 2 and VCAM-1 encoding for vascular cell adhesion molecule 1. Both play a critical role in MSCs mediated immunosuppression. They

play several functions in facilitating, cell to cell adhesion, transmigration and thus supporting interaction of MSCs with other immune cell (Ma et al., 2013). Another upregulated transcript was ADM that encodes for adrenomedullin that is an antiapoptotic factor that is also involved in promoting angiogenesis and with a possible role as an anti-fibrotic factor (Si et al., 2018, da Silva Meirelles et al., 2009). Then like previous finding, when we attempted to inspect for differences between cells responses on 3D-1 and 3D-2 subgroup in this gene family. Despite the big overlap between both subgroups, cells on 3D-1 subgroup also were found to upregulate more genes encoding for more bioactive molecules. These included: BMP1, BMP2, GDNF, IGF2, TGFBI, FGF11.

Collectively these data provided an evidence that UC-MSCs seeded on DC scaffolds upregulated transcript of many bioactive factors that may play major roles in mediating the therapeutic potentials of MSCs. These factors have diverse actions that included ECM remodeling, enhancing angiogenesis, antifibrosis, chemoattraction of other immune cells, immunomodulatory abilities of innate and adaptive immune system components. Encompassing the guidance towards the anti-inflammatory M2 macrophages, suppression of cytotoxic T cells and generation of Treg and T helper cells, inhibition of DC and NK cells. These are all favorable therapeutic effects that may contribute to the creation of a desirable microenvironment for promoting tissue repair and regeneration especially in the context of tissue engineering applications. Again, more research is required to correlate to *in vivo* models.

These data also substantiate the studies that showed that incorporation of MSCs on three dimensional (3D) substrates improves their functionalities as opposed to two dimensional (2D) cultures (Jing et al., 2018, Kusuma et al., 2017). In fact, the use of 3D scaffolds has been one of the approaches used to prime MSCs to enhance their efficacy and modulate their secretome toward a more suitable phenotype for therapeutic applications (Cunningham et al., 2018).

Of a particular interest was the notion that cells on 3D-1 appeared to upregulate more trophic factors in comparison to 3D-2 subgroup. These data along with the previous results that demonstrated higher stress on 3D-2 subgroup, suggests that maintaining the adventitial layer during decellularisation might provide a favorable niche for seeding cells on tracheal scaffolds and appear to support higher MSCs paracrine activities.

However future work needs to further investigate the differences between both matrices. Again, these findings have emphasised the crucial role of ECM biochemical and biophysical cues in directing cellular behavior. Of these cues many have been investigated such as substrate stiffness (Engler et al., 2006), topography (Wu et al., 2014), mechanical cues (De Lisio et al., 2014), ligand spatial context (Frith et al., 2012) and composition (Kusuma et al., 2017). One interesting study have provided glimpse of how the expression of some key paracrine factors (VEGF, TGFB, IL6) were varied between MSCs cultured on collagen and laminin variable substrates (De Lisio et al., 2014).
It is worth noting that the sample size especially the 3D-1 subgroup was a major study limitation due to the limited supply of human tracheal scaffolds and future work should aim to analyse more samples to confirm the findings. In addition to that, in the discussion above I have selected several gene families that were associated with MSCs therapeutic effects, however a full list of genes will be available upon request. Moreover, confirmatory proteomic and secretome analysis are warranted for future work. This study also did not address the cells differentiation potentials because it was not the scope of this work, although an overall general screening revealed the absence of known osteogenic (ALP, RUNX2, COL1A1, OCN) chondrogenic (ACAN,SOX9) and adiopogenic markers (PPARG), suggesting that *in vitro* differentiation is not a phenomenon which occurs during the early stages of MSC: scaffold interaction. However future work should aim to investigate for early differentiation markers with extension of cell cultivation time to confirm this.

6.4 Conclusion

To the best of our knowledge this study is the first study in tracheal bioengineering to address differential gene expression of MSCs seeded on decellularised tracheal scaffolds. The study has provided a comprehensive *in vitro* transcriptomic profile of UC-MSCs seeded on DC tracheal scaffolds. Moreover, it had demonstrated that seeded UC-MSCs have upregulated many genes associated with their paracrine therapeutic effects. Hence, providing evidence to support the paradigm of MSCs ability to create a pro-healing immunoregulatory environment that could support tissue repair and remodeling. The study also revealed an overall upregulation of many stress associated genes. In addition to that it has also suggested that the maintenance of the adventitial layer on DC scaffolds might provide a better niche for seeding cells as it was characterised by less stress signals and active upregulation of more paracrine bioactive molecules. This information shed lights to the importance of focusing on the manufacturing process in terms of scaffolds characterization and how it affects cells seeding as well as culture conditions to alleviate causes of cellular stress that might affect cellular functions.

The study has also provided lists of candidate genes and pathways related to inflammatory response, immunomodulation, wound healing and proangiogenic responses for further future studies to confirm their functions. These preliminary results have provided important insights into the role of MSCs in tracheal bioengineering and have expanded our understanding of the interactions between MSC and decellularised scaffolds. Extensive research is still required from basic *in vitro* studies parallel to thoughtful design of systematic preclinical animal *in vivo* studies in order to generate useful data and develop an understanding of the role of these cells in promoting engineered tissue repair and remodelling.

7 Final discussion, summery and conclusion

This thesis was undertaken for the sake of the development and characterisation of bioengineered MSCs-seeded decellularised scaffolds for long segmental tracheal defects. It has addressed and investigated three main research gaps: firstly, the evaluation of the decellularisation process efficiency with regards to cellular clearance, structural integrity, extracellular matrix components and mechanical properties of the generated tracheal grafts. We specifically focused on exploring and introducing better representative measures suitable for evaluating the mechanical properties of DC tracheal scaffolds. Secondly, we focused on improving passive MSC cell seeding efficiency, and then we explored cell-scaffolds interactions in terms of survival, attachment, proliferation, infiltration, and spatial distribution. Finally, we investigated the rationale of seeding MSCs onto DC tracheal scaffold for airway tissue engineering. This was achieved through examination of the *in vitro* differential gene expression of seeded MSCs seeded using RNA sequencing. Our results will be herein summarised highlighting important findings, areas of particular interest and limitations. All will be further discussed with perceived future directions that will help improvement of this tissue engineering approach.

7.1 Evaluation of the biochemical and mechanical properties of VAD decellularised tracheal scaffolds.

The target aim of any decellularisation protocol is to achieve efficient removal of cellular materials without jeopardising the structural, composition, and mechanical properties of the generated scaffolds. Therefore, our first part of this thesis aimed at providing a comprehensive structural and mechanical evaluation of tracheal scaffolds following VAD decellularisation protocol. VAD decellularisation protocol is a modified detergent enzymatic (DEM) protocol that incorporates the use of intermittent vacuum (negative pressure) during processing to expedite the processing time from more than 3 weeks to 9 days making it more clinically relevant (Lange et al., 2015).

This protocol is employed by our team for the generation of decellularised tracheal scaffolds for clinical use. Results revealed that the protocol was able to

preserve the overall macroscopic and microscopic structure of native trachea. With regards to decellularisation efficiency, microscopically, cellular clearance was evident by complete removal of the mucosal layer, yet residual nuclear materials were still seen in the submucosal layer and hyaline cartilage contrary to findings reported by Lange and colleagues showing a complete cellular clearance (Lange et al., 2015).My results are in keeping with previous studies of trachea decellularisation with similar detergent enzymatic/ no vacuum based protocols (Conconi et al., 2005, Macchiarini et al., 2008, Go et al., Haykal et al., 2012, Partington et al., 2013) where complete removal of chondrocytes was not achieved in the hyaline cartilage. But the results of total DNA level revealed a significant reduction of DNA post decellularisation in both human and porcine samples, where only human samples shows a DNA level of< 50ng/mg meeting the proposed minimal acceptable DNA level of DC tissues (Crapo et al., 2011).

Clinical and preclinical studies of decellularised tracheal scaffolds have demonstrated a minimal immune response to constructs despite presence of residual chondrocytes in the cartilage layer (Macchiarini et al., 2008, Hamilton et al., 2015, Gonfiotti et al., 2014, Elliott et al., 2012). It was suggested that the physical isolation of these cells within the dense avascular cartilage matrix helped evade immune cells (Benders et al., 2013). Whilst the VAD protocol might have expedited cellular clearance from outer layers, it is unlikely that the applied vacuum will lead to complete chondrocyte clearance due to the dense compact hyaline cartilage nature. That said owing to the nature of the trachea, achieving complete clearance within the cartilage might not be necessary, but it is unclear if these residual nuclear materials might cause a risk following implantation during scaffold degradation and remodelling. Therefore, it is necessary to inspect the long-term effect of these residual nuclear materials within the cartilage and future work should aim to establish a minimal residual DNA level specific for tracheal tissue in relevant *in vivo* models.

Our study also showed the presence of residual nuclear materials smeared within the submucosal layer. This observation suggests that the VAD protocol needs to be further optimised. A possible direction to solve this can be increasing washing steps or incorporating an extra DNase treatment step.

Our results also showed that the total level of collagen, fibronectin, and GAGs post VAD were maintained despite reduced expression of laminin, elastin, and collagen IV in both human and porcine samples. These are important components of the basement membrane and their disruption might interfere with epithelial cells attachment. Indeed, similar findings had been reported in another study that compared VAD to DEM protocol (Butler et al., 2017b). In fact, other studies have also demonstrated that the choice of detergent can affect the integrity of the basement membrane (Faulk et al., 2014). In addition to that, the applied physical pressure may have also contributed to this. Taken as a whole our results warrant the need to further optimise the VAD protocol and the utility of vacuum/no vacuum approach should be further investigated.

Because the main scope of this part of the study was to evaluate structural integrity of the decellularised scaffolds, we did not screen for bioactive growth factor retention or for the clearance of MHC antigens. However, these have been explored in other studies (Lange et al., 2015). That said, the ECM is a complex substrate and in order to provide comprehensive assessment of its components, future work should aim to utilise other techniques like proteomics analysis.

As previously described the trachea plays an important structural role maintaining the air way open despite the intrathoracic pressure during breathing. Preclinical and clinical studies in tracheal bioengineering have reported suboptimal mechanical properties leading to collapse or stenosis (Chiang et al., 2016).Therefore we focused on the mechanical evaluation of the generated DC scaffolds. Initially we conducted the conventional uniaxial tensile test that showed no significant difference between native and DC scaffolds. Yet it was difficult to compare our results with other studies because there was huge variations observed in the reported literature (Aoki and Moriya, 2018). These variations were mainly attributed to the differences in the experimental setups such as variations in: sample sizes, gripping techniques, loading protocols and data reporting system. The lack of a standardised protocol for conducting uniaxial tensile analysis in tracheal bioengineering is an identified limitation and warrants the need to standardise it to allow reproducible analysis and comparison among

studies. Although tensile test is helpful in reflecting the overall tensile strength of the scaffolds and its failure mechanics, it is unable to reflect the complex nonlinear mechanical properties of tracheal tissues and in particular cartilaginous rings (Boazak and Auguste, 2018). Therefore, there is an identified need to improve biomechanical assessment tools of decellularised tracheal scaffolds seeking better measures that can predict structural and mechanical stability of tissues post decellularisation.

The highlight of our work in this part of the thesis, is that we reported the first study that measured the viscoelastic mechanical properties of tracheal cartilage pre and post decellularisation using DMA analysis. Viscoelastic properties is a unique intrinsic mechanical feature of the cartilage that gives it its resilient properties allowing it to resist deformation in spite of changes of intrathoracic pressure which occur during respiration. We utilised DMA analysis for this purpose. Our results showed no significant difference between native and DC scaffolds, as well as demonstrating the elastomeric nature of the tissue being highly resilient with excellent shock absorbent properties.

DMA analysis offers many advantages which permits it to be used for quality control testing of scaffolds during the manufacturing process, such as: it allows non-destructive testing of the samples, it uses a relatively small size sample. Furthermore, physiological loading stresses can be easily simulated using multiple and simple loading configuration (bending, stretching, compression). It can also be tuned to test a sample over a wide range of stresses spanning over sub-failure and failure stresses. Moreover, the data generated can be used to aid computer simulations like Finite Element Analysis (FEA) or Computer Fluid Dynamics (CFD) modelling of trachea which can be later used to create models predicting tracheal collapse (Barnes et al., 2015).

Our work emphasizes the importance of developing an understanding of the tissue mechanical characteristics and the mechanical requirement that are essential for the normal functioning of the tissue in question. This understanding will aid selection of more reliable measures for assessing its function.

Several limitations to our study need to be acknowledged. Firstly, it was not possible to test the mechanical properties of the trachealis muscle or the annular ligaments because of the nature of porcine trachea having a very small trachealis muscle and annular ligaments. In addition to that, the human samples provided for the study were small and limited so only tracheal cartilage could be assessed. In order to perform a comprehensive mechanical analysis of the tracheal scaffold, we suggest that a minimum panel for mechanical testing to include: uniaxial or biaxial tensile test for the trachealis muscle and annular ligaments and viscoelastic properties of the cartilaginous rings. Furthermore, our analysis only provided information about the initial functional status of the scaffolds prior to implantation and does not predict the durability of the scaffolds. In order to assess scaffold durability, future work should aim to investigate several parameters like scaffold degradation kinetics (Gilbert et al., 2007), and determining what drives the constructive remodelling process to achieve a synchronised matrix regeneration to balance scaffold degradation.

While mechanical characterisation of scaffolds has been mostly done pre-implantation and at sacrifice an important direction in the field for future studies is the development of methods that can assess scaffold structural and mechanical properties *in vivo*. For example, development of assays to detect biological markers of tissue metabolism and degradation (Lohmander et al., 1995), other techniques like CT scanning, MRI and biomechanical probes (Butler et al., 2000) to assess tissue functions. In addition to that future work will have to utilise micromechanical assessment techniques of the generated scaffolds like atomic force microscopy (AFM) because local microscopic stiffness and topography might change as a result of decellularisation and consequently affect cellular attachment and responses (Suki, 2014).

It is also important to stress the importance of selecting relevant *in vivo* models for preclinical studies, for example differences between human and mice immune systems make studies in rodent not an ideal setup to predict immune response to engineered scaffolds (Webber et al., 2015). Recent efforts have been directed to prepare humanised mice models with an immune systems that more closely resemble that of a human to improve the prediction and investigation of body responses (Shultz et al., 2007).

7.2 Improvement of passive cell seeding efficiency and assessment, cellular attachment, infiltration, and spatial distribution.

Efficient and successful incorporation of cells within scaffolds is a central component of constructing tissue engineered grafts. A major downside in using passive cell seeding is the low cells seeding efficiency (10%-75%) and poor cell penetration (Villalona et al., 2010, Song et al., 2018). Therefore, the second part of this thesis aimed at improving passive MSC cell seeding into DC scaffolds. We hypothesised a novel modification of conventional passive seeding which we termed “partial surface dehydration” (PSD) and used this to condition the DC scaffold in to a CO_2 incubator prior to seeding. This pre-conditioning step was introduced prior to seeding in order to eliminate excess moisture from the surface of the scaffolds and enhance cells retention. Quantitative assessment of cell seeding efficiency (CSE) revealed an improved CSE up to (96.46% $\pm$1.710) compared to conventional passive seeding. Besides the high seeding efficiency reported, we report an improvement of reproducibility and consistency of results even when different, blinded operators seeded the scaffolds. Cell viability was also confirmed by quantitative live /dead staining and confocal microscopy over 14 days of culture indicating cytocompatibility of the scaffolds. In addition to that cells proliferative capacity was observed up to 7 days in culture using KI67 staining. This additional pre-conditioning step offered a simple, time and cost-effective method of attaining reproducible CSE of tracheal grafts compared to other methods that require specialised bioreactors (perfusion/ dynamic) which require lengthy culture setup and long periods and are labour-intensive. It is worth mentioning that this seeding technique was clinically translated to a GMP manufacturing process of a 40mm tissue engineered tracheal construct for one

compassionate case at Great Ormond Street Hospital manufactured at the Centre for Cell Gene and Tissue Therapeutics (CCGTT) at the Royal Free Hospital. This case had a successful clinical outcome, the patient is alive and well, with a functional airway 2 years after surgery but the case has not been reported at the request of the child's mother).

In our study we have utilised DNA quantification to measure CSE unlike most studies of tracheal bioengineering that relied mainly on histological assessment of tissue sections and where there is a rare mention of blinding of researchers to confirm the presence or absence of cells. That said it is important to mention a challenge we faced when attempting to quantitate cells attached directly to scaffolds due to the residual DNA present in the scaffolds and the non-homogeneous nature of trachea. Therefore, we used an indirect DNA quantification approach. Moreover, our study showed other limitations when using metabolic activity-based assays to quantitate cells survival and proliferation. These assays have limited linear range suitable only for lower cell numbers and thus are not suitable for tissue engineering applications that normally seed higher cell numbers. In addition to that, these assays mainly correlate to cellular activities that fluctuates with time and are affected by many other variables. This is in fact another challenge in the field, on which there is a need to develop new reliable non-invasive methods that can predict cellular survival proliferation and matrix deposition in these TE constructs.

Some of the suggested techniques include: the incorporation of the bioluminescent luciferase assay to seeded cells to detect cell viability and proliferation and matrix deposition (Close et al., 2011, Weinbaum et al., 2010), Raman spectroscopy (Owen et al., 2006) or oxygen saturation measurements (Westphal et al., 2017, Volkmer et al., 2012) and other techniques like azide proline-based method for the detection of new matrix deposition (Bardsley et al., 2017, Amgarten et al., 2015).

The most significant aspect of the work in this chapter was the development of an optical clearing technique coupled to fluorescently labelled reporter (Zs green) UC-MSCs and multiphoton imaging to visualise cell seeding distribution and

infiltration. This technique had not been reported in this setting before and the method was adapted from that used to image foetal tissues *in* vitro. Using this clearance method allowed interrogation of larger volumes of tissue and closer exploration of the spatial interactions between scaffolds and seeded cells. Dual photon microscopy allowed improved resolution of cell responses when seeded into the scaffolds compared to the classical histological sectioning or SEM imaging which provides either a two-dimensional (2D) snapshot of the constructs or topographical images that fail to reflect cells distribution and interactions. It also allows the examination of cells infiltration in the large opaque TE constructs and so improves multiphoton microscope resolution. Our study confirmed our hypothesis that the complex structure of the trachea impedes deep infiltration of cells.

The most interesting finding that emerged from these analyses was the recognition of two distinct cell morphology patterns that appeared to be related to the nature of the underlying matrix. Cells appeared to assume a fibroblastoid spread morphology when attached at the loose adventitial tracheal matrix. On the other hand, cells appeared round when attached to the dense tracheal matrix. These two distinct cell morphologies were confirmed with SEM imaging.

It is well known that the ECM composition, physical and biochemical cues interact with cells and influence cells behaviour including shape, attachment, proliferation, and fate. Since MSCs fibroblastic morphology has been found to strongly correlate with their actin cytoskeleton organization and the distribution of their focal adhesion points (Yin-Ping et al., 2016). We hypothesised that cells that displaying spindle spread morphology are cells that have found a niche to adhere better to the matrix unlike the round cells. So, we investigated the presence of known adhesive ligands of MSCs including: Collagen I, laminin, and fibronectin. Our results revealed that scaffolds with intact adventitial layer expressed collagen I, laminin, and fibronectin, but scaffolds lacking adventitial layer expressed only fibronectin. These finding support our hypothesis and suggests that cells appear to attach displaying the typical morphology when seeded on tracheal DC scaffolds where the adventitia layer is preserved. It is also possible that other factors like scaffold topography and matrix stiffness have also contributed to this

finding. These observations may also indicate changes related to cells acquiring different phenotypes. Future work should aim to confirm this and investigate further by performing comprehensive characterization of the adventitial layer in terms of composition and physical properties and cells adhesion. This is particularly important as our current protocol recommends the complete removal of the adventitial and excess tissue from the trachea during the decellularisation process. Therefore, in the light of the significance of the substrate effect on cell attachment and behaviour, it is important to characterise scaffold materials for their effects on cells to help optimise seeding protocols.

7.3 Differential gene expression analysis of MSCs seeded into DC tracheal scaffolds.

The rational of seeding MSCs in tracheal bioengineering is to benefit from their immunomodulatory capacity and their paracrine factors in creating a pro-regenerative environment that supports constructive remodelling and integration of tracheal constructs. Therefore, our final part of this thesis aimed to explore this paradigm though investigating the differential gene expression of cells post seeding into DC scaffolds compared to tissue culture plastic. For this purpose, we have utilised RNA seq analysis and confirmatory RT-PCR.

To the best of our knowledge this is the first study in tracheal bioengineering to address and provide gene expression data of MSCs seeded DC scaffolds. We have succeeded in providing a comprehensive transcriptomic portrait of MSCs seeded into DC tracheal scaffolds. Our data also provided an evidence that MSCs seeded on DC scaffolds upregulated transcripts of many bioactive paracrine factors that mediate the therapeutic potentials of MSCs. These factors as detailed in chapter 6 have diverse actions that include: ECM remodelling, enhancing angiogenesis, antifibrosis, chemoattraction, immunomodulatory abilities of innate and adaptive immune system components. All are considered favourable therapeutic effects that may contribute to the creation of a pro-healing microenvironment that might promote tissue repair and regeneration.

One interesting finding that emerged from our data was the recognition that cells seeded into scaffolds with intact adventitial layer had a distinct gene expression

pattern compared to cells seeded into scaffolds lacking the adventitial layer. Furthermore, there was an overall upregulation of many stress associated genes on the non-adventitial scaffolds whereas cells seeded into scaffolds maintaining an adventitial layer had fewer stress signals and appeared to upregulate more bioactive factors compared to cells seeded in to scaffolds lacking this layer. Future work will need to investigate this finding.

The most important limitation of this study was the small number of human tracheal scaffolds within the intact adventitial layer group. We could not control this issue as scaffolds were decellularised by the NHSBT staff and the presence or absence of the adventitial layer was random depending on the operator. Therefore, future studies should aim to repeat these analyses and confirm findings with larger sample number. Moreover, the present investigation has not considered screening for early differentiation markers of MSCs if any as the main focus was to investigate MSCs paracrine factors. Furthermore, the upregulation of stress associated genes suggests further investigation of cell scaffold interactions and culture conditions to improve the manufacturing process. Overall, this study has provided lists of candidate genes and pathways to serve as a basis for future studies. Future research should aim to utilise other techniques to explore cell secreatome like proteomic analysis to confirm findings. Extensive research is still required to correlate *in vitro* studies to preclinical animal *in vivo* studies in to develop an understanding of MSCs application in tracheal tissue engineering.

7.4 Conclusion

The work undertaken in this thesis has provided a significant contribution to the tracheal bioengineering field through improving methods of structural and mechanical evaluation of DC scaffolds, improvement of cell seeding techniques and cell scaffold evaluation. Moreover, our results have provided important insights and expanded our understanding of the cell-scaffolds interactions and the role of MSCs in tracheal bioengineering. This thesis emphasises that at this early stage of tracheal bioengineering, the race should be on comprehensive evaluations and in improvement of assessment techniques as key steps to facilitate clinical translation.

Bibliography

ADEBIYI, A. A., TASLIM, M. E. & CRAWFORD, K. D. 2011. The use of computational fluid dynamic models for the optimization of cell seeding processes. *Biomaterials,* 32**,** 8753-8770.

AGATHOS, E. A., TOMOS, P., LACHANAS, E., GAKIOPOULOU, H., PANTOPOULOU, A. & PERREA, D. 2010. Experimental Replacement of Pig Trachea with Novel Bioprosthesis from Harp Seal. *Asian Cardiovascular and Thoracic Annals,* 18**,** 557-562.

AGGARWAL, B. B. 2003. Signalling pathways of the TNF superfamily: a double-edged sword. *Nature Reviews Immunology,* 3**,** 745-756.

AGGARWAL, S. & PITTENGER, M. F. 2005. Human mesenchymal stem cells modulate allogeneic immune cell responses. *Blood,* 105**,** 1815.

AGRAWAL, H., THOLPADY, S. S., CAPITO, A. E., DRAKE, D. B. & KATZ, A. J. 2012. Macrophage phenotypes correspond with remodeling outcomes of various acellular dermal matrices %J Open Journal of Regenerative Medicine. Vol.01No.03**,** 9.

AJALLOUEIAN, F., LIM, M. L., LEMON, G., HAAG, J. C., GUSTAFSSON, Y., SJÖQVIST, S., BELTRÁN-RODRÍGUEZ, A., DEL GAUDIO, C., BAIGUERA, S., BIANCO, A., JUNGEBLUTH, P. & MACCHIARINI, P. 2014. Biomechanical and biocompatibility characteristics of electrospun polymeric tracheal scaffolds. *Biomaterials,* 35**,** 5307-5315.

AKIYAMA, K., CHEN, C., WANG, D., XU, X., QU, C., YAMAZA, T., CAI, T., CHEN, W., SUN, L. & SHI, S. 2012. Mesenchymal-stem-cell-induced immunoregulation involves FAS-ligand-/FAS-mediated T cell apoptosis. *Cell stem cell,* 10**,** 544-555.

ALLMAN, J. A., MCPHERSON, B. T., BADYLAK, F. S., MERRILL, C. L., KALLAKURY, H. B., SHEEHAN, W. C., RAEDER, W. R. & METZGER, W. D. 2001. XENOGENEIC EXTRACELLULAR MATRIX GRAFTS ELICIT A TH2-RESTRICTED IMMUNE RESPONSE1. *Transplantation,* 71**,** 1631-1640.

ALMALKI, S. G. & AGRAWAL, D. K. 2016. Effects of matrix metalloproteinases on the fate of mesenchymal stem cells. *Stem cell research & therapy,* 7**,** 129-129.

AMGARTEN, B., RAJAN, R., MARTÍNEZ-SÁEZ, N., OLIVEIRA, B. L., ALBUQUERQUE, I. S., BROOKS, R. A., REID, D. G., DUER, M. J. & BERNARDES, G. J. L. 2015. Collagen labelling with an azide-proline chemical reporter in live cells. *Chemical Communications,* 51**,** 5250-5252.

ANSARI, T., LANGE, P., SOUTHGATE, A., GRECO, K., CARVALHO, C., PARTINGTON, L., BULLOCK, A., MACNEIL, S., LOWDELL, M. W., SIBBONS, P. D. & BIRCHALL, M. A. 2017. Stem Cell-Based Tissue-Engineered Laryngeal Replacement. *Stem Cells Translational Medicine , 6 (2) pp. 677-687. (2017)*.

AOKI, F. G. & MORIYA, H. T. 2018. Mechanical Evaluation of Tracheal Grafts on Different Scales. *Artificial Organs,* 42**,** 476-483.

ARZI, B., DURAINE, G. D., LEE, C. A., HUEY, D. J., BORJESSON, D. L., MURPHY, B. G., HU, J. C. Y., BAUMGARTH, N. & ATHANASIOU, K. A.

2015. Cartilage immunoprivilege depends on donor source and lesion location. *Acta Biomaterialia,* 23**,** 72-81.

ASNAGHI, M. A., JUNGEBLUTH, P., RAIMONDI, M. T., DICKINSON, S. C., REES, L. E. N., GO, T., COGAN, T. A., DODSON, A., PARNIGOTTO, P. P., HOLLANDER, A. P., BIRCHALL, M. A., CONCONI, M. T., MACCHIARINI, P. & MANTERO, S. 2009. A double-chamber rotating bioreactor for the development of tissue-engineered hollow organs: From concept to clinical trial. *Biomaterials,* 30**,** 5260-5269.

ATHANASIOU, K. A., ESWARAMOORTHY, R., HADIDI, P. & HU, J. C. 2013. Self-Organization and the Self-Assembling Process in Tissue Engineering. *Annual Review of Biomedical Engineering,* 15**,** 115-136.

AZHIM, A., ONO, T., FUKUI, Y., MORIMOTO, Y., FURUKAWA, K. & USHIDA, T. Preparation of decellularized meniscal scaffolds using sonication treatment for tissue engineering. 2013 35th Annual International Conference of the IEEE Engineering in Medicine and Biology Society (EMBC), 3-7 July 2013 2013. 6953-6956.

BADER, A. & MACCHIARINI, P. 2010. Moving towards in situ tracheal regeneration: the bionic tissue engineered transplantation approach. *Journal of cellular and molecular medicine,* 14**,** 1877-1889.

BADYLAK, S. 2014. Decellularized Allogeneic and Xenogeneic Tissue as a Bioscaffold for Regenerative Medicine: Factors that Influence the Host Response. *Ann Biomed Eng,* 42**,** 1517-1527.

BADYLAK, S. F., FREYTES, D. O. & GILBERT, T. W. 2009. Extracellular matrix as a biological scaffold material: Structure and function. *Acta Biomaterialia,* 5**,** 1-13.

BADYLAK, S. F. & GILBERT, T. W. 2008. Immune Response to Biologic Scaffold Materials. *Seminars in immunology,* 20**,** 109-116.

BADYLAK, S. F., RECORD, R., LINDBERG, K., HODDE, J. & PARK, K. 1998. Small intestinal submucosa: a substrate for in vitro cell growth. *Journal of Biomaterials Science, Polymer Edition,* 9**,** 863-878.

BADYLAK, S. F., TAYLOR, D. & UYGUN, K. 2011. Whole-Organ Tissue Engineering: Decellularization and Recellularization of Three-Dimensional Matrix Scaffolds. *Annual Review of Biomedical Engineering,* 13**,** 27-53.

BADYLAK, S. F., TULLIUS, R., KOKINI, K., SHELBOURNE, K. D., KLOOTWYK, T., VOYTIK, S. L., KRAINE, M. R. & SIMMONS, C. 1995. The use of xenogeneic small intestinal submucosa as a biomaterial for Achille's tendon repair in a dog model. *Journal of Biomedical Materials Research,* 29**,** 977-985.

BADYLAK, S. F., VALENTIN, J. E., RAVINDRA, A. K., MCCABE, G. P. & STEWART-AKERS, A. M. 2008. Macrophage phenotype as a determinant of biologic scaffold remodeling. *Tissue engineering. Part A,* 14**,** 1835.

BADYLAK, S. F., WEISS, D. J., CAPLAN, A. & MACCHIARINI, P. 2012. Engineered whole organs and complex tissues. *Lancet,* 379**,** 943-952.

BAI, L., LI, D., LI, J., LUO, Z., YU, S., CAO, S., SHEN, L., ZUO, Z. & MA, X. 2016. Bioactive molecules derived from umbilical cord mesenchymal stem cells. *Acta Histochemica,* 118**,** 761-769.

BAIGUERA, S., BIRCHALL, M. A. & MACCHIARINI, P. 2010a. Tissue-engineered tracheal transplantation. *Transplantation,* 89**,** 485-491.

BAIGUERA, S., JUNGEBLUTH, P., BURNS, A., MAVILIA, C., HAAG, J., DE COPPI, P. & MACCHIARINI, P. 2010b. Tissue engineered human tracheas for in vivo implantation. *Biomaterials,* 31**,** 8931-8938.

BARDSLEY, K., YANG, Y. & EL HAJ, A. 2017. Fluorescent Labeling of Collagen Production by Cells for Noninvasive Imaging of Extracellular Matrix Deposition. *Tissue Engineering Part C: Methods,* 23**,** 228-236.

BARNES, S. C., SHEPHERD, D. E. T., ESPINO, D. M. & BRYAN, R. T. 2015. Frequency dependent viscoelastic properties of porcine bladder. *Journal of the Mechanical Behavior of Biomedical Materials,* 42**,** 168-176.

BARTHES, J., #XD6, #XE7, ELIK, H., HINDI, #XE9, , M., NDREU-HALILI, A., HASAN, A. & VRANA, N. E. 2014. Cell Microenvironment Engineering and Monitoring for Tissue Engineering and Regenerative Medicine: The Recent Advances. *BioMed Research International,* 2014**,** 18.

BARTLETT, R. D., CHOI, D. & PHILLIPS, J. B. 2016. Biomechanical properties of the spinal cord: implications for tissue engineering and clinical translation. *Regenerative Medicine,* 11**,** 659-673.

BARTOSH, T. J., YLÖSTALO, J. H., BAZHANOV, N., KUHLMAN, J. & PROCKOP, D. J. 2013. Dynamic compaction of human mesenchymal stem/precursor cells into spheres self-activates caspase-dependent IL1 signaling to enhance secretion of modulators of inflammation and immunity (PGE2, TSG6, and STC1. *STEM CELLS,* 31**,** 2443-2456.

BATIOGLU-KARAALTIN, A., KARAALTIN, M., OVALI, E., YIGIT, O., KONGUR, M., INAN, O., BOZKURT, E. & CANSIZ, H. 2015. In Vivo Tissue-Engineered Allogenic Trachea Transplantation in Rabbits: A Preliminary Report. *Stem Cell Rev and Rep,* 11**,** 347-356.

BECKERMANN, B. M., KALLIFATIDIS, G., GROTH, A., FROMMHOLD, D., APEL, A., MATTERN, J., SALNIKOV, A. V., MOLDENHAUER, G., WAGNER, W., DIEHLMANN, A., SAFFRICH, R., SCHUBERT, M., HO, A. D., GIESE, N., BÜCHLER, M. W., FRIESS, H., BÜCHLER, P. & HERR, I. 2008. VEGF expression by mesenchymal stem cells contributes to angiogenesis in pancreatic carcinoma. *British Journal of Cancer,* 99**,** 622.

BELSEY, R. 1950. Resection and reconstruction of the intrathoracic trachea. *British Journal of Surgery,* 38**,** 200-205.

BENDERS, K. E. M., VAN WEEREN, P. R., BADYLAK, S. F., SARIS, D. B. F., DHERT, W. J. A. & MALDA, J. 2013. Extracellular matrix scaffolds for cartilage and bone regeneration. *Trends in Biotechnology,* 31**,** 169-176.

BERNARDO, MARIA E. & FIBBE, WILLEM E. 2013. Mesenchymal Stromal Cells: Sensors and Switchers of Inflammation. *Cell Stem Cell,* 13**,** 392-402.

BEYERSMANN, D. 2002. Homeostasis and Cellular Functions of Zinc. *Materialwissenschaft und Werkstofftechnik,* 33**,** 764-769.

BIRCHALL, M. A., ELLIOTT, M. J., LOWDELL, M. & DE COPPI, P. 2013. Authors' reply. *The Lancet,* 381**,** 113.

BLENDSPACE, T. 2019. *Resiratory system* [Online]. Available: https://www.tes.com/lessons/iEVWIqJpz6l4hQ/respiratory-system [Accessed].

BOAZAK, E. M. & AUGUSTE, D. T. 2018. Trachea Mechanics for Tissue Engineering Design. *Acs Biomaterials Science & Engineering,* 4**,** 1272-1284.

BOAZAK, E. M., BENSON, J. M. & AUGUSTE, D. T. 2017. R- and Z-Axis Patterned Scaffolds Mimic Tracheal Circumferential Compliance and Longitudinal Extensibility. *Acs Biomaterials Science & Engineering,* 3**,** 3222-3229.

BOGAN, S. L., TEOH, G. Z. & BIRCHALL, M. A. 2016. Tissue Engineered Airways: A Prospects Article. *Journal of Cellular Biochemistry,* 117**,** 1497-1505.

BOLANO, L. & KOPTA, J. 1991. THE IMMUNOLOGY OF BONE AND CARTILAGE TRANSPLANTATION. *Orthopedics,* 14**,** 987-996.

BONNANS, C., CHOU, J. & WERB, Z. 2014. Remodelling the extracellular matrix in development and disease. *Nature Reviews Molecular Cell Biology,* 15**,** 786-801.

BOOMSMA, R. A. & GEENEN, D. L. 2012. Mesenchymal Stem Cells Secrete Multiple Cytokines That Promote Angiogenesis and Have Contrasting Effects on Chemotaxis and Apoptosis (Stem Cells Effect Chemotaxis and Apoptosis). *PLoS ONE,* 7**,** e35685.

BOUHUYS, A. 1977. *The physiology of breathing : a textbook for medical students /Arend Bouhuys,* New York, New York : Grune & Stratton.

BOWLIN, G. L., MEYER, A., FIELDS, C., CASSANO, A., MAKHOUL, R. G., ALLEN, C. & RITTGERS, S. E. 2001. The Persistence of Electrostatically Seeded Endothelial Cells Lining a Small Diameter Expanded Polytetrafluoroethylene Vascular Graft. *Journal of Biomaterials Applications,* 16**,** 157-173.

BRAND-SABERI, B. E. M. & SCHÄFER, T. 2014. Trachea: Anatomy and Physiology. *Thoracic Surgery Clinics,* 24**,** 1-5.

BRIAN, O. D., NICOLAS, C., VINCENT, P. W., HAOSI, S., JOHANNAH, S.-A., KAM, W. L. & FARSHID, G. 2012. Cartilage tissue engineering using differentiated and purified induced pluripotent stem cells. *Proceedings of the National Academy of Sciences,* 109**,** 19172.

BROWN, B. N. & BADYLAK, S. F. 2014. Extracellular matrix as an inductive scaffold for functional tissue reconstruction. *Translational Research,* 163**,** 268-285.

BROWN, B. N., LONDONO, R., TOTTEY, S., ZHANG, L., KUKLA, K. A., WOLF, M. T., DALY, K. A., REING, J. E. & BADYLAK, S. F. 2011. Macrophage phenotype as a predictor of constructive remodeling following the implantation of biologically derived surgical mesh materials. *Acta Biomaterialia,* 8.

BROWN, B. N., RATNER, B. D., GOODMAN, S. B., AMAR, S. & BADYLAK, S. F. 2012. Macrophage polarization: An opportunity for improved outcomes in and regenerative medicine. *Biomaterials,* 33**,** 3792-3802.

BROWN, B. N., VALENTIN, J. E., STEWART-AKERS, A. M., MCCABE, G. P. & BADYLAK, S. F. 2009. Macrophage phenotype and remodeling outcomes in response to biologic scaffolds with and without a cellular component. *Biomaterials,* 30**,** 1482-1491.

BURTON, H., FREIJ, J. & ESPINO, D. 2017. Dynamic Viscoelasticity and Surface Properties of Porcine Left Anterior Descending Coronary Arteries. *Cardiovasc Eng Tech,* 8**,** 41-56.

BUSTIN, S. A., BENES, V., GARSON, J., HELLEMANS, J., HUGGETT, J., KUBISTA, M., MUELLER, R., NOLAN, T., PFAFFL, M. W., SHIPLEY, G., WITTWER, C. T., SCHJERLING, P., DAY, P. J., ABREU, M., AGUADO,

B., BEAULIEU, J.-F., BECKERS, A., BOGAERT, S., BROWNE, J. A., CARRASCO-RAMIRO, F., CEELEN, L., CIBOROWSKI, K., CORNILLIE, P., COULON, S., CUYPERS, A., DE BROUWER, S., DE CEUNINCK, L., DE CRAENE, J., DE NAEYER, H., DE SPIEGELAERE, W., DECKERS, K., DHEEDENE, A., DURINCK, K., FERREIRA-TEIXEIRA, M., FIEUW, A., GALLUP, J. M., GONZALO-FLORES, S., GOOSSENS, K., HEINDRYCKX, F., HERRING, E., HOENICKA, H., ICARDI, L., JAGGI, R., JAVAD, F., KARAMPELIAS, M., KIBENGE, F., KIBENGE, M., KUMPS, C., LAMBERTZ, I., LAMMENS, T., MARKEY, A., MESSIAEN, P., METS, E., MORAIS, S., MUDARRA-RUBIO, A., NAKIWALA, J., NELIS, H., OLSVIK, P. A., PÉREZ-NOVO, C., PLUSQUIN, M., REMANS, T., RIHANI, A., RODRIGUES-SANTOS, P., RONDOU, P., SANDERS, R., SCHMIDT-BLEEK, K., SKOVGAARD, K., SMEETS, K., TABERA, L., TOEGEL, S., VAN ACKER, T., VAN DEN BROECK, W., VAN DER MEULEN, J., VAN GELE, M., VAN PEER, G., VAN POUCKE, M., VAN ROY, N., VERGULT, S., WAUMAN, J., TSHUIKINA-WIKLANDER, M., WILLEMS, E., ZACCARA, S., ZEKA, F. & VANDESOMPELE, J. 2013. The need for transparency and good practices in the qPCR literature. *Nature Methods,* 10**,** 1063.

BUTLER, C. R., HYNDS, R. E., CROWLEY, C., GOWERS, K. H. C., PARTINGTON, L., HAMILTON, N. J., CARVALHO, C., PLATE, M., SAMUEL, E. R., BURNS, A. J., URBANI, L., BIRCHALL, M. A., LOWDELL, M. W., DE COPPI, P. & JANES, S. M. 2017a. Vacuum-assisted decellularization: an accelerated protocol to generate tissue-engineered human tracheal scaffolds. *Biomaterials,* 124**,** 95-105.

BUTLER, C. R., HYNDS, R. E., CROWLEY, C., GOWERS, K. H. C., PARTINGTON, L., HAMILTON, N. J., CARVALHO, C., PLATÉ, M., SAMUEL, E. R., BURNS, A. J., URBANI, L., BIRCHALL, M. A., LOWDELL, M. W., DE COPPI, P. & JANES, S. M. 2017b. Vacuum-assisted decellularization: an accelerated protocol to generate tissue-engineered human tracheal scaffolds. *Biomaterials,* 124**,** 95-105.

BUTLER, C. R., HYNDS, R. E., GOWERS, K. H. C., LEE, D. D. H., BROWN, J. M., CROWLEY, C., TEIXEIRA, V. H., SMITH, C. M., URBANI, L., HAMILTON, N. J., THAKRAR, R. M., BOOTH, H. L., BIRCHALL, M. A., DE COPPI, P., GIANGRECO, A., O'CALLAGHAN, C. & JANES, S. M. 2016. Rapid Expansion of Human Epithelial Stem Cells Suitable for Airway Tissue Engineering. *American journal of respiratory and critical care medicine,* 194**,** 156.

BUTLER, D. L., GOLDSTEIN, S. A. & GUILAK, F. 2000. Functional Tissue Engineering: The Role of Biomechanics. *Journal of Biomechanical Engineering,* 122**,** 570-575.

BUTLER, D. L., JUNCOSA-MELVIN, N., BOIVIN, G. P., GALLOWAY, M. T., SHEARN, J. T., GOOCH, C. & AWAD, H. 2008. Functional tissue engineering for tendon repair: A multidisciplinary strategy using mesenchymal stem cells, bioscaffolds, and mechanical stimulation. *Journal of Orthopaedic Research,* 26**,** 1-9.

CALEY, M. P., MARTINS, V. L. C. & O'TOOLE, E. A. 2015. Metalloproteinases and Wound Healing. *Advances in wound care,* 4**,** 225-234.

CALIARI, S. R. & HARLEY, B. A. 2014. Collagen-GAG scaffold biophysical properties bias MSC lineage choice in the presence of mixed soluble signals. *Tissue Engineering Part A,* 20**,** 2463-2472.

CALVE, S., READY, A., HUPPENBAUER, C., MAIN, R. & NEU, C. P. 2015. Optical Clearing in Dense Connective Tissues to Visualize Cellular Connectivity In Situ (Optical Clearing of ECM-Rich Tissues). 10**,** e0116662.

CARTMELL, J. S. & DUNN, M. G. 2000. Effect of chemical treatments on tendon cellularity and mechanical properties. *Journal of Biomedical Materials Research,* 49**,** 134-140.

CASEY, A., DIRKS, F., LIANG, O. D., HARRACH, H., SCHUETTE-NUETGEN, K., LEEMAN, K., KIM, C. F., GERARD, C. & SUBRAMANIAM, M. 2014. Bone Marrow-Derived Multipotent Stromal Cells Attenuate Inflammation in Obliterative Airway Disease in Mouse Tracheal Allografts. *Stem Cells International,* 2014.

CHANG, S., PURYEAR, J. & CAIRNEY, J. 1993. A simple and efficient method for isolating RNA from pine trees. *Plant Mol Biol Rep,* 11**,** 113-116.

CHANG, S. H. & DONG, C. 2009. IL-17F: regulation, signaling and function in inflammation. *Cytokine,* 46**,** 7-11.

CHAO, T.-Y. & RAINES, R. T. 2011. Mechanism of ribonuclease A endocytosis: analogies to cell-penetrating peptides. *Biochemistry,* 50**,** 8374.

CHEN, F., YOO, J. J. & ATALA, A. 1999. Acellular collagen matrix as a possible "off the shelf" biomaterial for urethral repair. *Urology,* 54**,** 407.

CHEN, R.-N., HO, H.-O., TSAI, Y.-T. & SHEU, M.-T. 2004. Process development of an acellular dermal matrix (ADM) for biomedical applications. *Biomaterials,* 25**,** 2679-2686.

CHIANG, T., PEPPER, V., BEST, C., ONWUKA, E. & BREUER, C. K. 2016. Clinical Translation of Tissue Engineered Trachea Grafts. *The Annals of otology, rhinology, and laryngology,* 125**,** 873-885.

CHINNAPAKA, S., ATUL, K., DARILANG, M., AMIT, S., SURAJ DASHARATH, P., JINA, B., RAJARAM, S. & BITHIAH GRACE, J. 2015. Collagen Promotes Higher Adhesion, Survival and Proliferation of Mesenchymal Stem Cells. *PLoS ONE,* 10**,** e0145068.

CHOMCZYNSKI, P. & MACKEY, K. 1995. Short technical reports. Modification of the TRI reagent procedure for isolation of RNA from polysaccharide- and proteoglycan-rich sources. *Biotechniques,* 19**,** 942-5.

CLAESSON-WELSH, L. & HANSSON, G. K. 2016. Tracheobronchial transplantation: The Royal Swedish Academy of Sciences' concerns. *The Lancet,* 387**,** 942.

CLARK, E. S., BEST, C., ONWUKA, E., SUGIURA, T., MAHLER, N., BOLON, B., NIEHAUS, A., JAMES, I., HIBINO, N., SHINOKA, T., JOHNSON, J. & BREUER, C. K. 2016. Effect of cell seeding on neotissue formation in a tissue engineered trachea. *Journal of Pediatric Surgery,* 51**,** 49-55.

CLOSE, D. M., XU, T., SAYLER, G. & RIPP, S. 2011. In Vivo Bioluminescent Imaging (BLI): Noninvasive Visualization and Interrogation of Biological Processes in Living Animals. *Sensors,* 11**,** 180-206.

CONCONI, M. T., COPPI, P. D., LIDDO, R. D., VIGOLO, S., ZANON, G. F., PARNIGOTTO, P. P. & NUSSDORFER, G. G. 2005. Tracheal matrices, obtained by a detergent-enzymatic method, support in vitro the adhesion

of chondrocytes and tracheal epithelial cells. *Transplant International,* 18**,** 727-734.
CRAPO, P. M., GILBERT, T. W. & BADYLAK, S. F. 2011. An overview of tissue and whole organ decellularization processes. *Biomaterials,* 32**,** 3233-3243.
CRUPI, A., COSTA, A., TARNOK, A., MELZER, S. & TEODORI, L. 2015. Inflammation in tissue engineering: The Janus between engraftment and rejection. *European Journal of Immunology,* 45**,** 3222-3236.
CUENDA, A. & ROUSSEAU, S. 2007. p38 MAP-Kinases pathway regulation, function and role in human diseases. *Biochimica et Biophysica Acta (BBA) - Molecular Cell Research,* 1773**,** 1358-1375.
CUNNINGHAM, C. J., REDONDO-CASTRO, E. & ALLAN, S. M. 2018. The therapeutic potential of the mesenchymal stem cell secretome in ischaemic stroke. *Journal of cerebral blood flow and metabolism : official journal of the International Society of Cerebral Blood Flow and Metabolism,* 38**,** 1276-1292.
CYRANOSKI, D. 2014. Artificial tracheas under scrutiny. *Nature,* 516**,** 16-17.
D638-02A, A. S. 2003. Standard Test Method for Tensile Properties of Plastics *ASTM standard D638-02a.* West Conshohocken: ASTM international.
DA SILVA MEIRELLES, L., FONTES, A. M., COVAS, D. T. & CAPLAN, A. I. 2009. Mechanisms involved in the therapeutic properties of mesenchymal stem cells. *Cytokine & Growth Factor Reviews,* 20**,** 419-427.
DARLING, E. M. & ATHANASIOU, K. A. 2003. Articular Cartilage Bioreactors and Bioprocesses. *Tissue Engineering,* 9**,** 9-26.
DAVISSON, T., SAH, R. L. & RATCLIFFE, A. 2002. Perfusion increases cell content and matrix synthesis in chondrocyte three-dimensional cultures. *Tissue engineering,* 8**,** 807.
DE LISIO, M., JENSEN, T., SUKIENNIK, R. A., HUNTSMAN, H. D. & BOPPART, M. D. 2014. Substrate and strain alter the muscle-derived mesenchymal stem cell secretome to promote myogenesis. *Stem cell research & therapy,* 5**,** 74.
DELAERE, P. 2010. Stem-cell "hype" in tracheal transplantation? *Transplantation,* 90**,** 927-8; author reply 928-9.
DELAERE, P., VRANCKX, J., VERLEDEN, G., DE LEYN, P. & VAN RAEMDONCK, D. 2010. Tracheal Allotransplantation after Withdrawal of Immunosuppressive Therapy. *The New England Journal of Medicine,* 362**,** 138-145.
DELAERE, P. R. 2013. Stem-cell-based, tissue-engineered tracheal replacement in a child. *Lancet (London, England),* 381**,** 113.
DELAERE, P. R. & VAN RAEMDONCK, D. 2014. The trachea: The first tissue-engineered organ? *The Journal of Thoracic and Cardiovascular Surgery,* 147**,** 1128-1132.
DELAERE, P. R., VRANCKX, J. J., MEULEMANS, J., VANDER POORTEN, V., SEGERS, K., VAN RAEMDONCK, D., DE LEYN, P., DECALUWÉ, H., DOOMS, C. & VERLEDEN, G. 2012. Learning Curve in Tracheal Allotransplantation. *American Journal of Transplantation,* 12**,** 2538-2545.
DEN HONDT, M., VANAUDENAERDE, B. M., MAUGHAN, E. F., BUTLER, C. R., CROWLEY, C., VERBEKEN, E. K., VERLEDEN, S. E. & VRANCKX, J. J. 2017. An optimized non-destructive protocol for testing mechanical

properties in decellularized rabbit trachea. *Acta Biomaterialia,* 60**,** 291-301.
DEN HONDT, M. & VRANCKX, J. 2017. Reconstruction of defects of the trachea. *J Mater Sci: Mater Med,* 28**,** 1-11.
DESHMANE, S., KREMLEV, S., AMINI, S. & SAWAYA, B. 2009. Monocyte Chemoattractant Protein-1 (MCP-1): An Overview. *Journal Of Interferon And Cytokine Research,* 29**,** 313-326.
DEY, G., RADHAKRISHNAN, A., SYED, N., THOMAS, J. K., NADIG, A., SRIKUMAR, K., MATHUR, P. P., PANDEY, A., LIN, S.-K., RAJU, R. & PRASAD, T. S. K. 2013. Signaling network of Oncostatin M pathway. *Journal of cell communication and signaling,* 7**,** 103-108.
DIKINA, A. D., STROBEL, H. A., LAI, B. P., ROLLE, M. W. & ALSBERG, E. 2015. Engineered cartilaginous tubes for tracheal tissue replacement via self-assembly and fusion of human mesenchymal stem cell constructs. *Biomaterials,* 52**,** 452-462.
DOMINICI, M., LE BLANC, K., MUELLER, I., SLAPER-CORTENBACH, I., MARINI, F., KRAUSE, D., DEANS, R., KEATING, A., PROCKOP, D. & HORWITZ, E. 2006a. Minimal criteria for defining multipotent mesenchymal stromal cells. The International Society for Cellular Therapy position statement. *Cytotherapy,* 8**,** 315.
DOMINICI, M., LE BLANC, K., MUELLER, I., SLAPER-CORTENBACH, I., MARINI, F. C., KRAUSE, D. S., DEANS, R. J., KEATING, A., PROCKOP, D. J. & HORWITZ, E. M. 2006b. Minimal criteria for defining multipotent mesenchymal stromal cells. The International Society for Cellular Therapy position statement. *Cytotherapy,* 8**,** 315-317.
DUNKELMAN, N. S., ZIMBER, M. P., LEBARON, R. G., PAVELEC, R., KWAN, M. & PURCHIO, A. F. 1995. Cartilage production by rabbit articular chondrocytes on polyglycolic acid scaffolds in a closed bioreactor system. *Biotechnology and Bioengineering,* 46**,** 299-305.
DURBEEJ, M. 2009. Laminins. *Cell and Tissue Research,* 339**,** 259-268.
EDEN, E., NAVON, R., STEINFELD, I., LIPSON, D. & YAKHINI, Z. 2009. GOrilla : a tool for discovery and visualization of enriched GO terms in ranked gene lists. *BMC Bioinformatics,* 10**,** 48-48.
EL OMAR, R., BEROUD, J., STOLTZ, J.-F., MENU, P., VELOT, E. & DECOT, V. 2014. Umbilical Cord Mesenchymal Stem Cells: The New Gold Standard for Mesenchymal Stem Cell-Based Therapies? *Tissue Engineering Part B: Reviews,* 20**,** 523-544.
ELLIOTT, M. J., BUTLER, C. R., VARANOU-JENKINS, A., PARTINGTON, L., CARVALHO, C., SAMUEL, E., CROWLEY, C., LANGE, P., HAMILTON, N. J., HYNDS, R. E., ANSARI, T., SIBBONS, P., FIERENS, A., MCLAREN, C., ROEBUCK, D., WALLIS, C., MUTHIALU, N., HEWITT, R., CRABBE, D., JANES, S. M., DE COPPI, P., LOWDELL, M. W. & BIRCHALL, M. A. 2017. Tracheal Replacement Therapy with a Stem Cell-Seeded Graft: Lessons from Compassionate Use Application of a GMP-Compliant Tissue-Engineered Medicine. *Stem Cells Translational Medicine,* 6**,** 1458-1464.
ELLIOTT, M. J., DE COPPI, P., SPEGGIORIN, S., ROEBUCK, D., BUTLER, C. R., SAMUEL, E., CROWLEY, C., MCLAREN, C., FIERENS, A., VONDRYS, D., COCHRANE, L., JEPHSON, C., JANES, S., BEAUMONT, N. J., COGAN, T., BADER, A., SEIFALIAN, A. M., HSUAN, J. J.,

LOWDELL, M. W. & BIRCHALL, M. A. 2012. Stem-cell-based, tissue engineered tracheal replacement in a child: a 2-year follow-up study. *Lancet,* 380**,** 994-1000.
ELLIOTT, M. J., HAW, M. P., JACOBS, J. P., BAILEY, C. M., EVANS, J. N. G. & HERBERHOLD, C. 1996. Tracheal reconstruction in children using cadaveric homograft trachea. *European Journal of Cardio-Thoracic Surgery,* 10**,** 707-712.
ENGLER, A. J., GRIFFIN, M. A., SEN, S., BÖNNEMANN, C. G., SWEENEY, H. L. & DISCHER, D. E. 2004. Myotubes differentiate optimally on substrates with tissue-like stiffness: pathological implications for soft or stiff microenvironments. *The Journal of Cell Biology,* 166**,** 877-887.
ENGLER, A. J., SEN, S., SWEENEY, H. L. & DISCHER, D. E. 2006. Matrix Elasticity Directs Stem Cell Lineage Specification. *Cell,* 126**,** 677-689.
ENGLISH, K. 2013. Mechanisms of mesenchymal stromal cell immunomodulation.
EPSTEIN, S. K. 2005. Anatomy and physiology of tracheostomy. *Respiratory care,* 50**,** 476.
ETIENNE, H., FABRE, D., CARO, A. G., KOLB, F., MUSSOT, S., MERCIER, O., MITILIAN, D., STEPHAN, F., FADEL, E. & DARTEVELLE, P. 2018. Tracheal replacement. *European Respiratory Journal,* 51.
FAULK, D. M., CARRUTHERS, C. A., WARNER, H. J., KRAMER, C. R., REING, J. E., ZHANG, L., D'AMORE, A. & BADYLAK, S. F. 2014. The effect of detergents on the basement membrane complex of a biologic scaffold material. *Acta Biomaterialia,* 10**,** 183-193.
FIEL, S. B. 1992. Principles of pulmonary medicine, 2nd ed. By Steven Weinberger. Philadelphia: W.B. Saunders, 1992, 353 pp. *Pediatric Pulmonology,* 13**,** 130-130.
FIONA, M. W. & WILHELM, T. S. H. 2013. Role of the extracellular matrix in regulating stem cell fate. *Nature Reviews Molecular Cell Biology,* 14**,** 467.
FISHMAN, J. M., DE COPPI, P., ELLIOTT, M. J., ATALA, A., BIRCHALL, M. A. & MACCHIARINI, P. 2011. Airway tissue engineering. *Expert Opinion on Biological Therapy,* 11**,** 1623-1635.
FISHMAN, J. M., LOWDELL, M. & BIRCHALL, M. A. 2014a. Stem cell-based organ replacements-Airway and lung tissue engineering. *Seminars in Pediatric Surgery,* 23.
FISHMAN, J. M., LOWDELL, M. W., URBANI, L., ANSARI, T., BURNS, A. J., TURMAINE, M., NORTH, J., SIBBONS, P., SEIFALIAN, A. M., WOOD, K. J., BIRCHALL, M. A. & DE COPPI, P. 2013. Immunomodulatory effect of a decellularized skeletal muscle scaffold in a discordant xenotransplantation model. *Proceedings of the National Academy of Sciences of the United States of America,* 110**,** 14360-14365.
FISHMAN, J. M., WILES, K., LOWDELL, M. W., DE COPPI, P., ELLIOTT, M. J., ATALA, A. & BIRCHALL, M. A. 2014b. Airway tissue engineering: An update. *Expert Opinion on Biological Therapy,* 14**,** 1477-1491.
FLYNN, L. E. 2010. The use of decellularized adipose tissue to provide an inductive microenvironment for the adipogenic differentiation of human adipose-derived stem cells. *Biomaterials,* 31**,** 4715-4724.
FORMIGLI, L., PATERNOSTRO, F., TANI, A., MIRABELLA, C., QUATTRINI LI, A., NOSI, D., D'ASTA, F., SACCARDI, R., MAZZANTI, B., LO RUSSO, G. & ZECCHI-ORLANDINI, S. 2015. MSCs seeded on bioengineered

scaffolds improve skin wound healing in rats. *Wound Repair and Regeneration,* 23**,** 115-123.
FRANTZ, C., STEWART, K. M. & WEAVER, V. M. 2010. The extracellular matrix at a glance. *Journal of Cell Science,* 123**,** 4195-4200.
FREYMAN, T., POLIN, G., OSMAN, H., CRARY, J., LU, M., CHENG, L., PALASIS, M. & WILENSKY, R. L. 2006. A quantitative, randomized study evaluating three methods of mesenchymal stem cell delivery following myocardial infarction. *European Heart Journal,* 27**,** 1114-1122.
FRIEDENSTEIN, A. J., PIATETZKY-SHAPIRO, I. I. & PETRAKOVA, K. V. 1966. Osteogenesis in transplants of bone marrow cells. *Journal of embryology and experimental morphology,* 16**,** 381.
FRITH, J., MILLS, R. & COOPER-WHITE, J. 2012. Lateral spacing of adhesion peptides influences human mesenchymal stem cell behaviour. *Journal Of Cell Science,* 125**,** 317-327.
FROSTELL, C., BJÖRLING, G., STRÖMBERG, E., KARLSSON, S. & AUNE, R. E. 2017. Tracheal implants revisited. *The Lancet,* 389**,** 1191.
FUCHS, J. R., HANNOUCHE, D., TERADA, S., VACANTI, J. P. & FAUZA, D. O. 2003. Fetal tracheal augmentation with cartilage engineered from bone marrow-derived mesenchymal progenitor cells. *Journal of Pediatric Surgery,* 38**,** 984-987.
FULCHER, M. L. & RANDELL, S. H. 2013. Human Nasal and Tracheo-Bronchial Respiratory Epithelial Cell Culture. *In:* RANDELL, H. S. & FULCHER, L. M. (eds.) *Epithelial Cell Culture Protocols: Second Edition.* Totowa, NJ: Humana Press.
FURLOW, P. W. & MATHISEN, D. J. J. A. O. C. S. 2018. Surgical anatomy of the trachea. *2018,* 7**,** 255-260.
GALDERISI, U. & GIORDANO, A. 2014. The Gap Between the Physiological and Therapeutic Roles of Mesenchymal Stem Cells. *Medicinal Research Reviews,* 34**,** 1100-1126.
GATTAZZO, F., URCIUOLO, A. & BONALDO, P. 2014. Extracellular matrix: A dynamic microenvironment for stem cell niche. *Biochimica Et Biophysica Acta-General Subjects,* 1840**,** 2506-2519.
GEHRSITZ, A., MCKENNA, L. A., SÖDER, S., KIRCHNER, T. & AIGNER, T. 2001. Isolation of RNA from small human articular cartilage specimens allows quantification of mRNA expression levels in local articular cartilage defects. *Journal of Orthopaedic Research,* 19**,** 478-481.
GHANAVI, P., KABIRI, M. & DORAN, M. R. 2012. The rationale for using microscopic units of a donor matrix in cartilage defect repair. *Cell and Tissue Research,* 347**,** 643-648.
GHEZZI, C. E., RISSE, P.-A., MARELLI, B., MUJA, N., BARRALET, J. E., MARTIN, J. G. & NAZHAT, S. N. 2013. An airway smooth muscle cell niche under physiological pulsatile flow culture using a tubular dense collagen construct. *Biomaterials,* 34**,** 1954-1966.
GHORBANI, F., FEIZABADI, M., FARZANEGAN, R., VAZIRI, E., SAMANI, S., LAJEVARDI, S., MORADI, L. & SHADMEHR, M. 2017. An Investigation of Topics and Trends of Tracheal Replacement Studies Using Co-Occurrence Analysis. *Tissue Engineering Part B: Reviews,* 23**,** 118-127.
GILBERT, T., STEWART-AKERS, A., SIMMONS-BYRD, A. & BADYLAK, S. 2007. Degradation and remodeling of small intestinal submucosa in canine

Achilles tendon repair. *Journal Of Bone And Joint Surgery-American Volume,* 89A**,** 621-630.
GILBERT, T. W., FREUND, J. & BADYLAK, S. F. 2009. Quantification of DNA in Biologic Scaffold Materials. *The Journal of surgical research,* 152**,** 135-139.
GILBERT, T. W., GILBERT, S., MADDEN, M., REYNOLDS, S. D. & BADYLAK, S. F. 2008. Morphologic Assessment of Extracellular Matrix Scaffolds for Patch Tracheoplasty in a Canine Model. *The Annals of Thoracic Surgery,* 86**,** 967-974.
GILBERT, T. W., SELLARO, T. L. & BADYLAK, S. F. 2006. Decellularization of tissues and organs. *Biomaterials,* 27**,** 3675-3683.
GILL, S. E. & PARKS, W. C. 2008. Metalloproteinases and their inhibitors: Regulators of wound healing. *International Journal of Biochemistry and Cell Biology,* 40**,** 1334-1347.
GILLIAN, M. 2008. The ADAMs: signalling scissors in the tumour microenvironment.
GILPIN, D. A., WEIDENBECHER, M. S. & DENNIS, J. E. 2010. Scaffold-free tissue-engineered cartilage implants for laryngotracheal reconstruction. *The Laryngoscope,* 120**,** 612.
GIORDANO, A., GALDERISI, U. & MARINO, I. R. 2007. From the laboratory bench to the patient's bedside: an update on clinical trials with mesenchymal stem cells. *Journal of cellular physiology,* 211**,** 27-35.
GO, T., JUNGEBLUTH, P., BAIGUERO, S., ASNAGHI, A., MARTORELL, J., OSTERTAG, H., MANTERO, S., BIRCHALL, M., BADER, A. & MACCHIARINI, P. 2010. Both epithelial cells and mesenchymal stem cell-derived chondrocytes contribute to the survival of tissue-engineered airway transplants in pigs. *Journal of Thoracic and Cardiovascular Surgery,* 139**,** 437-443.
GODBEY, W. T., STACEY HINDY, B. S., SHERMAN, M. E. & ATALA, A. 2004. A novel use of centrifugal force for cell seeding into porous scaffolds. *Biomaterials,* 25**,** 2799-2805.
GOH, C. S.-L., JOETHY, J.-V., TAN, B.-K. & WONG, M. 2018. Large animal models for long-segment tracheal reconstruction: a systematic review. *Journal of Surgical Research,* 231**,** 140-153.
GONFIOTTI, A., JAUS, M. O., BARALE, D., BAIGUERA, S., COMIN, C., LAVORINI, F., FONTANA, G., SIBILA, O., ROMBOLA, G., JUNGEBLUTH, P. & MACCHIARINI, P. 2014. The first tissue-engineered airway transplantation: 5-year follow-up results. *Lancet,* 383**,** 238-244.
GONG, Y. Y., XUE, J. X., ZHANG, W. J., ZHOU, G. D., LIU, W. & CAO, Y. 2011. A sandwich model for engineering cartilage with acellular cartilage sheets and chondrocytes. *Biomaterials,* 32**,** 2265-2273.
GRANDI, C., BAIGUERA, S., MARTORINA, F., LORA, S., AMISTA, P., DALZOPPO, D., DEL GAUDIO, C., BIANCO, A., DI LIDDO, R., CONCONI, M. T. & PARNIGOTTO, P. P. 2011. Decellularized bovine reinforced vessels for small-diameter tissue-engineered vascular grafts. *Int J Mol Med,* 28**,** 315-25.
GRAY, F. L., TURNER, C. G., AHMED, A., CALVERT, C. E., ZURAKOWSKI, D. & FAUZA, D. O. 2012. Prenatal tracheal reconstruction with a hybrid amniotic mesenchymal stem cells–engineered construct derived from decellularized airway. *Journal of Pediatric Surgery,* 47**,** 1072-1079.

GRILLO, C. H. & MCKHANN, F. C. 1964. THE ACCEPTANCE AND EVOLUTION OF DERMAL HOMOGRAFTS FREED OF VIABLE CELLS. *Transplantation,* 2**,** 48-59.

GRILLO, H. C. 2002. Tracheal replacement: a critical review. *The Annals of Thoracic Surgery,* 73**,** 1995-2004.

GRILLO, H. C. 2004. *Surgery of the trachea and bronchi /Hermes C. Grillo,* Hamilton, Ont.

London, Hamilton, Ont.

London : BC Decker.

GRIMMER, J. F., GUNNLAUGSSON, C. B., ALSBERG, E., MURPHY, H. S., KONG, H. J., MOONEY, D. J. & WEATHERLY, R. A. 2004. Tracheal Reconstruction Using Tissue-Engineered Cartilage. *Archives of Otolaryngology–Head & Neck Surgery,* 130**,** 1191-1196.

GROSSMANN, J. 2002. Molecular mechanisms of "detachment-induced apoptosis-Anoikis". *Apoptosis,* 7**,** 247-260.

GUILAK, F., BUTLER, D. L., GOLDSTEIN, S. A. & BAAIJENS, F. P. T. 2014. Biomechanics and mechanobiology in functional tissue engineering. *Journal of Biomechanics,* 47**,** 1933-1940.

GUNATILLAKE, P. A., ADHIKARI, R. & GADEGAARD, N. 2003. Biodegradable synthetic polymers for tissue engineering. *European Cells and Materials,* 5**,** 1-16.

HAMILTON, N. J., KANANI, M., ROEBUCK, D. J., HEWITT, R. J., CETTO, R., CULME-SEYMOUR, E. J., TOLL, E., BATES, A. J., COMERFORD, A. P., MCLAREN, C. A., BUTLER, C. R., CROWLEY, C., MCINTYRE, D., SEBIRE, N. J., JANES, S. M., O'CALLAGHAN, C., MASON, C., DE COPPI, P., LOWDELL, M. W., ELLIOTT, M. J. & BIRCHALL, M. A. 2015. Tissue-Engineered Tracheal Replacement in a Child: A 4-Year Follow-Up Study. *American Journal of Transplantation,* 15**,** 2750-2757.

HAMILTON, N. J. I., HYNDS, R. E., GOWERS, K. H. C., TAIT, A., BUTLER, C. R., HOPPER, C., BURNS, A. J., BIRCHALL, M. A., LOWDELL, M. & JANES, S. M. 2019. Using a Three-Dimensional Collagen Matrix to Deliver Respiratory Progenitor Cells to Decellularized Trachea In Vivo. *Tissue Engineering Part C: Methods,* 25**,** 93-102.

HAN, Y., LAN, N., PANG, C. & TONG, X. 2011. Bone Marrow-Derived Mesenchymal Stem Cells Enhance Cryopreserved Trachea Allograft Epithelium Regeneration and Vascular Endothelial Growth Factor Expression. *Transplantation,* 92**,** 620-626.

HAYKAL, S., SALNA, M., WADDELL, T. K. & HOFER, S. O. 2014a. Advances in tracheal reconstruction. *Plastic and reconstructive surgery. Global open,* 2**,** e178.

HAYKAL, S., SALNA, M., ZHOU, Y., MARCUS, P., FATEHI, M., FROST, G., MACHUCA, T., HOFER, S. O. P. & WADDELL, T. K. 2014b. Double-Chamber Rotating Bioreactor for Dynamic Perfusion Cell Seeding of Large-Segment Tracheal Allografts: Comparison to Conventional Static Methods. *Tissue Engineering. Part C, Methods,* 20**,** 681-692.

HAYKAL, S., SOLEAS, J. P., SALNA, M., HOFER, S. O. P. & WADDELL, T. K. 2012. Evaluation of the Structural Integrity and Extracellular Matrix Components of Tracheal Allografts Following Cyclical Decellularization Techniques: Comparison of Three Protocols. *Tissue Engineering Part C-Methods,* 18**,** 614-623.

HAYKAL, S., ZHOU, Y., MARCUS, P., SALNA, M., MACHUCA, T., HOFER, S. O. P. & WADDELL, T. K. 2013. The effect of decellularization of tracheal allografts on leukocyte infiltration and of recellularization on regulatory T cell recruitment. *Biomaterials,* 34**,** 5821.

HELJASVAARA, R., AIKIO, M., RUOTSALAINEN, H. & PIHLAJANIEMI, T. 2017. Collagen XVIII in tissue homeostasis and dysregulation — Lessons learned from model organisms and human patients. *Matrix Biology,* 57-58**,** 55-75.

HERARD, A. L., PIERROT, D., HINNRASKY, J., KAPLAN, H., SHEPPARD, D., PUCHELLE, E. & ZAHM, J. M. 1996. Fibronectin and its alpha 5 beta 1-integrin receptor are involved in the wound-repair process of airway epithelium. *American Journal of Physiology - Lung Cellular and Molecular Physiology,* 271**,** L726-L733.

HERLAAR, E. & BROWN, Z. 1999. p38 MAPK signalling cascades in inflammatory disease. *Molecular Medicine Today,* 5**,** 439-447.

HERMAN, I. P. 2016. *Physics of the human body*, Cham : Springer.

HIEMER, B., GENZ, B., JONITZ-HEINCKE, A., PASOLD, J., WREE, A., DOMMERICH, S. & BADER, R. 2016. Devitalisation of human cartilage by high hydrostatic pressure treatment: Subsequent cultivation of chondrocytes and mesenchymal stem cells on the devitalised tissue. *Scientific Reports,* 6**,** 33747.

HIZAWA, N., KAWAGUCHI, M., HUANG, S.-K. & NISHIMURA, M. 2006. Role of interleukin-17F in chronic inflammatory and allergic lung disease. 36**,** 1109-1114.

HOCKING, D. C. & CHANG, C. H. 2003. Fibronectin matrix polymerization regulates small airway epithelial cell migration. *American Journal of Physiology - Lung Cellular and Molecular Physiology,* 285**,** L169-L179.

HOFFMAN, B., MARTIN, M., BROWN, B. N., BONASSAR, L. J. & CHEETHAM, J. 2015. Biomechanical and biochemical characterization of porcine tracheal cartilage. *The Laryngoscope***,** n/a-n/a.

HONG, H. J., CHANG, J. W., PARK, J. K., CHOI, J. W., KIM, Y. S., SHIN, Y. S., KIM, C. H. & CHOI, E. C. 2014. Tracheal reconstruction using chondrocytes seeded on a poly(L-lactic-co-glycolic acid)-fibrin/hyaluronan. *J Biomed Mater Res A,* 102**,** 4142-50.

HONG, H. J., LEE, J. S., CHOI, J. W., MIN, B.-H., LEE, H.-B. & KIM, C.-H. 2012. Transplantation of Autologous Chondrocytes Seeded on a Fibrin/Hyaluronan Composite Gel Into Tracheal Cartilage Defects in Rabbits: Preliminary Results. *Artificial Organs,* 36**,** 998-1006.

HOOVER, D. J., ZHU, V., CHEN, R., BRILEY, K., JR., RAMESHWAR, P., COHEN, S. & COFFMAN, F. D. 2013. Expression of the chitinase family glycoprotein YKL-40 in undifferentiated, differentiated and trans-differentiated mesenchymal stem cells. *PloS one,* 8**,** e62491-e62491.

HORI, Y., NAKAMURA, T., KIMURA, D., KAINO, K., KUROKAWA, Y., SATOMI, S. & SHIMIZU, Y. 2002. Experimental Study on Tissue Engineering of the Small Intestine by Mesenchymal Stem Cell Seeding. *Journal of Surgical Research,* 102**,** 156-160.

HUANG, Z., GODKIN, O. & SCHULZE-TANZIL, G. 2017. The Challenge in Using Mesenchymal Stromal Cells for Recellularization of Decellularized Cartilage. *Stem Cell Reviews and Reports,* 13**,** 50-67.

HÜBNER, G., BRAUCHLE, M., SMOLA, H., MADLENER, M., FÄSSLER, R. & WERNER, S. 1996. DIFFERENTIAL REGULATION OF PRO-INFLAMMATORY CYTOKINES DURING WOUND HEALING IN NORMAL AND GLUCOCORTICOID-TREATED MICE. *Cytokine,* 8**,** 548-556.

HYNES, R. O. 2002. Integrins: Bidirectional, Allosteric Signaling Machines. *Cell,* 110**,** 673-687.

IANNOTTI, J. P., DERWIN, K. A., BAKER, A. R., SPRAGG, R. K., LEIGH, D. R. & IANNOTTI, J. P. 2006. Commercial extracellular matrix scaffolds for rotator cuff tendon repair. biomechanical, biochemical, and cellular properties. *Journal of Bone and Joint Surgery,* 88**,** 2665.

IGAI, S. H., CHANG, S. S., GOTOH, S. M., YAMAMOTO, S. Y., YAMAMOTO, S. M., TABATA, S. Y. & YOKOMISE, S. H. 2008. Tracheal Cartilage Regeneration and New Bone Formation by Slow Release of Bone Morphogenetic Protein (BMP)-2. *ASAIO Journal,* 54**,** 104-108.

IMPENS, S., CHEN, Y., MULLENS, S., LUYTEN, F. & SCHROOTEN, J. 2010. Controlled cell-seeding methodologies: a first step toward clinically relevant bone tissue engineering strategies. *Tissue engineering. Part C, Methods,* 16**,** 1575.

INOUE, K. I., TAKANO, H., SHIMADA, A. & SATOH, M. 2009. Metallothionein as an Anti-Inflammatory Mediator. *Mediators Of Inflammation,* 2009.

JAKOBSEN, K., GRONHOJ, C., JENSEN, D., FISCHER-NIELSEN, A., HJULER, T. & VON BUCHWALD, C. 2017. Mesenchymal stem cell therapy for laryngotracheal stenosis: A systematic review of preclinical studies. *Plos One,* 12.

JAMES, A. A., JOON FAII, O. & JEFFREY, M. K. 2014. Mesenchymal stem cells: immune evasive, not immune privileged. *Nature Biotechnology,* 32**,** 252.

JAROSZ, M., OLBERT, M., WYSZOGRODZKA, G., MLYNIEC, K. & LIBROWSKI, T. 2017. Antioxidant and anti-inflammatory effects of zinc. Zinc-dependent NF-kappa B signaling. *Inflammopharmacology,* 25**,** 11-24.

JIN, C. Z., PARK, S. R., CHOI, B. H., PARK, K. & MIN, B.-H. 2007. In Vivo Cartilage Tissue Engineering Using a Cell-Derived Extracellular Matrix Scaffold. 31**,** 183-192.

JING, L., TONG, C., XIAHE, H., YUNSHAN, Z., BIN, W., YANYUN, Y., YI, C., YANNAN, Z., RUIPING, Z., XIUJIE, W., YINGCHUN, W. & JIANWU, D. 2018. Substrate-independent immunomodulatory characteristics of mesenchymal stem cells in three-dimensional culture. *PLoS ONE,* 13**,** e0206811.

JOHNSTON, C. J. C., SMYTH, D. J., DRESSER, D. W. & MAIZELS, R. M. 2016. TGF-β in tolerance, development and regulation of immunity. *Cellular immunology,* 299**,** 14-22.

JONATHAN, H., SAMUEL, L.-R., HELEDD, J.-G. & MICHAEL, M. 2019. Tumour necrosis factor signalling in health and disease [version 1
referees: 2 approved]. *F1000Research,* 8.

JONES, M. C., RUEGGEBERG, F. A., FAIRCLOTH, H. A., CUNNINGHAM, A. J., BUSH, C. M., PROSSER, J. D., WALLER, J. L., POSTMA, G. N. & WEINBERGER, P. M. 2014. Defining the Biomechanical Properties of the Rabbit Trachea. *Laryngoscope,* 124**,** 2352-2358.

JUNG, Y., NG, J. H., KEATING, C. P., SENTHIL-KUMAR, P., ZHAO, J., RANDOLPH, M. A., WINOGRAD, J. M. & EVANS, C. L. 2014.

Comprehensive Evaluation of Peripheral Nerve Regeneration in the Acute Healing Phase Using Tissue Clearing and Optical Microscopy in a Rodent Model. *PLoS ONE,* 9.

JUNGEBLUTH, P., ALICI, E., BAIGUERA, S., BLANC, K. L., BLOMBERG, P., BOZÓKY, B., CROWLEY, C., EINARSSON, O., GRINNEMO, K. H., GUDBJARTSSON, T., GUYADER, S. L., HENRIKSSON, G., HERMANSON, O., JUTO, J. E., LEIDNER, B., LILJA, T., LISKA, J., LUEDDE, T., LUNDIN, V., MOLL, G., NILSSON, B., RODERBURG, C., STRÖMBLAD, S., SUTLU, T., TEIXEIRA, A. I., WATZ, E., SEIFALIAN, A. & MACCHIARINI, P. 2011. Tracheobronchial transplantation with a stem-cell-seeded bioartificial nanocomposite: A proof-of-concept study. *The Lancet,* 378**,** 1997-2004.

JUNGEBLUTH, P., BADER, A., BAIGUERA, S., MÖLLER, S., JAUS, M., LIM, M. L., FRIED, K., KJARTANSDÓTTIR, K. R., GO, T., NAVE, H., HARRINGER, W., LUNDIN, V., TEIXEIRA, A. I. & MACCHIARINI, P. 2012. The concept of in vivo airway tissue engineering. *Biomaterials,* 33**,** 4319-4326.

JUNGEBLUTH, P., GO, T., ASNAGHI, A., BELLINI, S., MARTORELL, J., CALORE, C., URBANI, L., OSTERTAG, H., MANTERO, S., CONCONI, M. T. & MACCHIARINI, P. 2009. Structural and morphologic evaluation of a novel detergent–enzymatic tissue-engineered tracheal tubular matrix. *The Journal of Thoracic and Cardiovascular Surgery,* 138**,** 586-593.

JUNGEBLUTH, P., HAAG, J. C., LIM, M. L., LEMON, G., SJÖQVIST, S., GUSTAFSSON, Y., AJALLOUEIAN, F., GILEVICH, I., SIMONSON, O. E., GRINNEMO, K. H., CORBASCIO, M., BAIGUERA, S., DEL GAUDIO, C., STRÖMBLAD, S. & MACCHIARINI, P. 2013. Verification of cell viability in bioengineered tissues and organs before clinical transplantation. *Biomaterials,* 34**,** 4057-4067.

KAJBAFZADEH, A.-M., SABETKISH, S., SABETKISH, N., MUHAMMADNEJAD, S., AKBARZADEH, A., TAVANGAR, S., MOHSENI, M. & AMANPOUR, S. 2015. In-vivo trachea regeneration: fabrication of a tissue-engineered trachea in nude mice using the body as a natural bioreactor. *Surg Today,* 45**,** 1040-1048.

KAMIL, S. H., EAVEY, R. D., VACANTI, M. P., VACANTI, C. A. & HARTNICK, C. J. 2004. Tissue-Engineered Cartilage as a Graft Source for Laryngotracheal Reconstruction: A Pig Model. *Archives of Otolaryngology–Head & Neck Surgery,* 130**,** 1048-1051.

KANDJOV, I. M. 2001. Heat and Water Rate Transfer Processes in the Human Respiratory Tract at Various Altitudes. *Journal of Theoretical Biology,* 208**,** 287-293.

KANZAKI, M., YAMATO, M., HATAKEYAMA, H., KOHNO, C., YANG, J., UMEMOTO, T., KIKUCHI, A., OKANO, T. & ONUKI, T. 2006. Tissue Engineered Epithelial Cell Sheets for the Creation of a Bioartificial Trachea. *Tissue Engineering,* 12**,** 1275-83.

KARP, J. M. & LENG TEO, G. S. 2009. Mesenchymal Stem Cell Homing: The Devil Is in the Details. *Cell Stem Cell,* 4**,** 206-216.

KATO, A., OKAMOTO, O., ISHIKAWA, K., SUMIYOSHI, H., MATSUO, N., YOSHIOKA, H., NOMIZU, M., SHIMADA, T. & FUJIWARA, S. 2011. Dermatopontin interacts with fibronectin, promotes fibronectin fibril

formation, and enhances cell adhesion. *The Journal of biological chemistry,* 286**,** 14861-14869.
KAWECKI, M., LABUS, W., KLAMA-BARYLA, A., KITALA, D., KRAUT, M., GLIK, J., MISIUGA, M., NOWAK, M., BIELECKI, T. & KASPERCZYK, A. 2018. A review of decellurization methods caused by an urgent need for quality control of cell-free extracellular matrix' scaffolds and their role in regenerative medicine. *Journal of Biomedical Materials Research Part B-Applied Biomaterials,* 106**,** 909-923.
KEANE, T. J., LONDONO, R., TURNER, N. J. & BADYLAK, S. F. 2012. Consequences of ineffective decellularization of biologic scaffolds on the host response. *Biomaterials,* 33**,** 1771-1781.
KI, U. H. 2016. The macchiarini case-Investiation of the synthetic transplantation at Karolinska university hospital. Sweden: Karolinska university hospital.
KIM, B. S., PUTNAM, A. J., KULIK, T. J. & MOONEY, D. J. 1998. Optimizing seeding and culture methods to engineer smooth muscle tissue on biodegradable polymer matrices. *Biotechnology and Bioengineering,* 57**,** 46-54.
KIM, H. 2013. Influence of mesenchymal stem cells on cryopreserved tracheal allografts in rabbits. *Korean Journal of Thoracic and Cardiovascular Surgery,* 46**,** 328-339.
KIM, J., KIM, N., PARK, S. & CHOI, B. 2019. GM-CSF Enhances Mobilization of Bone Marrow Mesenchymal Stem Cells via a CXCR4-Medicated Mechanism. *Tissue Eng Regen Med,* 16**,** 59-68.
KIM, J., SUH, S. W., SHIN, J. Y., KIM, J. H., CHOI, Y. S. & KIM, H. 2004. Replacement of a tracheal defect with a tissue-engineered prosthesis: early results from animal experiments. *J Thorac Cardiovasc Surg,* 128**,** 124-9.
KINDT, E., ROSSI, D. T., GUENEVA-BOUCHEVA, K. & HALLAK, H. 2000. Quantitative Method for Biomarkers of Collagen Degradation Using Liquid Chromatography Tandem Mass Spectrometry. *Analytical Biochemistry,* 283**,** 71-76.
KLINKER, M. & WEI, C. 2015. Mesenchymal stem cells in the treatment of inflammatory and autoimmune diseases in experimental animal models. *World Journal Of Stem Cells,* 7**,** 556-567.
KNUDSON, C. B. & KNUDSON, W. 2001. Cartilage proteoglycans. *Seminars in Cell and Developmental Biology,* 12**,** 69-78.
KOBAYASHI, K., NOMOTO, Y., SUZUKI, T., TADA, Y., MIYAKE, M., HAZAMA, A., KANEMARU, S., NAKAMURA, T. & OMORI, K. 2006. Effect of fibroblasts on tracheal epithelial regeneration in vitro. *Tissue engineering,* 12**,** 2619-2628.
KOBAYASHI, K., SUZUKI, T., NOMOTO, Y., TADA, Y., MIYAKE, M., HAZAMA, A., WADA, I., NAKAMURA, T. & OMORI, K. 2010. A tissue-engineered trachea derived from a framed collagen scaffold, gingival fibroblasts and adipose-derived stem cells. *Biomaterials,* 31**,** 4855-63.
KOJIMA, K., BONASSAR, L. J., IGNOTZ, R. A., SYED, K., CORTIELLA, J. & VACANTI, C. A. 2003a. Comparison of tracheal and nasal chondrocytes for tissue engineering of the trachea. *The Annals of Thoracic Surgery,* 76**,** 1884-1888.
KOJIMA, K., BONASSAR, L. J., ROY, A. K., MIZUNO, H., CORTIELLA, J. & VACANTI, C. A. 2003b. A composite tissue-engineered trachea using

sheep nasal chondrocyte and epithelial cells. *FASEB Journal,* 17**,** 823-828.
KOJIMA, K., BONASSAR, L. J., ROY, A. K., VACANTI, C. A. & CORTIELLA, J. 2002. Autologous tissue-engineered trachea with sheep nasal chondrocytes. *The Journal of Thoracic and Cardiovascular Surgery,* 123**,** 1177-1184.
KOJIMA, K., IGNOTZ, R. A., KUSHIBIKI, T., TINSLEY, K. W., TABATA, Y. & VACANTI, C. A. 2004. Tissue-engineered trachea from sheep marrow stromal cells with transforming growth factor β2 released from biodegradable microspheres in a nude rat recipient. *The Journal of Thoracic and Cardiovascular Surgery,* 128**,** 147-153.
KOJIMA, K. & VACANTI, C. A. 2014. Tissue Engineering in the Trachea. *The Anatomical Record,* 297**,** 44-50.
KOMURA, M., KOMURA, H., KANAMORI, Y., TANAKA, Y., SUZUKI, K., SUGIYAMA, M., NAKAHARA, S., KAWASHIMA, H., HATANAKA, A., HOSHI, K., IKADA, Y., TABATA, Y. & IWANAKA, T. 2008. An animal model study for tissue-engineered trachea fabricated from a biodegradable scaffold using chondrocytes to augment repair of tracheal stenosis. *Journal of Pediatric Surgery,* 43**,** 2141-2146.
KOMURA, M., KOMURA, H., OTANI, Y., SUZUKI, K., SATAKE, R., KODAKA, T., TERAWAKI, K., YONEKAWA, H., IKEBUKURO, K., HOSHI, K., TAKATO, T., TABATA, Y., KOMURO, H. & IWANAKA, T. 2015. Tracheoplasty with cartilage-engineered esophagus environments. *J Pediatr Surg,* 50**,** 1093-8.
KRÄMER, A., GREEN, J., POLLARD, J. & TUGENDREICH, S. 2014. Causal analysis approaches in Ingenuity Pathway Analysis. *Bioinformatics,* 30**,** 523-530.
KRAMPERA, M. 2011. Mesenchymal stromal cell 'licensing': a multistep process. *Leukemia,* 25**,** 1408.
KRISHNASWAMY, V., MANIKANDAN, M., MUNIRAJAN, A., VIJAYARAGHAVAN, D. & KORRAPATI, P. 2014. Expression and integrity of dermatopontin in chronic cutaneous wounds: a crucial factor in impaired wound healing. *Cell Tissue Res,* 358**,** 833-841.
KUCHROO, P., DAVE, V., VIJAYAN, A., VISWANATHAN, C. & GHOSH, D. 2015. Paracrine Factors Secreted by Umbilical Cord-Derived Mesenchymal Stem Cells Induce Angiogenesis In Vitro by a VEGF-Independent Pathway. *Stem Cells and Development,* 24**,** 437-450.
KUNISAKI, S. M., FREEDMAN, D. A. & FAUZA, D. O. 2006. Fetal tracheal reconstruction with cartilaginous grafts engineered from mesenchymal amniocytes. *Journal of Pediatric Surgery,* 41**,** 675-682.
KUSUMA, G. D., CARTHEW, J., LIM, R. & FRITH, J. E. 2017. Effect of the Microenvironment on Mesenchymal Stem Cell Paracrine Signaling: Opportunities to Engineer the Therapeutic Effect. *Stem Cells and Development,* 26**,** 617-631.
KUTTEN, J. C., MCGOVERN, D., HOBSON, C. M., LUFFY, S. A., NIEPONICE, A., TOBITA, K., FRANCIS, R. J., REYNOLDS, S. D., ISENBERG, J. S. & GILBERT, T. W. 2015. Decellularized tracheal extracellular matrix supports epithelial migration, differentiation, and function. *Tissue engineering. Part A,* 21**,** 75-84.

KYURKCHIEV, D., BOCHEV, I., IVANOVA-TODOROVA, E., MOURDJEVA, M., ORESHKOVA, T., BELEMEZOVA, K. & KYURKCHIEV, S. 2014. Secretion of immunoregulatory cytokines by mesenchymal stem cells. *World Journal of Stem Cells,* 6**,** 552-570.

LANGE, P., GRECO, K., PARTINGTON, L., CARVALHO, C., OLIANI, S., BIRCHALL, M. A., SIBBONS, P. D., LOWDELL, M. W. & ANSARI, T. 2015. Pilot study of a novel vacuum-assisted method for decellularization of tracheae for clinical tissue engineering applications. *Journal of Tissue Engineering and Regenerative Medicine***,** n/a-n/a.

LANGER, R. & VACANTI, J. 1993. Tissue engineering. *Science,* 260**,** 920-926.

LAVOIE, M. & ABOU ELELA, S. 2008. Yeast ribonuclease III uses a network of multiple hydrogen bonds for RNA binding and cleavage. *Biochemistry,* 47**,** 8514.

LAWLESS, B. M., SADEGHI, H., TEMPLE, D. K., DHALIWAL, H., ESPINO, D. M. & HUKINS, D. W. L. 2017. Viscoelasticity of articular cartilage: Analysing the effect of induced stress and the restraint of bone in a dynamic environment. *Journal of the Mechanical Behavior of Biomedical Materials,* 75**,** 293-301.

LE BLEU, H. K., KAMAL, F. A., KELLY, M., KETZ, J. P., ZUSCIK, M. J. & ELBARBARY, R. A. 2017. Extraction of high-quality RNA from human articular cartilage. *Analytical biochemistry,* 518**,** 134-138.

LEE, C., MOON, K., CHOI, H. & WOO, J. 2002. Tissue engineered tracheal prosthesis with acceleratedly cultured homologous chondrocytes as an alternative of tracheal reconstructionq. *Journal of Cardiovascular Surgery,* 43**,** 275-9.

LEE, J. T. Y., CHEUNG, K. M. C. & LEUNG, V. Y. L. 2015. Extraction of RNA from tough tissues with high proteoglycan content by cryosection, second phase separation and high salt precipitation. *2015*.

LEE, M. J., SONG, H. Y., KIM, M. R., SUNG, S.-M., JUNG, J. S. & KIM, J. H. 2007. Oncostatin M stimulates expression of stromal-derived factor-1 in human mesenchymal stem cells. *International Journal of Biochemistry and Cell Biology,* 39**,** 650-659.

LEVASHOV YU, N., YABLONSKY, P. K., CHERNY, S. M., ORLOV, S. V., SHAFIROVSKY, B. B. & KUZNETZOV, I. M. 1993. One-stage allotransplantation of thoracic segment of the trachea in a patient with idiopathic fibrosing mediastinitis and marked tracheal stenosis. *Eur J Cardiothorac Surg,* 7**,** 383-6.

LI, L., JIANG, G., CHEN, Q. & ZHENG, J. 2015. Ki67 is a promising molecular target in the diagnosis of cancer. *Molecular Medicine Reports,* 11**,** 1566-1572.

LI, M. O., WAN, Y. Y., SANJABI, S., ROBERTSON, A.-K. L. & FLAVELL, R. A. 2006. TRANSFORMING GROWTH FACTOR-β REGULATION OF IMMUNE RESPONSES. 24**,** 99-146.

LI, W., LI, M., CHEN, Y., ZHANG, S. & QI, N. 2014. Various seeding methods for tissue development of human umbilical-cord-derived mesenchymal stem cells in 3-dimensional PET matrix. *Biotechnol Bioproc E,* 19**,** 108-117.

LIANG, X., DING, Y., ZHANG, Y., TSE, H.-F. & LIAN, Q. 2014. Paracrine Mechanisms of Mesenchymal Stem Cell-Based Therapy: Current Status and Perspectives. Los Angeles, CA.

LIN, C.-H., HSU, S.-H., HUANG, C.-E., CHENG, W.-T. & SU, J.-M. 2009. A scaffold-bioreactor system for a tissue-engineered trachea. *Biomaterials,* 30**,** 4117-4126.
LIU, R., GAO, J., YANG, Y. & ZENG, W. 2015. Preparation of Rat Whole-kidney Acellular Matrix via Peristaltic Pump. *Urology Journal,* 12**,** 2457-2461.
LIU, T., ZHANG, L., JOO, D. & SUN, S.-C. 2017. NF-κB signaling in inflammation. *Signal Transduction And Targeted Therapy,* 2**,** 17023.
LLC, R. 2019. *Respiratory system* [Online]. Available: http://www.clker.com [Accessed 2019].
LOHMANDER, L., ROOS, H., DAHLBERG, L. & LARK, M. 1995. The role of molecular markers to monitor disease, intervention and cartilage breakdown in osteoarthritis. *Acta Orthopaedica Scandinavica,* 66**,** 84-87.
LONDONO, R., DZIKI, J. L., HALJASMAA, E., TURNER, N. J., LEIFER, C. A. & BADYLAK, S. F. 2017. The effect of cell debris within biologic scaffolds upon the macrophage response. 105**,** 2109-2118.
LONG, G., SUSAN, T., RENÉE, M. H., CARMEN, T., MASSIMO, L. & BARRETT, J. R. 2000. Control of TH2 polarization by the chemokine monocyte chemoattractant protein-1. *Nature,* 404**,** 407.
LOVETT, M., LEE, K., EDWARDS, A. & KAPLAN, D. L. 2009. Vascularization Strategies for Tissue Engineering. *Tissue Engineering Part B-Reviews,* 15**,** 353-370.
LUO, X., LIU, Y., ZHANG, Z., TAO, R., LIU, Y., HE, A., YIN, Z., LI, D., ZHANG, W., LIU, W., CAO, Y. & ZHOU, G. 2013. Long-term functional reconstruction of segmental tracheal defect by pedicled tissue-engineered trachea in rabbits. *Biomaterials,* 34**,** 3336.
LUO, X., ZHOU, G., LIU, W., ZHANG, W. J., CEN, L., CUI, L. & CAO, Y. 2009. Tubular cartilage engineering in rabbits. *Tubular cartilage engineering in rabbits,* 4**,** 025006.
LUTOLF, M. P. & HUBBELL, J. A. 2005. Synthetic biomaterials as instructive extracellular microenvironments for morphogenesis in tissue engineering. *Nat Biotech,* 23**,** 47-55.
LYNES, M., HIDALGO, J., MANSO, Y., DEVISSCHER, L., LAUKENS, D. & LAWRENCE, D. 2014. Metallothionein and stress combine to affect multiple organ systems. *Cell Stress & Chaperones,* 19**,** 605-11.
MA, S., XIE, N., LI, W., YUAN, B., SHI, Y. & WANG, Y. 2013. Immunobiology of mesenchymal stem cells.
MACCHIARINI, P. & BIRCHALL, M. 2010. Stem-cell hype in tracheal transplantation? A response. *Transplantation,* 90**,** 928-929.
MACCHIARINI, P., JUNGEBLUTH, P., GO, T., ASNAGHI, M. A., REES, L. E., COGAN, T. A., DODSON, A., MARTORELL, J., BELLINI, S., PARNIGOTTO, P. P., DICKINSON, S. C., HOLLANDER, A. P., MANTERO, S., CONCONI, M. T. & BIRCHALL, M. A. 2008. Clinical transplantation of a tissue-engineered airway. *The Lancet,* 372**,** 2023-2030.
MACCHIARINI, P., WALLES, T., BIANCOSINO, C. & MERTSCHING, H. 2004. First human transplantation of a bioengineered airway tissue. *The Journal of Thoracic and Cardiovascular Surgery,* 128**,** 638-641.
MACKLEM, P. T. & MEAD, J. 1968. Factors determining maximum expiratory flow in dogs. *Journal of applied physiology,* 25**,** 159.

MAJDA, D., BHATTARAI, A., RIIKONEN, J., NAPRUSZEWSKA, B. D., ZIMOWSKA, M., MICHALIK-ZYM, A., TÖYRÄS, J. & LEHTO, V. P. 2017. New approach for determining cartilage pore size distribution: NaCl-thermoporometry. *Microporous and Mesoporous Materials,* 241**,** 238-245.
MALVÈ, M., DEL PALOMAR, A. P., TRABELSI, O., LÓPEZ-VILLALOBOS, J., GINEL, A. & DOBLARÉ, M. 2011. Modeling of the fluid structure interaction of a human trachea under different ventilation conditions. *International Communications in Heat and Mass Transfer,* 38**,** 10-15.
MARCHANT, W. 2005. Anatomy of the larynx, trachea and bronchi. *Anaesthesia and Intensive Care Medicine,* 6**,** 253-255.
MARTIN, D. E. 1988. *Respiratory anatomy and physiology / David E. Martin, John W. Youtsey,* St. Louis, St. Louis : Mosby.
MARTIN, I., WENDT, D. & HEBERER, M. 2004. The role of bioreactors in tissue engineering. *Trends in Biotechnology,* 22**,** 80-86.
MARTINDALE, J. L. & HOLBROOK, N. J. 2002. Cellular response to oxidative stress: Signaling for suicide and survival*. New York.
MATSUNAGA, K., FUJISAWA, K., TAKAMI, T., BURGANOVA, G., SASAI, N., MATSUMOTO, T., YAMAMOTO, N. & SAKAIDA, I. 2019. NUPR1 acts as a pro-survival factor in human bone marrow-derived mesenchymal stem cells and is induced by the hypoxia mimetic reagent deferoxamine. *Journal of Clinical Biochemistry and Nutrition,* advpub.
MAUGHAN, E. F., HYNDS, R. E., PROCTOR, T. J., JANES, S. M., ELLIOTT, M., BIRCHALL, M. A., LOWDELL, M. W. & DE COPPI, P. 2017. Autologous Cell Seeding in Tracheal Tissue Engineering. *Current Stem Cell Reports,* 3**,** 279-289.
MAUMUS, M., JORGENSEN, C. & NOËL, D. 2013. Mesenchymal stem cells in regenerative medicine applied to rheumatic diseases: Role of secretome and exosomes. *Biochimie,* 95**,** 2229-2234.
MAXSON, S., LOPEZ, E. A., YOO, D., DANILKOVITCH - MIAGKOVA, A. & LEROUX, M. A. 2012. Concise Review: Role of Mesenchymal Stem Cells in Wound Repair. *STEM CELLS Translational Medicine,* 1**,** 142-149.
MCDEVITT, C. A., WILDEY, G. M. & CUTRONE, R. M. 2003. Transforming growth factor-β1 in a sterilized tissue derived from the pig small intestine submucosa. *Journal of Biomedical Materials Research Part A,* 67**,** 637-640.
MCKEE, C. & CHAUDHRY, G. R. 2017. Advances and challenges in stem cell culture. *Colloids and Surfaces B: Biointerfaces,* 159**,** 62-77.
MEEZAN, E., HJELLE, J. T., BRENDEL, K. & CARLSON, E. C. 1975. A simple, versatile, nondisruptive method for the isolation of morphologically and chemically pure basement membranes from several tissues. *Life Sciences,* 17**,** 1721-1732.
MINGUELL, J. J., ALLERS, C. & LASALA, G. P. 2013. Mesenchymal Stem Cells and the Treatment of Conditions and Diseases: The Less Glittering Side of a Conspicuous Stem Cell for Basic Research. *Stem Cells and Development,* 22**,** 193-203.
MINNICH, D. J. & MATHISEN, D. J. 2007. Anatomy of the trachea, carina, and bronchi. *Thoracic surgery clinics,* 17**,** 571-585.
MOHD HEIKAL, M. Y., AMINUDDIN, B. S., JEEVANAN, J., CHEN, H. C., SHARIFAH, S. H. & RUSZYMAH, B. H. I. 2010. Autologous Implantation of Bilayered Tissue-Engineered Respiratory Epithelium for Tracheal

Mucosal Regenesis in a Sheep Model. *Cells Tissues Organs,* 192**,** 292-302.
MORRIS, A. H., STAMER, D. K. & KYRIAKIDES, T. R. 2017. The host response to naturally-derived extracellular matrix biomaterials. *Seminars in Immunology,* 29**,** 72-91.
MORRISSEY, M. A. & SHERWOOD, D. R. 2015. An active role for basement membrane assembly and modification in tissue sculpting. *Journal of cell science,* 128**,** 1661-1668.
MORTICELLI, L., THOMAS, D., ROBERTS, N., INGHAM, E. & KOROSSIS, S. 2013. Investigation of the suitability of decellularized porcine pericardium in mitral valve reconstruction. *J Heart Valve Dis,* 22**,** 340-53.
MOSMANN, T. 1983. Rapid colorimetric assay for cellular growth and survival: Application to proliferation and cytotoxicity assays. *Journal of Immunological Methods,* 65**,** 55-63.
MOUSAVIZADEH, R., SCOTT, A., LU, A., ARDEKANI, G. S., BEHZAD, H., LUNDGREEN, K., GHAFFARI, M., MCCORMACK, R. G. & DURONIO, V. 2016. Angiopoietin-like 4 promotes angiogenesis in the tendon and is increased in cyclically loaded tendon fibroblasts. *The Journal of physiology,* 594**,** 2971-2983.
MOY, A. J., LO, P. C. & CHOI, B. 2013. High-resolution visualization of mouse cardiac microvasculature using optical histology. *Biomedical optics express,* 5**,** 69.
MULLIKEN, J. B. & GRILLO, H. C. 1968. The limits of tracheal resection with primary anastomosis: further anatomical studies in man. *J Thorac Cardiovasc Surg,* 55**,** 418-21.
MURISON, P. J., JONES, A., MITCHARD, L., BURT, R. & BIRCHALL, M. A. 2009. Development of perioperative care for pigs undergoing laryngeal transplantation: a case series. *Laboratory Animals,* 43**,** 338-343.
MURPHY, M. B., MONCIVAIS, K. & CAPLAN, A. I. 2013. Mesenchymal stem cells: environmentally responsive therapeutics for regenerative medicine. *Experimental & molecular medicine,* 45**,** e54.
NAGATA, S., HANAYAMA, R. & KAWANE, K. 2010. Autoimmunity and the clearance of dead cells. *Cell,* 140**,** 619.
NAKAGAWA, T., TSURUOKA, M., OGURA, H., OKUYAMA, Y., ARIMA, Y., HIRANO, T. & MURAKAMI, M. 2010. IL-6 positively regulates Foxp3+CD8+ T cells in vivo. *International immunology,* 22**,** 129.
NAKAMURA, T., OHMORI, K. & KANEMARU, S.-I. 2011. Tissue-engineered airway and “in situ tissue engineering”. *Gen Thorac Cardiovasc Surg,* 59**,** 91-97.
NAKAMURA, T., SATO, T., ARAKI, M., ICHIHARA, S., NAKADA, A., YOSHITANI, M., ITOI, S.-I., YAMASHITA, M., KANEMARU, S.-I., OMORI, K., HORI, Y., ENDO, K., INADA, Y. & HAYAKAWA, K. 2009. In situ tissue engineering for tracheal reconstruction using a luminar remodeling type of artificial trachea. *The Journal of Thoracic and Cardiovascular Surgery,* 138**,** 811-819.
NEHRER, S., BREINAN, H. A., RAMAPPA, A., YOUNG, G., SHORTKROFF, S., LOUIE, L. K., SLEDGE, C. B., YANNAS, I. V. & SPECTOR, M. 1997. Matrix collagen type and pore size influence behaviour of seeded canine chondrocytes. *Biomaterials,* 18**,** 769-776.

NEVILLE, W. E., BOLANOWSKI, J. P. & KOTIA, G. G. 1990. Clinical experience with the silicone tracheal prosthesis. *J Thorac Cardiovasc Surg,* 99**,** 604-12; discussion 612-3.
NEVILLE, W. E., BOLANOWSKI, P. J. & SOLTANZADEH, H. 1976. Homograft replacement of the trachea using immunosuppression. *J Thorac Cardiovasc Surg,* 72**,** 596-601.
NG, K. W., DAVID, T. W. L. & HUTMACHER, D. W. 2005. The Challenge to Measure Cell Proliferation in Two and Three Dimensions. *Tissue Engineering,* 11**,** 182-91.
NICHOLSON, A. W. 2001. *Ribonucleases edited by Allen W. Nicholson,* San Diego
London, San Diego
London : Academic Press.
NIEPONICE, A., SOLETTI, L., GUAN, J., DEASY, B. M., HUARD, J., WAGNER, W. R. & VORP, D. A. 2008. Development of a tissue-engineered vascular graft combining a biodegradable scaffold, muscle-derived stem cells and a rotational vacuum seeding technique. *Biomaterials,* 29**,** 825-833.
NOMOTO, Y., KOBAYASHI, K., TADA, Y., WADA, I., NAKAMURA, T. & OMORI, K. 2008. Effect of Fibroblasts on Epithelial Regeneration on the Surface of a Bioengineered Trachea. *Annals of Otology, Rhinology & Laryngology,* 117**,** 59-64.
NOMOTO, Y., OKANO, W., IMAIZUMI, M., TANI, A., NOMOTO, M. & OMORI, K. 2012. Bioengineered prosthesis with allogenic heterotopic fibroblasts for cricoid regeneration. *The Laryngoscope,* 122**,** 805-809.
O' BRIEN, J., WILSON, I., ORTON, T. & POGNAN, F. 2000. Investigation of the Alamar Blue (resazurin) fluorescent dye for the assessment of mammalian cell cytotoxicity. *European Journal of Biochemistry,* 267**,** 5421-5426.
O'LEARY, C., GILBERT, J. L., O'DEA, S., O'BRIEN, F. J. & CRYAN, S.-A. 2015. Respiratory Tissue Engineering: Current Status and Opportunities for the Future. *Tissue Engineering Part B: Reviews,* 21**,** 323-344.
OGURA, T., TSUCHIYA, A., MINAS, T. & MIZUNO, S. 2015. Methods of high integrity RNA extraction from cell/agarose construct. *BMC Res Notes,* 8**,** 644.
OHKIMOTO, K., MOURI, M., AMATSU, M. & TERAOKA, M. 1997. Histological study of the tracheal adventitia, perichondrium and annular ligament. *Nihon Jibiinkoka Gakkai kaiho,* 100**,** 1394.
OKAMOTO, O. & FUJIWARA, S. 2006. Dermatopontin, a Novel Player in the Biology of the Extracellular Matrix. Taylor & Francis.
OMORI, K., NAKAMURA, T., KANEMARU, S., ASATO, R., YAMASHITA, M., TANAKA, S., MAGRUFOV, A., ITO, J. & SHIMIZU, Y. 2005. Regenerative Medicine of the Trachea: The First Human Case. *Annals of Otology, Rhinology & Laryngology,* 114**,** 429-433.
OMORI, K., TADA, Y., SUZUKI, T., NOMOTO, Y., MATSUZUKA, T., KOBAYASHI, K., NAKAMURA, T., KANEMARU, S., YAMASHITA, M. & ASATO, R. 2008. Clinical Application of in Situ Tissue Engineering Using a Scaffolding Technique for Reconstruction of the Larynx and Trachea. *Annals of Otology, Rhinology & Laryngology,* 117**,** 673-678.
ORTIZ, L. A., DUTREIL, M., FATTMAN, C., PANDEY, A. C., TORRES, G., GO, K. & PHINNEY, D. G. 2007. Interleukin 1 receptor antagonist mediates the antiinflammatory and antifibrotic effect of mesenchymal stem cells during

lung injury. *Proceedings of the National Academy of Sciences of the United States of America,* 104**,** 11002-11007.
OTT, H. C. & MATHISEN, D. J. 2011. Bioartificial tissues and organs: are we ready to translate? *The Lancet,* 378**,** 1977-1978.
OTT, H. C., MATTHIESEN, T. S., GOH, S. K., BLACK, L. D., KREN, S. M., NETOFF, T. I. & TAYLOR, D. A. 2008. Perfusion-decellularized matrix: using nature's platform to engineer a bioartificial heart. *Nature Medicine,* 14**,** 213-221.
OTT, L. M., WEATHERLY, R. A. & DETAMORE, M. S. 2011. Overview of Tracheal Tissue Engineering: Clinical Need Drives the Laboratory Approach. *Annals of Biomedical Engineering,* 39**,** 2091-2113.
OWEN, C., NOTINGHER, I., HILL, R., STEVENS, M. & HENCH, L. 2006. Progress in Raman spectroscopy in the fields of tissue engineering, diagnostics and toxicological testing. *J Mater Sci: Mater Med,* 17**,** 1019-1023.
PARK, C. W., KIM, K.-S., BAE, S., SON, H. K., MYUNG, P.-K., HONG, H. J. & KIM, H. 2009. Cytokine secretion profiling of human mesenchymal stem cells by antibody array. *International journal of stem cells,* 2**,** 59.
PARMAKSIZ, M., DOGAN, A., ODABAS, S., ELÇIN, A. E. & ELÇIN, Y. M. 2016. Clinical applications of decellularized extracellular matrices for tissue engineering and regenerative medicine.
PARMAKSIZ, M., ELCIN, A. E. & ELCIN, Y. M. 2017. Decellularization of bovine small intestinal submucosa and its use for the healing of a critical-sized full-thickness skin defect, alone and in combination with stem cells, in a small rodent model. *Journal of Tissue Engineering and Regenerative Medicine,* 11**,** 1754-1765.
PARTINGTON, L., MORDAN, N., MASON, C., KNOWLES, J., KIM, H., LOWDELL, M., BIRCHALL, M. A. & WALL, I. 2013. Biochemical changes caused by decellularization may compromise mechanical integrity of tracheal scaffolds. *Acta biomaterialia,* 9**,** 5251-5261.
PATEL, N. M., YAZDI, I. K., TASCIOTTI, E. & BIRLA, R. K. 2016. Optimizing cell seeding and retention in a three-dimensional bioengineered cardiac ventricle: The two-stage cellularization model. *Biotechnology and Bioengineering,* 113**,** 2275-2285.
PAWLOWSKI, K. J., RITTGERS, S. E., SCHMIDT, S. P. & BOWLIN, G. L. 2004. Endothelial cell seeding of polymeric vascular grafts. *Front Biosci,* 9**,** 1412-21.
PAZZANO, D., MERCIER, K. A., MORAN, J. M., FONG, S. S., DIBIASIO, D. D., RULFS, J. X., KOHLES, S. S. & BONASSAR, L. J. 2000. Comparison of Chondrogensis in Static and Perfused Bioreactor Culture. *Biotechnology Progress,* 16**,** 893-896.
PEREZ, R. A. & MESTRES, G. 2016. Role of pore size and morphology in musculo-skeletal tissue regeneration. *Materials Science & Engineering C,* 61**,** 922-939.
PERSAUD, L., DE JESUS, D., BRANNIGAN, O., RICHIEZ-PAREDES, M., HUAMAN, J., ALVARADO, G., RIKER, L., MENDEZ, G., DEJOIE, J. & SAUANE, M. 2016. Mechanism of Action and Applications of Interleukin 24 in Immunotherapy. *International journal of molecular sciences,* 17**,** 869.
PETERSEN, T. H., CALLE, E. A., ZHAO, L., LEE, E. J., GUI, L., RAREDON, M. B., GAVRILOV, K., YI, T., ZHUANG, Z. W., BREUER, C., HERZOG, E. &

NIKLASON, L. E. 2010. Tissue-engineered lungs for in vivo implantation. *Science (New York, N.Y.),* 329**,** 538.
PFAFFL, M. W. 2001. A new mathematical model for relative quantification in real-time RT-PCR. *Nucleic acids research,* 29**,** e45-e45.
PHILIPP, J., JOHANNES, C. H., SEBASTIAN, S., YLVA, G., ANTONIO BELTRÁN, R., COSTANTINO DEL, G., ALESSANDRA, B., IVAR, D., PER, U., SILVIA, B., GREG, L., MEI LING, L. & PAOLO, M. 2014. Tracheal tissue engineering in rats. *Nature Protocols,* 9**,** 2164.
PLAYER, S. 2019. *The respiratory system* [Online]. Available: https://slideplayer.com/slide/4921818/ [Accessed 2019].
PLUNKETT, N. & O'BRIEN, F. J. 2011. Bioreactors in tissue engineering. *Technology and Health Care,* 19**,** 55-69.
PONOMARENKO, M., STEPANENKO, I. & KOLCHANOV, N. 2013. Heat Shock Proteins. *In:* MALOY, S. & HUGHES, K. (eds.) *Brenner's Encyclopedia of Genetics (Second Edition).* San Diego: Academic Press.
PROPST, E. J., PRAGER, J. D., MEINZEN-DERR, J., CLARK, S. L., COTTON, R. T. & RUTTER, M. J. 2011. Pediatric Tracheal Reconstruction Using Cadaveric Homograft. *Archives of Otolaryngology–Head & Neck Surgery,* 137**,** 583-590.
QIN, Z., MUSTAFA, R., YU, C., YUKA, S., TOLGA, S., WOLFGANG, J., KARIM, B., KIYOSHI, I. & CARL, J. H. 2010. Circulating mitochondrial DAMPs cause inflammatory responses to injury. *Nature,* 464**,** 104.
RAIMONDI, M. T., BOSCHETTI, F., FALCONE, L., MIGLIAVACCA, F., REMUZZI, A. & DUBINI, G. 2004. The effect of media perfusion on three-dimensional cultures of human chondrocytes: integration of experimental and computational approaches. *Biorheology,* 41**,** 401.
RAINS, J. K., BERT, J. L., ROBERTS, C. R. & PARE, P. D. 1992. Mechanical properties of human tracheal cartilage. *J Appl Physiol (1985),* 72**,** 219-25.
RAMADAN, S., PAUL, N. & NAGUIB, H. E. 2017. Standardized static and dynamic evaluation of myocardial tissue properties. *Standardized static and dynamic evaluation of myocardial tissue properties,* 12**,** 025013.
RAMPERSAD, S. 2012. Multiple Applications of Alamar Blue as an Indicator of Metabolic Function and Cellular Health in Cell Viability Bioassays. *Sensors,* 12**,** 12347-12360.
RAWLINS, E. L. & HOGAN, B. L. M. 2008. Ciliated epithelial cell lifespan in the mouse trachea and lung. *American Journal of Physiology. Lung Cellular and Molecular Physiology,* 295**,** L231-L234.
REHMAN, J. J., TRAKTUEV, E. D., LI, L. J., MERFELD-CLAUSS, H. S., TEMM-GROVE, V. C., BOVENKERK, L. J., PELL, L. C., JOHNSTONE, L. B., CONSIDINE, L. R. & MARCH, L. K. 2004. Secretion of Angiogenic and Antiapoptotic Factors by Human Adipose Stromal Cells. *Circulation: Journal of the American Heart Association,* 109**,** 1292-1298.
REING, J. E., BROWN, B. N., DALY, K. A., FREUND, J. M., GILBERT, T. W., HSIONG, S. X., HUBER, A., KULLAS, K. E., TOTTEY, S., WOLF, M. T. & BADYLAK, S. F. 2010. The effects of processing methods upon mechanical and biologic properties of porcine dermal extracellular matrix scaffolds. *Biomaterials,* 31**,** 8626-8633.
REN, X., TAPIAS, L. F., JANK, B. J., MATHISEN, D. J., LANUTI, M. & OTT, H. C. 2015. Ex vivo non-invasive assessment of cell viability and proliferation in bio-engineered whole organ constructs. *Biomaterials,* 52**,** 103-112.

REVELL, C. M. & ATHANASIOU, K. A. 2009. Success rates and immunologic responses of autogenic, allogenic, and xenogenic treatments to repair articular cartilage defects. *Tissue engineering. Part B, Reviews,* 15**,** 1-15.

RHEE, K., LEE, J. & EOM, Y. 2015. Mesenchymal Stem Cell-Mediated Effects of Tumor Support or Suppression. *International Journal Of Molecular Sciences,* 16**,** 30015-30033.

ROBERTS, C. & PARE, P. 1991. Composition changes in human tracheal cartilage in growth and aging, including changes in proteoglycan structure. *American Journal of Physiology-Lung Cellular and Molecular Physiology,* 261**,** L92-L101.

ROBERTS, C. R., RAINS, J. K., PARÉ, P. D., WALKER, D. C., WIGGS, B. & BERT, J. L. 1997. Ultrastructure and tensile properties of human tracheal cartilage. *Journal of Biomechanics,* 31**,** 81-86.

ROSE, K. G., SESTERHENN, K. & WUSTROW, F. 1979. TRACHEAL ALLOTRANSPLANTATION IN MAN. *The Lancet,* 313**,** 433-433.

RUETTGER, A., NEUMANN, S., WIEDERANDERS, B. & HUBER, R. 2010. Comparison of different methods for preparation and characterization of total RNA from cartilage samples to uncover osteoarthritis in vivo. *BMC research notes,* 3**,** 7-7.

RUOSLAHTI, E. 1984. Fibronectin in cell adhesion and invasion. *Cancer and Metastasis Reviews,* 3**,** 43-51.

RUSZYMAH, B. H. I., CHUA, K., LATIF, M. A., HUSSEIN, F. N. & SAIM, A. B. 2005. Formation of in vivo tissue engineered human hyaline cartilage in the shape of a trachea with internal support. *International Journal of Pediatric Otorhinolaryngology,* 69**,** 1489-1495.

RUTTKAY-NEDECKY, B., NEJDL, L., GUMULEC, J., ZITKA, O., MASARIK, M., ECKSCHLAGER, T., STIBOROVA, M., ADAM, V. & KIZEK, R. 2013. The Role of Metallothionein in Oxidative Stress. *International Journal of Molecular Sciences,* 14**,** 6044-6066.

SAFSHEKAN, F., TAFAZZOLI-SHADPOUR, M., ABDOUSS, M., BEHGAM SHADMEHR, M. & GHORBANI, F. 2017a. Investigation of the Mechanical Properties of the Human Tracheal Cartilage. *Tanaffos,* 16**,** 107-114.

SAFSHEKAN, F., TAFAZZOLI-SHADPOUR, M., ABDOUSS, M. & SHADMEHR, M. B. 2017b. Viscoelastic Properties of Human Tracheal Tissues. *J Biomech Eng,* 139.

SAKATA, J., VACANTI, C. A., SCHLOO, B., HEALY, G. B., LANGER, R. & VACANTI, J. P. 1994. Tracheal composites tissue engineered from chondrocytes, tracheal epithelial cells, and synthetic degradable scaffolding. *Transplant Proc,* 26**,** 3309-10.

SALACINSKI, H. J., TIWARI, A., HAMILTON, G. & SEIFALIAN, A. M. 2001. Cellular engineering of vascular bypass grafts: Role of chemical coatings for enhancing endothelial cell attachment. *Medical and Biological Engineering and Computing,* 39**,** 609-618.

SALASSA, J. R., PEARSON, B. W. & PAYNE, W. S. 1977. Gross and microscopical blood supply of the trachea. *Ann Thorac Surg,* 24**,** 100-7.

SALCEDO, R., PONCE, M. L., YOUNG, H. A., WASSERMAN, K., WARD, J. M., KLEINMAN, H. K., OPPENHEIM, J. J. & MURPHY, W. J. 2000. Human endothelial cells express CCR2 and respond to MCP-1: direct role of MCP-1 in angiogenesis and tumor progression. *Blood,* 96**,** 34.

SALZIG, D., LEBER, J., MERKEWITZ, K., LANGE, M. C., KÖSTER, N. & CZERMAK, P. 2016. Attachment, Growth, and Detachment of Human Mesenchymal Stem Cells in a Chemically Defined Medium. *Stem Cells International,* 2016.

SANTACRUZ, J. F. & MEHTA, A. C. 2009. Airway complications and management after lung transplantation: ischemia, dehiscence, and stenosis. *Proceedings of the American Thoracic Society,* 6**,** 79.

SATO, M. & BREMNER, I. 1993. Oxygen free radicals and metallothionein.

SATO, T., ARAKI, M., NAKAJIMA, N., OMORI, K. & NAKAMURA, T. 2010. Biodegradable polymer coating promotes the epithelization of tissue-engineered airway prostheses. *The Journal of Thoracic and Cardiovascular Surgery,* 139**,** 26-31.

SCHELLER, J., CHALARIS, A., SCHMIDT-ARRAS, D. & ROSE-JOHN, S. 2011. The pro- and anti-inflammatory properties of the cytokine interleukin-6. *BBA - Molecular Cell Research,* 1813**,** 878-888.

SCHLIE-WOLTER, S., NGEZAHAYO, A. & CHICHKOV, B. N. 2013. The selective role of ECM components on cell adhesion, morphology, proliferation and communication in vitro. *Experimental cell research,* 319**,** 1553.

SCHOLZEN, T. & GERDES, J. 2000. The Ki-67 protein: From the known and the unknown. New York.

SCHULZ, R. & BADER, A. 2007. Cartilage tissue engineering and bioreactor systems for the cultivation and stimulation of chondrocytes. *Eur Biophys J,* 36**,** 539-568.

SCOTT, G. D., BLUM, E. D., FRYER, A. D. & JACOBY, D. B. 2014. Tissue optical clearing, three-dimensional imaging, and computer morphometry in whole mouse lungs and human airways. *American journal of respiratory cell and molecular biology,* 51**,** 43.

SEGUIN, A., BACCARI, S., HOLDER-ESPINASSE, M., BRUNEVAL, P., CARPENTIER, A., TAYLOR, D. A. & MARTINOD, E. 2013. Tracheal regeneration: evidence of bone marrow mesenchymal stem cell involvement. *The Journal of thoracic and cardiovascular surgery,* 145**,** 1297.

SEGUIN, A., RADU, D., HOLDER-ESPINASSE, M., BRUNEVAL, P., FIALAIRE-LEGENDRE, A., DUTERQUE-COQUILLAUD, M., CARPENTIER, A. & MARTINOD, E. 2009. Tracheal Replacement With Cryopreserved, Decellularized, or Glutaraldehyde-Treated Aortic Allografts. *The Annals of Thoracic Surgery,* 87**,** 861-867.

SHAIK, S., HAYES, D., GIMBLE, J. & DEVIREDDY, R. 2017. Inducing Heat Shock Proteins Enhances the Stemness of Frozen–Thawed Adipose Tissue-Derived Stem Cells. *Stem Cells and Development,* 26**,** 68-616.

SHERWOOD, J. K., RILEY, S. L., PALAZZOLO, R., BROWN, S. C., MONKHOUSE, D. C., COATES, M., GRIFFITH, L. G., LANDEEN, L. K. & RATCLIFFE, A. 2002. A three-dimensional osteochondral composite scaffold for articular cartilage repair. *Biomaterials,* 23**,** 4739-4751.

SHIMIZU, K., ITO, A., ARINOBE, M., MURASE, Y., IWATA, Y., NARITA, Y., KAGAMI, H., UEDA, M. & HONDA, H. 2007. Effective cell-seeding technique using magnetite nanoparticles and magnetic force onto decellularized blood vessels for vascular tissue engineering. *Journal of Bioscience and Bioengineering,* 103**,** 472-478.

SHULTZ, L. D., ISHIKAWA, F. & GREINER, D. L. 2007. Humanized mice in translational biomedical research. *Nat Rev Immunol,* 7**,** 118-30.
SHUTTERSTOCK. 2019. *Trachea* [Online]. Available: https://www.shutterstock.com/home [Accessed 2019].
SI, H., ZHANG, Y., SONG, Y. & LI, L. 2018. Overexpression of adrenomedullin protects mesenchymal stem cells against hypoxia and serum deprivation-induced apoptosis via the Akt/GSK3β and Bcl-2 signaling pathways. *International journal of molecular medicine,* 41**,** 3342-3352.
SILVESTRI, L., COSTANTINI, I., SACCONI, L. & PAVONE, F. 2016. Clearing of fixed tissue: a review from a microscopist's perspective. *Journal Of Biomedical Optics,* 21.
SIMON-ASSMANN, P., OREND, G., MAMMADOVA-BACH, E., SPENLÉ, C. & LEFEBVRE, O. 2011. Role of laminins in physiological and pathological angiogenesis. *International Journal of Developmental Biology,* 55**,** 455-465.
SIMONE, F., ADRIENNE, M. G., OSAMU, H. & AFSHIN, S. 2010. Cellular Stress Responses: Cell Survival and Cell Death. *International Journal of Cell Biology,* 2010.
SKIBINSKI, G., ELBORN, J. S. & ENNIS, M. 2007. Bronchial epithelial cell growth regulation in fibroblast cocultures: the role of hepatocyte growth factor. *American journal of physiology. Lung cellular and molecular physiology,* 293**,** L69.
SOLETTI, L., NIEPONICE, A., GUAN, J., STANKUS, J. J., WAGNER, W. R. & VORP, D. A. 2006. A seeding device for tissue engineered tubular structures. *Biomaterials,* 27**,** 4863-4870.
SONG, H. H. G., RUMMA, R. T., OZAKI, C. K., EDELMAN, E. R. & CHEN, C. S. 2018. Vascular Tissue Engineering: Progress, Challenges, and Clinical Promise. *Cell Stem Cell,* 22**,** 340-354.
SOTRES-VEGA, A., BALTAZARES-LIPP, M., VILLALBA-CALOCA, J., GAXIOLA-GAXIOLA, M. O., SANTIBAÑEZ-SALGADO, J. A., OLMOS-ZÚÑIGA, J. R. & JASSO-VICTORIA, R. 2009. Tracheal cryopreservation: caspase-3 immunoreactivity in tracheal epithelium and in mixed glands. *Brazilian Journal of Medical and Biological Research,* 42**,** 1156-1162.
SPECTOR, M. 2016. Decellularized tissues and organs: an historical perspective and prospects for the future. *Decellularized tissues and organs: an historical perspective and prospects for the future,* 11**,** 020201.
STAMENKOVIC, I. 2003. Extracellular matrix remodelling: the role of matrix metalloproteinases. *In:* BOSMAN, F. T. & STAMENKOVIC, I. (eds.). Chichester, UK.
STREULI, C. 1999. Extracellular matrix remodelling and cellular differentiation. *Current Opinion in Cell Biology,* 11**,** 634-640.
SUKI, B. 2014. Assessing the Functional Mechanical Properties of Bioengineered Organs With Emphasis on the Lung. *Journal of Cellular Physiology,* 229**,** 1134-1140.
SUN, S. & KARSDAL, M. A. 2016. Chapter 6 - Type VI Collagen. *In:* KARSDAL, M. A. (ed.) *Biochemistry of Collagens, Laminins and Elastin.* Academic Press.
SUN, Y., YAN, L., CHEN, S. & PEI, M. 2018. Functionality of decellularized matrix in cartilage regeneration: A comparison of tissue versus cell sources. *Acta Biomaterialia,* 74**,** 56-73.

SUTHERLAND, A. J., CONVERSE, G. L., HOPKINS, R. A. & DETAMORE, M. S. 2015. The bioactivity of cartilage extracellular matrix in articular cartilage regeneration. *Advanced healthcare materials,* 4**,** 29-39.

SUZUKI, T., KOBAYASHI, K., TADA, Y., SUZUKI, Y., WADA, I., NAKAMURA, T. & OMORI, K. 2008. Regeneration of the Trachea Using a Bioengineered Scaffold with Adipose-Derived Stem Cells. *Annals of Otology, Rhinology & Laryngology,* 117**,** 453-463.

SYKES, M. 2010. Immune Evasion by Chimeric Trachea. *The New England Journal of Medicine,* 362**,** 172-174.

TADA, Y., SUZUKI, T., TAKEZAWA, T., NOMOTO, Y., KOBAYASHI, K., NAKAMURA, T. & OMORI, K. 2008. Regeneration of Tracheal Epithelium Utilizing a Novel Bipotential Collagen Scaffold. *Annals of Otology, Rhinology & Laryngology,* 117**,** 359-365.

TAKAHASHI, S. 2012. Molecular functions of metallothionein and its role in hematological malignancies. *Journal of Hematology & Oncology,* 5**,** 41.

TAN, Q., HILLINGER, S., VAN BLITTERSWIJK, C. A. & WEDER, W. 2009. Intra-scaffold continuous medium flow combines chondrocyte seeding and culture systems for tissue engineered trachea construction. *Interactive cardiovascular and thoracic surgery,* 8**,** 27-30.

TAN, Q., STEINER, R., YANG, L., WELTI, M., NEUENSCHWANDER, P., HILLINGER, S. & WEDER, W. 2007. Accelerated angiogenesis by continuous medium flow with vascular endothelial growth factor inside tissue-engineered trachea. *European Journal of Cardio-Thoracic Surgery,* 31**,** 806-811.

TANJORE, H. & KALLURI, R. 2006. The role of type IV collagen and basement membranes in cancer progression and metastasis. *The American journal of pathology,* 168**,** 715-717.

TAPIAS, L. F., GILPIN, S. E., REN, X., WEI, L., FUCHS, B. C., TANABE, K. K., LANUTI, M. & OTT, H. C. 2015. Assessment of Proliferation and Cytotoxicity in a Biomimetic Three-Dimensional Model of Lung Cancer. *The Annals of Thoracic Surgery,* 100**,** 414-421.

TENG, Z., OCHOA, I., LI, Z., LIAO, Z., LIN, Y. & DOBLARE, M. 2009a. Study on tracheal collapsibility, compliance, and stress by considering nonlinear mechanical property of cartilage. *Ann Biomed Eng,* 37**,** 2380-9.

TENG, Z. Z., OCHOA, I., LI, Z. Y. & DOBLARE, M. 2009b. Study of tracheal collapsibility, compliance and stress by considering its asymmetric geometry. *Medical Engineering & Physics,* 31**,** 328-336.

TENG, Z. Z., OCHOA, I., LI, Z. Y., LIN, Y. H., RODRIGUEZ, J. F., BEA, J. A. & DOBLARE, M. 2008. Nonlinear mechanical property of tracheal cartilage: A theoretical and experimental study. *Journal of Biomechanics,* 41**,** 1995-2002.

TENG, Z. Z., TRABELSI, O., OCHOA, I., HE, J., GILLARD, J. H. & DOBLARE, M. 2012. Anisotropic material behaviours of soft tissues in human trachea: An experimental study. *Journal of Biomechanics,* 45**,** 1717-1723.

THE, L. 2018. The final verdict on Paolo Macchiarini: guilty of misconduct. *The Lancet,* 392**,** 2.

THE LANCET, E. 2016. Expression of concern—Tracheobronchial transplantation with a stem-cell-seeded bioartificial nanocomposite: a proof-of-concept study. *The Lancet,* 387**,** 1359-1359.

TRABELSI, O., DEL PALOMAR, A. P., LOPEZ-VILLALOBOS, J. L., GINEL, A. & DOBLARE, M. 2010. Experimental characterization and constitutive modeling of the mechanical behavior of the human trachea. *Med Eng Phys,* 32**,** 76-82.

TSAO, C.-K., KO, C.-Y., YANG, S.-R., YANG, C.-Y., BREY, E. M., HUANG, S., CHU, I. M. & CHENG, M.-H. 2014. An ectopic approach for engineering a vascularized tracheal substitute. *Biomaterials,* 35**,** 1163-1175.

UCL 2017. Special Inquiry into Regenerative Medicine Research at UCL.

UDELSMAN, B., MATHISEN, D. J. & OTT, H. C. 2018. A reassessment of tracheal substitutes-a systematic review. *Annals of Cardiothoracic Surgery,* 7**,** 175-182.

URBANI, L., CAMILLI, C., PHYLACTOPOULOS, D.-E., CROWLEY, C., NATARAJAN, D., SCOTTONI, F., MAGHSOUDLOU, P., MCCANN, C. J., PELLEGATA, A. F., URCIUOLO, A., DEGUCHI, K., KHALAF, S., ARUTA, S. F., SIGNORELLI, M. C., KIELY, D., HANNON, E., TREVISAN, M., WONG, R. R., BARADEZ, M. O., MOULDING, D., VIRASAMI, A., GJINOVCI, A., LOUKOGEORGAKIS, S., MANTERO, S., THAPAR, N., SEBIRE, N., EATON, S., LOWDELL, M., COSSU, G., BONFANTI, P. & DE COPPI, P. 2018. Multi-stage bioengineering of a layered oesophagus with in vitro expanded muscle and epithelial adult progenitors. *Nature Communications,* 9**,** 4286.

UZARSKI, J. S., DIVITO, M. D., WERTHEIM, J. A. & MILLER, W. M. 2017. Essential design considerations for the resazurin reduction assay to noninvasively quantify cell expansion within perfused extracellular matrix scaffolds. *Biomaterials,* 129**,** 163-175.

VACANTI, C. A., PAIGE, K. T., KIM, W. S., SAKATA, J., UPTON, J. & VACANTI, J. P. 1994. Experimental tracheal replacement using tissue-engineered cartilage. *Journal of Pediatric Surgery,* 29**,** 201-205.

VIELREICHER, M., SCHÜRMANN, S., DETSCH, R., SCHMIDT, M. A., BUTTGEREIT, A., BOCCACCINI, A. & FRIEDRICH, O. 2013. Taking a deep look: modern microscopy technologies to optimize the design and functionality of biocompatible scaffolds for tissue engineering in regenerative medicine. *Journal of the Royal Society, Interface,* 10**,** 20130263.

VIGNESH, K. S. & DEEPE, G. S. 2017. Metallothioneins: Emerging Modulators in Immunity and Infection. *International Journal of Molecular Sciences,* 18.

VILLALONA, G., UDELSMAN, B., DUNCAN, D., MCGILLICUDDY, E., SAWH-MARTINEZ, R., HIBINO, N., PAINTER, C., MIRENSKY, T., ERICKSON, B., SHINOKA, T. & BREUER, C. 2010. Cell-Seeding Techniques in Vascular Tissue Engineering. *Tissue Engineering Part B: Reviews,* 16**,** 341-50.

VITACOLONNA, M., BELHARAZEM, D., HOHENBERGER, P. & ROESSNER, E. 2013. *Effect of static seeding methods on the distribution of fibroblasts within human*
acellular dermis.

VOGEL, G. 2013. Trachea transplants test the limits. *Science (New York, N.Y.),* 340**,** 266.

VOLKMER, E., OTTO, S., POLZER, H., SALLER, M., TRAPPENDREHER, D., ZAGAR, D., HAMISCH, S., ZIEGLER, G., WILHELMI, A., MUTSCHLER, W. & SCHIEKER, M. 2012. Overcoming hypoxia in 3D culture systems for

tissue engineering of bone in vitro using an automated, oxygen-triggered feedback loop. *J Mater Sci: Mater Med,* 23**,** 2793-2801.
VRTAČNIK, P., KOS, Š., BUSTIN, S. A., MARC, J. & OSTANEK, B. 2014. Influence of trypsinization and alternative procedures for cell preparation before RNA extraction on RNA integrity. *Analytical Biochemistry,* 463**,** 38-44.
WAGNER, J., KEAN, T., YOUNG, R., DENNIS, J. E. & CAPLAN, A. I. 2009. Optimizing mesenchymal stem cell-based therapeutics. *Current Opinion in Biotechnology,* 20**,** 531-536.
WAHL, S. M., SWISHER, J., MCCARTNEY-FRANCIS, N. & CHEN, W. 2004. TGF-β: the perpetrator of immune suppression by regulatory T cells and suicidal T cells. *Journal of Leukocyte Biology,* 76**,** 15-24.
WALLES, T., GIERE, B., HOFMANN, M., SCHANZ, J., HOFMANN, F., MERTSCHING, H. & MACCHIARINI, P. 2004a. Experimental generation of a tissue-engineered functional and vascularized trachea. *The Journal of Thoracic and Cardiovascular Surgery,* 128**,** 900-906.
WALLES, T., GIERE, B., MACCHIARINI, P. & MERTSCHING, H. 2004b. Expansion of chondrocytes in a three-dimensional matrix for tracheal tissue engineering. *The Annals of Thoracic Surgery,* 78**,** 444-448.
WANG, L. & STEGEMANN, J. P. 2010. Extraction of high quality RNA from polysaccharide matrices using cetlytrimethylammonium bromide. *Biomaterials,* 31**,** 1612-1618.
WANG, L.-T., TING, C.-H., YEN, M.-L., LIU, K.-J., SYTWU, H.-K., WU, K. K. & YEN, B. L. 2016. Human mesenchymal stem cells (MSCs) for treatment towards immune- and inflammation-mediated diseases: review of current clinical trials. *Journal of biomedical science,* 23**,** 76.
WARD, J. P. T., WARD, J., LEACH, R. M. & WIENER, C. M. 2010. *The Respiratory System at a Glance,* Hoboken, Hoboken: John Wiley & Sons, Incorporated.
WATT, F. M. & HUCK, W. T. S. 2013. Role of the extracellular matrix in regulating stem cell fate. *Nat Rev Mol Cell Biol,* 14**,** 467-473.
WEBBER, M., KHAN, O., SYDLIK, S., TANG, B. & LANGER, R. 2015. A Perspective on the Clinical Translation of Scaffolds for Tissue Engineering. *Ann Biomed Eng,* 43**,** 641-656.
WEIDENBECHER, M., TUCKER, H. M., AWADALLAH, A. & DENNIS, J. E. 2008. Fabrication of a Neotrachea Using Engineered Cartilage. *Laryngoscope,* 118**,** 593-598.
WEIDENBECHER, M., TUCKER, H. M., GILPIN, D. A. & DENNIS, J. E. 2009. Tissue-engineered trachea for airway reconstruction. *Laryngoscope,* 119**,** 2118-2123.
WEINBAUM, J., QI, J. & TRANQUILLO, R. 2010. Monitoring Collagen Transcription by Vascular Smooth Muscle Cells in Fibrin-Based Tissue Constructs. *Tissue Engineering Part C: Methods,* 16**,** 459-67.
WEISS, D. J., ELLIOTT, M., YANG, Q., POOLE, B. & BIRCHALL, M. 2014. Tracheal bioengineering: The next steps: Proceeds of an international society of cell therapy pulmonary cellular therapy signature series workshop, Paris, France, April 22, 2014. *Cytotherapy,* 16**,** 1601-1613.
WEK, R. C., JIANG, H. & ANTHONY, T. 2006. Coping with stress: eIF2 kinases and translational control. *Biochemical Society Transactions,* 34**,** 7-11.

WENDT, D., MARSANO, A., JAKOB, M., HEBERER, M. & MARTIN, I. 2003. Oscillating perfusion of cell suspensions through three-dimensional scaffolds enhances cell seeding efficiency and uniformity. *Biotechnology and Bioengineering,* 84**,** 205-214.

WESTPHAL, I., JEDELHAUSER, C., LIEBSCH, G., WILHELMI, A., ASZODI, A. & SCHIEKER, M. 2017. Oxygen mapping: Probing a novel seeding strategy for bone tissue engineering. *Biotechnology and Bioengineering,* 114**,** 894-902.

WEYMANN, A., PATIL, N. P., SABASHNIKOV, A., KORKMAZ, S., LI, S., SOOS, P., ISHTOK, R., CHAIMOW, N., PATZOLD, I., CZERNY, N., SCHMACK, B., POPOV, A.-F., SIMON, A. R., KARCK, M. & SZABO, G. 2015. Perfusion-Decellularization of Porcine Lung and Trachea for Respiratory Bioengineering. *Artificial Organs,* 39**,** 1024-1032.

WIGGENHAUSER, P. S., SCHANTZ, J. T. & ROTTER, N. 2017. Cartilage engineering in reconstructive surgery: auricular, nasal and tracheal engineering from a surgical perspective. *Regenerative medicine,* 12**,** 303.

WILES, K., FISHMAN, J. M., DE COPPI, P. & BIRCHALL, M. A. 2016. The Host Immune Response to Tissue-Engineered Organs: Current Problems and Future Directions. *Tissue Engineering Part B: Reviews,* 22**,** 28-219.

WISZNIEWSKI, L., JORNOT, L., DUDEZ, T. & PAGANO, A. 2006. Long-Term Cultures of Polarized Airway Epithelial Cells from Patients with Cystic Fibrosis. *American Journal of Respiratory Cell and Molecular Biology,* 34**,** 39-48.

WON SUH, S., KIM, J., HWAN BAEK, C., HAN, J. & KIM, H. 2001. Replacement of a Tracheal Defect with Autogenous Mucosa Lined Tracheal Prosthesis Made from Polypropylene Mesh. *ASAIO Journal,* 47**,** 496-500.

WOOD, M. W., MURPHY, S. V., FENG, X. & WRIGHT, S. C. 2014. Tracheal Reconstruction in a Canine Model. *Otolaryngology–Head and Neck Surgery,* 150**,** 428-433.

WOODS, T. & GRATZER, P. F. 2005. Effectiveness of three extraction techniques in the development of a decellularized bone–anterior cruciate ligament–bone graft. *Biomaterials,* 26**,** 7339-7349.

WU, Y.-N., LAW, J. B. K., HE, A. Y., LOW, H. Y., HUI, J. H. P., LIM, C. T., YANG, Z. & LEE, E. H. 2014. Substrate topography determines the fate of chondrogenesis from human mesenchymal stem cells resulting in specific cartilage phenotype formation. *Nanomedicine: Nanotechnology, Biology, and Medicine,* 10**,** 1507-1516.

WURTZ, A., PORTE, H., CONTI, M., DUSSON, C., DESBORDES, J., COPIN, M.-C. & MARQUETTE, C.-H. 2010. Surgical technique and results of tracheal and carinal replacement with aortic allografts for salivary gland–type carcinoma. *The Journal of Thoracic and Cardiovascular Surgery,* 140**,** 387-393.e2.

XIAO, Y. L., RIESLE, J. & BLITTERSWIJK, C. 1999. Static and dynamic fibroblast seeding and cultivation in porous PEO/PBT scaffolds. *Journal of Materials Science: Materials in Medicine,* 10**,** 773-777.

XING, Z., GAULDIE, J., COX, G., BAUMANN, H., JORDANA, M., LEI, X. F. & ACHONG, M. K. 1998. IL-6 is an antiinflammatory cytokine required for controlling local or systemic acute inflammatory responses. *Journal of Clinical Investigation,* 101**,** 311-320.

XINYU, Q., SHIYU, L., HAO, Z., BIN, Z., YUTING, S., CHENXI, Z., RONG, T., MIAO, W., HUIJUAN, K., XINYI, Z. & YAN, J. 2018. Mesenchymal stem cells and extracellular matrix scaffold promote muscle regeneration by synergistically regulating macrophage polarization toward the M2 phenotype. *Stem Cell Research & Therapy,* 9**,** 1-15.

XU, Y., LI, D., YIN, Z., HE, A., LIN, M., JIANG, G., SONG, X., HU, X., LIU, Y., WANG, J., WANG, X., DUAN, L. & ZHOU, G. 2017. Tissue-engineered trachea regeneration using decellularized trachea matrix treated with laser micropore technique. *Acta Biomaterialia,* 58**,** 113-121.

YAMASHITA, J., FURMAN, B. R., RAWLS, H. R., WANG, X. & AGRAWAL, C. M. 2001. The use of dynamic mechanical analysis to assess the viscoelastic properties of human cortical bone. 58**,** 47-53.

YANG, Q., PENG, J., GUO, Q., HUANG, J., ZHANG, L., YAO, J., YANG, F., WANG, S., XU, W., WANG, A. & LU, S. 2008. A cartilage ECM-derived 3-D porous acellular matrix scaffold for in vivo cartilage tissue engineering with PKH26-labeled chondrogenic bone marrow-derived mesenchymal stem cells. *Biomaterials,* 29**,** 2378-2387.

YIN-PING, L., YI-SHIUAN, L., MARILYN, G. R., JENNIFER HUI-CHUN, H., KENG-HUI, L. & OSCAR, K. L. 2016. Three-dimensional spherical spatial boundary conditions differentially regulate osteogenic differentiation of mesenchymal stromal cells. *Scientific Reports,* 6.

YOON, M., KIM, J., OAK, C., JANG, T., JUNG, M., CHUN, B., LEE, S. & HEO, J. 2013. Tracheal cartilage regeneration by progenitor cells derived from the perichondrium. *Tissue Eng Regen Med,* 10**,** 286-292.

YU, C., YOUNG, S., RUSSO, V., AMSDEN, B. G. & FLYNN, L. E. 2013. Techniques for the Isolation of High-Quality RNA from Cells Encapsulated in Chitosan Hydrogels. *Tissue Engineering Part C: Methods,* 19**,** 829-838.

YUE, Y., HUANG, W., LIANG, J., GUO, J., JI, J., YAO, Y., ZHENG, M., CAI, Z., LU, L. & WANG, J. 2015. IL4I1 Is a Novel Regulator of M2 Macrophage Polarization That Can Inhibit T Cell Activation via L-Tryptophan and Arginine Depletion and IL-10 Production. *PloS one,* 10**,** e0142979-e0142979.

ZALATA, LAMMERTIJN, CHRISTOPHE & COMHAIRE 1998. The correlates and alleged biochemical background of the resazurin reduction test in semen. *International Journal of Andrology,* 21**,** 289-294.

ZHANG, H., FU, W. & XU, Z. 2015. Re-epithelialization: A key element in tracheal tissue engineering. *Regenerative Medicine,* 10**,** 1005-1023.

ZHANG, Y., HE, Y., BHARADWAJ, S., HAMMAM, N., CARNAGEY, K., MYERS, R., ATALA, A. & VAN DYKE, M. 2009. Tissue-specific extracellular matrix coatings for the promotion of cell proliferation and maintenance of cell phenotype. *Biomaterials,* 30**,** 4021-4028.

ZHAO, J., GRIFFIN, M., CAI, J., LI, S., BULTER, P. E. M. & KALASKAR, D. M. 2016. Bioreactors for tissue engineering: An update. *Biochemical Engineering Journal,* 109**,** 268-281.

ZHENG, M. H., CHEN, J., KIRILAK, Y., WILLERS, C., XU, J. & WOOD, D. 2005. Porcine small intestine submucosa (SIS) is not an acellular collagenous matrix and contains porcine DNA: Possible implications in human implantation. *Journal of Biomedical Materials Research Part B: Applied Biomaterials,* 73B**,** 61-67.

ZHOU, P., HUANG, Y., GUO, Y., WANG, L., LING, C., GUO, Q., WANG, Y., ZHU, S., FAN, X., ZHU, M., HUANG, H., LU, Y. & WANG, Z. 2016. Decellularization and Recellularization of Rat Livers With Hepatocytes and Endothelial Progenitor Cells. *Artif Organs,* 40**,** E25-38.

ZILLER, A. & FRAISSINET-TACHET, L. 2018. Metallothionein diversity and distribution in the tree of life: a multifunctional protein. *Metallomics,* 10**,** 1549-1559.

ZUND, G., YE, Q., HOERSTRUP, S. P., SCHOEBERLEIN, A., SCHMID, A. C., GRUNENFELDER, J., VOGT, P. & TURINA, M. 1999. Tissue engineering in cardiovascular surgery: MTT, a rapid and reliable quantitative method to assess the optimal human cell seeding on polymeric meshes. *European Journal of Cardio-thoracic Surgery,* 15**,** 519-524.

ZWOLANEK, D., FLICKER, M., KIRSTÄTTER, E., ZAUCKE, F., VAN OSCH, G. & ERBEN, R. 2015. [beta]1 Integrins Mediate Attachment of Mesenchymal Stem Cells to Cartilage Lesions. *BioResearch Open Access,* 4**,** 39-53.